ANALYZING GENOME INTEGRITY DURING DNA REPLICATION USING iPOND (iSOLATION OF PROTEINS ON NASCENT DNA)

By

Bianca Maria Sirbu

Dissertation

Submitted to the Faculty of the

Graduate School of Vanderbilt University

in partial fulfillment of the requirements

for the degree of

DOCTOR OF PHILOSOPHY

in

Biochemistry

August 2013

Nashville, Tennessee

Approved:

Professor David Cortez

Professor Scott Hiebert

Professor Kathy Gould

Professor Lawrence Marnett

Professor William Tansey

Pentru iubiții mei părinți, Mama şi Tata

Pentru surioara mea incredibila, Cristi

Pentru minunatul meu draguț, Geoffrey

ACKNOWLEGEMENTS

“Explore the world. Nearly everything is interesting if you go into it deep enough.” Richard Feynman

The incredible opportunities to research my curiosities have made graduate school an amazing journey. I am grateful to the Vanderbilt University Interdisciplinary Program, the Biochemistry Department, the Molecular Toxicology Center, the Department of Defense Breast Cancer Research Program, and the Swim Across America Foundation for their kind support of this research.

The last six years of graduate school have been a thrilling and humbling scientific and life journey that would have been impossible without the amazing mentors, colleagues and friends that have supported me along the way.

My thesis committee members Professors Kathy Gould, Scott Hiebert, Bill Tansey and Larry Marnett have provided me invaluable guidance throughout the years. I am indebted to them for their time, patience, advice on how to make iPOND work, and their kind mentorship. Professor Hiebert shared his expertise and contagious passion for the chromatin field with our laboratory and continues to be an encouraging collaborator and friend. Professor Gould has watched me grow since the IMPACT group she led in the first year of IGP. She has been supportive of all my endeavors and I am grateful for her caring nature.

None of this would have been possible without my thesis mentor Dave Cortez. Professor Cortez came up with the elegant solution to purify replication forks using click chemistry. I feel fortunate to have been the student whom he patiently guided and encouraged through the numerous trials and tribulations called iPOND. His clear and critical thinking humble me every day and I've tried to absorb as much of his nature as possible. I admire his remarkable work ethic and passion for science. He has been the best mentor I could have hoped for and he will remain an inspiration to me.

My colleagues in the Cortez lab have been without a doubt the most talented team of scientists with whom I could have hoped to spend these years. They have furthermore been my loving friends whose perseverance, intelligence, and overall thoughtfulness are commendable. Dan Mordes, Courtney Lovejoy, Carol Bansbach Robbins, and Eddie Nam have been my confidants and have provided amazing amounts of encouragement from the time I joined the lab. Dan patiently discussed his insights into DNA replication with me and has remained a dear friend over the years. Courtney, Carol and Eddie have been family to me. I love their beautiful minds and kind souls and miss us being together. Jami Couch joined us a couple of years later and has been my partner in crime since the earlier days of iPOND. He continues to impress me with his brilliance and gentle, insightful nature. I am fortunate to have him as a friend. The success of my project would have been impossible without him. Rémy Betous is one of the most passionate scientists I've ever met. His dedication is contagious and he

benevolently imparted the best scientific advice. Gloria Glick has made life in the lab smooth for all of us with her immaculate organization and generous cookie jar. I am grateful for her patience with my messes.

Our newest lab members have brightened the last couple of years in lab. Gina Kavanaugh's heart is big enough for two people and her inner peace is inspirational. I really appreciate Jessica Luzwick's clarity in thinking and lack of fluff. Akosua Badu-Nkansah's work ethic is incredible as are her stories about growing up in other lands. Kareem Mohni provides smiles and insightful comments to everyone and I'm glad our times in the lab have overlapped. I am also thankful to have had time to know Lisa Poole, Kami Bhat, Clint Caroll and Huzefa Dungrawala who have brought greatness to the Cortez team.

The environment at Vanderbilt has helped me flourish and this is due in large part to my colleagues in the Biochemistry department. Professors Guengerich and Wagner have kindly shared their time with me over the years to provide advice on life. The smiles of my friends in the Toxicology Center have made even the hardest days pleasant. My collaborators Hayes McDonald, Yaoyi Chen, David Tabb, Simona Codreanu, Dan Liebler, Ned Porter, Keri Tallman, Natalia Isaeva, Jordan Feigerle, Alex Trevisan and Rose Follis have generously helped me numerous times. I am privileged to have the friendship of Vidya Bhaskara and Mahesh Chandrasekharan. They are passionate scientists, devoted and kind friends.

My old friends from before graduate school (Elnaz Naseri, Boris Paskalev, Miriam Makhlouf, and Elina Shustef) and new friends from my time during graduate school (my girls Meghana Rao and Laura Burns, Mike Burns, Josh Arnold, Tarjani Thaker, Steven Pitts, Amicia Elliott, Chris Ververis, my TVC team members, Achumboro Aatande, Evan Lund, Wenjun Xu, Rob Havens and Mike Pickup) have shared the best of times and worst of times with me. They have taught me the importance of balancing work and life, being adventurous, taking chances, and embracing changes. Meghana and Laura have compassionately shared the experience of graduate school, inspired me to persevere, and loved me even when I failed at being a good friend. Undeservingly, I am blessed to have such amazing people in my life.

Lastly, my family is my source of energy. When my parents moved my sister and I from Romania to America as teenagers, they packed two suitcases and uprooted from a comfortable life to start anew in hopes of providing real opportunities for their children in a foreign land. They spoke no English at that time, had few acquaintances and small life savings. They immigrated and struggled working several difficult jobs to provide us a better life and they've succeeded. I couldn't be more proud of them and my sister Cristina. They are the roots of all my strength and I am humbled by their sacrifices and immense love. Vă mulțumesc din toata inima şi vă iubesc, dragii mei. Cristi, you know me better than anyone. Te iubesc, bebeluşa. Geoffrey Becker. I could not live without you. You are my best friend and soul mate. I still can't believe you picked me.

TABLE OF CONTENTS

LIST OF TABLES

Page

LIST OF FIGURES

Page

LIST OF ABBREVIATIONS

53BP1	p53 Binding Protein 1
9-1-1	RAD9-HUS1-RAD1
APH	aphidicolin
APIM	AlkB homologue 2 PCNA-interacting motif
ATAD5	ATPase family, AAA domain containing 5
ATM	Ataxia Telangiectasia Mutated
ATP	adenosine tri-phosphate
ATR	ATM- and RAD3-Related
ATRIP	ATR-interacting protein
BAZ1B	bromodomain adjacent to zinc finger domain, 1B
BLM	Bloom Syndrome, Recq Helicase-Like
BP	Base Pairs of DNA
BRCA1	breast and ovarian cancer gene 1
BRCT	Breast Cancer Suppressor Protein (BRCA1), carboxy-terminal domain
BrdU	bromodeoxyuridine
BRIP1	Brca1 Interacting Protein C-Terminal Helicase 1
BSA	bovine serum albumin
CAF-1	Chromatin Assembly Factor 1
CDC6	cell division cycle 6
CDK	cyclin dependent kinase
CDT1	CDC10-dependent transcript 1
CHAF1A (B)	Chromatin Assembly Factor 1 Subunit A (B)
CHD1L	Chromodomain Helicase Dna Binding Protein 1-Like
ChIP	Chromatin Immunoprecipitation
CHK1	checkpoint kinase 1
CHK2	checkpoint kinase 2
CldU	Chlorodeoxyuridine
CMG	Cdc45-MCM-GINS
CP110	centrosomal protein 110
CPT	camptothecin
DDK	DBF4-dependent kinase
DDR	DNA damage response
DDRi	DDR kinase inhibitors
DNA	deoxyribonucleic acid
DNA-PK	DNA-dependent protein kinase
DNMT1	DNA (cytosine-5-)-methyltransferase 1
dNTP	deoxyribonucleotide triphosphate
DSB	double strand break

DSBR	double strand break repair
dsDNA	double stranded DNA
dUTP	deoxyuridine triphosphate
EdU	5-ethynyl-2'-deoxyuridine
EHMT1	euchromatic histone-lysine N-methyltransferase 1
EXO1	exonuclease 1
FA	Fanconi Anemia
FANCD2	Fanconi anemia, complementation group D2
FANCI	anconi anemia, complementation group I
GAPDH	Glyceraldehyde 3-phosphate dehydrogenase
GFP	green fluorescent protein
GINS	Go (5), Ichi (1), Nii (2), San (3): Sld5, Psf1, Psf2, Psf3
H1	Histone 1
H2B	Histone 2B
H3	Histone 3
H4	Histone 4
HA	hemagglutinin
HAT1	Histone Acetyltransferase 1
HDAC	Histone deacetylase
HR	homologous recombination
HU	hydroxyurea
ICL	Interstrand CrossLink
ID	Complex of FANCI and FANCD2
IdU	5-iodo-2′-deoxyuridine
IGEPAL	octylphenoxypolyethoxyethanol (detergent)
IP	immunoprecipitation
iPOND	isolation of Proteins On Nascent DNA
IR	ionizing radiation
iTRAQ	isobaric tag for relative and absolute quantification
KAP1	KRAB domain-associated protein 1
KBP	thousand base pairs
Ku70/80	Lupus Ku autoantigen protein p70/p80
LIG1	ligase I, DNA, ATP-dependent
LTQ	linear trap quadrupole
MCM	minichromosome maintenance
MDC1	Mediator of DNA damage checkpoint protein 1
Mec1	mitotic entry checkpoint protein 1
MEF	mouse embryonic fibroblast
MMC	Mitomycin C
MMR	Mismatch Repair
MMS	methyl methane sulfonate
MMS22L	Chromosome 6 Open Reading Frame 167
MRE11	meiotic recombination 11
MRN	MRE11-RAD50-NBS1

MS	Mass Spectrometry
MSH2	mutS homolog 2
MSH3	mutS homolog 3
MSH6	mutS homolog 6
MuDPIT	Multi-Dimensional Protein Identification Technology
NBS1	Nijmegen breakage syndrome
NER	nucleotide excision repair
NHEJ	non-homologous end joining
ORC	origin recognition complex
PAGE	polyacrylamide gel electrophoresis
PBS	phosphate buffered saline
PCNA	proliferating cell nuclear antigen
PIGT	phosphatidylinositol glycan anchor biosynthesis, class T
PIKK	PI-3 kinase-related kinase
PIP	PNCA Interacting Protein
POLD1	DNA polymerase delta catalytic subunit 1
POLE2	Polymerase Epsilon Subunit 2
POLE3	Polymerase Epsilon Subunit 3
PPP1R10	Protein Phosphatase 1, Regulatory (Inhibitor) Subunit 10
Pre-RC	pre-replication complex
PTM	Post-Translational Modification
RECQL1	RecQ protein-like (DNA helicase Q1-like)
RFC	replication factor C
RNF8	ring finger protein 8
RNR	ribonucleotide reductase
RPA	replication protein A
SDS	sodium dodecyl sulfate
SILAC	stable isotope labelling by amino acids in cell culture
SIOD	Schimke immuno-osseous dysplasia
siRNA	small interfering RNA
SMARCAD1	SWI/SNF-related matrix-associated actin-dependent regulator of chromatin subfamily A containing DEAD/H box 1
SMARCAL1	SWI/SNF, matrix associated, actin dependent regulator of chromatin A-like 1
SNF2	sucrose non-fermenting 2
SNF2H	SWI/SNF related, matrix associated, actin dependent regulator of chromatin, subfamily A, member 5
SNF2L	SWI/SNF related, matrix associated, actin dependent regulator of chromatin, subfamily A, member 1
SRM	Selected Reaction Monitoring mode
SSBR	single strand break repair
ssDNA	singe stranded DNA
Thd	Thymidine
TIPIN	timeless interacting protein

TONSL	Nuclear Factor Of Kappa Light Polypeptide Gene Enhancer In B-Cells Inhibitor-Like 2
TOP3A	Topoisomerase (Dna) Iii Alpha
TopBP1	Topoisomerase II-beta binding protein 1
TRMT6	tRNA methyltransferase homolog 6
UBR5	ubiquitin protein ligase E3 component n-recognin 5
UHRF1	ubiquitin-like with PHD and ring finger domains 1
UNG	Uracil-Dna Glycosylase
UV	ultraviolet radiation
VPS26	vacuolar protein sorting 26 homolog B
WDHD1	WD repeat and HMG-box DNA binding protein 1
WIZ	widely interspaced zinc finger motifs
WRN	Werner Syndrome, Recq Helicase-Like
WSTF	Williams syndrome transcription factor
XRCC1	X-ray repair complementing defective repair in Chinese hamster cells 1
γH2AX	H2AX phospho-serine 139

CHAPTER I

INTRODUCTION*

The task of developing from a single cell into a multicellular organism is remarkable. It requires ultimate precision every time a cell commits to duplicate its genetic material, the genome. In human cells, this means making copies of more than 6,000,000,000 base pairs of DNA during each DNA replication cycle. These copies have to be accurately divided between two daughter cells during mitosis. Mistakes made in the cell cycle cause mutations and chromosomal aberrations that eventually lead to diseases such as cancer.

However, to become a multicellular organism, it is insufficient to just replicate DNA. Cells must also differentiate to form tissues. Although all cells contain the same DNA, some cells differentiate into muscle cells while others differentiate into bone cells. This tissue-specific differentiation is driven in part by changes that occur 'on top of' the genome. This is called the 'epigenome' and it must also be inherited accurately for daughter cells to express the same genes and differentiate into the same tissue as the parental cell. Mistakes in copying the parental epigenome results in aberrant gene expression and human disease.

*Excerpts of this chapter are published in reference [1]. Sirbu BM, Couch FB and Cortez D, *Genes & Development 2011* and are in press Sirbu BM and Cortez D, *CSHL Perspectives in Biology* 2013.

And yet, maintaining genomic and epigenomic integrity during the cell cycle is still insufficient to become a healthy multicellular organism. Cells must also coordinate genome and epigenome inheritance with the given daily dose of damage. For example, exposure to UV light or the reactive byproducts of our metabolism stops cell growth to check the severity of the damage. Such a 'checkpoint' in the cell cycle allows time for DNA repair to occur. If left unrepaired, these types of damages accumulate, cause mutations, chromosomal abnormalities and eventually lead to severe human syndromes such as cancer.

How does a cell maintain integrity throughout the cell cycle and after DNA damage? By activating the DNA damage response system. This alert pathway preserves the genetic and epigenetic material to promote the development of one cell into a specific tissue that forms a healthy multicellular organism.

In this chapter, I will discuss the events of chromatin and DNA replication, epigenomic inheritance during replication, and how cells confront and repair DNA damage that disrupts these events. Exploring how these events are coordinated in a timely manner relative to one another has been difficult to study and is the topic of my thesis project.

Chromatin replication

Within the nucleus, DNA is tightly packaged into chromatin fibers that are assembled from repeating units of nucleosomes. Each nucleosome contains 147 base pairs of DNA wrapped around eight histone proteins (Fig. 1.1). This highly organized chromatin structure poses a physical barrier to duplication of the underlying DNA and must be disassembled. This process of chromatin decondensation begins with unraveling of histones from parental DNA at the end of the G1 (gap 1) phase of the cell cycle and continues throughout S phase when the underlying DNA is replicated.

DNA replication causes a large disturbance in chromatin structure and must be properly restored after passage of the replication fork [2]. After completion of DNA replication, DNA is repackaged into nucleosomes and higher order chromatin structure is reestablished. The duplicated genetic material is then segregated to two daughter cells during mitosis (Fig. 1.1).

The dynamic process of chromatin disassembly and reassembly is tightly coupled to DNA replication to ensure the accurate inheritance of the genome [3]. Histones are removed from their location on parental DNA 'in front' of the replication fork and captured by the histone chaperone CAF1 (Fig. 1.2). CAF1 interacts with the proliferating nuclear antigen (PCNA) protein, which serves as the processivity factor for DNA polymerases. This physical coupling to PCNA ensures that chromatin assembly is coordinated with DNA replication [4].

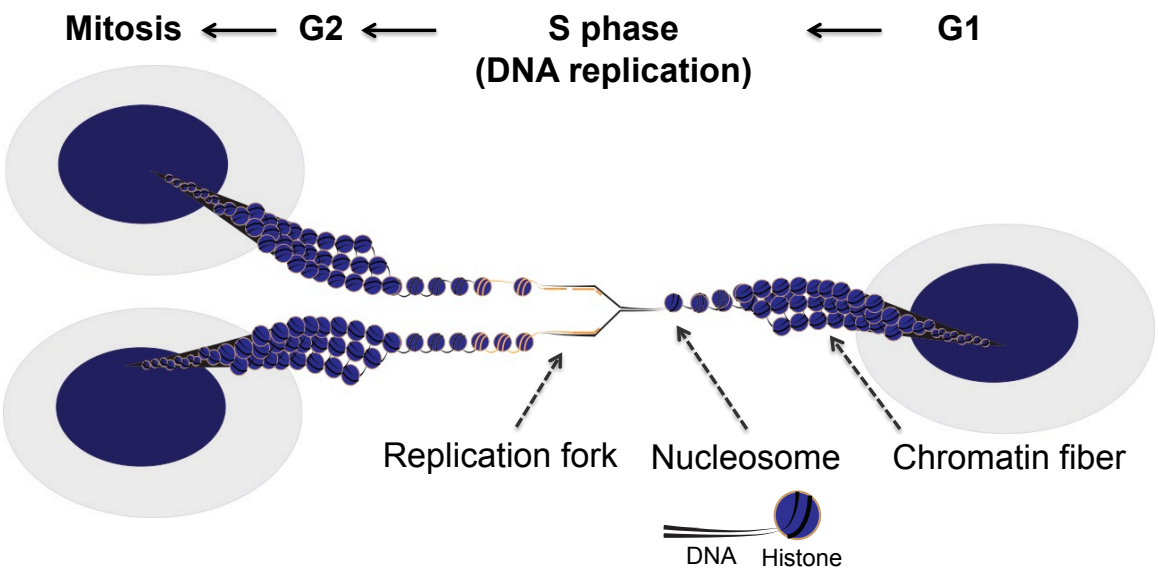

Figure 1.1. Maintaining genome integrity through the cell cycle. Decondensation of the chromatin fiber within the nucleus starts at the end of G1 phase. Nucleosomes (DNA wrapped around histones) are removed from parental DNA during S phase to allow the replication fork machinery to duplicate DNA. Chromatin is reestablished behind the replication fork into chromatin fibers and the duplicated genome is distributed to two daughter cells during mitosis.

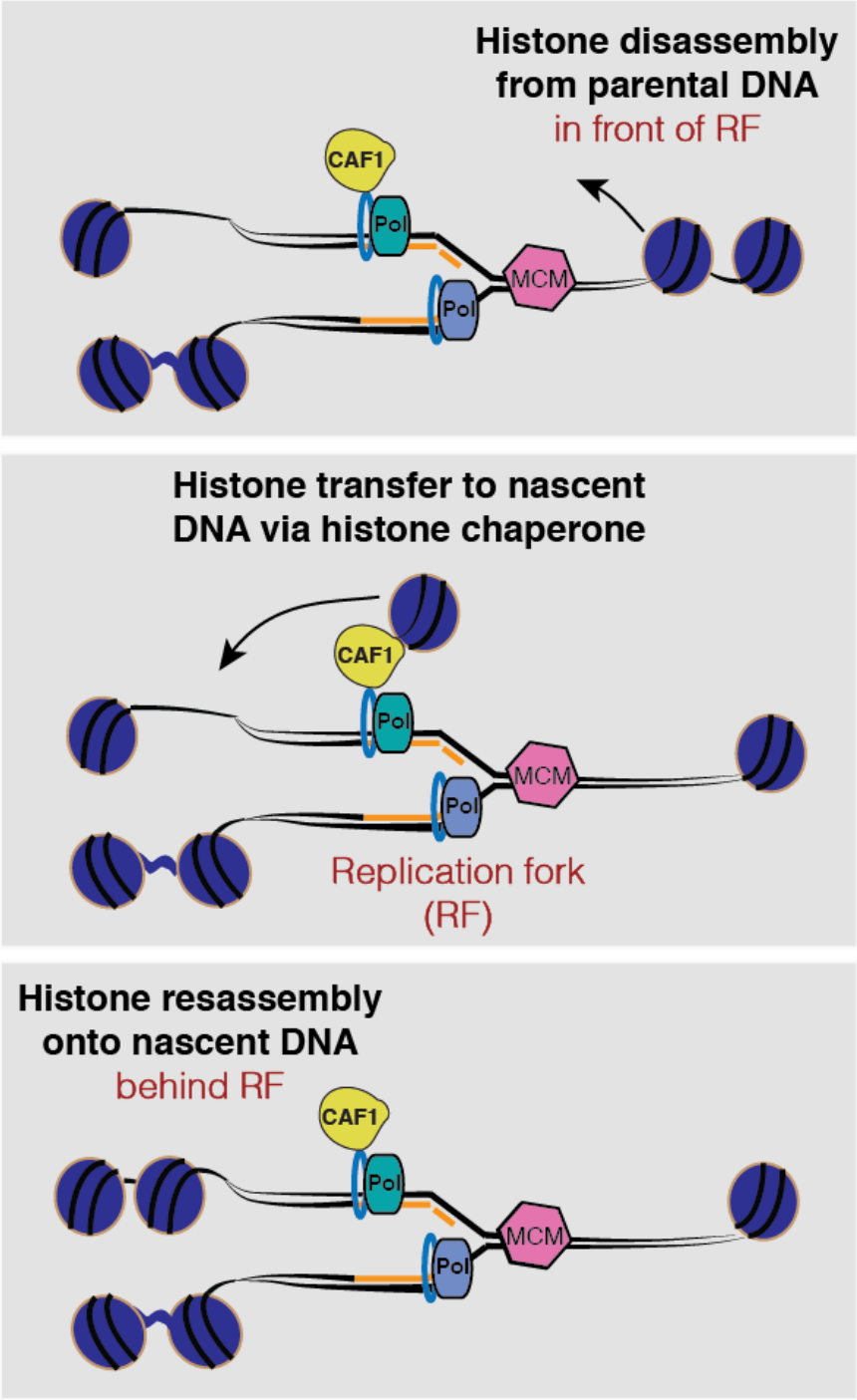

Figure 1.2. Chromatin replication. Parental histones on parental DNA in front of the replication fork (RF) are disassembled and recycled by histone chaperones onto nascent DNA behind the replication fork. Chromatin disassembly and reassembly are coordinated with replication fork passage and only a few histones are removed at any one time ahead of the replication fork.

CAF1 facilitates assembly of nascent chromatin behind the replication fork by recycling histones for deposition onto the nascent DNA (Fig. 1.2)

Since the amount of DNA is doubled during replication, twice the number of histones is needed to assemble nascent chromatin. Newly synthesized histones are imported from the cytosol into the nucleus as an H3-H4 dimer in complex with the histone chaperone ASF1. Nascent histones are distinguished from parental histones by the presence of an evolutionarily conserved di-acetylation mark on lysines 5 and 12 of histone H4 (H4K5ac/K12ac) [5] (Fig. 1.3). How the nascent and parental histones mix prior to being deposited onto nascent DNA remains unclear, but is hypothesized to be an asymmetric process, although some level of semi-conservative and random mixing may occur [6].

Epigenomic integrity during chromatin replication

Epigenetic inheritance refers to the faithful maintenance of parental modifications present on histones and DNA. For example, the removal of specific post-translational modifications on histones through DNA replication is essential for progression from nascent to parental histone, a process termed chromatin maturation. The prominent example involves the removal of the pre-deposition di-acetyl marks from H4K5/K12, which facilitates chromatin assembly and the formation of higher order chromatin structures [3, 7].

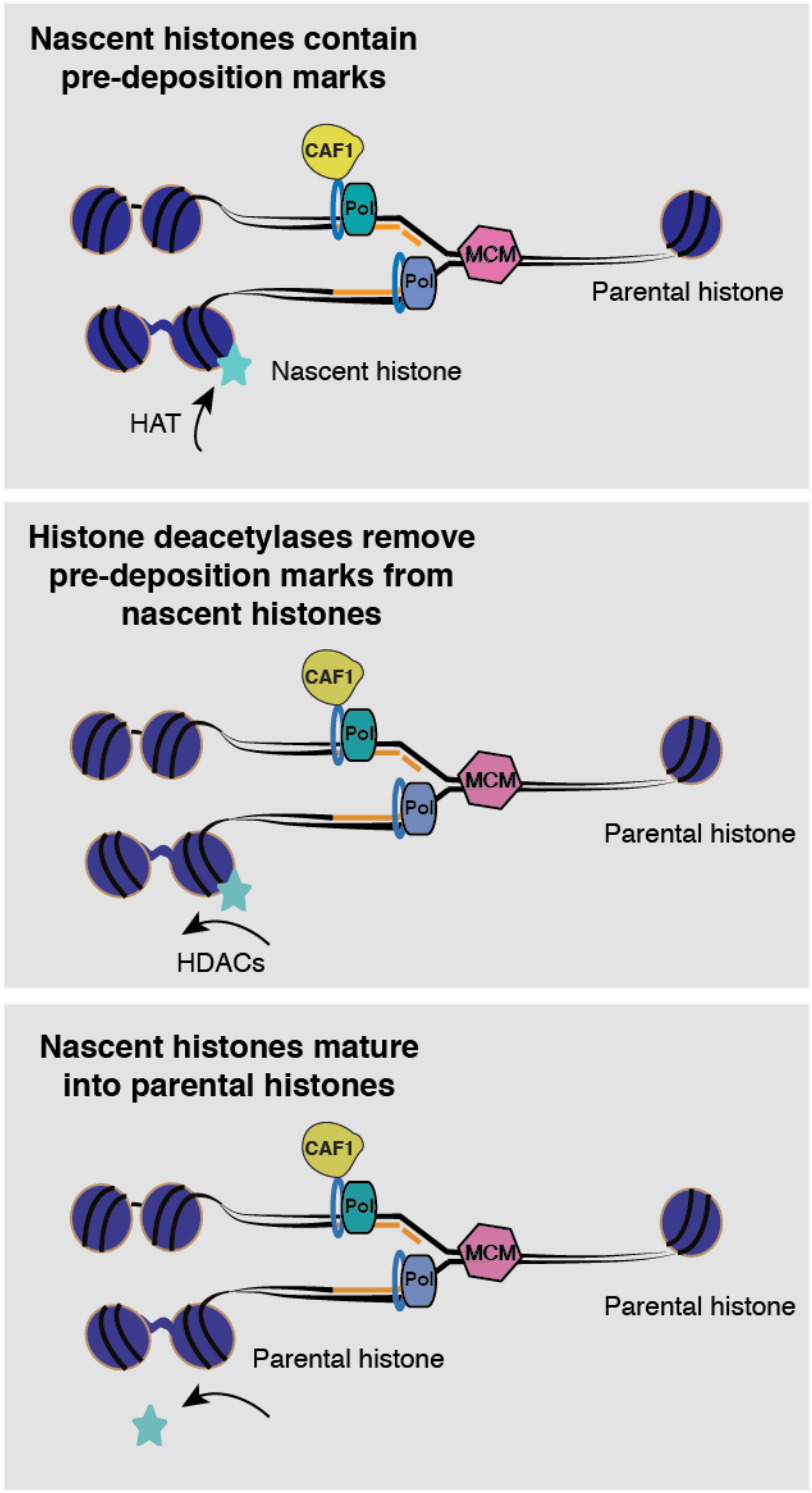

Figure 1.3. Chromatin maturation. Newly synthesized histones imported from the cytosol into the nucleus contain pre-deposition marks. Following assembly into nascent chromatin, histone acetyltransferases remove pre-deposition marks to faithfully transmit epigenetic information to the next cell cycle.

Chromatin maturation is a dynamic balance between histone deacetylases (HDACs) and histone acetyltransferases (HATs) that catalyze removal and addition of acetyl groups on histones, respectively. In yeast, the HAT1 acetyltransferase modifies H4 on K5/K12 in the cytosol where nascent histones are synthesized. Following catalysis, HAT1 remains bound to nascent histones that are imported into the nucleus for deposition onto nascent chromatin [8]. How this dynamic event is coupled to progression through replication has remained poorly characterized in higher organisms and is a topic explored in this thesis.

Epigenetic inheritance involves not only propagating the parental histone marks during chromatin assembly and maturation, but also transmitting the marks on DNA to the next generation. Parental DNA is methylated and serves as the template for the faithful transmission of methylation to newly replicated DNA. PCNA links semi-conservative DNA methylation to replication by recruiting the DNA methyltrasferase DNMT1 to replication forks [9]. Proper methylation of nascent DNA occurs at CpG sites (cytosine followed by guanine) also requires the ubiquitin ligase UHRF1 (Ubiquitin-like, containing PHD and RING finger domains 1), a coordinating factor for DNA methylation and histone deacetylation [2, 10]. Hypermethylation of CpG sites in the promoter regions of genes is a hallmark of the epigenetic instability underlying several cancer types and has contributed to the methylator phenotype hypothesis for tumorigenesis [11].

In addition to DNA methylation and chromatin maturation, chromatin remodeling enzymes catalyze nucleosome sliding, histone eviction and histone

exchange to restore higher order chromatin structure after disruption during DNA replication [2]. It remains largely unresolved how these enzymatic activities are coordinated at replication forks due to the lack of tools to study replication-coupled chromatin assembly and maturation, particularly in mammalian cells.

DNA replication

Following removal of histones from parental DNA during chromatin disassembly, the underlying DNA is exposed and ready to be copied. The process of DNA replication is tightly controlled to ensure the genetic material is duplicated once and only once per cell cycle. DNA replication begins at origins of replication that are present throughout the genome of eukaryotic cells. Unlike in yeast (e.g. *S. cerevisiae*), origins of replication are poorly defined regions of the genome in higher organisms [12].

Beginning in late mitosis and early G1 phases of the cell cycle, protein complexes are recruited to origins of replication to form the pre-replication complex (pre-RC) (Fig. 1.4). The pre-RC consists of several proteins including the origin recognition complex (ORC), Cdt1, Cdc6 and the MCM helicase that unwinds the two parental DNA strands. This unwinding begins in S phase, depends on the enzymatic activities of the CDK (cyclin dependent kinase) and DDK (Cdc7/Dbf4-dependent kinase) kinases, and provides the DNA template used for bi-directional DNA replication [13].

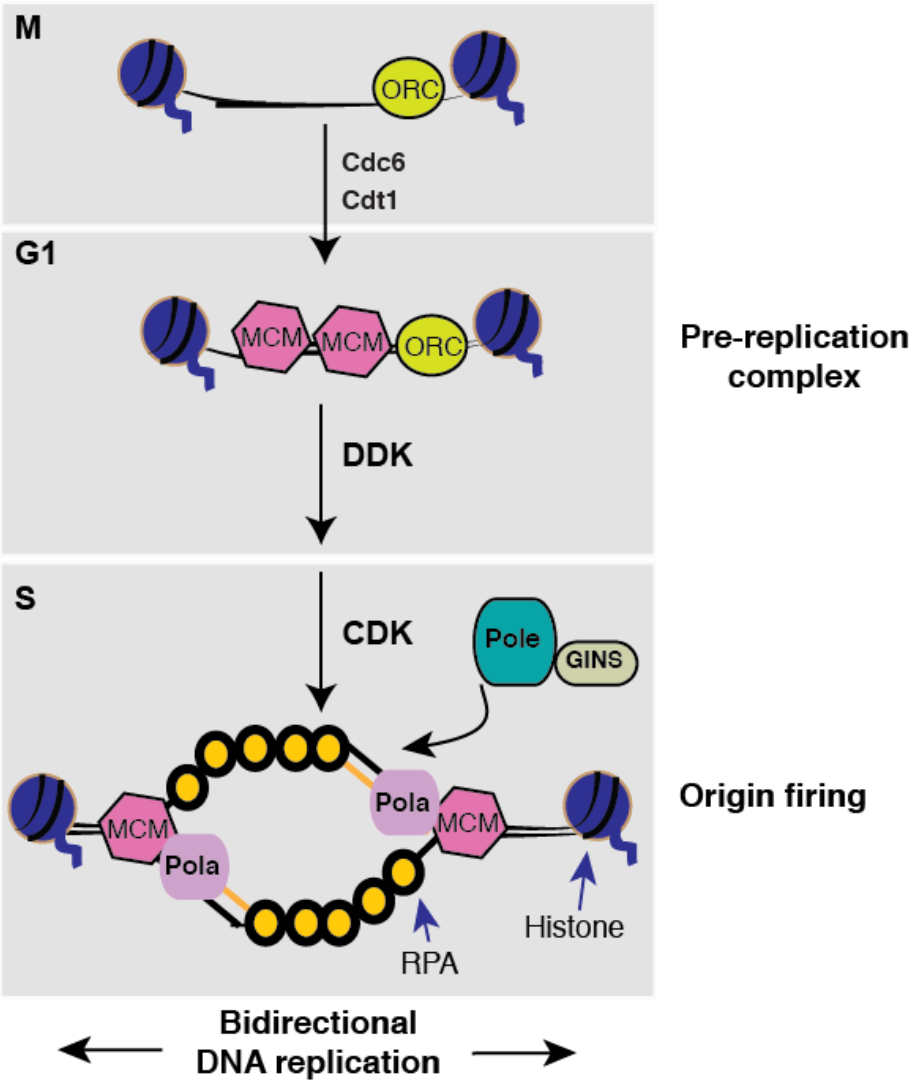

Figure 1.4. Initiation of DNA replication. ORC loading begins at the end of mitosis, followed by recruitment of Cdc6 and Cdt1. In G1, the pre-replication complex is formed and the double hexamer MCM2-7 helicase is loaded head-to-head onto DNA. The kinases CDK and DDK are needed for firing of origins of replication upon entry into S phase. DNA replication proceeds bi-directionally from a fired origin.

Binding of the Replication Protein A (RPA) to parental DNA maintains the parental strands separated to allow the loading of the replicative polymerases and initiation of leading and lagging strand DNA synthesis. Since DNA polymerases delta and epsilon cannot initiate DNA synthesis *de novo,* an RNA primer is first provided by DNA primase/polymerase alpha. Once DNA synthesis begins, an origin is said to have 'fired.'

DNA synthesis occurs asymmetrically with continuous polymerization on the leading strand and in a discontinuous manner on the lagging strand. The replication factor C (RFC) 1-5 complex loads the replicative polymerases epsilon and delta on the leading and lagging strands, respectively. RFC1-5 likely facilitates the recycling of the DNA polymerase processivity factor PCNA once synthesis of the Okazaki fragment (nascent DNA fragment on the lagging strand) is completed. Thus, constant loading and unloading of PCNA and polymerase delta occurs on the lagging strand. DNA replication continues until the parental DNA is completely duplicated exactly once and replication is then terminated.

DNA replication occurs in the context of chromatin, yet how histone and DNA replication are coordinated at the elongating replication fork has remained poorly understood. This unanswered question is addressed in this thesis.

DNA damage response

DNA damage occurs in each and every cell cycle and threatens the integrity of the genome and epigenome. Fortunately, cells have evolved an evolutionarily conserved mechanism to deal with DNA damage called the DNA damage response (DDR).

The major coordinators of the DDR are a family of related phosphatidylinositol 3-kinase-related kinases (PIKK). These kinases include DNA dependent protein kinase (DNA-PKcs), ataxia telangiectasia-mutated (ATM), and ATM and Rad3-related (ATR). DNA-PKcs and ATM are primarily involved in DSB repair, whereas ATR responds to a wide range of DNA lesions, especially those associated with DNA replication [14] (Fig. 1.5). ATR's versatility makes it essential for the viability of replicating cells in mice and humans [15-17]. Rare hypomorphic ATR mutations are found in some cases of Seckel Syndrome, which is characterized by growth and mental retardation, and short stature [18, 19]. In the case of ATM, inherited biallelic mutations cause ataxia-telangiectasia, characterized by neurodegeneration, immunodeficiency, and cancer [20, 21]. ATM mutations are also frequently found in several types of tumors [22].

The DDR kinases share several common regulatory mechanisms of activation [23]. All three DDR kinases sense damage through protein–protein interactions that serve to recruit the kinases to damage sites. Once localized, post-translational modifications and other protein–protein interactions fully activate the kinases to initiate a cascade of phosphorylation events.

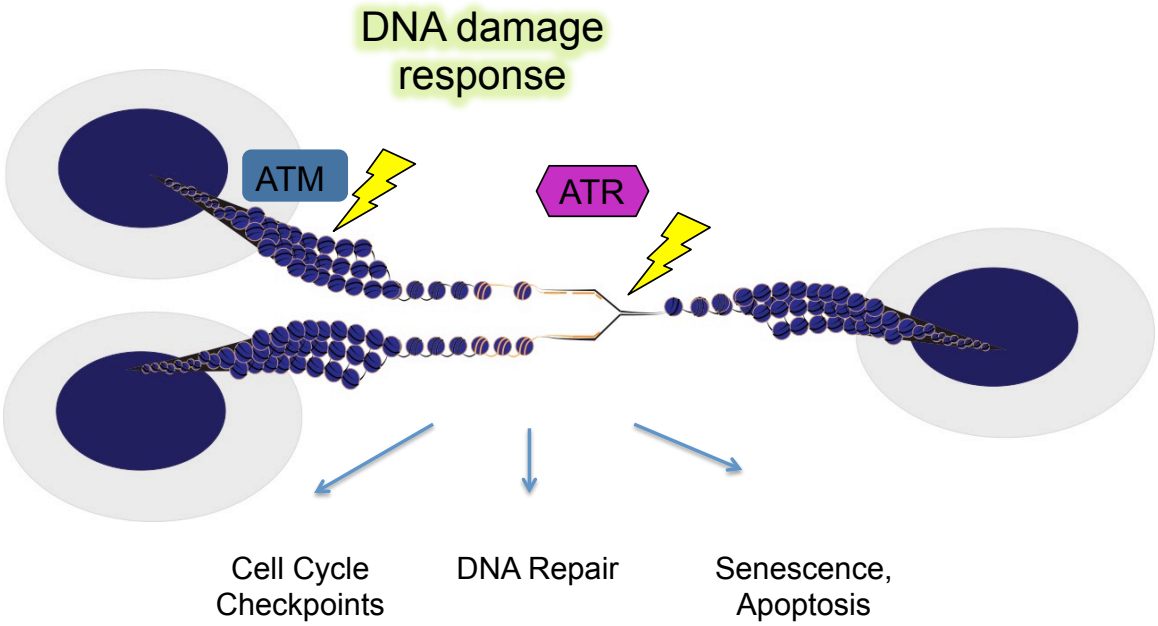

Figure 1.5. DNA damage response. The ATM and ATR kinases are two of the apical coordinators of the DNA damage response and are recruited to so sites of double-strand breaks (in the case of ATM) and damaged replication forks (in the case of ATR). Together, the DNA damage response halts the cell cycle to allow time for repair and initiates senescence or apoptosis of heavily damaged cells.

ATM and ATR have both unique and shared substrates that participate in DNA repair, checkpoint signaling, and determining cell fate decisions such as apoptosis and senescence.

Responding to DNA damage at the replication fork

Where does damage come from and how does it affect the crucial events coordinated at the replication fork? Thousands of DNA lesions, the lack of nucleotides, and other types of stress are encountered during every round of DNA replication and cause what is collectively termed replication stress.

The majority of lesions are removed and repaired before the replication fork encounters the damage site using one of several choices of repair mechanism. Base excision repair (BER) removes damaged bases, mismatch repair (MMR) recognizes base incorporation errors and base damage, nucleotide excision repair (NER) removes bulky DNA adducts, and crosslink repair (ICL) removes interstrand crosslinks. In addition, breaks in the DNA backbone are repaired via double-strand break (DSB) repair pathways including homologous recombination (HR) and nonhomologous end joining (NHEJ). Some of these mechanisms can operate independently to repair simple lesions. However, the repair of more complex lesions involving multiple DNA processing steps is regulated by the DNA damage response (DDR). For the most difficult to repair lesions, the DDR can be essential for successful repair.

When damage is not repaired before the replication fork reaches the damage site or when a lesion is encountered directly at the replication fork, the replication fork stalls until the damage is removed. A stalled fork itself may not be a particularly devastating event to a cell because DNA replication will usually be completed from an adjacent origin of replication. In such cases, the DDR stabilizes the damaged fork to prevent aberrant DNA processing. In other cases, such as in replication of fragile sites that contain few replication origins, fork stabilization may be insufficient and DDR-kinase dependent restart of the stalled fork becomes essential [24].

How are stalled forks repaired? Depending on the DNA strand affected (leading or lagging), the type of damage, and the severity of damage, cells employ different DNA repair mechanisms to allow DNA polymerases to accurately read and duplicate the information in the genome. Damage encountered on the leading strand that halts movement of the replicative polymerase but allows DNA unwinding by the helicase creates large stretches of RPA-coated ssDNA [14]. This is the signaling platform that recruits the ATR kinase through its obligatory interacting partner ATRIP that binds RPA- ssDNA (Fig. 1.6). Other fork stalling mechanisms include the bypass of damage using low fidelity polymerases or switching DNA template strands for translesion synthesis. If the damage is observed on the lagging strand, it is typically easier to bypass since repriming occurs naturally to synthesize Okazaki fragments [25].

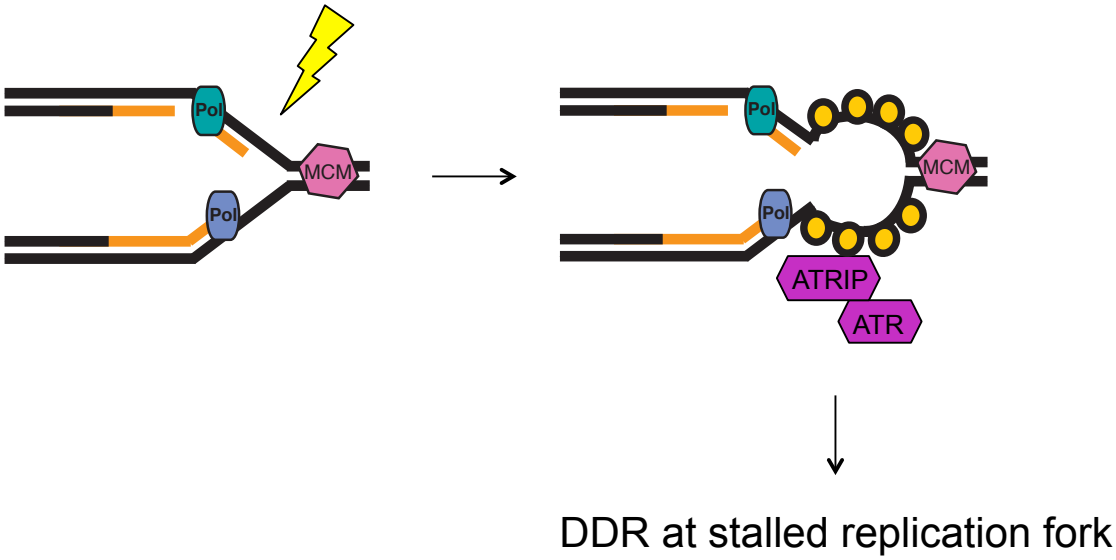

Figure 1.6. ATR kinase responds to damage at replication forks. Stalling of the replicative polymerase and continued unwinding by the replicative helicase generates parental ssDNA. The replication protein A (RPA, depicted as yellow dots) has high affinity for ssDNA and forms a recruiting platform for the ATR-ATRIP complex that initiates the DNA damage response to stalled replication forks.

Lesions that halt movement of both helicase and polymerases elicit a specialized repair type called interstrand crosslink repair (ICL). ICL repair provides the best mechanistic understanding of repair of damaged replication forks (see below).

Interstrand crosslink repair during DNA replication

Engineering of site-specific DNA crosslink lesions in *Xenopus* egg extracts has provided an excellent tool for studies of fork repair [26, 27]. Such lesions are highly effective in stalling both the replicative polymerase and helicase. Interstrand crosslinks are perhaps the most difficult lesions to repair, requiring specialized repair mechanisms governed by genes mutated in patients with Fanconi anemia (FA), as well as components of nucleotide excision and DSB repair [28]. In the context of DNA replication, interstrand crosslinks are potent fork stalling lesions that activate ATR. Perhaps for these reasons, the ATR kinase has critical function in ICL repair.

When the ICL stalls a replication fork, the DNA structure signals the recruitment of several Fanconi proteins beginning with the FANCM translocase [26, 29]. FANCM may remodel the damaged fork to help recruit the FA core complex, a multisubunit ubiquitin ligase (Fig. 1.7). An essential activity of the core complex is monoubiquitination of FANCD2 and FANCI within the FANCI-FANCD2 (ID) complex [30]. Repair then initiates with synchronized incision on both sides of the crosslink and may be mediated by the flap endonuclease FAN1 or SLX4-associated nucleases.

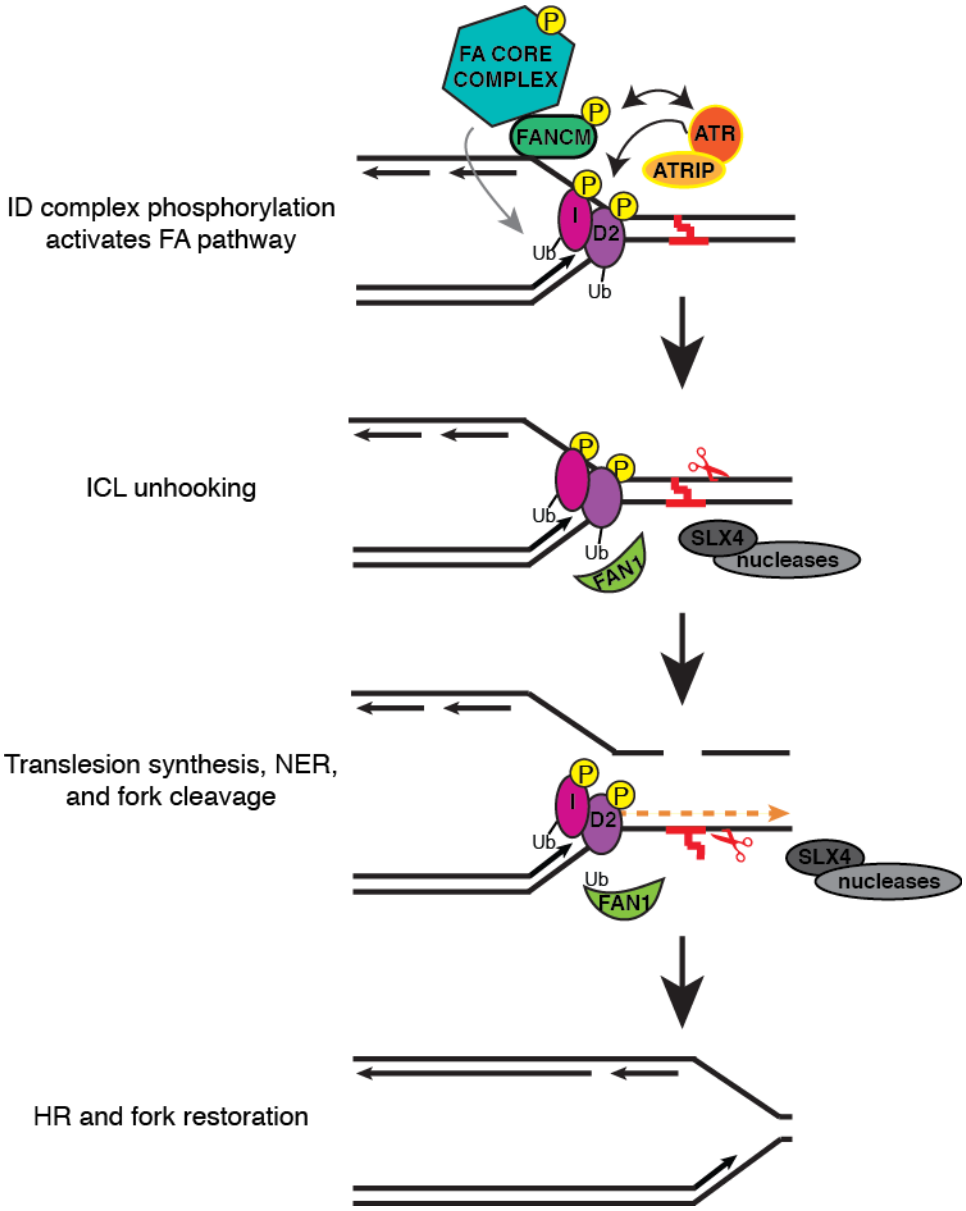

Figure 1.7. Replication fork repair of interstrand crosslink damage. Interstrand crosslinks prevent both helicase and polymerase activities and stall replication forks. FANCM remodels the stalled fork and results in recruitment of the FA core complex and activation of the ATR pathway. Repair involves nucleolytic cleavage to unhook the ICL and allow for translesion synthesis past the damaged base to restore the replication fork. These steps involve components of the nucleotide excision repair and homologous recombination pathways and ATR-mediated phosphorylation.

The ubiquitin-binding UBZ motif of FAN1 is essential for ICL repair as it recognizes mono-ub FANCD2 [31-33]. Fork cleavage results in “unhooking” of the crosslink allowing error-prone polymerases to extend past the lesion and NER to remove the crosslinked base. The unhooking reaction also generates a DSB intermediate that is processed by HR to restore the fork [34]. These complex steps of fork repair are coordinated by the ATR kinase, which stabilizes damaged replication forks.

ATR stabilizes stalled replication forks to prevent fork collapse

The fork stabilization activity of ATR is functionally defined either in terms of the ability to restart replication once a blockage is removed or by the changes in DNA or protein composition at the fork. Yeast mutants deficient in the ATR pathway lose the replicative polymerases from the fork [35-37] and accumulate abnormal DNA structures including long stretches of ssDNA and reversed fork structures [38, 39]. Polymerase epsilon is lost from replicating chromatin in *Xenopus* egg extracts when ATR is depleted. This results in replication fork collapse into a DSB [40]. Therefore, ATR may promote genome integrity by stabilizing replisomes and limiting nucleolytic processing of replication forks.

In addition, other replication fork proteins including RPA, CLASPIN, and members of the replication fork pausing complex like TIMELESS, TIPIN, and AND1 are ATR substrates [41]. Deficiencies in these proteins cause hypersensitivity to replication stress agents [42-45]. The significance of the DDR

to replication stress is highlighted by the fact that numerous ATR substrates are mutated in human diseases [46].

ATR directly targets several repair enzymes that remodel damaged forks including WRN, FANCM, and SMARCAL1. The WRN helicase and FANCM translocase proteins can unwind a variety of complex DNA structures. SMARCAL1 is a SNF2 family ATPase that is activated by complex DNA structures and uses the energy of ATP hydrolysis to re-anneal DNA strands and branch migrate model fork structures [47, 48]. RPA directly influences these SMARCAL1-dependent fork remodeling activities. For example, when damage is encountered on the leading strand, RPA stimulates regression of the replication fork into a complex chicken foot structure that may be a necessary intermediate structure for repair of forks [48]. The presence of RPA subsequently promotes restoration of the chicken foot structure into a normal fork structure containing a gap on the lagging strand. These mechanisms are essential to promote the accurate repair of damaged replication forks and provide valuable insights into how the ATR pathway maintains fork stability.

Unfortunately, such studies provide only glimpses of the numerous proteins implicated in replication fork stability, replication-associated DNA repair and fork restart. Identifying the proteins implicated in these functions has been difficult due to the inability to purify stalled and damaged replication forks from mammalian systems. How ATR maintains genome stability at stalled replication forks is explored in this thesis.

Studying genome and epigenome maintenance at replication forks

Overall, the response and repair of damaged replication forks remains poorly understood in comparison with the response to double-strand breaks (DSBs). Several investigators have used site specific DSBs combined with chromatin immunoprecipitation (ChIP) to examine proteins localizing to breaks with high resolution [49-52]. These studies have revealed that chromatin surrounding a DSB is extensively modified, that nucleosomes are destabilized, chromatin is remodeled, and histones are modified with post-translational marks [53-56]. These changes increase access to the repair machinery and recruit proteins involved in repair and DDR signaling. The extent to which chromatin changes at a stalled fork mimic those at a DSB is unknown because site-specific analyses of active and stalled replisomes have not been achieved in mammalian systems.

Thesis project

My thesis project has focused on gaining insights into how the genome and epigenome are inherited during DNA replication. Specifically, the spatial and temporal regulation of replication-coupled chromatin assembly and maturation have been poorly understood due to the technical limitations of studying elongating replication forks *in vivo* in mammalian cells. Additionally, how stalled replication forks transition to a state of irreversible collapse has been unclear.

To address these questions, in Chapter III, I describe the development of the iPOND (isolation of proteins on nascent DNA) methodology for studies of the dynamic mechanisms at replication forks. In Chapter IV, I used iPOND to examine the changes that accompany chromatin deposition and maturation following DNA synthesis. I also defined the timing and several genetic requirements involved in switching from a stalled to a collapsed replication fork. In Chapter V, I coupled iPOND to proteomics approaches to demonstrate the capacity of iPOND-MS as a discovery technology for studies of the mechanisms that preserve normal, stalled and collapsed replication forks. In Chapter VI, I further discuss the implications of my findings for comprehending how the genome and epigenome are inherited during DNA replication and following DNA damage. Overall, my thesis findings are significant for understanding the dynamic processes coordinated at replication forks and furthermore provide a tool for studying genomic and epigenomic instability, which are hallmarks of human diseases such as cancer.

CHAPTER II

MATERIALS AND METHODS*

Cell culture

HEK293T cells were cultured in DMEM supplemented with 7.5% FBS and maintained at 37°C and 5% CO_2. Stable cell lines expressing POLE2-HA and POLE3-HA were generated by retroviral infection and selection in puromycin-containing medium. HAT1-/- and HAT1+/+ MEF cells were cultured in DMEM supplemented with 15% FBS. HEK293T suspension cells were cultured in Freestyle medium (Invitrogen) supplemented with 1%FBS, 1% glutamine and 1% penicillin/streptomycin and maintained at 37°C, 5% CO_2, 80 humidity setting, and spinning at 130rpm in a shaking incubator.

Plasmid constructs

POLE2-HA and POLE3-HA retroviral vectors were generated by gateway cloning. pENTR POLE2 and pENTR POLE3 were recombined with pLPCX-GW-HA3X (pDC1127) to generate a C-terminal HA-tagged POLE2 and POLE3 retroviral vectors. pDC1127 was created by subcloning a 3XHA epitope into pLPCX between the Not1 and Cla1 restriction sites, then subcloning the gateway cassette containing attR1, ccdB gene, and attR2 as an EcoRV fragment between EcoR1 and Not1 sites.

*This Chapter contains the iPOND protocol from reference [57] and experimental details from reference [1].

Antibodies

Antibody incubations were performed in 1% milk in TBST buffer for 1-2 hours at room temperature for all of the following antibodies

Table 2.1. Antibody list and dilutions.

Protein	Source	Catalog Number	Dilution
CAF1/p60	Bethyl Laboratories	A301-085A	1:1,000
H1	Millipore	05-457	1 to 200
H2A	Abcam	ab18255	1:1,000
H2AX	Bethyl Laboratories	A300-082A	1:1,000
H2B	Abcam	ab1790	1:5,000
H3	Abcam	ab46765	1:5,000
H4	Abcam	ab31830	1:1,000
H4K12ac	Active Motif	39166	1:2,000
H4K20me1	Active Motif	39176	1:1,000
H4K5ac	Abcam	ab51997	1:1,000
HA.11	Covance	MMS-101P	1:1,000
HDAC1	Abcam	ab7028	1 to 500
HDAC2	Abcam	ab7029	1 to 500
HDAC3	Abcam	ab16047	1 to 500
KU70	Abcam	ab3114	1 to 500
KU80	Abcam	ab33242	1 to 500
MRE11 (12D7)	GeneTex, Inc.	GTX70212	1 to 500
PCNA	Santa Cruz Biotechnology	SC-56	1 to 200
pRPA S33	Bethyl Laboratories	A300-246A	1:1,000
pRPA32 S4/S8	Bethyl Laboratories	A300-245A	1:1,000
pSMC1 S966	Bethyl Laboratories	A300-050A	1:1,000
RAD51	Santa Cruz Biotechnology	SC-8349	1 to 200
RPA32	Bethyl Laboratories	A300-244A	1:1,000
SMARCA1/SNF2L	Cell Signaling	9450	1 to 500
SMARCA5/SNF2H	Abcam	ab3749	1 to 500
yH2AX (S139), clone JBW302	Upstate Biotechnology	05-636	1:1,000

iPOND materials

The following materials were used for iPOND experiments:

EdU (Invitrogen, cat. no. E10187 to be used at 10 μM or synthesized at Vanderbilt Core to be used at 12 μM); thymidine (Sigma, cat. no. T1895); formaldehyde solution (37% (wt/vol); Sigma, cat. no. F1635); PBS, pH 7.2 (10x; Gibco, cat. no. 70013); glycine (Fisher, cat. no. BP 381); cell lifter (Corning, cat. no. 3008); Triton X-100 (Sigma, cat. no. T8787); BSA (Sigma, cat. no. A7030); dimethyl sulfoxide (DMSO; Fisher, cat. no. A4034); copper (II) sulfate pentahydrate (CuSO4·5H2O; Fisher, cat. no. C489); (+) sodium l-ascorbate (Sigma, cat. no. A4034); biotin azide (Invitrogen, cat. no. B10184, photocleavable biotin azide synthesized in Professor Ned Porter's laboratory at Vanderbilt, or TEV cleavable biotin azide synthesized in Vanderbilt Sythesis Core); SDS (Sigma, cat. no. L4390); Tris, pH 8.0 and 6.7; sodium chloride (NaCl); RNase A solution (Sigma, cat. no. R6148); proteinase K (Sigma, cat. no. P5568); glycerol; bromophenol blue; EDTA; agarose (Bio-Rad Laboratories, cat. no. 161-3101); dithioerythritol (DTT; Sigma, cat. no. D-8255); aprotinin (Sigma, cat. no. A6279); leupeptin (Sigma, cat. no. L2884); streptavidin agarose (Novagen, cat. no. 69203-3); magnetic streptavidin beads used for iPOND-MS (Novagen, cat. no. 21344); trichloroacetic acid (TCA); acetone; Western Lightning Plus enhanced chemilluminescence substrate; Igepal CA-630; Odyssey infrared imaging system (Li-Cor Biosciences); click reaction stock solutions (biotin azide, CuSO4 and sodium l-ascorbate; see below for iPOND reagent setup).

iPOND equipment

The following equipment was used for iPOND experiments:

Nylon mesh (90 µm; Small Parts, cat. no. B000FN0PGQ); glass vial screw thread with cap attached for UV photocleavage (Fisher, cat. no. 03-338AA); magnetic micro-stirring bar (2 mm diameter x 7 mm length; Fisher, cat. no. 1451363); microtip sonicator for cell lysis and chromatin fragmentation (Misonix 4000 or Fisher Scientific Sonic Dismembrator, model 500); rotating platform for biotin captures; UV lamp (UVP, cat. no. UVLMS-38 EL Series 3UV lamp, 365/302/254 nm UV 8 Watt); magnetic stir plate; microcentrifuge for 1.5-ml microcentrifuge tubes; tabletop centrifuge for 15-ml and 50-ml conical tubes

iPOND reagent setup

The reagents for iPOND were prepared as follows:

EdU: Dissolve EdU in DMSO to obtain a final concentration of 10 mM. Protect from light. Store in aliquots at – 20 °C for up to 1 year. Before use, thaw at 37 °C. To EdU-label cells, pipette 1:1,000 of EdU directly into medium for a final concentration of 10 µM.

Thymidine: Dissolve in water to a final concentration of 10 mM. Store in aliquots at –20 °C for up to 1 year. Thaw the solution before use. Use at a final concentration of 10 µM.

PBS, 1x: Prepare 1x PBS from 10• PBS stock by diluting 1:10 with water; store at room temperature (RT, 25 °C) for up to 1 year.

Formaldehyde/PBS, 1% (wt/vol): Dilute 37% (wt/vol) formaldehyde 1:37 with PBS. Freshly prepare this reagent and keep it at RT until cell fixation (see detailed iPOND procedure, Step 12).

Glycine, 1.25 M: Prepare 1.25 M glycine stock in water and store at RT for up to 1 year. Use at 1:10 dilution for a final concentration of 0.125 M glycine.

Permeabilization buffer: Prepare a 20% (vol/vol) stock of Triton X-100 in water and keep it at RT. Dilute to 0.25% (vol/vol) Triton X-100 in PBS. Store at 4 °C for several months.

BSA in PBS wash buffer, 0.5% (wt/vol): Prepare 0.5% (wt/vol) BSA in PBS. Filter-sterilize the solution and store it at 4 °C for a couple of weeks.

Biotin azide (1 mM): Dissolve biotin azide in DMSO to a final concentration of 1 mM. Aliquot and store at – 20 °C for up to 1 year.

CuSO4 (100 mM): Prepare a stock of 100 mM CuSO4 in H2O; store at RT for several months.

Sodium l-ascorbate: Freshly prepare 20 mg/ ml of (+) sodium l-ascorbate (reducing agent) in H2O; limit exposure to air and store on ice until needed.

Click reaction mixes: To prepare click reaction cocktails, please see **Table 2.1** for details. Cocktails are freshly prepared for each experiment before the click reaction (see detailed iPOND procedure, Step 28).

Lysis buffer: Prepare 1% (wt/vol) SDS in 50 mM Tris (pH 8.0). Store at RT for several months. Before use, add protease inhibitors aprotinin and leupeptin to a final concentration of 1 μg ml – 1.

Salt wash: Prepare 5 M NaCl in water. Dilute to 1 M NaCl with water before use. Store at RT for 1 year.

SDS Laemmli sample buffer (2xSB): Mix 0.4 g of SDS, 2 ml of 100% glycerol, 1.25 ml of 1 M Tris (pH 6.8), and 0.01 g of bromophenol blue in 8 ml of H2O. Store at – 20 °C for up to 1 year. Before use, add 1 M DTT to a final concentration of 0.2 M.

Cross-link reversal solution: Mix 2 µl of 0.5 M EDTA, 4 µl of 1 M Tris (pH 6.7) and 1 µl of Proteinase K. Freshly prepare this solution. Prepare sufficient cross-link reversal solution mix to add 7 µl to each sample (in step 8 of Crosslink reversal and DNA analysis).

Cell lysis buffer: Mix 10 mM Tris (pH 8.0), 2 mM MgCl2 and 1% (vol/vol) Igepal CA-630. Before use, add protease inhibitors aprotinin and leupeptin to a final concentration of 1 µg ml – 1. Freshly prepare this buffer.

Nuclei buffer: Mix 15 mM Tris (pH 8.0), 0.125 M sucrose, 15 mM NaCl, 40 mM KCl, 0.5 mM spermidine and 0.15 M spermine. Freshly prepare this buffer.

Extraction buffer: Mix 1x PBS with 350 mM NaCl, 2 mM EDTA and 0.1% (vol/vol) Triton X-100. Freshly prepare this buffer.

Detailed iPOND Procedure

Below is the detailed iPOND protocol that includes **CRITICAL STEPS,** PAUSE POINTS and a **TROUBLESHOOTING** guide provided in table format that addresses the most pertinent issues encountered in the iPOND procedure [57].

Cell culture preparation ● TIMING 1–7 d

1l Calculate the number of dishes of cells needed for the experiment. Each sample requires at least 1.0 x10^8 cells at the time of the EdU pulse. I typically use three 150 mm dishes of HEK293T cells per sample. The number of cells may need to be increased depending on the application and cell type.

2l Expand cell cultures 1 d before EdU incubation (Step 3) to ensure that the cells are growing optimally. Include one extra dish of cells for counting the cell number in Step 3.

□ **CRITICAL STEP** For HEK293T cells, the experiment works best when cell confluence is between 4 and 6 x10^7cells per dish on the day of the EdU pulse. Cells must be in log phase of growth and should not be overgrown. Monitor proper incubator temperature and CO_2 content. EdU incorporation is not maximal unless these crucial parameters are met. If you are performing chases, equilibrate the medium to 37 °C and the proper CO_2 content overnight.

EdU labeling of nascent DNA● TIMING 10 min–8 h

3l Determine the cell number in the extra dish of cells from Step 2. This cell number will be used to calculate the amount of the reagents used for each sample in Step 29.

4l Plan out times to pulse, chase, fix, quench, collect and wash the samples.

□ **CRITICAL STEP** Stagger the samples to ensure that each is treated equally throughout the processing steps.

5l To pulse cells with EdU, remove the dishes from the incubator and place them in a biological safety cabinet.

6l Add 23 µl of the 10 mM EdU stock into 23 ml of cell culture medium in each dish to achieve a final EdU concentration of 10 µM. Return the dishes to the incubator for the desired pulse time (e.g., 10 min).

7l If thymidine chases or drug treatments are not being performed, skip to Step 11.

8l To perform thymidine chase or addition of drug, remove the dishes from the incubator and decant the medium.

9l Carefully wash the cells with 5 ml of chase medium and decant. The chase medium should have been pre-equilibrated to 37 °C and the proper CO_2 content.

10l Add 20 ml of chase medium containing 10 µM thymidine or the desired concentration of DNA damaging drug. Return the dishes to the incubator for the desired length of time.

□ **CRITICAL STEP** It is important to perform Steps 5–10 as quickly as possible to prevent pH and temperature changes in the medium, which can affect replication rates.

Formaldehyde cross-linking and collection of cells ● TIMING 1 h

11l After EdU pulse and/or chase, decant the medium.

12l Immediately fix the cells on a dish by adding 10 ml of 1% (wt/vol) formaldehyde in PBS and incubating for 20 min at RT.

13l Quench cross-linking by adding 1 ml of 1.25 M glycine.

14l Collect the sample by scraping with a cell lifter and transfer it to a 50-ml conical tube. Note the volume. This is the same volume that should be used for PBS washes in Step 17.

15l Centrifuge for 5 min at 900*g*, 4 °C.

16l Decant the supernatant.

17l Wash pellets three times with 1x PBS and centrifuge for 5 min at 900*g*, 4 °C. PBS wash volume is same as fixation volume noted in Step 14. Vortex to resuspend pellets in PBS.

18l After the last wash, decant PBS.

 PAUSE POINT The samples can be flash-frozen and stored at – 80 °C for several weeks.

Cell permeabilization ● TIMING 1 h

19l Resuspend the cells in permeabilization buffer at a concentration of 1 x10^7 cells per ml.

20l Incubate the cells at RT for 30 min. During incubation, thaw and prepare the reagents necessary for the click reaction cocktail (see Steps 28 and 29).

21l Spin down for 5 min at 900*g*, 4 °C.

22l Carefully decant the supernatant.

23l Wash the cells once with cold 0.5% (wt/vol) BSA in PBS, using the same volume as used for permeabilization in Step 19.

CRITICAL STEP BSA prevents the cell pellet from detaching from the wall of a 50-ml conical flask. A loose pellet will lead to the loss of cells in this step.

24l Centrifuge the cells for 5 min at 900*g*, 4 °C, and then decant the supernatant.

TROUBLESHOOTING

25l Wash the cells once with PBS using the same volume as used for permeabilization in Step 19.

26l Spin down for 5 min at 900*g*, 4 °C.

27l Decant the supernatant and place the pellets on ice while completing the preparation for the click reaction cocktail.

Click reaction ● TIMING 2 h

28l Thaw an aliquot of stock biotin azide by placing it on a 37 °C heat block.

CRITICAL STEP If you are using photocleavable biotin azide, keep the reagent protected from light and prepare the click reaction cocktail in the dark.

29l To calculate click reaction cocktail volumes, **Table 2.1** lists the amounts of each reagent needed per reaction with an example sample size of 1 x10^8 cells. The actual volumes should be adjusted on the basis of the cell number measured per sample (Step 3). Note that two click reaction cocktails need to be prepared: one for the control, which contains DMSO, and one for the experimental samples, which contains the biotin azide.

30l Combine the click reaction cocktail reagents on ice in the order listed in **Table 2.1**.

Table 2.1. Click reaction cocktails for a sample with 1 x 10^8 cells.

Reagent	[stock]	[final]	Control reaction volume (ml)	Experimental reaction volume (ml)
1×PBS			4.35	4.35
DMSO			0.05	
Biotin-azide	1mM	10μM		0.05
Sodium ascorbate	100mM	10mM	0.5	0.5
$CuSO_4$	100mM	2mM	0.1	0.1
Total Volume			5.0	5.0

31l Resuspend the cell pellets from Step 27 in the click reaction cocktail from Step 30 by vortexing.

32l Rotate the reactions at RT for 1–2 h.

33l Centrifuge the samples for 5 min at 900*g*, 4 °C, and decant the supernatants.

34l Wash the cells once with cold 0.5% (wt/vol) BSA in PBS, using the same volume as used in click reaction for one sample.

35l Centrifuge for 5 min at 900*g,* 4 °C and decant supernatant.

36l Wash the cells once with PBS, using the same volume as used in click reaction for one sample.

37l Decant the PBS and invert the tubes on a paper towel to remove all PBS.

 PAUSE POINT The samples can be flash-frozen and stored at – 80 °C for a few days.

Cell lysis and sonication ● TIMING 1 h

38l Prepare the lysis buffer by adding aprotinin and leupeptin before use (see REAGENT SETUP) and place on ice.

39l Resuspend the samples from Step 37 at a concentration of 1.5 x 10^7 cells per 100 µl of lysis buffer and transfer them to 1.5-ml centrifuge tubes on ice. To examine DNA fragment size at this step (see Crosslink reversal and DNA analysis).

40l Sonicate the cells by using a microtip sonicator and the following settings: pulse: 20 s constant pulse, 40 s pause; power: 13–16 Watts; repeat pulse 1x for every 200 µl of cell lysate; total pulse time: 4–5 min per sample.

□ **CRITICAL STEP** Lysates should appear translucent after sonication and not cloudy. Cloudiness is an indicator of an improper ratio of SDS to protein in the lysate or of insufficient sonication. Keep the samples on an ice slurry during sonication to prevent overheating.

TROUBLESHOOTING

41l Centrifuge the samples for 10 min at 16,100*g*, RT in a tabletop centrifuge.

□ **CRITICAL STEP** Lysate should appear clear after centrifugation. The presence of a white precipitate or a white film on top of the lysate is indicative of insufficient clearing of the lysate.

42l Filter the supernatant through a 90-µm nylon mesh into a new tube. Place the tube on ice.

43l Note the lysate volume.

44l To examine DNA fragment size at this step (see Cross-link reversal and DNA analysis).

45l Dilute the lysate 1:1 (vol/vol) with cold PBS containing 1 µg ml – 1 of aprotinin and leupeptin.

 CRITICAL STEP Samples have been diluted to contain 0.5% (wt/vol) SDS and 25 mM Tris because less efficient biotin capture is observed in lysates containing 1% (wt/vol) SDS.

46l Note the final capture volume.

47l Remove 15 µl of the lysate to save as the input sample for use in Step 64 and place it on ice. Immediately add 15 µl of 2x SB to this input sample and store at – 80 °C. The remaining lysate is used for the streptavidin capture, which is described below.

Streptavidin capture of biotin-tagged nascent DNA and associated proteins

● TIMING 16–20 h

48l To capture biotin-tagged nascent DNA, each sample from Step 47 is incubated with streptavidin-agarose beads at a concentration of 100 µl of bead slurry (50 µl packed volume) per $1x10^8$ cells. First, wash sufficient beads for all samples together by centrifuging the bead slurry at 1,800*g* for 1 min at RT.

49l Slowly and carefully aspirate the storage buffer from the beads.

50l Wash the beads twice with 1:1 (vol/vol) lysis buffer containing protease inhibitors.

51l Carefully and slowly aspirate the supernatant after each wash in Step 50.

52l Wash the beads once with 1:1 (vol/vol) PBS containing aprotinin and leupeptin; carefully aspirate the supernatant.

53l Resuspend the beads in 1:1 (vol/vol) PBS containing protease inhibitors.

54l Add an equal volume of beads to each sample from Step 47 with a pipette tip that is cut at the end.

55l Rotate the biotin captures in a cold room for 16–20 h (in the dark if photocleavable biotin azide is used).

56l Centrifuge the streptavidin-agarose beads with the captured DNA and associated proteins for 3 min at 1,800*g*, RT.

57l Very slowly and carefully aspirate most of the supernatant.

□ **CRITICAL STEP** The supernatant should be light blue/clear with no precipitate.

TROUBLESHOOTING

58l Add 1 ml of cold lysis buffer (no additives needed) to wash the beads.

59l Rotate at RT for 5 min.

60l Centrifuge for 1 min at 1,800*g* at RT and carefully aspirate and discard the supernatant.

61l Wash the beads once with 1 ml of 1 M NaCl.

62l Rotate and pellet the beads by repeating Steps 59 and 60.

63l Repeat the lysis buffer washes (Steps 58–60) two more times.

Elution of proteins bound to nascent DNA● TIMING 1–4 h

64l Protein elution can be performed using option A (boiling in 2x SB) or option B (UV photocleavage), depending on the amount of background observed in the negative control. Option B is best suited for proteins that show substantial background and require larger amounts of starting material for detection.

(Elution option A) Boiling in 2x SB

(i) After the last wash in Step 63, aspirate all of the supernatant. Protein-DNA complexes isolated on the beads are called the capture sample.

(ii) To elute proteins bound to nascent DNA, add 2x SB to packed beads from Step 64A(i) (1:1, vol/vol of packed beads; e.g., 100 µl 2xSB/100µl packed beads).

(iii) Incubate the capture sample from Step 64A(ii) and the input sample from Step 47 for 25 min at 95 °C to reverse cross-links.

□ **CRITICAL STEP** Typically, both the input and iPOND-purified capture samples should be examined concurrently.

(iv) Centrifuge the boiled samples for 1 min at 1,800*g*, RT. The supernatant is the '2x eluted capture' sample and is ready to use in standard SDS-PAGE and immunoblotting procedures (see Step 65).

(Elution option B) UV photocleavage, TCA concentration and boiling in 2x SB

(i) After the last wash in Step 63, wash one additional time with 1x PBS containing leupeptin and aprotinin as in Steps 59 and 60.

(ii) Centrifuge for 1 min at 1,800*g*, RT, and carefully aspirate the supernatant.

(iii) Add 1:1 (vol/vol) of 1x PBS containing protease inhibitors to the packed beads and resuspend by pipetting.

(iv) Transfer the resuspended beads into a glass vial with a mini magnetic stir bar.

(v) Place the glass vial containing the sample on a magnetic stir plate and adjust to stir on the lowest possible speed.

(vi) Position a UV lamp as close to the glass vial as possible. UV-photoelute at 365 nm for 2 h at RT.

(vii) Transfer the bead slurry from the glass vial into a 1.5-ml centrifuge tube.

(viii) Centrifuge the tube for 1 min at 1,800*g*, RT to pellet the beads.

(ix) Carefully remove the supernatant into a fresh tube. This is the 'UV-photoeluted capture' sample in PBS.

(x) Optionally, to concentrate the sample using TCA precipitation, proceed to the next step. Otherwise, add 1:1 (vol/vol) of 2x SB to the UV-photoeluted capture sample, boil at 95 °C for 25 min to reverse cross-links, and then proceed to analysis of proteins (Step 65).

(xi) Add ice-cold 100% TCA to the UV photoeluted capture sample from Step 64B(ix) to achieve a final concentration of 15% (vol/vol) TCA.

(xii) Incubate the sample on ice for 30 min.

(xiii) Centrifuge at 16,100*g* for 30 min in a cold room.

(xiv) Carefully remove the supernatant and save it for troubleshooting.

(xv) Wash the pellet with 1 ml of ice-cold acetone.

(xvi) Centrifuge for 10 min at 16,100*g* in cold room.

(xvii) Carefully remove the supernatant and save it for troubleshooting.

(xviii) Air-dry the pellet for 2–3 min until the smell of acetone is undetectable.

□ **CRITICAL STEP** If the pellet is not visible at this step, spin down the supernatant saved from Step 64B(xiv), and then repeat Step 64B(xv–xviii). If no pellet is observed, spin down the supernatant previously saved from Step 64B(xvii) and repeat Step 64B(xviii).

TROUBLESHOOTING

(xix) Add 30 µl of 2x SB to the protein pellet to resuspend the sample.

(xx) Incubate the capture sample (from Step 64B(x) if it is not TCA precipitated or from Step 64B(xix) if it is TCA precipitated) and the input sample (from Step 47) for 25 min at 95 °C. The samples are ready for use in standard SDS-PAGE and immunoblotting procedures.

Analysis of eluted proteins using western blotting ● TIMING 2–3 d

65l Prepare a standard SDS-PAGE gel [58]. To examine purification of positive controls concurrently (a replication protein and a histone, e.g., PCNA and H3, respectively), it is useful to prepare a 15% (wt/vol) gel.

66l To detect purified proteins from input and capture samples (from Step 64A(iv) or Step 64B(xx)), load the equivalent of 3 to 6 x 10^7 cells per well from the total protein capture (e.g., 3 to 6 x 10^7 of 1 x 10^8). This means that each sample of 1 x

10^8 cells yields sufficient sample for analysis of 2–3 immunoblots. For input samples, load the equivalent of 0.1% (vol/vol) input per well.

 CRITICAL STEP Depending on antibody quality, different proteins may require more cells for detection than others. This will require empirical determination.

67l Perform electrophoresis to resolve proteins on the basis of molecular weight, and then proceed with standard immunoblotting with desired antibodies according to supplier instructions or with MS analysis [59].

68l Proteins can be detected by using chemiluminescence (e.g., Western Lightning Plus) or quantitative immunoblotting with the Odyssey infrared imaging system.

Table 2.2. iPOND troubleshooting table.

Step	Problem	Reason	Solution
24	Poor cell recovery	The cells were not pelleted sufficiently during the centrifugation.	Increase the time or speed of the centrifugation. Be sure wash solution contains BSA.
40	Cell lysate is cloudy after sonication	Sonication did not completely lyse cells or SDS-protein complexes precipitate from solution.	Increase sonication times and be sure to avoid foaming of samples. Ensure the proper volume of lysis buffer was used in Step 39.
56	White precipitate layer observed above beads after centrifugation of biotin captures	Lipids from cell membranes were not properly pelleted after sonication	Make certain that lysate is clear after sonication and centrifugation. If white layer is observed on top of cell lysate, remove lysate, and clear again by centrifugation.
64, Elution Option B, xviii	No pellet is observed after air drying the TCA concentrated iPOND eluate	Sample was lost during TCA precipitation	Centrifuge the supernatant saved in Step xiv. Proceed with steps xv-xviii. If no pellet is observed, centrifuge supernatant previously saved in Step xvii. Continue with step xix.
68	High background signal in the control sample	Protein binds to streptavidin beads non-specifically.	Use elution option B, increase the number of washes in Steps 62-63.
68	Poor signal for control proteins like PCNA in the experimental sample	Poor EdU incorporation.	Increase the number of cells used in each sample and ensure the cells are growing well prior to experiment.
68	Poor detection of protein of interest in the input samples	Poor antibody or formaldehyde crosslinking interferes with epitope detection.	Optimize immunoblotting conditions or change antibody. Consider increasing the boiling time in Step 65Aiii or Step 65Bxx to completely reverse the formaldehyde crosslinks.

Crosslink reversal and DNA analysis

To examine DNA fragmentation size, cross-links are reversed from lysates collected before and after DNA sonication, bound proteins are digested, DNA fragments are separated on an agarose gel and analyzed under UV light.

1. Before sonication (iPOND protocol above Step 39), remove 5 µl of lysate and place it on ice. This is the presonication sample.

2. After sonication and sample filtration (Step 44), remove 5 µl of lysate and place it on ice. This represents the postsonication sample.

3. To all samples, add 90 µl of H2O and 4 µl of 5 M NaCl.

4. Incubate the samples at 65 °C for 4–16 h.

5. Add 1 µl of RNase A (20 mg/ ml) to each sample.

6. Incubate the samples in a 37 °C water bath for 30 min.

7. Prepare the cross-link reversal solution (see Reagent Setup).

8. Add 7 µl of cross-link reversal solution to each sample.

9. Incubate the samples at 45 °C for 1–2 h.

10. During the incubation time, pour a 1.5% (wt/vol) agarose/TAE gel without ethidium bromide.

11. Add DNA loading dye to 20 µl of sample and load it on a 1.5% (wt/vol) agarose gel.

12. Perform electrophoresis at 75 V for 3 h in 1x TAE buffer to resolve DNA fragments.

13. Stain the gel with ethidium bromide.

14. Visualize DNA fragments under UV light.

Native iPOND (developed by Jami Couch)

iPOND performed without formaldehyde cross-linking (native iPOND) may simplify mass spectrometry analyses of purified histones.

1. Culture 5 x 10^7 cells in one 150 mm dish per sample.

2. Label the samples with 10 μM EdU for 60 min.

3. Collect the cells by scraping on ice.

4. Collect the pellets by centrifuging at 100*g* for 5 min at 4 °C.

5. Discard the supernatant and wash the cells with 5 ml of ice-cold PBS. Collect the cells by centrifuging at 100*g* for 5 min at 4 °C.

6. Discard the supernatant and lyse the cells by resuspension in ice-cold cell lysis buffer with Igepal CA-630 at 1 x 10^7 cells per ml.

7. Vortex five times for 5 s with 5 s between pulses.

8. Collect nuclei by centrifugation at 100*g* for 5 min at 4 °C.

9. Discard the supernatant and wash twice in 5 ml cell lysis buffer without Igepal CA-630.

10. Collect nuclei by centrifugation at 100*g* for 5 min at 4 °C.

11. Discard the supernatant and resuspend the cells in ice-cold nuclei buffer at 2.5 x10^7cells per ml.

12. Set up click reactions using the formula in Table 2.1.

13. Incubate for 1 h on a shaker at 4 °C and protect from light.

14. Collect the nuclei by centrifugation at 100*g* for 5 min at 4 °C.

15. Discard the supernatant and resuspend in ice-cold nuclei buffer at 2 x 10^7 cells per ml.

16. Add EDTA to a final concentration of 1 mM and $CaCl_2$ to 2 mM.

17. Warm to 37 °C in a water bath and add micrococcal nuclease to 20 Kurntz units per 1 x 10^7 cells.

18. Incubate the cells at 37 °C for 3.5 min.

19. Add EDTA to a final concentration of 2 mM to quench the reactions. Collect nuclei by centrifugation at 100*g* for 5 min at 4 °C.

20. Extract chromatin by discarding the supernatant and resuspending the nuclei in ice-cold extraction buffer at 5 x 10^7 cells per 3 ml. Rotate for 2 h to overnight at 4 °C, protected from light.

21. Centrifuge at 16,100*g* for 5 min at 4 °C to remove all insoluble material. Transfer the supernatant to a fresh tube and discard the pellet.

22. Remove 0.5% of the total volume and save it as the 'input' sample. To the remaining lysate, add 20 µl of streptavidin-agarose beads per 1 x 10^7 cells. Rotate for 1.5 h to overnight at 4 °C, protected from light.

23. Collect the beads by centrifugation at 1,800*g* for 1 min. Let the beads stand for another min to settle completely. Aspirate and discard the supernatant.

24. Transfer the beads to a 1.5-ml centrifuge tube.

25. Wash the beads twice with 1 ml of extraction buffer for 5 min at 4 °C.

26. Add an equal volume of 2x SB and heat to 95 °C for 10 min.

27. Separate the recovered proteins with SDS-PAGE and analyze by immunoblotting or mass spectrometry.

iPOND methodology for adherent 293T cells

The iPOND protocol, experimental frameworks and treatments used in [1] and discussed in Chapters III and IV are described below.

HEK 293T cells (~1.5-3 x 10^8 cells per sample) were incubated with 12 μM EdU (Vanderbilt Synthesis Core). For pulse-chase experiments with thymidine (Sigma), EdU-labeled cells were washed once with temperature and pH-equilibrated medium containing 10 mM thymidine to remove the EdU, then chased into 10 μM thymidine. Other chemicals were added to the cell cultures at the following concentrations: HU (3 mM; Sigma), HAT inhibitor anacardic acid (30 mM; Enzo), HDAC inhibitor FK228 (100 nM; kindly provided by Dineo Khabele), Mre11 inhibitor Mirin (100 mM; Sigma), ATM inhibitor (KU55933, 10 mM; AstraZeneca), DNAPK inhibitor (KU57788, 1 mM; AstraZeneca), and caffeine (10 mM; ICN Biomedicals). DMSO was used as a vehicle control where appropriate.

After labeling, cells were cross-linked, quenched, washed, permeabilized, and washed as described in the detailed iPOND protocol above. For the click reaction, cells were incubated in click reaction buffer (Invitrogen) for 1–2 h at a concentration of 2-3 x 10^7 cells per milliliter of click reaction buffer. The click reaction buffer contains Invitrogen's Click-iT cell reaction buffer and cell buffer additive (C10269), 2mM copper (II) sulfate (CuSO4), and 1 mM photocleavable

biotin azide [60] (kindly provided by Ned Porter). DMSO was added instead of biotin-azide to the negative control samples (no clk in all figures). Cell pellets were washed once with 0.5% BSA/PBS and once with PBS.

Cell lysis, sonication, purifications using streptavidin-agarose beads (Novagen), washes, elution of nascent DNA bound proteins, crosslink reversal, SDS-PAGE and immunoblotting were performed as detailed in the iPOND protocol above. In most cases, quantitative immunoblotting was performed using the Odyssey infrared imaging system.

iPOND sample preparation for optimizations and iPOND-MS

The iPOND protocol used for proteomics approaches in Chapter III (iPOND-MS optimizations) and Chapter V (iPOND-MS screens) employed suspension 293T cells. The click reaction cocktail was reconstituted using PBS buffer and sodium ascorbate as detailed in the iPOND protocol above.

For iPOND-MS optimization experiments (Chapter III), UV photocleavage elution and TCA precipitation was performed as described in detail in the iPOND protocol above with the following modification. Purified proteins subjected to UV photocleavage were incubated at RT for 2 hours without magnetic stirring but with gentle mixing by hand every 30 mins. iPOND purifications performed using streptavidin-conjugated magnetic beads (Novagen, cat. no. 21344) were submitted to MudPIT analysis on a scale of $6x10^7$cells and purifications using

streptavidin-conjugated agarose beads (Novagen, cat. no. 69203-3) were submitted to MudPIT analyses on a scale of $4x10^7$cells.

The iPOND-MS screens (Chapter V) used suspension 293T cells logarithmically growing at $3.3x10^6$ cells per mL of 500ml cultures (total of $1.6x10^9$ cells) were pulsed with 12μM EdU (Vanderbilt Proteomics Core) for 15 mins. To collect cells for the 'no click' and elongating fork samples, formaldehyde was added to the suspension culture for 20 mins at a final concentration of 1% to halt cell processes, and crosslinking was quenched using glycine to a final concentration of 0.125M. For stalled and collapsed fork samples, EdU pulsed samples were chased into 3mM of HU by directly adding HU to EdU-containing cell cultures for 2 hours. In addition, the collapsed fork sample was co-treated with 3μM of ATR inhibitor (Vertex) [61, 62]. The thymidine chase sample was pulsed with EdU for 13 mins, cells were spun down at 1,000rpm for 4 mins, media was decanted carefully and cells were resuspended by pipetting using media equilibrated for temperature and pH (overnight) containing 10μM thymidine. The thymidine chase was conducted for 60 mins, cells were fixed with 1% formaldehyde for 20 mins at RT, and crosslinking was quenched for 5 mins at RT using a final glycine concentration of 0.125M.

Fixed samples were split evenly into 6 of 50ml conical tubes, spun down at 2,000rpm at 4°C for 6 mins, washed 3 times with 1x PBS at RT and frozen at -80°C. Five of the 6 tubes were independently processed on a scale of 2.7x10^8 cells per sample for iPOND purifications. The conditions for permeabilization,

click chemistry, cell lysis, sonication, 18 hour purifications using streptavidin-conjugated agarose beads (Novagen, cat. no. 69203-3) and washes are described in detail in the iPOND protocol above and detailed [57]. Purified replication fork proteins were eluted under reducing conditions by boiling in 2x sample buffer for 25 mins. The equivalent of $4x10^7$ cells per sample were resolved 1cm into on a 10% Novex precast gel (Invitrogen) for 5 mins. Gels were stained using Coomassie Blue (Invitrogen) and de-stained over-night according to manufacturer's standard instructions. The resolved proteins were excised from the gels at the Vanderbilt Proteomics Core, alkylated, and in-gel trypsin digested using standard procedures (performed by Hayes McDonald).

Multidimensional Protein Identification Technology (MudPIT) (performed by Hayes McDonald)

Recovered tryptic peptides were subjected to two-dimensional LC-MS/MS (MudPIT) separation as previously described [63] and [64]. Briefly, digested peptides were loaded onto a pre-column containing materials for reversed phase (RP) followed by strong cation exchange (SCX) separations. Peptides eluted from the SCX using seven 10 min salt pulses of increasing concentrations were separated by an RP gradient, ionized into an LTQ-XL mass spectrometer (Thermo Fisher Scientific), and MS/MS spectra were collected.

Mass spectrometric data analysis (performed by Hayes McDonald)

The peptide spectral data was searched against the UniProt human protein database using the Myrimatch [65], Sequest [66], and Myrimatch and Sequest [67] database search engines. Protein groups were assembled using IDPicker, which uses parsimony to report the minimum number of confident protein identifications [68]. Matched peptides were filtered at a 5% peptide and protein false discovery rate and each protein required a minimum of 2 independent peptides for identification. Protein identifiers were converted to EntrezID unique identifiers using the UniProt ID mapping database [69] and the DAVID bioinformatics database [70, 71]. Unmapped identifiers were excluded from the final protein list reporting enriched proteins.

QuasiTel statistical analysis and protein enrichment filtering criteria

To determine fold enrichments of proteins relative to the negative controls, spectral count data was imported into the statistical software program QuasiTel [72] for pair-wise comparisons (performed by Hayes McDonald). QuasiTel applies a quasi-likelihood model to raw spectral count data and reports protein fold enrichment and statistical significance as a quasi p-value. Spectral count data is normalized for each MudPIT run using the total number of spectra reported for the run. The threshold for spectral counts was set at an average of 1 spectral count per 1 experimental sample. For example, when comparing the 5 replicates from the replication fork sample to the 5 replicates from the chromatin

chase sample, a minimum of 5 spectral counts was required in the replication fork sample for consideration in QuasiTel. Furthermore, to be considered a protein significantly enriched on nascent DNA, the filtering criteria required a minimum of 1.5-fold enrichment above both negative controls and a quasi p-value of less than or equal to 0.05.

These filtering criteria were applied to proteins identified using each of the three protein identification search types (Myrimatch plus Sequest, Myrimatch alone and Sequest alone). Therefore, 3 separate lists of enriched proteins were generated independently. The final lists reported in Tables 5.2, 5.3, and 5.4 represent the union of all 3 lists and contain all the proteins that passed the fold enrichment and p-value filtering criteria in at least 1 of the 3 lists. The tables report the median number derived for fold enrichment relative to the chromatin-bound negative control, p-value, and spectral counts.

Bioinformatics data analyses

Proteins identified at elongating, stalled and collapsed replication forks were classified based on gene ontology using ToppGene [73]. To display median fold enrichment relative to the chromatin chase control, median quasi p-value, and median spectral counts from the experimental sample were graphed using R (performed by Yaoyi Chen). Protein network modeling was performed using the GeneMANIA prediction server [74] and queried for physical interactions, functional pathways, and shared protein motifs.

Hypergeometric hypothesis testing of the significance of ATM/ATR substrates identified in the iPOND-MS screen was performed in R using the following command line: > phyper(18,700,20000-700,290, lower.tail=F). The values represent the following: 18 is the number of proteins identified at normal replication forks to be ATM/ATR substrates, according to reference [41] where over 700 ATM/ATR substrates were identified; 20,000 represents a conservative estimation of the total number of proteins in the human proteome [75]; 290 is the number of total proteins significantly enriched at normal, stalled and collapsed replication forks in the iPOND-MS screen.

Selected reaction monitoring (SRM) label-free quantitative MS (performed by David Friedman)

Sample preparation on a smaller scale was performed similarly to iPOND purifications detailed for MudPIT analyses. Three independent biological replicates were prepared in 200mL HEK 293T suspension cultures at a concentration of 3x $x10^6$ cells per ml. Five iPOND samples were processed using the experimental frameworks detailed in the MudPIT section above. Unscheduled runs were performed to examine the signal intensity and retention times for 60 proteins of interest by monitoring 3 transition states per peptide. Peak picking and signal intensity was performed using Skyline [76]. Signal intensities for each peptide were normalized to the sum of the intensities of the internal reference peptides.

DNA fiber labeling

Loss of function studies with SMARCA1 were performed using the following siRNAs (Dharmacon):

SMARCA1_1 target sequence GAAGAAACCAGUACGUGUA

SMARCA1_2 target sequence CAACGAGAAUGGUAUACAA

Briefly, U2OS cells were plated at $2x10^5$ cells and reverse transfected with 40pmol of siRNA using Dharmafect1 lipid reagent. Following 48 hours of knockdown, cells were pulse labeled for 20 mins with the nucleoside analog IdU (20μM), washed twice with pH and temperature equilibrated HBSS, pulsed with CldU (100μM), washed twice with HBSS, and collected with trypsin. Diluted and resuspended cells were lysed using spreading buffer (0.5% SDS, 200mM Tris-HCl pH 7.4, 50mM EDTA), fibers were spread by tilting slides at 15 degrees and fixed with methanol:acetic acid (3:1). For staining, slides were treated with 2.5M HCl, blocked with 10% goat serumin PBST (0.1% Triton), stained with rat monoclonal anti-BrdU antibody recognizing CldU and mouse anti-BrdU recognizing IdU. Secondary Alexa Fluor 594 and 488 antibodies were used to for fluorescent detection of fibers. Immunofluorescent images were captured using a Zeiss Axioplan microscope equipped with a Zeiss camera. To quantify fibers containing IdU (green) followed by CldU (red) tracks, immunofluorescent images captured from 2 independent slides per each sample were measured from 100 fibers per sample using the Axiovision software.

CHAPTER III

DEVELOPMENT OF iPOND (isolation of Proteins On Nascent DNA) TECHNIQUE*

Introduction

During S-phase, DNA replication and chromatin assembly are coordinated at the replication fork to duplicate the genome and epigenome rapidly and accurately. DNA template damage and other forms of replication stress challenge genetic stability and activate a DNA damage response [14]. This signaling pathway protects and repairs damaged replication forks to promote successful completion of chromosome replication and prevent diseases such as cancer [77].

To date, the main tool available for detecting protein accumulation at replication forks or damaged sites has primarily relied on immunofluorescence imaging. While a useful method, immunofluorescence imaging suffers from low resolution, poor sensitivity and a requirement for highly specific antibodies [52]. Other methods such as chromatin immunoprecipitation (ChIP) have limited applicability to mammalian cell replication because of difficulties in obtaining synchronous cultures and the lack of highly efficient, sequence-specified origins of replication [12]. Purification of replisome protein complexes through protein-protein interactions is useful to identify potential components, but it provides limited spatial information about protein localization.

*This Chapter contains the iPOND protocol from reference [57] and excerpts from reference [1].

To overcome these technical challenges, I developed iPOND (isolation of Proteins On Nascent DNA) [1, 57]. In this chapter, I describe the development of iPOND as a useful tool for purifying and monitoring replisome and chromatin assembly dynamics in mammalian cells. In addition, I describe several iPOND experimental frameworks useful for monitoring the recruitment of proteins to elongating and damaged replication forks with spatial and temporal resolution previously unachievable. This chapter provides evidence for the power of employing iPOND in studies of genome and epigenome inheritance during DNA replication.

Results

iPOND overview

The iPOND methodology enables the purification of proteins bound directly or indirectly to the nascent DNA at replication forks. The method relies on labeling short fragments of nascent DNA with EdU, a nucleoside analog of thymidine [78]. EdU contains an alkyne functional group that permits copper-catalyzed cycloaddition (click chemistry) [79] to a biotin azide to yield a stable covalent linkage (Fig. 3.1). This reaction effectively biotin tags the EdU-labeled nascent DNA. The cells are then fixed with formaldehyde, which serves to both stop DNA replication and cross-link protein-DNA complexes (Fig. 3.2). Some DNA fragmentation occurs during this step because of copper-catalyzed hydrolysis of the DNA [80]. Cells are then lysed in denaturing conditions and sonication completes the DNA fragmentation producing solubilized DNA-protein complexes. Streptavidin-coated beads purify the nascent, EdU-labeled DNA-protein complexes.

Next, the proteins are eluted from the complexes. For most applications, boiling in SDS sample buffer is sufficient to reverse cross-links and solubilize proteins after purification (Fig. 3.2, see elution option A discussed in Chapter II). However, this method also releases any proteins that bind to the bead matrix nonspecifically and does not release the DNA from the beads. The use of a cleavable biotin azide in the click reaction facilitates elution in milder conditions to improve specificity and recovery of the DNA (discussed in Chapter II).

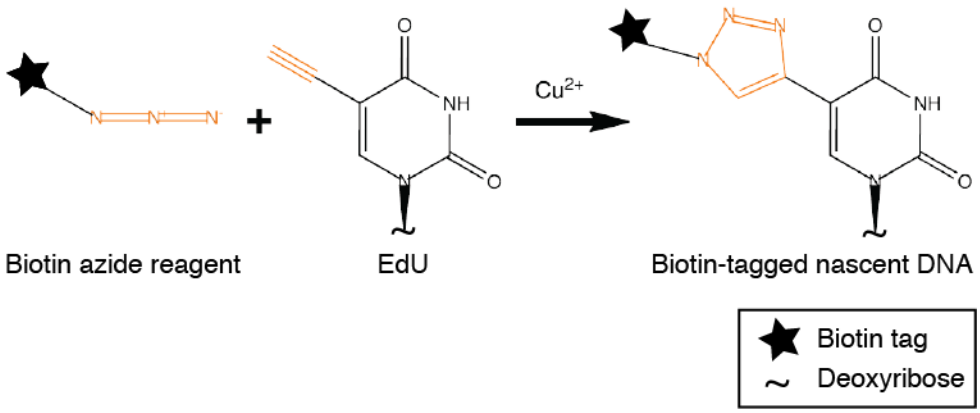

Figure 3.1. Click chemistry addition of biotin tags to nascent DNA. EdU incorporated into nascent DNA is covalently tagged with biotin in the copper-catalyzed click reaction. Orange color represents the azide (biotin-N3) and alkyne (EdU) functional groups involved in the click chemistry reaction.

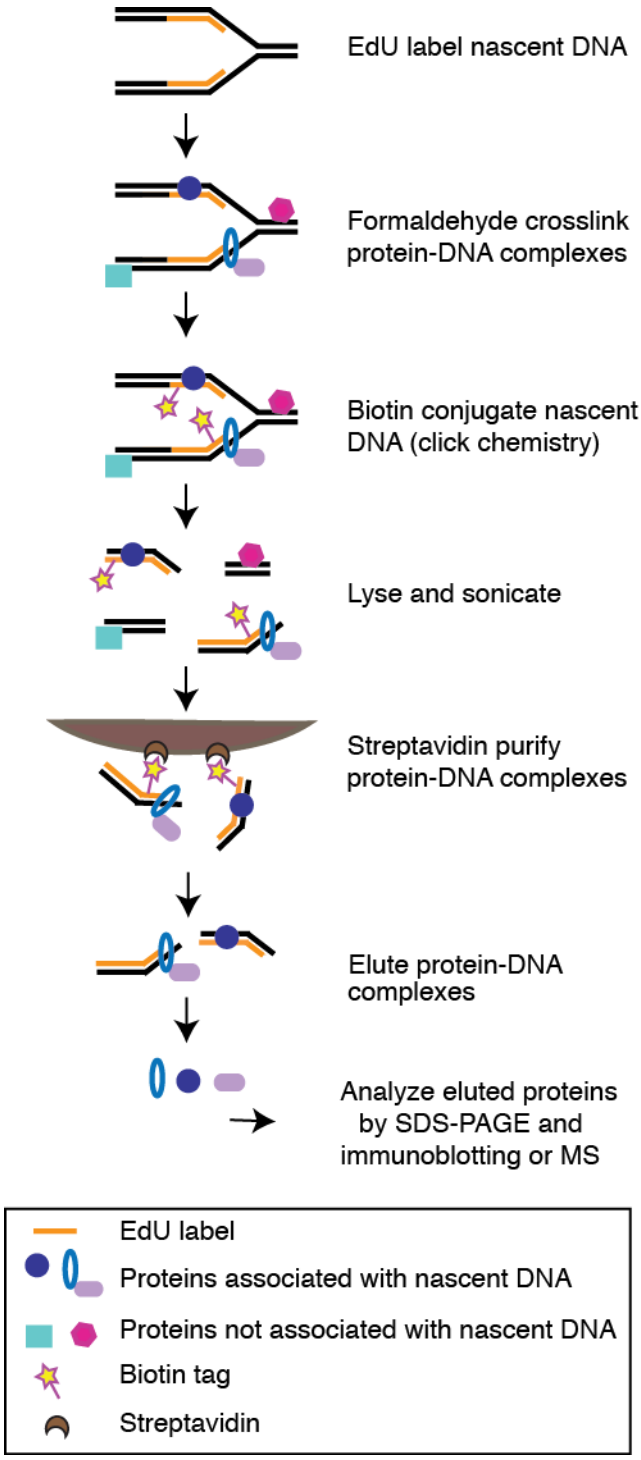

Figure 3.2. Schematic overview of the iPOND procedure. The iPOND procedure consists of pulsing cells with EdU to label nascent DNA *in vivo*, formaldehyde cross-linking protein-DNA complexes, covalently tagging EdU-labeled DNA with biotin by using click chemistry, lysing and sonicating cells, purifying the solubilized protein-DNA complexes and eluting bound proteins for analysis by SDS-PAGE, and immunoblotting or MS.

.

This elution option may be useful in experimental systems where biotinylation of endogenous proteins is a concern. Several cleavable biotin azides have been described and we have used a UV-photocleavable biotin-azide synthesized by Ned Porter's group at Vanderbilt [60, 81].

Lastly, to detect the purified proteins and post-translational modifications (PTMs) we can use standard immunoblotting or mass spectrometry (MS) methodologies. It may be beneficial to omit the formaldehyde cross-linking step, which may complicate proteomics analyses of proteins and particularly PTMs on lysine residues if the cross-links are not fully reversed. Jami FB Couch has adapted the iPOND protocol without cross-linking using the Igepal nondenaturing detergent in the lysis step and a reduced salt concentration in the wash steps (see Chapter II for native iPOND protocol developed by Jami FB Couch).

iPOND proof of concept

To validate the iPOND methodology, I first asked whether I could specifically detect replisome proteins on purified nascent DNA. I labeled cells with EdU for 10 mins, then performed iPOND. One important control to interpret iPOND results is analogous to the pre-immune control used in co-immunoprecipation experiments. To test whether detection of replication proteins is specific to the purification of nascent DNA, the biotin azide was omitted from the click reaction of one sample (Fig. 3.3B lane 3, labeled 'no clk'). No replication proteins were detected in this sample, indicating that protein-DNA complexes are

not purified in the absence of click chemistry (Fig. 3.3B, lane 3). An alternative control was a sample in which the cells were not incubated with EdU (Fig. 3.3C, labeled EdU min 0). If any protein were detected in the 'no click' negative control, it would represent nonspecific protein interactions with the streptavidin matrix.

In contrast, after covalent tagging of EdU-labeled nascent DNA with biotin using click chemistry, we detected proliferating cell nuclear antigen (PCNA), chromatin assembly factor 1 (CAF-1), replication protein A (RPA), and two subunits of polymerase epsilon (Fig. 3.3B). These results indicate that iPOND can purify replisome proteins, including those indirectly bound to DNA such as CAF-1 [4]. Furthermore, they indicate that iPOND is a sensitive methodology that detects proteins such as POLE2 and POLE3, which are replisome components expected to be at a density of only one or two molecules per replication fork. Thus, unlike immunofluorescence, iPOND does not require high concentrations of proteins within a small nuclear region to track protein localization. It should be noted that proteins such as GAPDH that are not affiliated with DNA replication are not detectable in iPOND captures (data not shown).

To ensure that a purified protein is enriched particularly at replication forks, a second control is essential. This is a sample in which EdU labeling of cells is followed by incubation with thymidine for several mins before sample collection (a chase sample). A true replisome protein that travels with the replication fork should be associated with DNA only before the thymidine chase

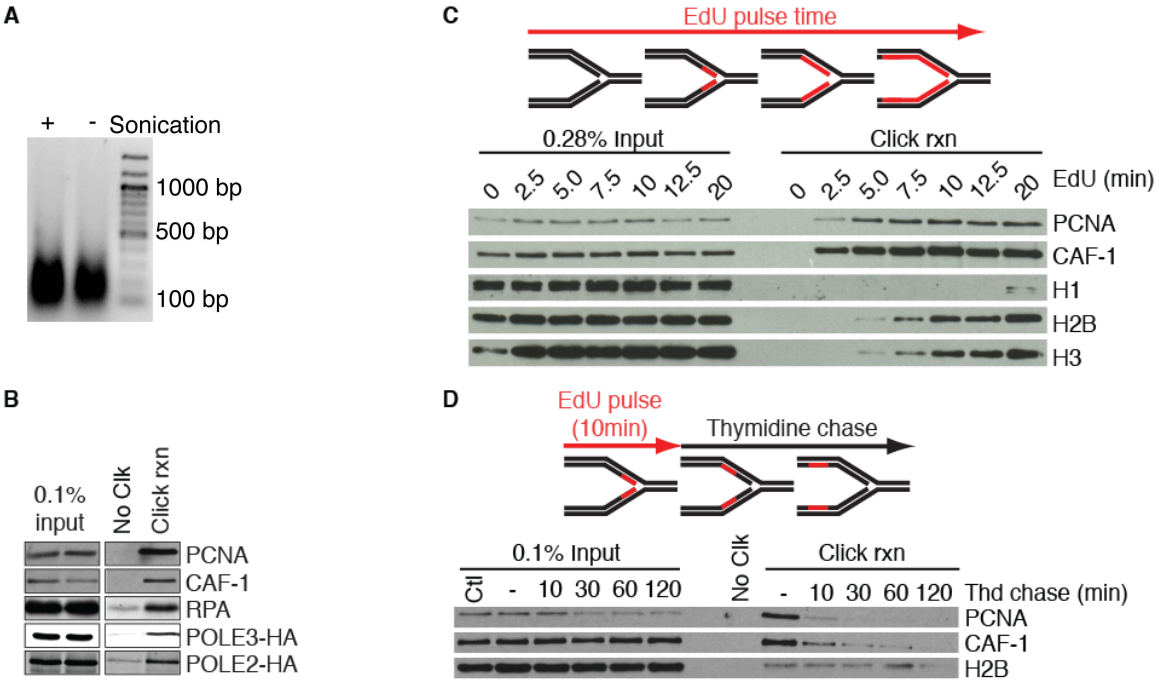

Figure 3.3. Development and proof-of-concept of the iPOND technology. (A) Average DNA fragments obtained before and after sonication of cell lysates used for iPOND purifications. (B) Cells were incubated with EdU for 10 mins prior to performing iPOND. Cells expressing POLE2-HA or POLE3-HA were used to detect these proteins with the HA antibody. (C) Cells were incubated in EdU-containing medium for increasing times prior to performing the iPOND protocol. (D) Cells were incubated with EdU for 10 mins. The EdU-containing medium was removed and cells were washed once before incubating for increasing times in medium containing 10 mM thymidine prior to performing iPOND. In all experiments, the No Clk control is the input sample in the first lane processed with no biotin-azide. Jami FB Couch performed the experiments in Fig. 3.3A and directed Jordan Feigerle in performing the experiment in Fig. 3.3B.

because the ‘chase’ fragment is located at a distance from the moving replication fork (Fig. 3.4A). In contrast, other chromatin-bound proteins such as histones may be detected in both samples because they are not specifically part of the replisome.

Such an experimental pulse-chase framework was used to monitor nascent DNA-associated proteins at greater and greater distances from the moving fork. Cells were labeled with EdU, and then chased into thymidine for increasing amounts of time (Fig. 3.3D). In these experiments, histone levels remain constant, indicating that the procedure effectively captures a maturing chromatin segment of constant length. However, the replication fork proteins PCNA and CAF-1 levels purified with the EdU-labeled segment decline rapidly following the thymidine chase (Fig. 3.3D). These data indicate that iPOND isolates chromatin-associated proteins specifically located at the replication fork. Furthermore, this evidence suggests that PCNA and CAF-1 are rapidly unloaded and recycled once DNA synthesis of Okazaki fragments is completed on the lagging strand.

To test the minimum amount of EdU pulse time needed to detect replisome proteins, time-course experiments were performed with increasing EdU labeling times (Fig. 3.3C). PCNA and CAF-1 were detected after a 2.5-min pulse of EdU, histones H2B and H3 after 5 mins, and the linker histone H1 at 20 mins after EdU addition (Fig. 3.3C). It should be noted that interpreting differences in the signal intensities between different proteins is difficult since

different antibodies have varying antigen avidities. Nonetheless, the deposition of H1 on maturing chromatin is supported by independent iPOND proteomics screens [82] and previous fractionation data indicating that H1 is added 10-20 mins after DNA replication to create higher-order chromatin structures [82, 83]. Therefore, my analysis indicates that a 2.5-min incubation with EdU is sufficient to capture replisome proteins and that longer incubations with EdU are required to isolate newly deposited chromatin.

The spatial and temporal resolution achieved with iPOND depends on the size of the DNA fragments generated after cell lysis, the rate of DNA synthesis and the EdU pulse time. In practice, we consistently obtain DNA fragments of ~100-300 base pairs (bp) (Fig. 3.3A), meaning that the latter two parameters dictate iPOND resolution. In mammalian cells, the rate of DNA synthesis varies between 0.75 and 2.5 kb/min [84]. Thus, a 2.5-min EdU pulse labels ~ 2–6 kbp, although this is likely a significant overestimation, since EdU must enter the cell and be phosphorylated before incorporation into DNA. Therefore, iPOND resolution is currently on the order of a few thousand base pairs.

Experimental designs

Thus far, I have described the utility of iPOND for identifying proteins associated with active replisomes (Fig. 3.3) by combining iPOND within a pulse-chase experimental framework (Fig 3.4). This experimental design is also the method of choice for the second major iPOND application—monitoring changes in chromatin located at various distances from the replication fork.

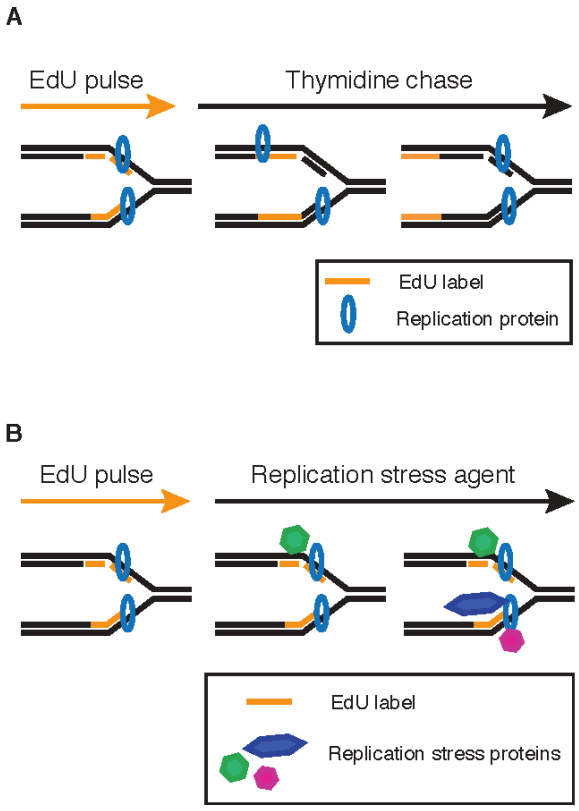

Figure 3.4. Schematic of the experimental designs used to identify replisome or DNA damage proteins and modifications at the replication fork. (A) To identify replisome proteins, a pulse-chase variation of the iPOND protocol uses a thymidine chase to move the nascent, EdU-labeled DNA segment away from the replication fork. The chase sample provides a control to distinguish replisome components from general chromatin-binding factors. (B) To study proteins and modifications associated with damaged replication forks, an agent that stalls replication forks, such as HU, is added after the EdU-labeling period.

Chromatin reassembly after passage of the replication fork occurs as a function of time and hence distance from the elongating fork [3]. iPOND can be used to purify histones on a segment of EdU-labeled DNA after various times of thymidine chase, which permits an analysis of how chromatin architecture is restored behind the elongating fork. In Chapter IV, I use this experimental design to document the timing of the deacetylation of newly synthesized histone H4 after deposition.

Additionally, iPOND can be used to detect protein recruitment or post-translational modifications of proteins at damaged forks. The procedure in this case is to pulse for a short time with EdU, then to add a replication stress agent such as hydroxyurea (HU) or camptothecin (Fig. 3.4B). HU is particularly useful as high concentrations largely stop fork movement, facilitating an analysis of transiently or persistently stalled forks (evidenced in Chapter IV). Combining the DNA damaging protocol with the pulse-chase procedure also enables an examination of DNA damage–dependent events at different distances from the damaged fork. In Chapter IV, an example of this procedure demonstrates the spreading of histone variant H2AX phosphorylation from an HU-stalled fork. Thus, the high spatial resolution of iPOND is derived from the capacity to measure the position of protein changes in relation to the replication fork.

Discussion

iPOND comparison to other methods

Compared with conventional indirect immunofluorescence, iPOND has an improved sensitivity of detection since even low-abundance replisome proteins such as polymerases are isolated (Fig. 3.3B). It also provides improved spatial and temporal resolution. Although an enhanced imaging technique permits single-molecule detection of replisome proteins in bacteria [85], unlike imaging, iPOND is compatible with unbiased approaches for protein identification such as MS.

ChIP is a powerful substitute for several iPOND capabilities in organisms such as *S. cerevisiae* that have highly efficient, sequence-defined origins of replication and cell cycle synchronization is easily achieved. ChIP has the advantage of being more sensitive than iPOND as it detects DNA sequences after PCR amplification. However, ChIP requires highly specific, often unavailable antibodies and is not compatible with unbiased approaches such as MS. Moreover, although ChIP has been used in mammalian systems to examine protein recruitment to origins of replication [86], it is generally not useful for studying the dynamic processes associated with fork elongation and chromatin maturation. Finally, adapting ChIP to studying damaged replication forks in mammalian cell culture awaits the development of ways to engineer site-specific

DNA lesions that stall forks with high efficiency as has been done using *Xenopus* egg extracts to study interstrand cross-link repair [26, 27].

The most comparable technology to iPOND is the immunoprecipitation of nascent DNA-protein complexes with antibodies to halogenated nucleoside analogs, which was used to examine the recruitment of the homologous recombination factor RAD51 to sites of replication fork stalling [87]. However, the relatively low affinity of this antibody-epitope interaction and the requirement for DNA denaturation for antibody access necessitated a long chlorodeoxyuridine (CldU)-labeling period (40 min), providing little advantage over biochemical fractionation of chromatin. In principle, biotin-dUTP could be used directly to label the nascent DNA, thus avoiding the need to perform the click chemistry reaction. However, biotin-dUTP is not cell permeable, thus necessitating some cellular manipulation to introduce it into cells, and the large biotin tag may interfere with DNA structure and protein associations with DNA.

iPOND limitations and other considerations

Currently, the major limitation of iPOND is the large amount of starting material needed. Each sample requires approximately $1x10^8$ cells for efficient iPOND capture of replisome proteins with a 10 min EdU incubation. The large number of cells needed for the procedure is dictated by the sensitivity of the immunoblotting and MS detection methods. This cell number is based on unsynchronized cultures of 293T cells in which about 50% of the cells are in S-

phase at the time of the experiment. Synchronizing cells such that 100% are in S-phase would reduce the cells needed, whereas the use of cell types with fewer replicating cells would increase it. Although these cell numbers are large, they are obtainable by using standard cell culture methods.

iPOND is currently an ensemble methodology, meaning that the data comes from hundreds of replication forks in millions of cells. It provides a picture of an average replication fork and cannot distinguish the significant heterogeneity between cells in the population or between forks within different genomic regions. Thus, identification of two proteins by iPOND does not mean the two proteins are necessarily recruited to the same nascent DNA segment. Coupling iPOND to single molecule analyses (iPOND-SM) of endogenous or tagged proteins of interest would provide improved resolution to the technique. iPOND-SM could answer questions about the relative location of proteins on nascent or mature DNA. For example, at what distance away from the replisome does a nascent histone become a parental histone? A broad answer to this question can be gained with current iPOND techniques (explored in Chapter IV). However, dissecting out the molecule per molecule differences in progressing from new to old histone could be achievable using iPOND-SM (discussed further in Chapter VI).

Finally, iPOND resolution may be improved in a system in which EdU exists as the sole nucleoside to pair with adenosine. This could be achieved in a cellular system such as *Xenopus*, in which dNTPs are added in a controlled

manner for incorporation into nascent DNA. Such studies have been successfully employed to study sister chromatin cohesion, which is a replication-coupled process (Susannah Rankin, Oklahoma Medical Research Foundation, unpublished results).

iPOND applications (detailed further in Chapter VI)

The iPOND experimental designs described above could be quite powerful when combined with genetic or small molecule–mediated inactivation of specific pathways that regulate DNA replication, chromatin deposition and maturation, and DNA repair. iPOND is compatible with proliferating cell types and we have used it successfully in HEK293T, NIH3T3 and mouse embryonic fibroblasts (see MEF results in Chapter IV). Thus, cell lines engineered to have mutations in specific pathways can be used directly with iPOND without any major modifications to the protocol.

iPOND can also be extended for use beyond mammalian cell culture. Any cell type that can incorporate EdU during DNA synthesis (or be engineered to use EdU) can be used. In fact, we have used iPOND to purify DNA-protein complexes from the yeast *Saccharomyces cerevisiae*, although substantial optimization will be required to improve purification efficiency (Jami FB Couch, unpublished observations).

Furthermore, combining iPOND with quantitative MS should be a valuable methodology for identifying new replisome and DNA damage response proteins. This application (iPOND-MS) is the topic of Chapter V.

CHAPTER IV

ANALYZING PROTEIN DYNAMICS AT NORMAL, STALLED AND COLLAPSED REPLICATION FORKS*

Introduction

In the previous chapter, I described the rationale and development of iPOND as a biochemical method to purify replication forks and the associated proteins from mammalian cells. In this chapter, various iPOND experimental frameworks are used to examine the timing and spatial distribution of processes that maintain the epigenome and genome after replication fork passage and DNA damage.

One mechanism necessary for maintaining epigenetic inheritance through DNA replication involves the timely removal of histone marks present on nascent histones (predeposition marks). This process of 'chromatin maturation' is coupled to replication fork passage. In the first part of this chapter, I demonstrate that histone deacetylases remove the replication-coupled pre-deposition marks on histone H4, which are catalyzed by the HAT1 acetyltransferase.

In the second part of this chapter, how replication forks respond to DNA damage that slows fork progression is analyzed. Replication fork stalling causes changes in the recruitment and phosphorylation of proteins at the damaged forks.

*The majority of this chapter has been published in reference [1] and a portion has been published in reference [88].

We show that checkpoint kinases catalyze phosphorylation of the histone variant H2AX and this mark spreads from the stalled fork to encompass adjacent chromatin domains. A switch in the damage response occurs at persistently stalled forks leading to assembly of the RAD51 recombinase. This loading depends on DNA end resection. Collectively, this chapter establishes the utility of iPOND for analyzing epigenomic and genomic processes occurring at active, stalled, and collapsed replication forks.

Results

Analysis of DNA-replication coupled chromatin maturation

Maturation of the new chromatin requires addition and removal of histone post-translational modifications. Newly synthesized histone H4 imported from the cytosol is acetylated on two lysines (5 and12), and these evolutionarily conserved marks are removed after deposition [5, 89].

The B type histone acetyltransferase HAT1 has been assumed to catalyze the formation of H4K5ac/H4K12ac during chromatin assembly [90, 91]. This hypothesis has not been formally tested in the mammalian system due to the lack of genetic and biochemical tools. Mark Parthun's laboratory has recently constructed a conditional mouse knockout model of HAT1 (in press). I used iPOND pulse-chase experiments to examine the acetylation status of H4 on K5 and K12 following histone deposition at replication forks (Fig. 4.1). In HAT1 homozygous null MEFs, H4K5/K12 acetylation is absent from nascent chromatin. This suggests that HAT1 is the replication-coupled acetyltransferase that modifies H4K5/K12 in higher organisms (Fig. 4.1).

Following deposition of acetylated H4K5 (H4K5ac) and H4K12ac, time course experiments reveal that acetylated H4K5 is removed rapidly and H4K12ac deacetylation is slightly delayed (Fig. 4.2.A,B). The delay in K12 deacetylation could be due to the activity of chromatin-associated histone acetyltransferases that promote the acetylation of this site in some chromatin domains.

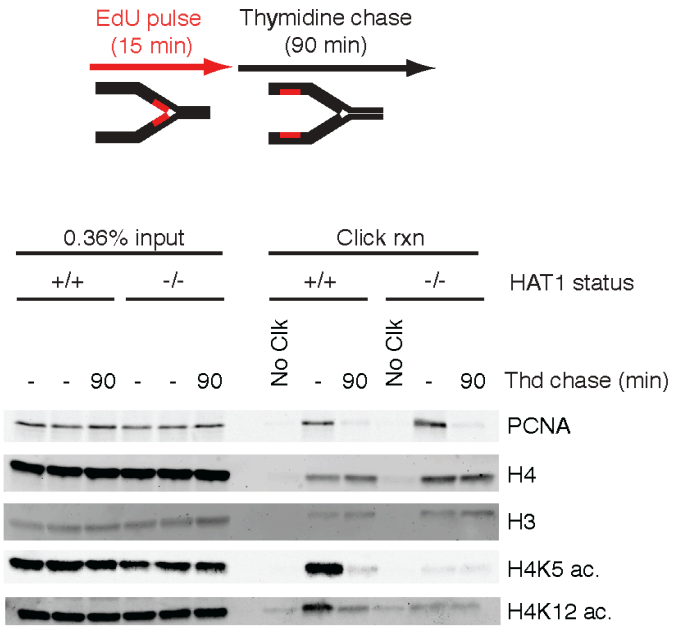

Figure 4.1. Hat1 is required for the acetylation of histone H4 deposited during replication-coupled chromatin assembly. Hat1+/+ and Hat1-/- MEFs were pulse-labeled with EdU for 15 mins and chased with thymidine for 90 mins as depicted in the experimental schematic. Proteins associated with nascent DNA were purified using iPOND and immunoblottted for the indicated proteins and histone post-translational marks. No clk represents the lack of biotin-azide in the click reaction that prevents biotin-tagging of nascent DNA.

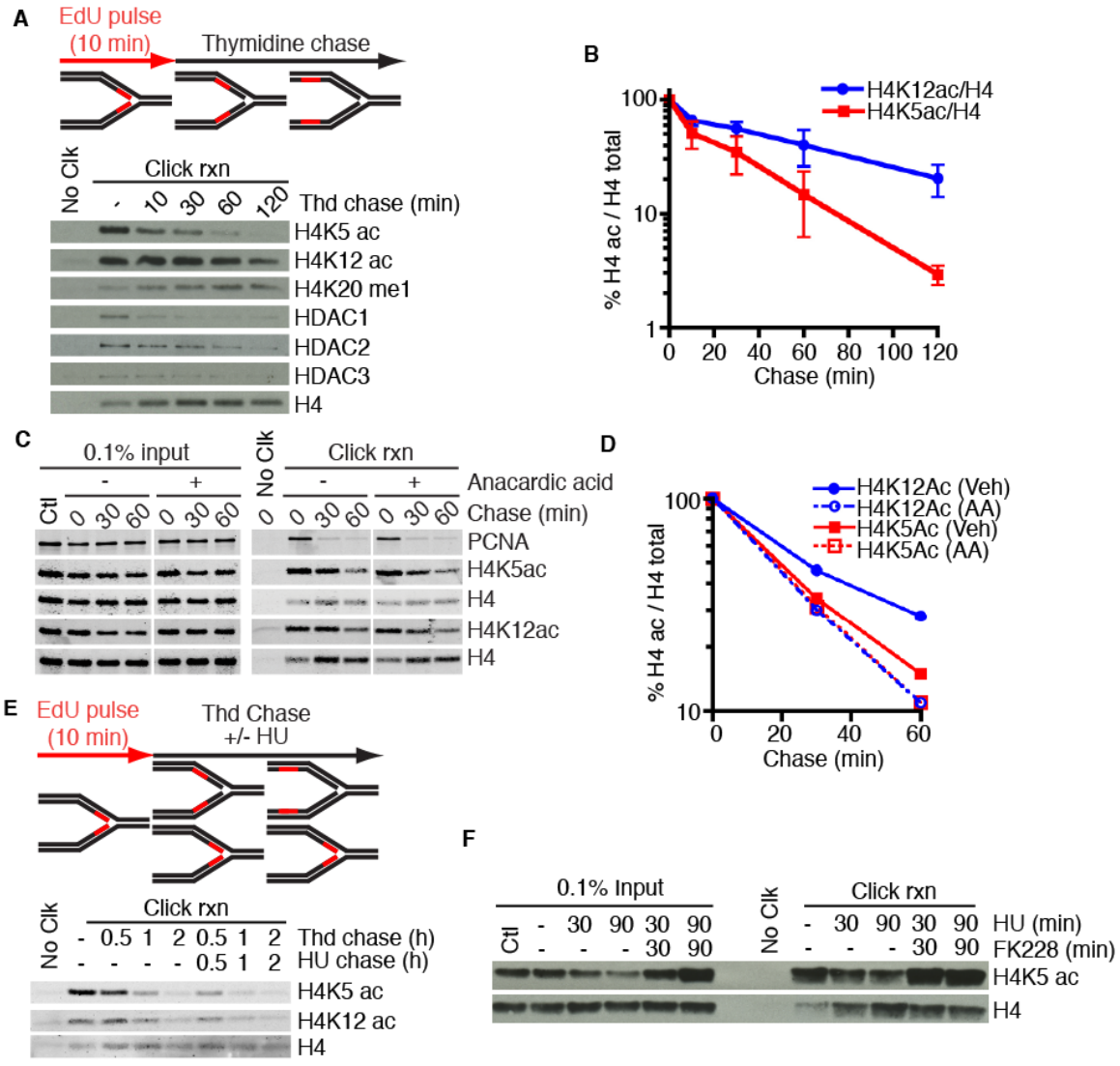

Figure 4.2. Deacetylation of newly deposited histone H4 depends on HDACs and is independent of replication fork movement. (A–E). Cells were labeled with EdU for 10 mins followed, by a chase into thymidine-containing medium for the indicated times prior to performing iPOND. (B) Quantitation of H4 acetylation levels compared with total H4 in the click reaction samples from three independent experiments. Error bars in all figures are standard deviations. (C,D) Anacardic acid (30 mM) was added to the indicated samples. (E) HU (3 mM) was added to the indicated samples. (F) Cells labeled with EdU were chased into 3 mM HU medium with or without 100 nM FK228 prior to performing iPOND. Experiments in panels C and D were performed by Jami FB Couch.

Indeed, in the presence of the nonselective HAT inhibitor anacardic acid, the rate of H4K12 deacetylation becomes identical to H4K5, with a half-life of <20 mins (Fig. 4.2C,D).

In principle, chromatin maturation—as measured by H4K5/K12 deacetylation—could be coupled to fork progression. To test this hypothesis, I used high concentrations of hydroxyurea (HU) to stall active replisomes and stop DNA synthesis. HU addition stalls the fork effectively in these cells, since the amount of histone capture does not increase appreciably during the HU treatment (Fig. 4.2E). Deacetylation of newly deposited H4 proceeds at the same rate regardless of whether DNA synthesis is inhibited. Thus, chromatin maturation can be uncoupled from replisome movement.

The histone deacetylase (HDAC) in human cells that catalyzes the deacetylation of H4K5 and K12 is unknown. HDAC1 and HDAC2 associate with CAF-1 [92], and HDAC3 is required—perhaps in late S phase or G2—to remove H4K5ac [93]. Indeed, in pulse-chase experiments, an enrichment of HDAC1, HDAC2, and HDAC3 is evident near the fork (Fig. 4.2A), and the selective class I HDAC inhibitor FK228 [94] prevented deacetylation of H4 (Fig. 4.2F), suggesting that all three of these HDACs are involved.

In addition to studying epigenetic events coordinated with ongoing DNA replication, iPOND permits the analysis of genome maintenance activities after damage encountered at replication forks. The next section analyzes replication forks that stall and eventually collapse after prolonged replication stress.

DDR response at stalled replication forks

HU treatment causes DDR activation to stabilize the stalled fork and induce a cell cycle checkpoint. Previous studies suggest that HU-stalled forks remain stable and competent to resume DNA synthesis for several hours; however, eventually, the stalled fork collapses and DSBs are formed [87].

To further examine this process, we monitored recruitment and modification of proteins at stalled forks. The amounts of PCNA and CAF-1 that are captured at the stalled fork decrease initially after adding HU to the medium, and then reach a steady state level of between 20% and 30% of that found at an elongating fork (Fig. 4.3A). This PCNA pattern is likely due to unloading of PCNA from the completed Okazaki fragments.

We detected RPA associated with the fork both before and after HU addition (Fig. 4.3A). The amount of RPA detected remained constant even though RPA accumulates at stalled forks [14]. This discrepancy is explained because RPA binds only to the single-stranded, template strand of DNA, which lacks incorporated EdU. Therefore, iPOND detects only the RPA immediately adjacent to the newly synthesized dsDNA (Fig. 4.3D).

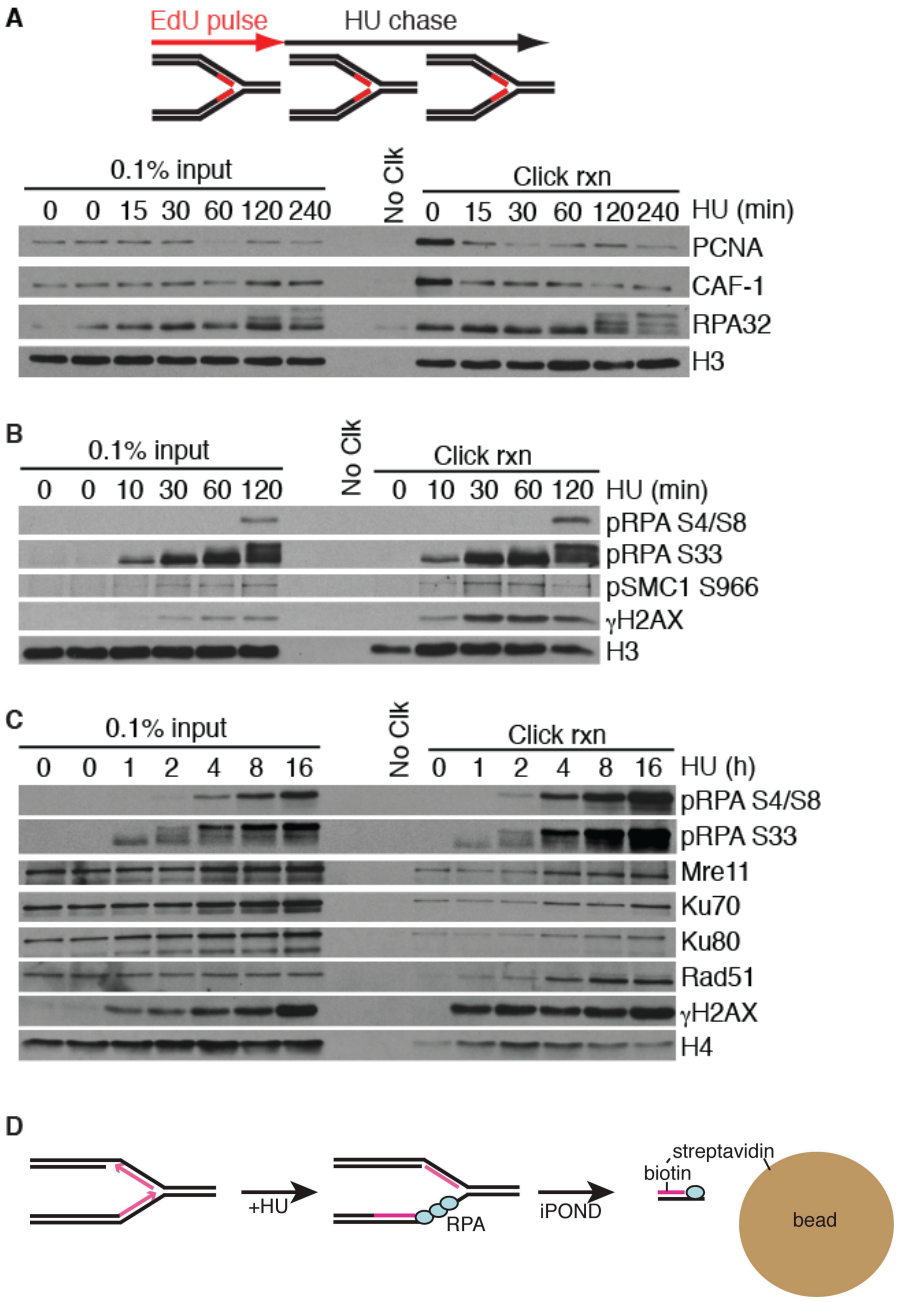

Figure 4.3. iPOND monitors post-translational modifications and recruitment of DDR proteins to stalled and collapsed replication forks. (A–D) Cells were labeled with EdU for 15 mins (A) or 10 mins (B–D), followed by a chase into HU for the indicated times prior to performing iPOND. (D) Diagram for iPOND isolation of RPA bound adjacent to ssDNA-dsDNA junction at stalled replication forks.

In time course experiments, I noticed that at 120 and 240 minutes after addition of HU, the electrophoretic mobility of RPA decreased, consistent with phosphorylation (Fig. 4.3A). RPA S33 phosphorylation could be detected within 10 minutes of HU addition, and S4/S8 phosphorylation appeared at 2 hours (Fig. 4.3B). DNA-PK catalyzes S4/S8 phosphorylation and ATR catalyzes S33 phosphorylation [95], suggesting that ATR phosphorylates RPA immediately after fork stalling, and DNA-PK phosphorylates RPA only at persistently stalled forks.

H2AX phosphorylation (γH2AX) is often considered a marker for DSBs [96]. However, I observed γH2AX at stalled replication forks at even the earliest time points (10 minutes) after HU addition (Fig. 4.3B), well before evidence of DSB formation [87]. These data prompted us to examine the timing of recruitment of DSB repair proteins. MRE11, KU70, and KU80 exhibited a recruitment profile in which low amounts were observable before the addition of HU, and remained unchanged for 2 hours after HU addition (Fig. 4.3C).

However, by 4 hours in HU, a significant increase was detected in all of these proteins near the stalled fork (Fig. 4.3C). RAD51 was first detectable after HU addition, but its levels also increased significantly by 4 hours, suggesting that DSBs may form between 2 and 4 hours after the fork is stalled. KU70 and KU80 may bind to some of the single-ended breaks, and RAD51 may bind to others. An additional interpretation is that RAD51-mediated recombination and fork regression occurs at some stalled replication forks [87]. It is likely that both DSBs and HR occur following prolonged exposures to replication stress.

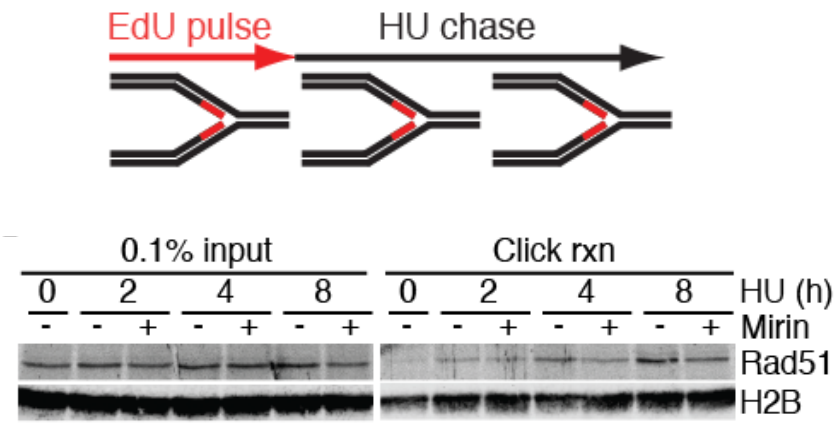

Figure 4.4. MRE11 promotes Rad51 accumulation at persistently stalled replication forks. EdU pulsed cells were treated with HU with or without the Mre11 inhibitor mirin (100 mM) as indicated. Experiment was performed by Jami FB Couch.

At DSBs, MRE11-dependent end resection is required to load RAD51 [97]. At collapsed forks, RAD51 may function to promote recombination-based methods to re-establish the replication fork [98]. To test whether the loading of RAD51 at stalled forks also requires MRE11, cells were treated with the MRE11 nuclease inhibitor mirin [99]. Although the early recruitment of RAD51 occurred independently of MRE11, later accumulation required MRE11 activity (Fig. 4.3D), suggesting that end resection promotes this loading. The timing of MRE11 recruitment also correlated with increased RPA S4/S8 phosphorylation (Fig. 4.3C), which was been previously linked to DNA end resection at camptothecin-damaged forks [100].

γH2AX *spreading from stalled forks before and after fork collapse*

I noticed that the rapid phosphorylation of H2AX near the fork saturates within 30 minutes; however, global levels (observed in inputs) continue to increase (Fig. 4.3B). One explanation for this observation is that the global increase stems from H2AX phosphorylation in regions adjacent to the stalled replication fork. This type of γH2AX spreading has been observed near DSBs where ATM promotes phosphorylation of H2AX immediately at the damage site and in chromatin surrounding the break to facilitate amplification of the DDR [101, 102].

To test the hypothesis that γH2AX spreads from stalled replication forks, cells were first labeled with EdU, then chased with thymidine for various lengths

of time to extend the distance between the EdU-labeled fragment and the fork, and finally added HU to stall the fork. We again observed maximum γH2AX at the fork 30 minutes after HU addition; however, the chromatin region distant from the fork contained low but detectable levels of γH2AX that increased when examined at 60 minutes after HU addition (Fig. 4.5A).

A more detailed analysis revealed that the density of γH2AX gradually declined as a function of distance from the stalled fork (Fig. 4.5B,C). Compared with the saturated density at the fork, the γH2AX density decreased approximately twofold for every 15 min of thymidine chase time when cells were treated with HU for 1 h. By 2 h, we observed increased γH2AX density in all chromatin segments analyzed, suggesting that γH2AX spreading contributes significantly to the global change in γH2AX levels.

To examine the chromatin at a single location distant from the fork, we repeated this experiment holding the thymidine chase time constant at 30 min, and treated with HU for varying times. We observed a steady increase in γH2AX at this distance from the fork (Fig. 4.5D). Importantly, these results indicate considerable spreading of the γH2AX signal even shortly after fork stalling. Assuming a conservative rate of fork elongation of 1 kb/min, these data imply that, within 1 h of fork stalling, γH2AX spreads to include a large domain containing tens of thousands of base pairs of DNA.

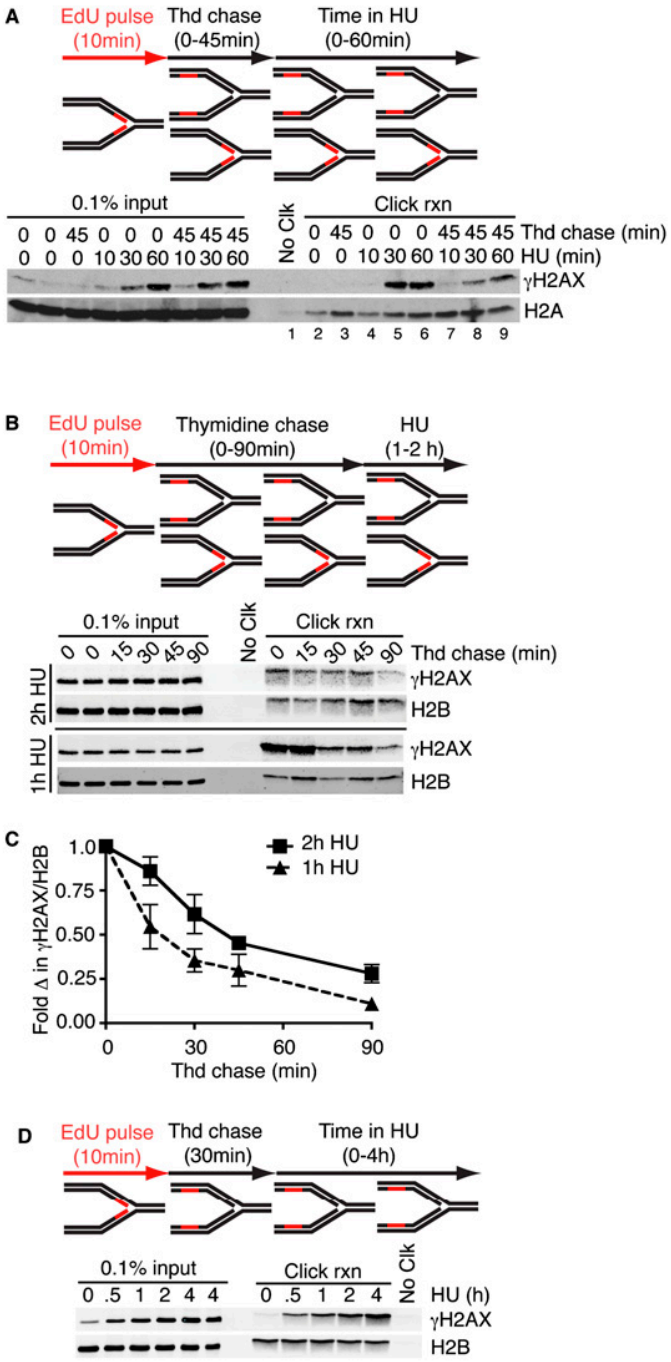

Figure 4.5. γH2AX spreads from a stalled replication fork. (A–D) Cells labeled with EdU for 10 min were chased into thymidine containing medium prior to addition of HU, then processed using iPOND. The length of the thymidine and HU treatments is indicated. Quantitation of the click reaction samples in C at the 2-h HU-treated samples is from three independent experiments, and at the 1-h HU treated samples is from two independent experiments. B,C and D were performed by Jami Couch.

To identify the kinases that phosphorylate H2AX adjacent to the stalled fork and that promote spreading, we used small molecule kinase inhibitors. The selective DNA-PK and ATM inhibitors NU7441 [103] and KU55933 [104] had minimal effects on the spreading or total levels of γH2AX induced by a short (30- to 60-min) HU treatment (Fig. 4.6A; Fig. 4.7A). However, these inhibitors did significantly reduce γH2AX levels at all chromosomal positions relative to the fork in cells treated with HU for 4 h (Fig. 4.6B,C, Fig. 4.7).

These results indicate that DNA-PK/ATM contributes to maintenance and spreading of γH2AX at persistently stalled forks. In contrast, treatment with caffeine, which preferentially inhibits ATR [105], significantly reduced γH2AX formation and spreading shortly after the fork is stalled (Fig. 4.6D). These results are consistent with a model in which ATR phosphorylates H2AX at a stalled fork and promotes initial spreading. At later time points, when DSBs likely form at the fork, ATM and DNA-PKcs maintain and further propagate the H2AX phosphorylation (Fig. 4.8).

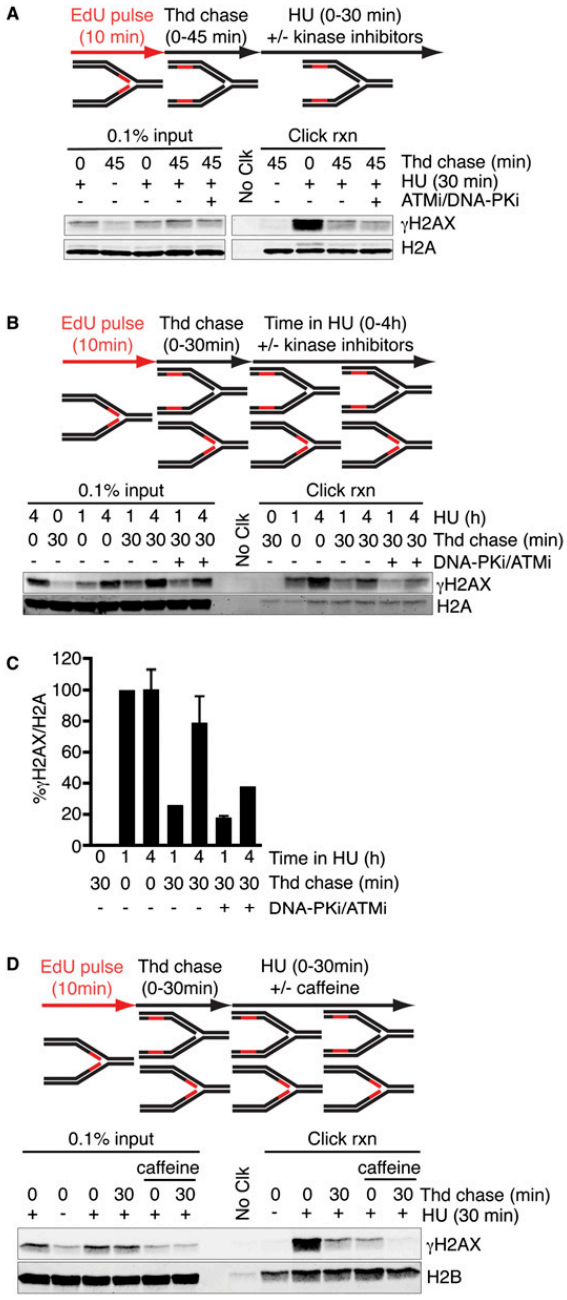

Figure 4.6. Checkpoint kinases propagate H2AX phosphorylation from stalled replication forks. (A–C) Cells labeled with EdU for 10 min were chased into thymidine, followed by treatment with HU. The length of thymidine and HU treatments are indicated. DNA-PK (KU7441, 1 mM) and ATM (KU5593, 10 mM) inhibitors were added at the same time as HU in the indicated samples. (C) Quantitation of the click reaction samples is the average from two independent experiments and is normalized to the 1-h HU treatment. (D) Cells labeled with EdU for 10 min were chased into thymidine for either 0 or 30 min, followed by a 30-min treatment with HU. Caffeine (10 mM) was added at the same time as HU in the indicated samples. Experiment in panel D was performed by Jami FB Couch.

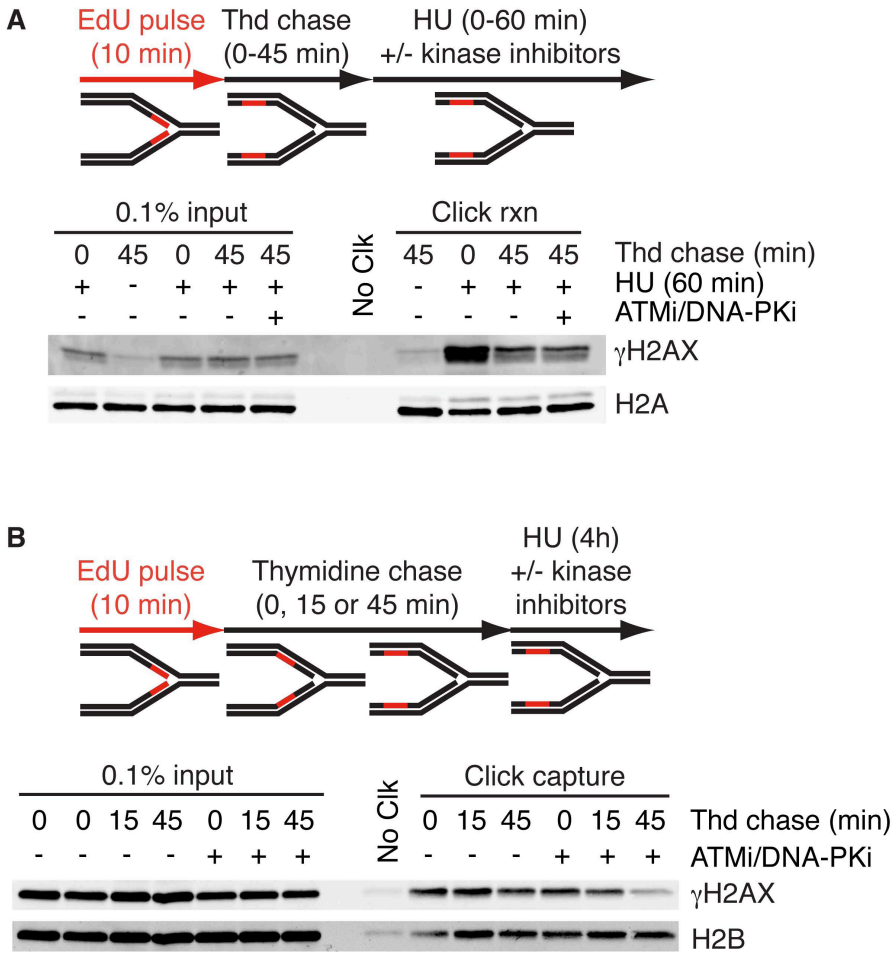

Figure 4.7. ATM/DNA-PK do not contribute to early γH2AX spreading from a stalled replication fork. (A, B) Cells labeled with EdU for 10 mins were chased into thymidine containing media prior to addition of HU, then processed using iPOND. The length of thymidine and HU treatments are indicated. DNA-PK (KU7441, 1mM) and ATM (KU5593, 10mM) inhibitors were added at the same time as HU in the indicate samples.

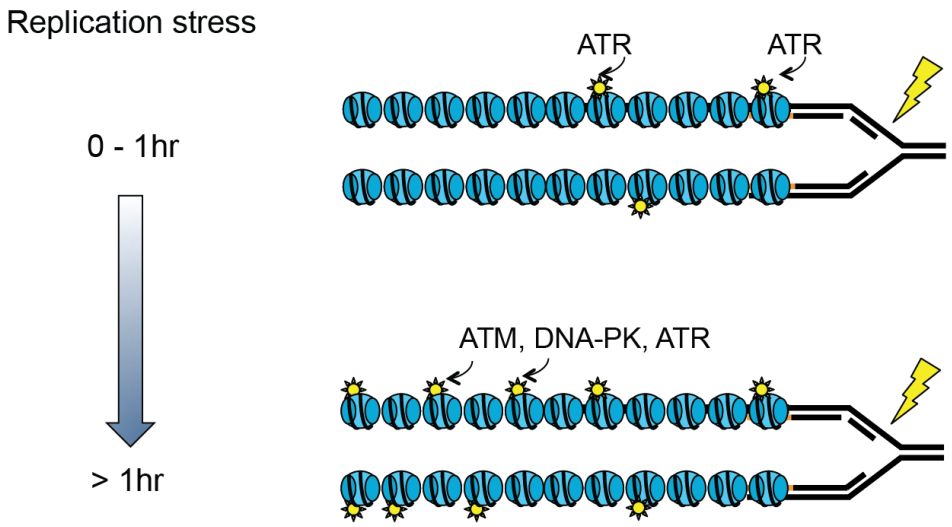

Figure 4.8. Model for the temporal mechanism of checkpoint kinase-dependent spreading of H2AX phosphorylation from stalled replication forks. At early time points after HU treatment (less than 2h), ATR is the most important kinase in phosphorylating H2AX both near the stalled fork and spreading the signal away from the fork. At later time points in HU (4h), ATM and DNA-PK become increasingly involved in both spreading the H2AX phosphorylation and in maintaining the phosphorylation near the stalled fork.

Discussion

In this chapter, I provided further validation for the use of iPOND as a method for studies of genome and epigenome maintenance processes. Using various experimental frameworks, I examined the timing and distance from the fork of replication-coupled chromatin deposition and maturation, and the replication stress response.

Chromatin assembly is thought to occur by a stepwise deposition of the core histones, followed by linker histones and changes in post-translational modifications [3]. My data confirm this assembly process in vivo in cultured mammalian cells. Furthermore, I found that at least some chromatin maturation processes, such as the removal of acetylation on H4K5 and H4K12, proceed even when decoupled from replisome movement. I showed that HAT1 is the mammalian acetyltransferase that catalyzes the replication-coupled modification on histone H4 K5/K12. HAT1 is essential to promote genome stability and homozygous deletion of HAT1 in murine models causes neonatal lethality (Prabakaran, in press).

HDAC1, HDAC2, and HDAC3 are enriched on newly synthesized DNA, and an inhibitor that targets all three of these enzymes prevents H4K5ac and H4K12ac deacetylation. Intriguingly, deacetylation of H4K5ac and H4K12ac occurred at the same rate, but acetyltransferases rapidly reacetylated H4K12, suggesting a specific need for this modification in some chromatin domains. In

the yeast *Saccharomyces cerevisiae*, H3K56 acetylation is also associated with newly deposited histones during DNA replication, and promotes survival in response to replication stress [106]. We were unable to detect this acetylation mark on newly deposited histones or after HU treatment (data not shown). This observation is consistent with other human cell studies that found low levels of this post-translational modification in total chromatin that further decreased in response to DNA damage [107].

Prominent changes in response to replication stress include protein phosphorylation. Importantly, our data indicate that H2AX phosphorylation spreads to a large chromatin domain early in the response to fork stalling. This early phosphorylation is catalyzed by ATR and is unlikely to be due to the processing of the fork into a DSB intermediate. Our data are consistent with previous analyses implicating both ATR-dependent [108] and ATR-independent [15, 109] H2AX phosphorylating activities in response to fork arrest.

Most models of ATR function suggest that it is active only when bound to the ssDNA at the stalled fork through an ATRIP–RPA interaction [14], but our data indicate that ATR helps spread the γH2AX signal. One possibility is that the early spreading of γH2AX is due to looping of the newly synthesized chromatin that brings it into proximity of ATR.

One role for such looping may be improved DNA repair. In yeast, increased chromosomal mobility has recently been observed following induction of a DSB [110, 111]. This movement depends on the yeast ATR kinase, DNA end

resection, and RAD51. It would be interesting to test whether ATR-dependent γH2AX in chromatin domains away from the replication fork depend upon RAD51 or the resection machinery.

An alternative method for propagation of H2AX phosphorylation may signify that ATR has a method of spreading its signal beyond the immediate ssDNA vicinity. Such a mechanism would be similar to the ability of active ATM to spread along the dsDNA away from the DSB end [112] MDC1 may be involved in such a process [113, 114] and I detected enrichment of MDC1 at stalled replication forks using iPOND-MS (Chapter V).

Persistent stalling of the fork for longer than 1–2 h causes a switch in the DDR. RPA is hyperphosphorylated on DNA-PK-dependent phosphorylation sites, ATM/ DNA-PK catalyzes further γH2AX spreading, and DSB repair proteins like MRE11, KU70/80, and RAD51 are enriched. RAD51 assembly at these persistently stalled forks depends on MRE11 activity, suggesting a requirement for end resection. The end resection may be on the template DNA strand, since we continued to capture EdU-labeled DNA and associated proteins. Resecting the leading strand template would yield a 3' overhang of newly synthesized DNA, which could be used in recombination-based methods of fork repair and restart [87].

Overall, these data provide the first high-resolution, time-dependent analyses of protein dynamics at active, stalled, and collapsed replication forks in mammalian cells.

CHAPTER V

iPOND PROTEOMIC IDENTIFICATION OF NOVEL GENOME AND EPIGENOME INHERITANCE PROTEINS*

Introduction

In the previous chapters, I described the utility of iPOND for monitoring the dynamics of known proteins that function in DNA replication and repair. While these represent a large fraction of the proteins that maintain genome integrity during chromosome duplication, a comprehensive view of the replisome and associated proteins has not been examined due to technical challenges of purifying replisomes from mammalian cells. In addition, how replisome composition is altered in response to DNA damage remains unclear. When replication forks encounter damage that halts the replicative polymerase but allows continued unwinding by the replicative helicase, single-stranded parental DNA accumulates [14, 115]. RPA coats the ssDNA and serves as the recruiting platform for many of the known checkpoint response proteins.

But what are all of the proteins that accumulate at sites of damaged replisomes? What enzymatic activities protect genome and epigenome integrity during DNA replication?

*Excerpts of the introduction and discussion of this chapter are in press Sirbu BM and Cortez D, *CSHL Perspectives in Biology.*

To answer these broad questions, I coupled iPOND to unbiased shotgun proteomics to probe the changes in replisome composition under different conditions. I propose to identify and validate new proteins recruited to replication forks.

In addition to exploring the active and stalled replisome, I was interested in how the ATR kinase stabilizes stalled replication forks to prevent genomic instability. In the absence of ATR activity, replication forks are said to 'collapse.' The mechanism of fork 'collapse' remains ambiguous, but changes in proteins and DNA at replication forks provide detectable evidence for fork breakdown. For example, *S. cerevisiae* mutants deficient in the ATR pathway lose the replicative polymerases from the fork [35-37] and accumulate abnormal DNA structures including long stretches of ssDNA and reversed fork structures resembling Holliday junctions [38, 39]. In yeast, the EXO1 nuclease generates the excess ssDNA at the stalled fork when the ATR pathway is inactivated [116]. Loss of ATR function in *Xenopus* egg extracts also causes loss of Polε and collapse of the fork into a DSB [40].

Studying fork collapse in human cells lacking ATR is difficult because ATR is essential for the viability of replicating cells [15]. Using a selective inhibitor of ATR kinase activity [61, 62], we observed that mammalian cells treated with the ATR inhibitor accumulate toxic levels of ssDNA that corresponds to the nascent DNA strand (Couch FB, results in press). The relevant targets of ATR in preventing replication fork collapse are unknown, but may include nucleases that

generate excess ssDNA and helicases that rearrange highly recombinogenic structures into detrimental fork structures. Hundreds of ATR substrates have been identified in large proteomics screens [41]. A portion of these substrates likely represents ATR targets that prevent fork collapse.

Probing the changes in the replisome using iPOND-MS and an ATR-specific inhibitor is of clinical relevance. Cancer cells exhibit high amounts of replication stress, which is partly due to the activation of oncogenes in precancerous lesions [117, 118]. Replication stress requires the ATR pathway for survival, making ATR an attractive therapeutic target for killing specific cancer types. Therefore, an examination of proteins that are enriched at stalled forks that collapse in the absence of ATR activity may offer mechanistic insights into how cancer cells treated with ATR inhibitors will respond to cancer therapies. Furthermore, we may gain information about the cancer patient population that may benefit the most from treatment with ATR inhibitors, which are currently being tested in Phase I clinical trials.

Results

iPOND optimizations for shotgun proteomics approaches

Prior to coupling iPOND purifications to quantitative proteomics approaches for identification of replication fork proteins, two MS strategies were considered. Stable isotope labeling offers high accuracy of protein identification, but requires extensive biochemical workup and cost [119]. We chose to pursue label-free spectral counting that provides relative quantitation of protein abundance across several samples simultaneously [120]. Preliminary experiments were performed in an effort to improve the signal to noise ratio prior to the iPOND-MS screens and are detailed in Chapter II and Appendix A.

iPOND proteomics quality control

To identify proteins associated with nascent DNA at replication forks and to explore the protein changes resulting from DNA damage, we coupled iPOND purifications to proteomics analyses. Five samples were prepared for iPOND-MS (Fig. 5.1A). For all samples, cells were treated for 15 mins with EdU to label nascent DNA. To examine proteins at normal, elongating replication forks, EdU pulsed cells were collected and proteins bound to nascent DNA were purified using iPOND (Fig. 5.1A). To monitor proteins associated with stalled replication forks, EdU labeled cells were treated with a high concentration of HU. This arrests fork movement and induces a DNA damage response (data not shown).

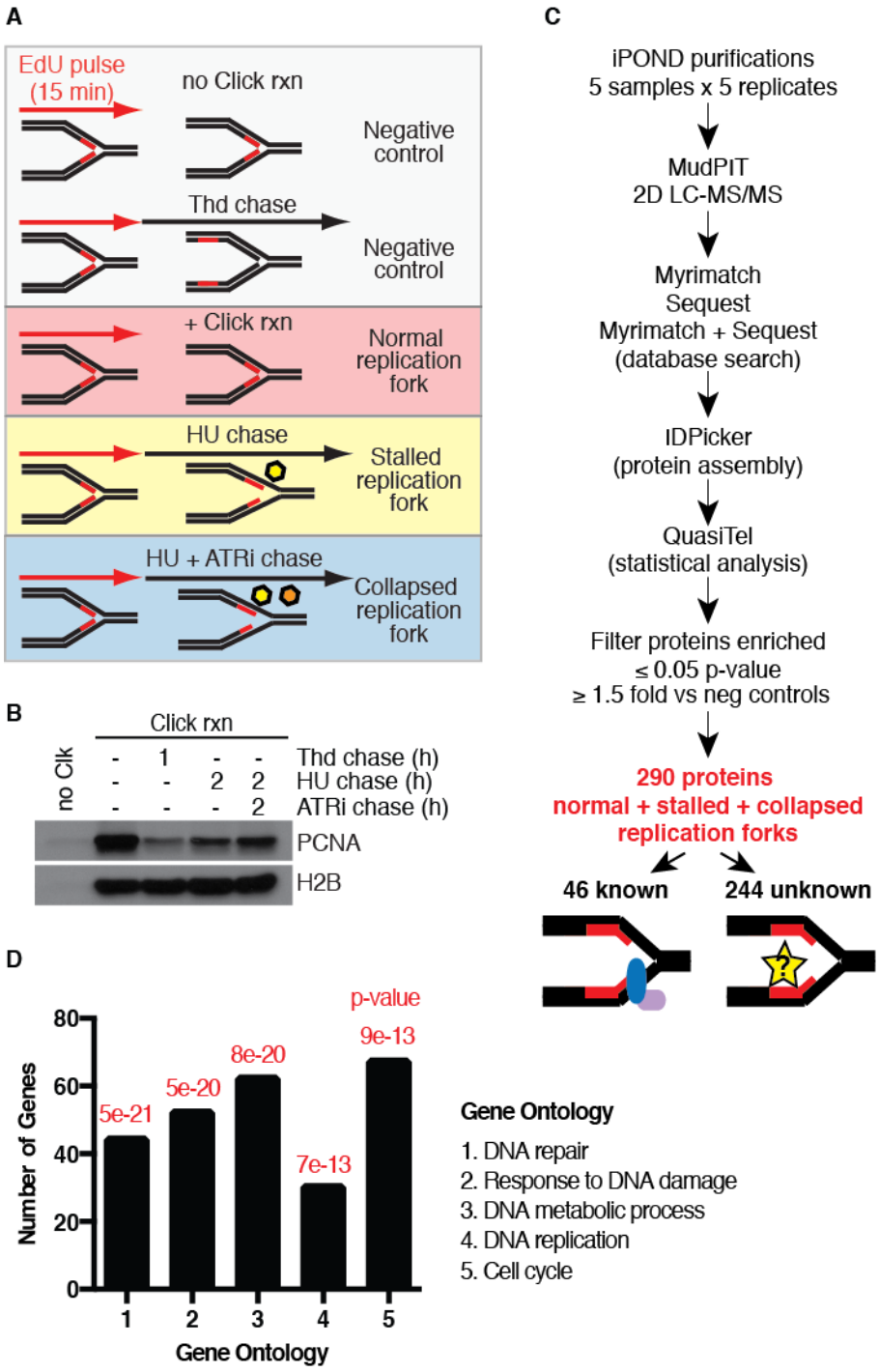

Figure 5.1. iPOND proteomics screen workflow. (A) Diagram of iPOND-MS pulse/chase frameworks. Cells pulsed with EdU for 15 mins were processed without the Click rxn reagent (Negative control) or treated with thymidine for one hour (Negative control) prior to iPOND. The experimental samples were collected immediately after the EdU pulse (Normal replication fork). EdU pulsed cells were treated with 3mM HU for 2 hours (Stalled replication fork), or simultaneously chased into 3mM HU and ATR inhibitor (Collapsed replication fork) without removing EdU, and samples were then collected for iPOND. (B) Representative iPOND purifications from one of the five replicates submitted for proteomic analyses. The five samples described in (A) were iPOND purified and blotted for PCNA and H2B. (C) iPOND-MS experimental workflow. (D) Toppgene analysis for classification of statistically significant proteins found enriched at normal, stalled, and collapsed replication forks.

The third experimental sample explored proteins recruited to stalled forks that collapse in the absence of ATR activity. Thus, EdU pulsed cells were chased into a combination of HU and an ATR specific inhibitor [61, 62], at an inhibitor concentration that causes the accumulation of RPA on nascent-strand ssDNA (Couch FB unpublished results).

The specificity of replication fork protein purifications was tested relative to two negative controls (Fig. 5.1A top panel). One negative control was treated identically to the normal replication fork sample but omitted the biotin azide that biotin tags nascent DNA. Proteins purified in this 'no Click rxn' sample represent those that interact non-specifically with streptavidin-conjugated beads. For the second negative control, cells pulsed with EdU were chased into thymidine for 1 hour to monitor proteins bound to mature chromatin, which are no longer close to the replication fork. Proteins detected in this sample represent chromatin-bound proteins that are not specific to replisomes or the surrounding nascent chromatin.

To test the relative enrichment of replication proteins in the samples submitted for MS analyses, iPOND purifications were examined for PCNA levels. As observed previously, PCNA was detected at elongating replication forks and its levels decreased upon chase into thymidine and replication stress (Fig. 5.1B). While still detectable, PCNA levels at stalled and ATR inhibited replication forks appear less enriched than at unperturbed forks. This may reflect unloading of PCNA from the lagging strand [121]. The relatively equal levels of histone H2B

detected on isolated chromatin (Fig. 5.1B) indicate that equivalent amounts of EdU-labeled DNA were purified in samples subsequently analyzed by MS.

iPOND-MS view of proteins at replication forks

Following the described conditions, the five samples were iPOND purified independently five times from one cell culture (5 technical replicates). The eluted proteins were analyzed using two-dimensional liquid chromatography coupled with tandem mass spectrometry (multidimensional protein identification technology MudPIT) (Fig. 5.1B). The MS/MS spectra were matched to the human protein database using the Myrimatch and Sequest search engines [65-67]. Proteins identified using at least one of these search engines had to pass filtering criteria described in detail below and reported in Tables 5.2, 5.3 and 5.4. The fold enrichment, p-value and spectral count data is the median value generated from each search engine applied.

To discern replication fork proteins from non-specific and chromatin-bound proteins, spectral counts were used to determine protein fold changes relative to the negative controls. The final lists include proteins enriched at least 1.5-fold (relative to both negative controls) with p-values less than or equal to 0.05, as calculated using QuasiTel [72]. To increase the stringency criteria, an additional filter required at least 5 spectral counts total per 5 experimental replicates. Tables 5.2, 5.3 and 5.4 contain the significantly enriched proteins found at normal, stalled and collapsed replication forks, respectively.

These filtering criteria led to the identification of a total of 290 proteins, some of which overlapped in two or all three experimental conditions (Table 5.1). At least sixteen percent of the enriched proteins had previously been documented to function in DNA replication and damage (Fig. 5.1B, C). Functional characterization of the dataset revealed that gene ontology categories such as DNA repair, response to DNA damage, DNA metabolic process, DNA replication and cell cycle were overrepresented above random chance of expectancy (Fig. 5.1D). This provides confidence that the iPOND-MS screen successfully identified DNA replication and damage proteins.

Of the total proteins enriched on nascent DNA, 84 were found to accumulate at normal forks, 139 at stalled forks and 137 at collapsed forks. Several established genome maintenance proteins were among the 11 proteins enriched in all three experimental conditions tested (Table 5.1). For example, the interstrand crosslink repair factor FANCI, which is found mutated in Fanconi anemia, the ATR-activating replication stress protein TOPBP1, and the chromatin remodeler SMARCAD1 were enriched at replication forks under unperturbed and stressed conditions. The identification of genome maintenance proteins in unperturbed conditions supports the idea that basal levels of replication stress occur during each cell cycle and that every S phase requires checkpoint proteins to ensure faithful DNA replication [14].

Table 5.1. Proteins enriched in common in the iPOND proteomics screens.

Normal Stalled Collapsed	Normal Stalled	Normal Collapsed	Stalled Collapsed	
ACO1	ACO1	ACO1	ACO1	POLD1
FANCI	CBS	CA2	ADD1	PTRH2
IMMT	CHAF1B	FANCI	CHTF18	RAD1
ISYNA1	FANCI	HEATR3	CUL2	RPA2
MRPL13	IMMT	IMMT	CUL3	SLC25A11
PDCD4	ISYNA1	ISYNA1	DAK	SMARCAD1
PIGT	MRPL13	MRPL13	DNAJC8	SPATA5
POLD1	MSH3	PDCD4	FANCD2	TMTC3
SMARCAD1	NAA10	PIGT	FANCI	TOPBP1
TOPBP1	NCAPH	POLD1	FKBP10	TRMT6
TRMT6	OSBPL9	POLE	GOT1	UGGT1
	PDCD4	RFC1	GSS	VAC14
	PHKB	RFC4	IMMT	XPO5
	PIGT	RFC5	ISYNA1	XRCC1
	POLD1	RPA3	KIAA1598	
	RPL6P10	SEPT11	MAOA	
	SKP1	SLC4A2	MDC1	
	SMARCAD1	SMARCAD1	MRPL13	
	SPTLC2	TIMELESS	MRPL28	
	SSB	TM9SF4	PDCD4	
	TOPBP1	TOPBP1	PDS5B	
	TRMT6	TRMT6	PIGT	

	Known proteins

At normal and ATR inhibited replication forks, I observed the core replisome components (polymerase epsilon, the large subunit of polymerase delta POLD1, and the replication clamp loader accessory factors RFC1-5) (Table 5.1). Most models pose that ATR prevents dissociation of the replisome to maintain a stable replication fork competent for restart of DNA synthesis after DNA damage [14]. The presence of POLD1, POLE and RFC1-5 at forks lacking ATR activity suggests that maintaining an intact replisome is independent of ATR activity in human cells.

The elongating replisome and associated proteins

The distribution of proteins identified at elongating replication forks revealed that the majority of proteins enriched with a p-value less than 0.01 (red colored dots in Fig. 5.2) are well-established replisome components. For example, PCNA, POLD1 and POLE were identified with numerous spectral counts, providing further confidence in the identification of these proteins (Fig. 5.2A). It should be noted that when no spectra were detected in the chromatin-bound negative control, QuasiTel calculates relative fold enrichment using a small, non-zero value in the denominator. This factor may lead to an overestimation of protein enrichment (see Table 5.2 fold enrichment for CP110 and PIGT). While these values are included in Tables 5.2, 5.3, and 5.4, they are omitted from Figures 5.2, 5.3 and 5.4. Overall, the highest confidence proteins from iPOND-MS have low p-values, are highly enriched relative to both negative controls and are detected with large spectral count numbers.

To examine potential genetic and biochemical connections among the identified proteins, I performed bioinformatics searches using the GeneMANIA prediction server [74]. The network modeling showed that approximately one third of the identified proteins form a cohesive network based on curated physical interactions (Fig. 5.2B). PCNA represents a prominent node in this network and is a known recruiting scaffold for numerous replication and DNA damage proteins.

A

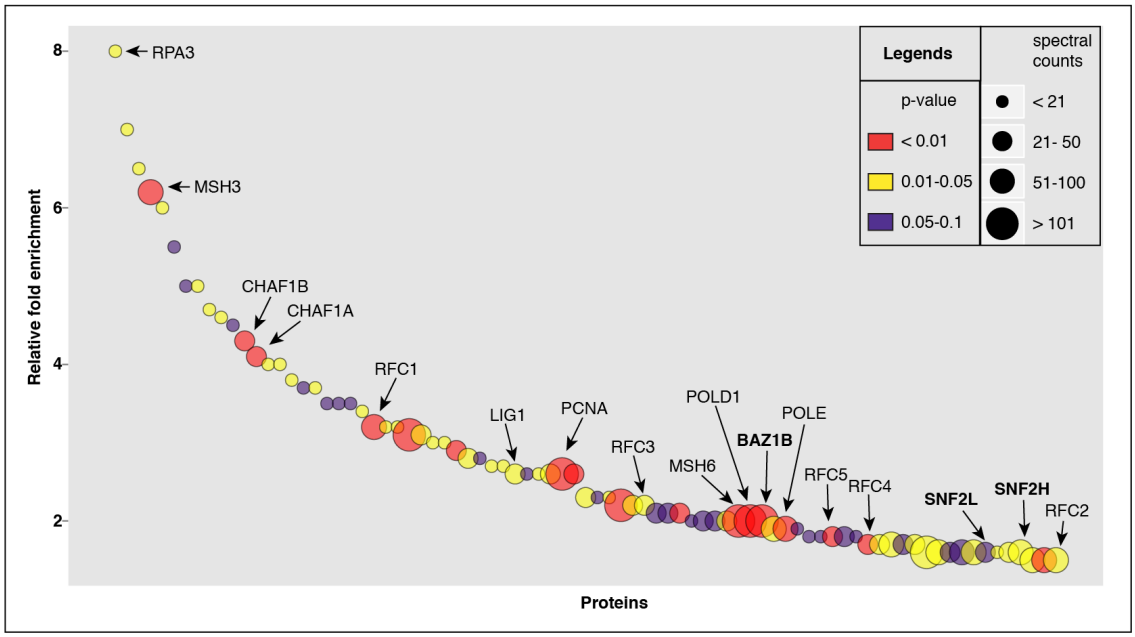

B

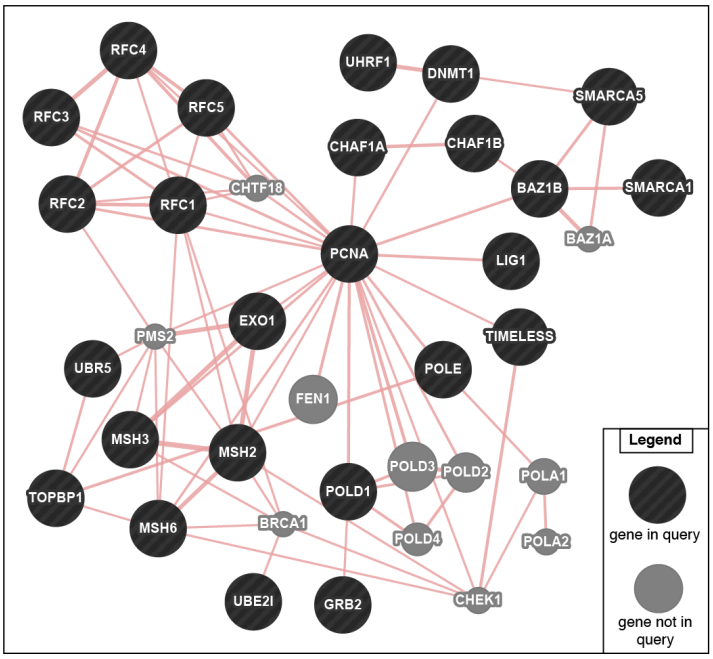

C

Proteins with PCNA-interacting motifs (PIP and APIM)	ATM/ATR putative substrates	Genome maintenance genes
BAZ1B	ATAD5	EP400
CCP110	BAZ1B	FANCI
DNMT1	CHAF1A	HSD17B7
EHMT1	EHMT1	PDCD4
LIG1	EXO1	PLOD1
MSH3	FANCI	RFC2
MSH6	MSH2	RPA3
SMARCA1	MSH3	SMARCA1
SMARCA5	MSH6	SNRPD1
UBR5	POLE	TIMELESS
UHRF1	RFC1	TRMT6
	RFC3	
	SMARCAD1	
	TOPBP1	
	TRMT6	
	UBR5	
	VPS26B	
	WDHD1	

Figure 5.2. iPOND-MS identifies proteins significantly enriched on replicating DNA in unperturbed S phase. (A) The fold enrichment relative to the chromatin chase negative control, the p-value and the spectral count data, which passed the filtering criteria described in the text, are depicted for the proteins listed in Table 5.2. The dot size indicates the total number of MS spectra counted in the normal replication fork samples from the five replicate purifications. The dot color represents p-value as calculated using QuasiTel. The proteins in bold are proteins that were followed up in subsequent validation experiments. The dot plots were generated in R by Yaoyi Chen. (B) Protein network analyses used GeneMANIA predictions [74] to probe the physical interactions within the normal replication fork dataset. (C) The iPOND-MS normal replication fork proteins that contain potential PCNA interacting motifs [122] or putative ATM/ATR phosphorylation sites [41, 123] are listed. iPOND-MS proteins were cross-referenced with genomics screens for genes that when knocked down cause significant H2AX phosphorylation [124, 125].

Table 5.2. Proteins significantly enriched on nascent chromatin during unperturbed DNA replication. Hayes McDonald performed QuasiTel comparisons between replication fork samples and negative controls.

Entrez ID	Official symbol	Name	Median Enrichment	Median p-value	Median Spectral counts
5982	RFC2	Replication Factor C (Activator 1) 2, 40Kda	1.5	0.0484	58
6128	RPL6P10	Ribosomal Protein L6 Pseudogene 10	1.5	0.0037	55
760	CA2	Carbonic Anhydrase Ii	1.5	0.0330	64
8467	SMARCA5	Swi/Snf Related, Matrix Associated, Actin Dependent Regulator Of Chromatin, Subfamily A, Member 5	1.6	0.0211	195
55215	FANCI	Fanconi Anemia, Complementation Group I	1.6	0.0408	87
51366	UBR5	Ubiquitin Protein Ligase E3 Component N-Recognin 5	1.6	0.0757	33
6594	SMARCA1	Swi/Snf Related, Matrix Associated, Actin Dependent Regulator Of Chromatin, Subfamily A, Member 1	1.6	0.0531	96
29128	UHRF1	Ubiquitin-Like With Phd And Ring Finger Domains 1	1.6	0.0214	59
10135	NAMPT	Nicotinamide Phosphoribosyltransferase	1.6	0.0535	42
5351	PLOD1	Procollagen-Lysine 1, 2-Oxoglutarate 5-Dioxygenase 1	1.6	0.0357	14.5
875	CBS	Cystathionine-Beta-Synthase	1.6	0.0431	28
6632	SNRPD1	Small Nuclear Ribonucleoprotein D1 Polypeptide 16Kda	1.6	0.0315	82
5984	RFC4	Replication Factor C (Activator 1) 4, 37Kda	1.7	0.0045	48
3251	HPRT1	Hypoxanthine Phosphoribosyltransferase 1	1.7	0.0310	36
5479	PPIB	Peptidylprolyl Isomerase B (Cyclophilin B)	1.7	0.0401	55
48	ACO1	Aconitase 1, Soluble	1.7	0.0891	34
54517	PUS7	Pus7 Pseudouridylate Synthase 7 Homolog	1.7	0.0334	29.5
2885	GRB2	Growth Factor Receptor-Bound Protein 2	1.8	0.0910	17
6500	SKP1	S-Phase Kinase-Associated Protein 1	1.8	0.0638	18
5985	RFC5	Replication Factor C (Activator 1) 5, 36.5Kda	1.8	0.0091	44.5
64975	MRPL41	Mitochondrial Ribosomal Protein L41	1.8	0.0701	22
10491	CRTAP	Cartilage Associated Protein	1.8	0.0659	10
6741	SSB	Sjogren Syndrome Antigen B (Autoantigen La)	1.9	0.0319	100
5426	POLE	Polymerase (Dna Directed), Epsilon	1.9	0.0003	53
8260	NAA10	Ard1 Homolog A, N-Acetyltransferase (S. Cerevisiae)	1.9	0.0625	17
57634	EP400	E1A Binding Protein P400	2.0	0.0794	15
8125	ANP32A	Acidic (Leucine-Rich) Nuclear Phosphoprotein 32 Family, Member A	2.0	0.0731	26
55752	SEPT11	Septin 11	2.0	0.0680	24
4436	MSH2	Muts Homolog 2, Colon Cancer, Nonpolyposis Type 1 (E. Coli)	2.0	0.0154	46
9031	BAZ1B	Bromodomain Adjacent To Zinc Finger Domain, 1B	2.0	0.0041	125
2956	MSH6	Muts Homolog 6 (E. Coli)	2.0	0.0005	288
5424	POLD1	Polymerase (Dna Directed), Delta 1, Catalytic Subunit 125Kda	2.0	0.0030	108.5
55027	HEATR3	Heat Repeat Containing 3	2.1	0.0502	25
10620	ARID3B	At Rich Interactive Domain 3B (Bright-Like)	2.1	0.0986	24
29089	UBE2T	Ubiquitin-Conjugating Enzyme E2T (Putative)	2.1	0.0066	40
26164	GTPBP5	Gtp Binding Protein 5 (Putative)	2.2	0.0002	266.5
29028	ATAD2	Atpase Family, Aaa Domain Containing 2	2.2	0.0180	45
5983	RFC3	Replication Factor C (Activator 1) 3, 38Kda	2.2	0.0457	41
5721	PSME2	Proteasome (Prosome, Macropain) Activator Subunit 2 (Pa28 Beta)	2.3	0.0474	37
9777	TM9SF4	Transmembrane 9 Superfamily Protein Member 4	2.3	0.0866	14
11073	TOPBP1	Topoisomerase (Dna) Ii Binding Protein 1	2.3	0.0378	9
11169	WDHD1	Wd Repeat And Hmg-Box Dna Binding Protein 1	2.6	0.0173	30
5257	PHKB	Phosphorylase Kinase, Beta	2.6	0.0553	10
9039	UBA3	Ubiquitin-Like Modifier Activating Enzyme 3	2.6	0.0450	13
3978	LIG1	Ligase I, Dna, Atp-Dependent	2.6	0.0438	47
5111	PCNA	Proliferating Cell Nuclear Antigen	2.6	0.0003	124
58525	WIZ	Widely Interspaced Zinc Finger Motifs	2.6	0.0004	37
902	CCNH	Cyclin H	2.7	0.0307	9
29925	GMPPB	Mitochondrial Ribosomal Protein L37	2.7	0.0441	11
8914	TIMELESS	Timeless Homolog (Drosophila)	2.8	0.0194	23

Table 5.2 continued. Proteins significantly enriched on nascent chromatin during unperturbed DNA replication.

Entrez ID	Official symbol	Name	Median Enrichment	Median p-value	Median Spectral counts
51477	ISYNA1	Inositol-3-Phosphate Synthase 1	2.8	0.0615	12
112936	VPS26B	Vacuolar Protein Sorting 26 Homolog B (S. Pombe)	2.9	0.0084	22
28998	MRPL13	Mitochondrial Ribosomal Protein L13	3.0	0.0297	15
79813	EHMT1	Euchromatic Histone-Lysine N-Methyltransferase 1	3.0	0.0289	9
1786	DNMT1	Dna (Cytosine-5-)-Methyltransferase 1	3.1	0.0001	201
79915	ATAD5	Atpase Family, Aaa Domain Containing 5	3.1	0.0437	26
5981	RFC1	Replication Factor C (Activator 1) 1, 145Kda	3.2	0.0018	61
25923	ATL3	Atlastin Gtpase 3	3.2	0.0440	13
7329	UBE2I	Ubiquitin-Conjugating Enzyme E2I (Ubc9 Homolog, Yeast)	3.2	0.0270	14
51605	TRMT6	Trna Methyltransferase 6 Homolog (S. Cerevisiae)	3.4	0.0485	16
283237	TTC9C	Tetratricopeptide Repeat Domain 9C	3.5	0.0679	7
1820	ARID3A	At Rich Interactive Domain 3A (Bright-Like)	3.5	0.0679	7
27250	PDCD4	Programmed Cell Death 4 (Neoplastic Transformation Inhibitor)	3.5	0.0768	11
6166	RPL36AL	Ribosomal Protein L36A-Like	3.7	0.0549	12
23397	NCAPH	Non-Smc Condensin I Complex, Subunit H	3.7	0.0245	12
54454	ATAD2B	Atpase Family, Aaa Domain Containing 2B	3.8	0.0158	19
84153	RNASEH2C	Ribonuclease H2, Subunit C	4.0	0.0379	8
114883	OSBPL9	Oxysterol Binding Protein-Like 9	4.0	0.0144	11.5
10036	CHAF1A	Chromatin Assembly Factor 1, Subunit A (P150)	4.1	0.0033	30
8208	CHAF1B	Chromatin Assembly Factor 1, Subunit B (P60)	4.3	0.0011	42
51478	HSD17B7	Hydroxysteroid (17-Beta) Dehydrogenase 7	4.5	0.0797	4.5
55559	HAUS7	Three Prime Repair Exonuclease 2; Haus Augmin-Like Complex, Subunit 7	4.6	0.0472	6.5
10166	SLC25A15	Solute Carrier Family 25 (Mitochondrial Carrier; Ornithine Transporter) Member 15	4.7	0.0237	11
6522	SLC4A2	Solute Carrier Family 4, Anion Exchanger, Member 2 (Erythrocyte Membrane Protein Band 3-Like 1)	5.0	0.0843	5
10989	IMMT	Inner Membrane Protein, Mitochondrial (Mitofilin)	5.0	0.0237	10
56916	SMARCAD1	Swi/Snf-Related, Matrix-Associated Actin-Dependent Regulator Of Chromatin, Subfamily A, Containing Dead/H Box 1	5.5	0.0732	11
55869	HDAC8	Histone Deacetylase 8	6.0	0.0311	8.5
4437	MSH3	Muts Homolog 3 (E. Coli)	6.2	0.0001	51
80142	PTGES2	Prostaglandin E Synthase 2	6.5	0.0452	6.5
9517	SPTLC2	Serine Palmitoyltransferase, Long Chain Base Subunit 2	7.0	0.0348	9
6119	RPA3	Replication Protein A3, 14Kda	8.0	0.0309	8
9156	EXO1	Exonuclease 1	24.0	0.0006	20
9738	CP110	Cp110 Protein	289859429.9	0.0371	6
51604	PIGT	Phosphatidylinositol Glycan Anchor Biosynthesis, Class T	1050559491.8	0.0044	8

Legend	Protein
	known
	discussed
	validated

Legend	p-value
	<0.01
	0.01-0.05
	0.05-0.1

Several of the iPOND-MS proteins contain predicted PCNA-interacting motifs (PIP boxes), as determined by cross-referencing [122] (Fig. 5.2C). For example, the Williams syndrome transcription factor WSTF (also known as BAZ1B), DNA methyltransferase (DNMT1), ligase 1, mismatch repair proteins MSH3 and MSH6, chromatin remodelers SNF2L and SNF2H, and the E3 ubiquitin ligase UBR5 have been shown to localize to replication forks. It is unknown if the PIP box of each factor is essential for localization to replication forks.

A second PCNA-interacting motif APIM (AlkB homologue 2 PCNA-interacting motif) is commonly found in proteins exhibiting damage-inducible PCNA interactions [122]. The centrosomal protein CP110, the DNMT1 recruiting protein UHRF1, and the euchromatic histone methyltransferase EHMT1 have predicted APIM motifs, suggesting these three proteins may function during replication stress.

To further analyze the proteins, the dataset was compared to published proteomics screens focused on finding new genome maintenance proteins. ATM and ATR regulate DDR proteins through phosphorylation. However, it is largely unknown which of the over 600 checkpoint kinase substrates are located at replication forks. Eighteen of the iPOND-MS enriched proteins are potential ATM/ATR substrates at unperturbed replication forks (Fig. 5.2C), according to cross-referencing with large-scale proteomics screens [41]. This represents a statistically significant fraction of proteins, as determined by hypergeometric hypothesis testing (p-value 0.0013, see Chapter II for bioinformatics analyses).

The majority of these kinase substrates are known DDR proteins, such as MSH2, MSH3, MSH6, POLE, RFC1, RFC3, TOPBP1, the TOPB1 ubiquitin ligase UBR5, FANCI, the exonuclease EXO1, the replication initiating factor WDHD1 (also known as AND1), and the alternative PCNA clamp loader ATAD5 (also known as ELG1). Other potential substrates that localized to forks have been affiliated with chromatin assembly and maturation during replication. These include the histone chaperone CAF1A, the chromatin remodeler SMARCAD1, and EHMT1. TRNA methyltransferase (TRMT6) and vacuolar protein sorting homolog B (VPS26) are putative ATM/ATR substrates that have not been previously linked to DNA replication, but were identified at elongating forks using iPOND-MS.

Lastly, the iPOND-MS list was cross-referenced with large-scale genomics screens that identified genes that when silenced activate the DNA damage response [124, 125]. Eleven iPOND-MS proteins may cause H2AX phosphorylation when depleted. Five of these have not been previously associated with functions during DNA replication, but may represent novel proteins of interest (Fig. 5.2C). Overall, the iPOND-MS screen for proteins associated with nascent DNA identified known replication fork proteins and novel proteins that may function during DNA replication. In later sections, I show validations of SNF2L recruitment to nascent chromatin and discuss the function of this chromatin remodeler in replication fork progression.

The stalled replisome and associated proteins

Enriched proteins were plotted as described for the undamaged fork dataset to visualize proteins found at stalled replication forks (Fig. 5.3A). Although few known DDR proteins were identified, the dataset was significantly enriched in gene ontologies classified under cellular response to stress (p-value 8e-5), DNA metabolic process (p-value 6e-4) and cell cycle (p-value 1.7e-3), as determined by Toppgene bioinformatics analyses. The low number of DDR proteins in this iPOND-MS sample may reflect poor iPOND purification of stalled replication forks where large stretches of parental RPA-ssDNA are generated from uncoupling of helicase and polymerase activities [115]. Since iPOND only purifies nascent DNA, this parental ssDNA signaling platform with bound checkpoint proteins may not be isolatable under these conditions.

However, of the known proteins, mediator of DNA damage checkpoint 1 (MDC1), RPA2, the DNA helicase RECQL1, the single-stranded DNA repair factor XRCC1, the Fanconi ID complex, and the Rad1 component of the checkpoint activating Rad9-Hus1-Rad1 (9-1-1) complex were clearly enriched. Several of the identified proteins are putative ATM/ATR substrates, harbor PCNA-interacting motifs, helicase domains, or cause DNA damage when depleted (Fig. 5.3B-D), linking the iPOND-MS stalled fork proteins to chromosome stability.

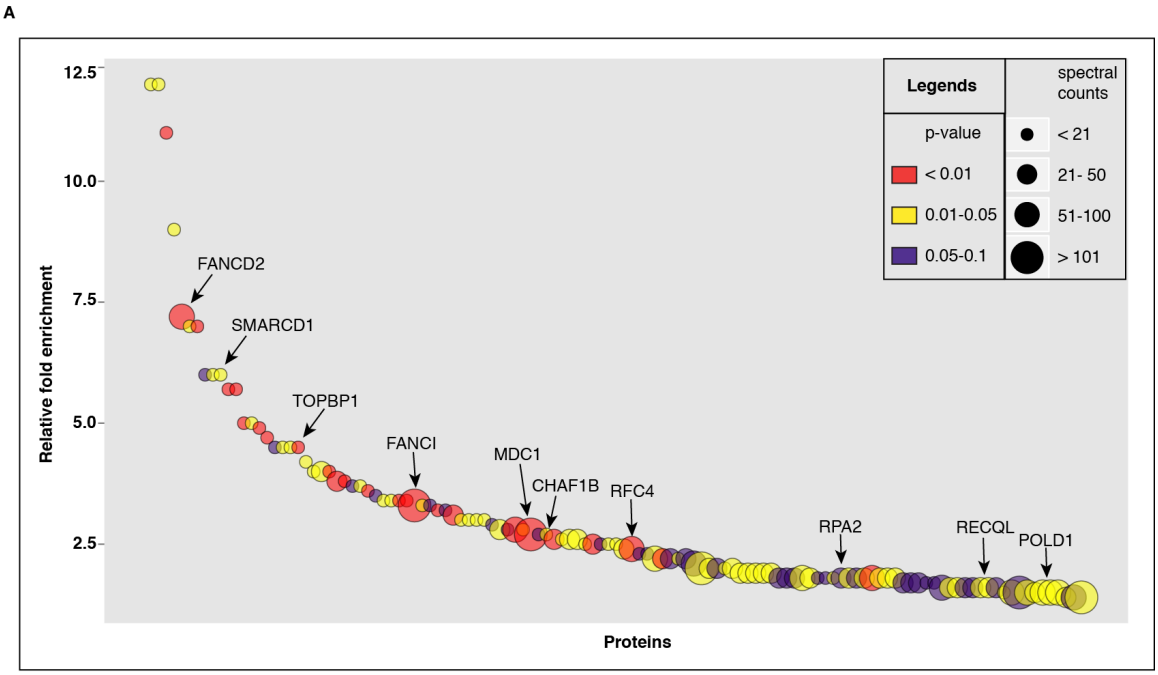

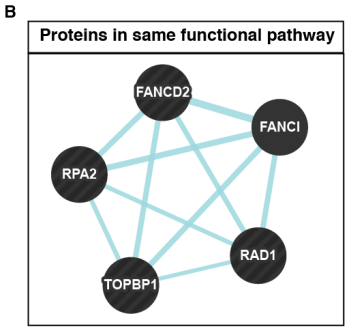

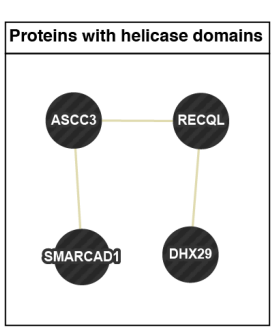

D

Proteins with PCNA-interacting motifs (PIP and APIM)	ATM/ATR putative substrates	Genome maintenance genes
ASCC3	AKAP12	ADD1
MSH3	CHTF18	ATP6V0D1
OBSCN	EHMT2	CALR
PHF14	EIF3D	COL6A1
RECQL	EPB41L2	CUL2
	FANCD2	FANCI
	FANCI	KIAA1598
	MDC1	MLL4
	MSH3	ORC7C2
	NIN	PDC4
	PDS5B	PSMD8
	SMARCAD1	RPA2
	SPG11	THUMPD1
	TOPBP1	TRMT6
	TRMT6	TTC27
	ZC3HAV1L	XPO5

Figure 5.3. iPOND-MS identifies proteins significantly enriched on replicating DNA during replication stress. (A) The fold enrichment relative to the chromatin chase negative control, the p-value and the spectral count data, which passed the filtering criteria described in the text, are depicted for the proteins listed in Table 5.3. The dot size indicates the total number of MS spectra counted in the stalled replication fork samples from the five replicate purifications. The dot color represents p-value as calculated using QuasiTel. The dot plots were generated in R by Yaoyi Chen. (B,C) Protein network analyses used GeneMANIA predctions to probe proteins in common functional pathways or those containing helicase domains. (D) The iPOND-MS stalled replication fork proteins that contain potential PCNA interacting motifs or putative ATM/ATR phosphorylation sites are listed. iPOND-MS proteins were cross-referenced with genomics screens for genes that when knocked down cause significant H2AX phosphorylation.

Table 5.3. Proteins significantly enriched on nascent chromatin during replication fork stalling. Hayes McDonald performed QuasiTel comparisons between stalled replication fork samples and negative controls.

Entrez ID	Official symbol	Name	Median Enrichment	Median p-value	Median Spectral counts
2820	GPD2	Glycerol-3-Phosphate Dehydrogenase 2 (Mitochondrial)	1.4	0.0125	48
178	AGL	Amylo-1, 6-Glucosidase, 4-Alpha-Glucanotransferase	1.4	0.0948	80
7086	TKT	Transketolase	1.4	0.0295	209
7372	UMPS	Uridine Monophosphate Synthetase	1.5	0.0251	20
5424	POLD1	Polymerase (Dna Directed), Delta 1, Catalytic Subunit 125Kda	1.5	0.0429	78
8664	EIF3D	Eukaryotic Translation Initiation Factor 3, Subunit D	1.5	0.0955	115
3064	HTT	Huntingtin	1.5	0.0470	67
54505	DHX29	Deah (Asp-Glu-Ala-His) Box Polypeptide 29	1.5	0.0288	42
5691	PSMB3	Proteasome (Prosome, Macropain) Subunit, Beta Type, 3	1.5	0.0257	68
6128	RPL6P10	Ribosomal Protein L6	1.5	0.0344	53
5965	RECQL	Recq Protein-Like (Dna Helicase Q1-Like)	1.5	0.0236	58
166378	SPATA5	Spermatogenesis Associated 5	1.6	0.0517	62
128	ADH5	Alcohol Dehydrogenase 5 (Class Iii), Chi Polypeptide	1.6	0.0270	39
7515	XRCC1	X-Ray Repair Complementing Defective Repair In Chinese Hamster Cells 1	1.6	0.0140	22
6599	SMARCC1	Swi/Snf Related, Matrix Associated, Actin Dependent Regulator Of Chromatin, Subfamily C, Member 1	1.6	0.0906	33
118	ADD1	Adducin 1 (Alpha)	1.6	0.0694	22
5515	PPP2CA	Protein Phosphatase 2 (Formerly 2A), Catalytic Subunit, Alpha Isoform	1.6	0.0396	39
8453	CUL2	Cullin 2	1.6	0.0473	41
22826	DNAJC8	Dnaj (Hsp40) Homolog, Subfamily C, Member 8	1.6	0.0957	23
2314	FLII	Flightless I Homolog (Drosophila)	1.7	0.0890	45
2475	MTOR	Mechanistic Target Of Rapamycin (Serine/Threonine Kinase)	1.7	0.0569	34
9675	TTI1	TELO2 interacting protein 1	1.7	0.0516	25
79187	FSD1	Fibronectin Type Iii And Spry Domain Containing 1	1.7	0.0585	11
9678	PHF14	Phd Finger Protein 14	1.7	0.0955	7
8604	SLC25A12	Solute Carrier Family 25 (Mitochondrial Carrier, Aralar), Member 12	1.8	0.0985	30
56886	UGGT1	Udp-Glucose Ceramide Glucosyltransferase-Like 1	1.8	0.0659	30
10973	ASCC3	Activating Signal Cointegrator 1 Complex Subunit 3	1.8	0.0859	49
8452	CUL3	Cullin 3	1.8	0.0297	57
2037	EPB41L2	Erythrocyte Membrane Protein Band 4.1-Like 2	1.8	0.0204	34
8260	NAA10	Ard1 Homolog A, N-Acetyltransferase (S. Cerevisiae)	1.8	0.0563	16
847	CAT	Catalase	1.8	0.0784	18
6500	SKP1	S-Phase Kinase-Associated Protein 1	1.8	0.0345	18
875	CBS	Cystathionine-Beta-Synthase	1.8	0.0853	29
51651	PTRH2	Peptidyl-Trna Hydrolase 2	1.8	0.0150	29
6118	RPA2	Replication Protein A2, 32Kda	1.8	0.0569	31
2805	GOT1	Glutamic-Oxaloacetic Transaminase 1, Soluble (Aspartate Aminotransferase 1)	1.8	0.0130	38
57510	XPO5	Exportin 5	1.8	0.0047	53
2224	FDPS	Farnesyl Diphosphate Synthase	1.8	0.0345	24
4128	MAOA	Monoamine Oxidase A	1.8	0.0245	48
80218	NAA50	N-Acetyltransferase 13 (Gcn5-Related)	1.8	0.0308	34
5714	PSMD8	Proteasome (Prosome, Macropain) 26S Subunit, Non-Atpase, 8	1.9	0.0311	26
381	ARF5	Adp-Ribosylation Factor 5	1.9	0.0364	27
811	CALR	Calreticulin	1.9	0.0472	48
55276	PGM2	Phosphoglucomutase 2	1.9	0.0311	23
11231	SEC63	Sec63 Homolog (S. Cerevisiae)	1.9	0.0212	30
6741	SSB	Sjogren Syndrome Antigen B (Autoantigen La)	2.0	0.0142	109
4976	OPA1	Optic Atrophy 1 (Autosomal Dominant)	2.0	0.0272	45
51552	RAB14	Rab14, Member Ras Oncogene Family	2.0	0.0830	21
10785	WDR4	Wd Repeat Domain 4	2.0	0.0432	12
4715	NDUFB9	Nadh Dehydrogenase (Ubiquinone) 1 Beta Subcomplex, 9, 22Kda	2.0	0.0406	23
347688	TUBB8	Tubulin, Beta 8	2.1	0.0937	66

Continued Table 5.3. Proteins significantly enriched on nascent chromatin during replication fork stalling.

Entrez ID	Official symbol	Name	Median Enrichment	Median p-value	Median Spectral counts
23047	PDS5B	Pds5, Regulator Of Cohesion Maintenance, Homolog B (S. Cerevisiae)	2.2	0.0206	57
8402	SLC25A11	Solute Carrier Family 25 (Mitochondrial Carrier; Oxoglutarate Carrier), Member 11	2.2	0.0069	41
5931	RBBP7	Retinoblastoma Binding Protein 7	2.2	0.0763	22
6251	RSU1	Ras Suppressor Protein 1	2.2	0.0138	17
2287	FKBP3	Fk506 Binding Protein 3, 25Kda	2.2	0.0515	38
5217	PFN2	Profilin 2	2.3	0.0776	12
55623	THUMPD1	Thump Domain Containing 1	2.3	0.0831	10.5
55622	TTC27	Tetratricopeptide Repeat Domain 27	2.4	0.0321	22
23193	GANAB	Glucosidase, Alpha; Neutral Ab	2.4	0.0057	59
55239	OGFOD1	2-Oxoglutarate And Iron-Dependent Oxygenase Domain Containing 1	2.5	0.0307	8
1500	CTNND1	Catenin (Cadherin-Associated Protein), Delta 1	2.5	0.0041	40
7410	VAV2	Vav 2 Guanine Nucleotide Exchange Factor	2.5	0.0615	10
55181	C17ORF71	Chromosome 17 Open Reading Frame 71	2.5	0.0355	10
8632	DNAH17	Dynein, Axonemal, Heavy Chain 17	2.5	0.0332	18
4437	MSH3	Muts Homolog 3 (E. Coli)	2.6	0.0030	23
10447	FAM3C	Family With Sequence Similarity 3, Member C	2.6	0.0392	19
6169	RPL38	Ribosomal Protein L38	2.6	0.0419	30
8208	CHAF1B	Chromatin Assembly Factor 1, Subunit B (P60)	2.6	0.0293	27
9656	MDC1	Mediator Of Dna-Damage Checkpoint 1	2.7	0.0001	117
55681	SCYL2	Scy1-Like 2 (S. Cerevisiae)	2.7	0.0856	17
8976	WASL	Wiskott-Aldrich Syndrome-Like	2.7	0.0441	11
6888	TALDO1	Transaldolase 1	2.8	0.0123	22
63922	CHTF18	Ctf18, Chromosome Transmission Fidelity Factor 18 Homolog (S. Cerevisiae)	2.8	0.0796	15
327	APEH	N-Acylaminoacyl-Peptide Hydrolase	2.8	0.0044	54
3052	HCCS	Holocytochrome C Synthase (Cytochrome C Heme-Lyase)	2.8	0.0184	15
1663	DDX11	Dead/H (Asp-Glu-Ala-Asp/His) Box Polypeptide 11 (Chl1-Like Helicase Homolog, S. Cerevisiae)	2.9	0.0572	13
51719	CAB39	Calcium Binding Protein 39	3.0	0.0303	14
3162	HMOX1	Heme Oxygenase (Decycling) 1	3.0	0.0301	12
55768	NGLY1	N-Glycanase 1	3.0	0.0289	9
10554	AGPAT1	1-Acylglycerol-3-Phosphate O-Acyltransferase 1	3.0	0.0289	9
160418	TMTC3	Transmembrane And Tetratricopeptide Repeat Containing 3	3.1	0.0029	45
9590	AKAP12	A Kinase (Prka) Anchor Protein 12	3.2	0.0097	16
9114	ATP6V0D1	Atpase, H+ Transporting, Lysosomal 38Kda, V0 Subunit D1	3.2	0.0708	10
55215	FANCI	Fanconi Anemia, Complementation Group I	3.3	0.0000	186
92092	ZC3HAV1L	Zinc Finger Cch-Type, Antiviral 1-Like	3.3	0.0411	12
119559	SFXN4	Sideroflexin 4	3.3	0.0553	10
5257	PHKB	Phosphorylase Kinase, Beta	3.4	0.0386	15
81502	HM13	Histocompatibility (Minor) 13	3.4	0.0339	13
51605	TRMT6	Trna Methyltransferase 6 Homolog (S. Cerevisiae)	3.4	0.0073	16
56889	TM9SF3	Transmembrane 9 Superfamily Member 3	3.4	0.0063	17
83732	RIOK1	Rio Kinase 1 (Yeast)	3.5	0.0679	8
2937	GSS	Glutathione Synthetase	3.6	0.0096	19
60681	FKBP10	Fk506 Binding Protein 10, 65 Kda	3.7	0.0813	10
259217	HSPA12A	Heat Shock 70Kda Protein 12A	3.7	0.0451	11
28998	MRPL13	Mitochondrial Ribosomal Protein L13	3.8	0.0067	21
26007	DAK	Dihydroxyacetone Kinase 2 Homolog (S. Cerevisiae)	3.8	0.0007	19
48	ACO1	Aconitase 1, Soluble	4.0	0.0195	13
10573	MRPL28	Mitochondrial Ribosomal Protein L28	4.0	0.0209	40
51477	ISYNA1	Inositol-3-Phosphate Synthase 1	4.0	0.0069	18
27250	PDCD4	Programmed Cell Death 4 (Neoplastic Transformation Inhibitor)	4.2	0.0102	17
55697	VAC14	Vac14 Homolog (S. Cerevisiae)	4.5	0.0328	17
23043	TNIK	Traf2 And Nck Interacting Kinase	4.5	0.0196	9

Continued Table 5.3. Proteins significantly enriched on nascent chromatin during replication fork stalling.

Entrez ID	Official symbol	Name	Median Enrichment	Median p-value	Median Spectral counts
11073	TOPBP1	Topoisomerase (Dna) Ii Binding Protein 1	4.5	0.0063	18
8634	RTCD1	Rna Terminal Phosphate Cyclase Domain 1	4.7	0.0019	14
114883	OSBPL9	Oxysterol Binding Protein-Like 9	4.9	0.0065	14
23397	NCAPH	Non-Smc Condensin I Complex, Subunit H	5.0	0.0045	19
8927	BSN	Bassoon (Presynaptic Cytomatrix Protein)	5.0	0.0423	5
9513	FXR2	Fragile X Mental Retardation, Autosomal Homolog 2	5.7	0.0027	17
57698	KIAA1598	Kiaa1598	5.7	0.0033	13
9368	SLC9A3R1	Solute Carrier Family 9 (Sodium/Hydrogen Exchanger), Member 3 Regulator 1	6.0	0.0557	6
56916	SMARCAD1	Swi/Snf-Related, Matrix-Associated Actin-Dependent Regulator Of Chromatin, Subfamily A, Containing Dead/H Box 1	6.0	0.0493	12
90231	KIAA2013	Kiaa2013	6.0	0.0313	6
55101	ATP5SL	Atp5S-Like	7.0	0.0203	6
10989	IMMT	Inner Membrane Protein, Mitochondrial (Mitofilin)	7.0	0.0076	12
2177	FANCD2	Fanconi Anemia, Complementation Group D2	7.2	0.0004	58
23167	EFR3A	Efr3 Homolog A (S. Cerevisiae)	9.0	0.0329	9
9517	SPTLC2	Serine Palmitoyltransferase, Long Chain Base Subunit 2	11.0	0.0029	11
51199	NIN	Ninein (Gsk3B Interacting Protein)	12.0	0.0101	12
1291	COL6A1	Collagen, Type Vi, Alpha 1	12.0	0.0437	12
5810	RAD1	Rad1 Homolog (S. Pombe)	57297.5	0.0425	5
399687	MYO18A	Myosin Xviiia	79037.2	0.0917	6
84033	OBSCN	Obscurin, Cytoskeletal Calmodulin And Titin-Interacting Rhogef	152603.8	0.0948	5
8688	KRT37	Keratin 37	195494434.4	0.0270	11
284110	GSDMA	Gasdermin A	241549526.6	0.0300	5
3658	IREB2	Iron-Responsive Element Binding Protein 2	264604246.8	0.0450	5.5
79646	PANK3	Pantothenate Kinase 3	289859428.7	0.0090	6
26292	MYCBP	C-Myc Binding Protein	656599691.0	0.0008	5
26658	OR7C2	Olfactory Receptor, Family 7, Subfamily C, Member 2	656599691.0	0.0008	5
147912	SIX5	Six Homeobox 5	656599691.0	0.0008	5
9833	MELK	Maternal Embryonic Leucine Zipper Kinase	656599694.6	0.0033	5
9757	MLL4	Myeloid/Lymphoid Or Mixed-Lineage Leukemia 4	656599700.1	0.0008	5
2717	GLA	Galactosidase, Alpha	656599703.2	0.0008	5
80208	SPG11	Spastic Paraplegia 11 (Autosomal Recessive)	656599713.7	0.0008	5
5598	MAPK7	Mitogen-Activated Protein Kinase 7	656599733.5	0.0008	5
51604	PIGT	Phosphatidylinositol Glycan Anchor Biosynthesis, Class T	1181879433.9	0.0003	9
10919	EHMT2	Euchromatic Histone-Lysine N-Methyltransferase 2	2855716504.9	0.0002	8
8554	PIAS1	Protein Inhibitor Of Activated Stat, 1	3192788694.0	0.0002	9
800	CALD1	Caldesmon 1	5821982068.5	0.0000	7

Legend	Protein
	known
	discussed

Legend	p-value
	<0.01
	0.01-0.05
	0.05-0.1

The ATR inhibited and collapsed replisome with associated proteins

The iPOND-MS proteins enriched at collapsed forks were plotted as described in Fig. 5.4 to examine the distribution of proteins at replication forks that become unstable during replication stress without ATR. As noted before, QuasiTel statistical analyses overestimate the relative fold enrichment when zero spectral counts are detected in the chromatin chase control. Thus, the top 18 most enriched proteins listed in Table 5.4 are outside the linear range plotted in Fig. 5.4.

One such highly enriched protein is the methyl methansulfonate-sensitivity protein MMS22L (Table 5.4). In complex with the DNA repair protein TONSL, MMS22L is recruited to sites of RPA-coated ssDNA to promote recombinatorial repair of damaged replication forks [126-128]. TONSL was also found highly enriched (8-fold) at collapsed replication forks (highlighted in Table 5.4). The MMS22L-TONSL complex facilitates HR after DNA end resection through promoting Rad51 filament formation. Interestingly, Rad51 was also found highly enriched at ATR inhibited forks (Table 5.4). Other known DDR proteins present at ATR inhibited forks play roles in DSB repair. Factors such as BRIP1 and MCD1 harbor BRCT motifs that bind phosphorylated proteins important for DNA repair. Collectively, this supports the idea that ATR prevents aberrant processing of unstable replication forks into DSBs and limits the accumulation of DNA repair factors at replication forks.

A

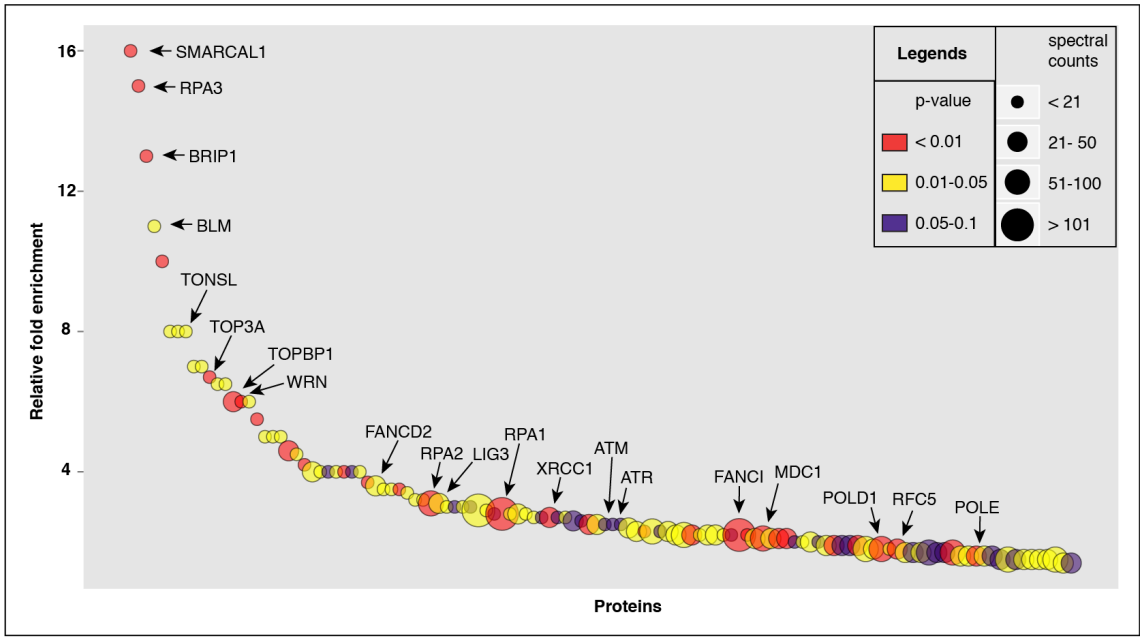

B

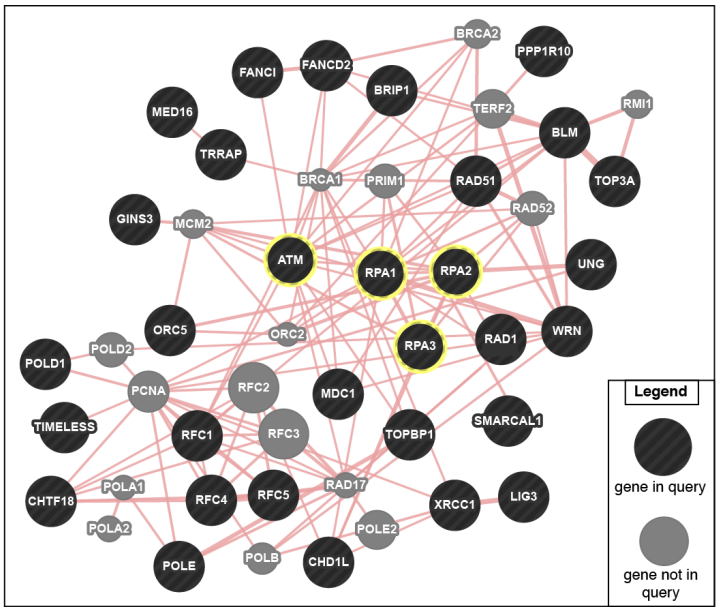

C

Proteins with PCNA-interacting motifs (PIP and APIM)	ATM/ATR putative substrates	Genome maintenance genes
BTAF1	ATM	ADD1
GTF3C3	CHTF18	BRIP1
MED16	FANCD2	COMT
TONSL	FANCI	CUL2
TRRAP	MDC1	DMD
UNG	PDS5B	DNPH1
WRN	POLE	FANCI
	RFC1	INCENP
RPA-interacting proteins	RPA1	JMJD6
	SART3	KIAA1598
BLM	SMARCAD1	NBAS
BRIP1	TOPBP1	PDCD4
CHD1L	TRMT6	PGM3
CUL3	WRN	PLIN3
ORC5		PLRG1
RAD1		RDH14
RAD51		RPA1
SMARCAL1		RPA2
TOP3A		RPA3
TOPBP1		SLC25A17
UNG		TIMELESS
WRN		TRMT6
		XPO5

Figure 5.4. iPOND-MS identifies proteins significantly enriched on replicating DNA after replication stress and ATR inhibition. (A) The fold enrichment relative to the chromatin chase negative control, the p-value and the spectral count data, which passed the filtering criteria described in the text, are depicted for the proteins listed in Table 5.4, which passed the filtering criteria described in the text. The dot size indicates the total number of MS spectra counted in the collapsed replication fork samples from the five replicate purifications. The dot color represents p-value as calculated using QuasiTel. The dot plots were generated in R by Yaoyi Chen. (B) Protein network analyses probed the physical interactions at collapsed replication forks using the GeneMANIA prediction server. Yellow highlight indicates proteins known to function or accumulate after ATR inhibition. (C) List of iPOND-MS collapsed replication fork proteins that either: contain potential PCNA interacting motifs, are annotated to interact with RPA1 or RPA2 according to GeneMANIA, are predicted ATM/ATR substrates, or cause DNA damage when depleted.

Table 5.4. Proteins significantly enriched on nascent chromatin during ATR inhibition at stalled replication forks. Hayes McDonald performed QuasiTel comparisons between collapsed replication fork samples and negative controls.

Entrez ID	Official symbol	Name	Median Enrichment	Median p-value	Median Spectral counts
26128	KIAA1279	Kiaa1279	1.4	0.0176	35
9733	SART3	Squamous Cell Carcinoma Antigen Recognized By T Cells 3	1.4	0.0719	43
9330	GTF3C3	General Transcription Factor Iiic, Polypeptide 3, 102Kda	1.5	0.0644	38
760	CA2	Carbonic Anhydrase Ii	1.5	0.0118	61
403	ARL3	Adp-Ribosylation Factor-Like 3	1.5	0.0607	22
57510	XPO5	Exportin 5	1.5	0.0221	44
65080	MRPL44	Mitochondrial Ribosomal Protein L44	1.5	0.0397	28
23196	FAM120A	Family With Sequence Similarity 120A	1.5	0.0154	33
64225	ATL2	Atlastin Gtpase 2	1.5	0.0469	25
5701	PSMC2	Proteasome (Prosome, Macropain) 26S Subunit, Atpase, 2	1.5	0.0105	66
118	ADD1	Adducin 1 (Alpha)	1.6	0.0205	22
51727	CMPK1	Cytidine Monophosphate (Ump-Cmp) Kinase 1, Cytosolic	1.6	0.0440	35
5426	POLE	Polymerase (Dna Directed), Epsilon	1.6	0.0042	45
5232	PGK2	Phosphoglycerate Kinase 2	1.6	0.0314	31
8453	CUL2	Cullin 2	1.6	0.0550	40
10613	ERLIN1	Er Lipid Raft Associated 1	1.7	0.0486	32
7174	TPP2	Tripeptidyl Peptidase Ii	1.7	0.0823	32
2805	GOT1	Glutamic-Oxaloacetic Transaminase 1, Soluble (Aspartate Aminotransferase 1)	1.7	0.0334	33
8452	CUL3	Cullin 3	1.7	0.0667	56
8295	TRRAP	Transformation/Transcription Domain-Associated Protein	1.7	0.0608	28
51651	PTRH2	Peptidyl-Trna Hydrolase 2	1.7	0.0629	26
166378	SPATA5	Spermatogenesis Associated 5	1.7	0.0025	72
5984	RFC4	Replication Factor C (Activator 1) 4, 37Kda	1.8	0.0131	51
4128	MAOA	Monoamine Oxidase A	1.8	0.0480	46
5424	POLD1	Polymerase (Dna Directed), Delta 1, Catalytic Subunit 125Kda	1.8	0.0027	97
23471	TRAM1	Translocation Associated Membrane Protein 1	1.8	0.0380	11
5985	RFC5	Replication Factor C (Activator 1) 5, 36.5Kda	1.8	0.0038	46
10226	PLIN3	Mannose-6-Phosphate Receptor Binding Protein 1	1.9	0.0369	34
7386	UQCRFS1	Ubiquinol-Cytochrome C Reductase, Rieske Iron-Sulfur Polypeptide-Like 1	1.9	0.0001	36
25873	RPL36P14	Ribosomal Protein L36 Pseudogene 14	1.9	0.0888	23
56886	UGGT1	Udp-Glucose Ceramide Glucosyltransferase-Like 1	1.9	0.0687	33
83743	GRWD1	Glutamate-Rich Wd Repeat Containing 1	1.9	0.0068	33
51234	TMEM85	Transmembrane Protein 85	2.0	0.0955	7
81609	SNX27	Sorting Nexin Family Member 27	2.0	0.0472	20
5558	PRIM2	Primase, Dna, Polypeptide 2 (58Kda)	2.0	0.0201	40
1962	EHHADH	Enoyl-Coenzyme A, Hydratase/3-Hydroxyacyl Coenzyme A Dehydrogenase	2.0	0.0659	9
8402	SLC25A11	Solute Carrier Family 25 (Mitochondrial Carrier; Oxoglutarate Carrier), Member 11	2.1	0.0205	38
9656	MDC1	Mediator Of Dna-Damage Checkpoint 1	2.1	0.0006	93
55027	HEATR3	Heat Repeat Containing 3	2.1	0.0261	26
5981	RFC1	Replication Factor C (Activator 1) 1, 145Kda	2.1	0.0067	40
2171	FABP5	Fatty Acid Binding Protein 5 (Psoriasis-Associated)	2.1	0.0093	23
160418	TMTC3	Transmembrane And Tetratricopeptide Repeat Containing 3	2.2	0.0123	32
9897	KIAA0196	Kiaa0196	2.2	0.0393	56
5356	PLRG1	Pleiotropic Regulator 1 (Prl1 Homolog, Arabidopsis)	2.2	0.0047	40
26263	FBXO22OS	F-Box Protein 22	2.2	0.0409	14
55752	SEPT11	Septin 11	2.2	0.0251	26
10914	PAPOLA	Poly(A) Polymerase Alpha	2.2	0.0489	22
9942	XYLB	Xylulokinase Homolog (H. Influenzae)	2.2	0.0466	14
9777	TM9SF4	Transmembrane 9 Superfamily Protein Member 4	2.2	0.0935	11
55215	FANCI	Fanconi Anemia, Complementation Group I	2.2	0.0009	125

Continued Table 5.4. Proteins significantly enriched on nascent chromatin during ATR inhibition at stalled replication forks.

Entrez ID	Official symbol	Name	Median Enrichment	Median p-value	Median Spectral counts
5001	ORC5L	Origin Recognition Complex, Subunit 5-Like (Yeast)	2.2	0.0030	20
9044	BTAF1	Btaf1 Rna Polymerase Ii, B-Tfiid Transcription Factor-Associated, 170Kda (Mot1 Homolog, S. Cerevisiae)	2.3	0.0260	21
55218	EXD2	Exonuclease 3'-5' Domain Containing 2	2.3	0.0018	16
23047	PDS5B	Pds5, Regulator Of Cohesion Maintenance, Homolog B (S. Cerevisiae)	2.3	0.0420	60
3619	INCENP	Inner Centromere Protein Antigens 135/155Kda	2.3	0.0821	15
8914	TIMELESS	Timeless Homolog (Drosophila)	2.3	0.0320	21
84342	COG8	Peptide Deformylase (Mitochondrial); Component Of Oligomeric Golgi Complex 8	2.4	0.0289	23
22826	DNAJC8	Dnaj (Hsp40) Homolog, Subfamily C, Member 8	2.5	0.0011	31
48	ACO1	Aconitase 1, Soluble	2.5	0.0154	50
84993	UBL7	Ubiquitin-Like 7 (Bone Marrow Stromal Cell-Derived)	2.5	0.0966	5
545	ATR*	Ataxia Telangiectasia And Rad3 Related	2.5	0.0546	20
472	ATM	Similar To Serine-Protein Kinase Atm (Ataxia Telangiectasia Mutated)	2.5	0.0602	15
10550	ARL6IP5	Adp-Ribosylation-Like Factor 6 Interacting Protein 5	2.6	0.0519	23
11344	TWF2	Twinfilin, Actin-Binding Protein, Homolog 2 (Drosophila)	2.6	0.0762	14
29105	C16ORF80	Chromosome 16 Open Reading Frame 80	2.7	0.0431	16
5238	PGM3	Phosphoglucomutase 3	2.7	0.0616	17
7515	XRCC1	X-Ray Repair Complementing Defective Repair In Chinese Hamster Cells 1	2.7	0.0012	35
25820	ARIH1	Ariadne Homolog, Ubiquitin-Conjugating Enzyme E2 Binding Protein, 1 (Drosophila)	2.7	0.0602	11
63875	MRPL17	Mitochondrial Ribosomal Protein L17	2.7	0.0441	11
55697	VAC14	Vac14 Homolog (S. Cerevisiae)	2.8	0.0926	9
6117	RPA1	Replication Protein A1, 70Kda	2.8	0.0000	287
23133	PHF8	Phd Finger Protein 8	2.8	0.0411	12
10573	MRPL28	Mitochondrial Ribosomal Protein L28	2.8	0.0217	29
28998	MRPL13	Mitochondrial Ribosomal Protein L13	2.8	0.0268	17
3305	HSPA1L	Heat Shock 70Kda Protein 1-Like	2.9	0.0223	136
10478	SLC25A17	Solute Carrier Family 25 (Mitochondrial Carrier; Peroxisomal Membrane Protein, 34Kda), Member 17	2.9	0.0365	13
2937	GSS	Glutathione Synthetase	3.0	0.0366	17
5514	PPP1R10	Protein Phosphatase 1, Regulatory (Inhibitor) Subunit 10	3.0	0.0529	12
5269	SERPINB6	Serpin Peptidase Inhibitor, Clade B (Ovalbumin), Member 6	3.0	0.0125	18
10016	PDCD6	Programmed Cell Death 6	3.0	0.0651	12
6118	RPA2	Replication Protein A2, 32Kda	3.1	0.0010	55
3980	LIG3	Ligase Iii, Dna, Atp-Dependent	3.1	0.0183	30
79654	HECTD3	Hect Domain Containing 3	3.2	0.0392	16
51594	NBAS	Neuroblastoma Amplified Sequence	3.2	0.0456	13
51605	TRMT6	Trna Methyltransferase 6 Homolog (S. Cerevisiae)	3.4	0.0249	16
60681	FKBP10	Fk506 Binding Protein 10, 65 Kda	3.5	0.0489	9
7570	ZNF22	Zinc Finger Protein 22 (Kox 15)	3.5	0.0387	7
29925	MRPL37	Mitochondrial Ribosomal Protein L37	3.5	0.0078	14
2177	FANCD2	Fanconi Anemia, Complementation Group D2	3.6	0.0172	30
8776	MTMR1	Myotubularin Related Protein 1	3.7	0.0011	18
63922	CHTF18	Ctf18, Chromosome Transmission Fidelity Factor 18 Homolog (S. Cerevisiae)	4.0	0.0269	21
1312	COMT	Catechol-O-Methyltransferase	4.0	0.0379	8
57665	RDH14	Retinol Dehydrogenase 14 (All-Trans/9-Cis/11-Cis); 5'-Nucleotidase, Cytosolic Ib	4.0	0.0571	8
51477	ISYNA1	Inositol-3-Phosphate Synthase 1	4.0	0.0173	19
23549	DNPEP	Aspartyl Aminopeptidase	4.0	0.0079	16
10025	MED16	Mediator Complex Subunit 16	4.0	0.0995	11
8526	DGKE	Diacylglycerol Kinase, Epsilon 64Kda	4.0	0.0313	7
27250	PDCD4	Programmed Cell Death 4 (Neoplastic Transformation Inhibitor)	4.2	0.0059	14
6811	STX5	Syntaxin 5	4.5	0.0102	9
26007	DAK	Dihydroxyacetone Kinase 2 Homolog (S. Cerevisiae)	4.6	0.0024	23

Continued Table 5.4. Proteins significantly enriched on nascent chromatin during ATR inhibition at stalled replication forks.

Entrez ID	Official symbol	Name	Median Enrichment	Median p-value	Median Spectral counts
5875	RABGGTA	Rab Geranylgeranyltransferase, Alpha Subunit	5.0	0.0423	6
253635	CCDC75	Coiled-Coil Domain Containing 75	5.0	0.0423	5
57698	KIAA1598	Kiaa1598	5.0	0.0348	14
10325	RRAGB	Ras-Related Gtp Binding B	5.5	0.0071	11
11073	TOPBP1	Topoisomerase (Dna) Ii Binding Protein 1	6.0	0.0005	24
7486	WRN	Similar To Werner Syndrome Protein; Werner Syndrome, Recq Helicase-Like	6.0	0.0089	14
7374	UNG	Uracil-Dna Glycosylase	6.0	0.0371	12
10989	IMMT	Inner Membrane Protein, Mitochondrial (Mitofilin)	6.5	0.0116	11
56916	SMARCAD1	Swi/Snf-Related, Matrix-Associated Actin-Dependent Regulator Of Chromatin, Subfamily A, Containing Dead/H Box 1	6.5	0.0322	13
7156	TOP3A	Topoisomerase (Dna) Iii Alpha	6.7	0.0036	20
9557	CHD1L	Chromodomain Helicase Dna Binding Protein 1-Like	7.0	0.0141	11
22904	SBNO2	Strawberry Notch Homolog 2 (Drosophila)	7.0	0.0203	7
10591	DNPH1	2'-Deoxynucleoside 5'-phosphate N-hydrolase 1	8.0	0.0309	8
4796	TONSL	Tonsoku-like; DNA repair protein	8.0	0.0309	8
9538	EI24	Etoposide Induced 2.4 Mrna	8.0	0.0120	7
6522	SLC4A2	Solute Carrier Family 4, Anion Exchanger, Member 2	10.0	0.0058	5
641	BLM	Bloom Syndrome, Recq Helicase-Like	11.0	0.0178	17
83990	BRIP1	Brca1 Interacting Protein C-Terminal Helicase 1	13.0	0.0025	13
6119	RPA3	Replication Protein A3, 14Kda	15.0	0.0024	15
50485	SMARCAL1	Swi/Snf Related, Matrix Associated, Actin Dependent Regulator Of Chromatin, Subfamily A-Like 1	16.0	0.0005	16
80856	KIAA1715	Kiaa1715	57297	0.0425	5
9527	GOSR1	Golgi Snap Receptor Complex Member 1	67795	0.0131	6
253714	MMS22L	MMS22-like, DNA repair protein	85755	0.0156	7.5
51604	PIGT	Phosphatidylinositol Glycan Anchor Biosynthesis, Class T	241288	0.0422	8.5
9910	RABGAP1L	Rab Gtpase Activating Protein 1-Like	289859431	0.0090	6
49855	SCAPER	S-Phase Cyclin A-Associated Protein In The Er	656599691	0.0161	5
201475	RAB12	Rab12, Member Ras Oncogene Family	656599691	0.0058	5
56955	MEPE	Matrix Extracellular Phosphoglycoprotein	656599696	0.0058	5
91875	TTC5	Tetratricopeptide Repeat Domain 5	656599708	0.0058	5
10776	ARPP19	Camp-Regulated Phosphoprotein, 19Kda	656599709	0.0058	5
118426	LOH12CR1	Loss Of Heterozygosity, 12, Chromosomal Region 1	656599732	0.0058	5
5810	RAD1	Rad1 Homolog (S. Pombe)	656599732	0.0008	5
195977	ANTXRL	Anthrax Toxin Receptor-Like	656599732	0.0008	5
23210	JMJD6	Jumonji Domain Containing 6	719268928	0.0007	5.5
5888	RAD51	Rad51 Homolog (Reca Homolog, E. Coli) (S. Cerevisiae)	787919631	0.0035	6
5908	RAP1B	Rap1B, Member Of Ras Oncogene Family	787919645	0.0035	6
1756	DMD	Dystrophin	35849128351	0.0000	5
64785	GINS3	Gins Complex Subunit 3 (Psf3 Homolog)	35849128461	0.0000	5

Legend	Protein
	known
	discussed

Legend	p-value
	<0.01
	0.01-0.05
	0.05-0.1

To examine physical interactions at collapsed replication forks, I queried the GeneMANIA bioinformatics database [74], which revealed that one-fourth of the identified proteins form a tight network (Fig. 5.4B). ATM and the heterotrimeric RPA complex are highlighted as major contributors to the system. The recruitment of ATM is consistent with genetic studies demonstrating that ATR inhibition activates ATM [61] and we have directly detected DSB formation after ATR inhibition using comet assays (Couch FB and Cortez, unpublished results). These findings support the idea that DSB formation is prevalent at ATR inhibited replication forks. Furthermore, RPA subunits were also highly enriched at collapsed forks (Table 5.4). This provides additional support to the idea that iPOND-MS purifies forks that have collapsed into DSBs and recombinogenic structures.

Since RPA accumulated at collapsed forks, I next assessed whether any of the identified proteins are known to interact with RPA. Several disease-associated helicases including the Blooms Syndrome protein BLM, the oncogene and chromodomain helicase CHD1L (also known as ALC1), the SIOD syndrome mutated annealing helicase SMARCAL1, and the Werner Syndrome RecQ helicase WRN were highly enriched at collapsed replication forks (Fig. 5.4C) [129, 130]. Other RPA1 or RPA2 binding proteins linked to DNA damage responses (BRIP1, CUL3, TOP3A, TOPBP1 and UNG) were also detected at ATR inhibited forks (Fig. 5.4C).

Furthermore, RPA-coated ssDNA is the checkpoint-activating structure for the recruitment of ATR [14]. Although slightly below the filtering criteria for significance (p-value of 0.0546), ATR was enriched at collapsed forks and included in Table 5.4 (marked * for insignificant). The ATR activating protein TOPBP1 accumulated as well, although most ATR molecules are likely inactive under these conditions. Collectively, iPOND-MS purification of collapsed replication forks identified numerous RPA-interacting proteins.

To determine if the collapsed fork protein dataset contains genes previously linked to DNA damage response signaling, I cross-referenced several genomic and proteomic screens [41, 123-125]. Sixteen identified proteins are potential ATM/ATR substrates (p-value 0.03, hypergeometric test, see Chapter II) and 23 of the proteins may cause DNA damage when deleted (Fig. 5.4C). Overall, iPOND purification of collapsed replication forks led to the identification of several high confidence genome maintenance proteins.

Prioritization and validation of replication fork proteins identified with iPOND-MS

To prioritize the 244 novel proteins identified in the iPOND-MS screens, my initial strategies for narrowing the list of proteins of interest included: (a) applying stringent filtering criteria for fold enrichment relative to two negative controls, requiring a low p-value derived from QuasiTel statistical analyses of raw spectral counts, and high spectral count values; (b) cross-referencing the dataset with genomic and proteomics screens that identified DNA damage response

proteins [41, 123-125]; (c) searching bioinformatics databases for references to predicted domains implicated in replication or repair [73, 74]; (d) performing extensive literature searches to find proteins of interest. Proteins containing domains linked to DNA replication (eg. PCNA-interacting motifs) [122], having predicted enzymatic activity (ATPase domains) [73], and other known functional domains were ranked with highest interest. A broad initial prioritization of proteins that fulfilled at least one of these criteria led to 148 proteins of interest (Appendix B).

To further narrow the list of replication fork proteins of interest, a high-throughput immunofluorescence screen was performed to find genes that function similarly to ATR (Kavanaugh G, unpublished data). Silencing of ATR causes DNA damage and compromises the restart of persistently stalled replication forks [14]. To find ATR-like genes, the 148 genes of interest were silenced using 4 siRNAs and the phosphorylation of H2AX and incorporation of EdU were measured after release from treatment with HU. ATR silencing results in high γH2AX and low EdU values since forks collapse into DSBs and do not resume DNA synthesis. Thus, an ATR-like gene would be predicted to have high γH2AX and low EdU values (a high 'ATR-like score') (Fig. 5.5).

Silencing of the chromatin remodeler SNF2L and the phosphatase PPP1R10 exhibited an ATR-like phenotype with 3 of 4 siRNAs (Fig 5.5). Interestingly, the chromatin remodeler SNF2H, which is highly related to SNF2L, did not phenocopy loss of SNF2L in this screen.

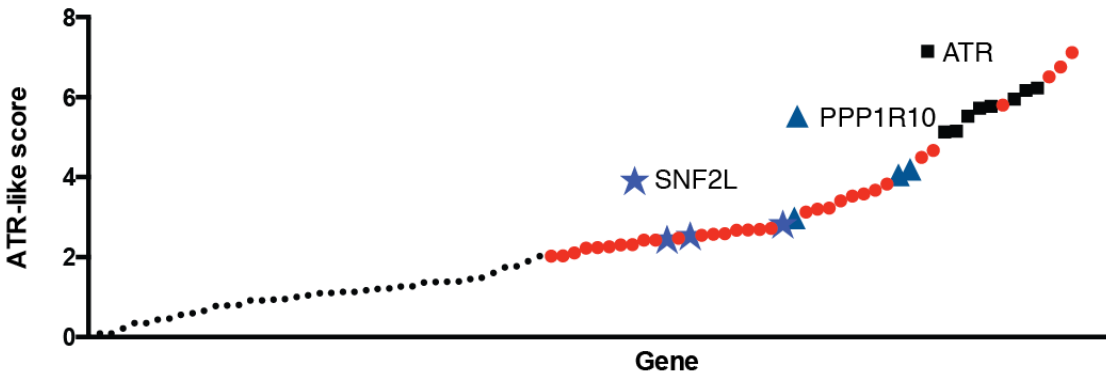

Figure 5.5 Functional genomic screen reveals SNF2L and PPP1R10 function in the DNA damage response. Cells depleted of SNF2L and PPP1R10 were treated with HU for 24 hours, released from replication stress, and pulse labeled with EdU to monitor restart of DNA replication. The immunofluorescence screen monitored fork restart (EdU incorporation) and phosphorylation of histone H2AX (a marker of DNA damage). The ATR-like score plotted on the y axis represents the average ratio of γH2AX to EdU values obtained for individual siRNAs targeting the genes of interest. ATR-like scores were calculated from individual nuclei visualized in the screen. The red dot color indicates a significant ATR-like score for the specified siRNA. Statistical significance relative to non-targeting siRNA negative control was calculated using Wilcoxin sum rank statistical testing. The plotted dots represent the 16 genes that exhibited significant ATR-like scores with at least 2 of 4 siRNAs tested.

While it is tempting to speculate that the two remodelers may function in separate genetic pathways, more experiments are needed to directly test this hypothesis (see Chapter VI). SNF2L was deemed of highest interest and pursued for further validation and preliminary functional characterization.

The chromatin remodeler SNF2L localizes to elongating replication forks

To validate SNF2L localization to elongating replication forks, two independent iPOND identification methods were employed. First, quantitative MS in selected reaction monitoring (SRM) mode was used to determine the enrichment of SNF2L on nascent chromatin. The same experimental framework was used for SRM analyses as that used in the original iPOND-MS screen (Fig. 5.1A). The signal intensities showed an enrichment of SNF2L and the positive control BAZ1B at elongating replication forks relative to the chromatin chase (Fig. 5.6B-E). Detection of RPA2 enrichment at collapsed replication forks (SRM sample 5) indicates that the iPOND-SRM method identified proteins enriched with a maximum 3-fold range of detection. The RPA binding protein UNG and the ATPase ATAD2 were also validated using iPOND-SRM (Fig. C.1.).

The second SNF2L validation method used a standard iPOND purification scheme followed by immunoblotting. SNF2L and the related chromatin remodeler SNF2H accumulated on nascent DNA at elongating replication forks (Fig. 5.6F).

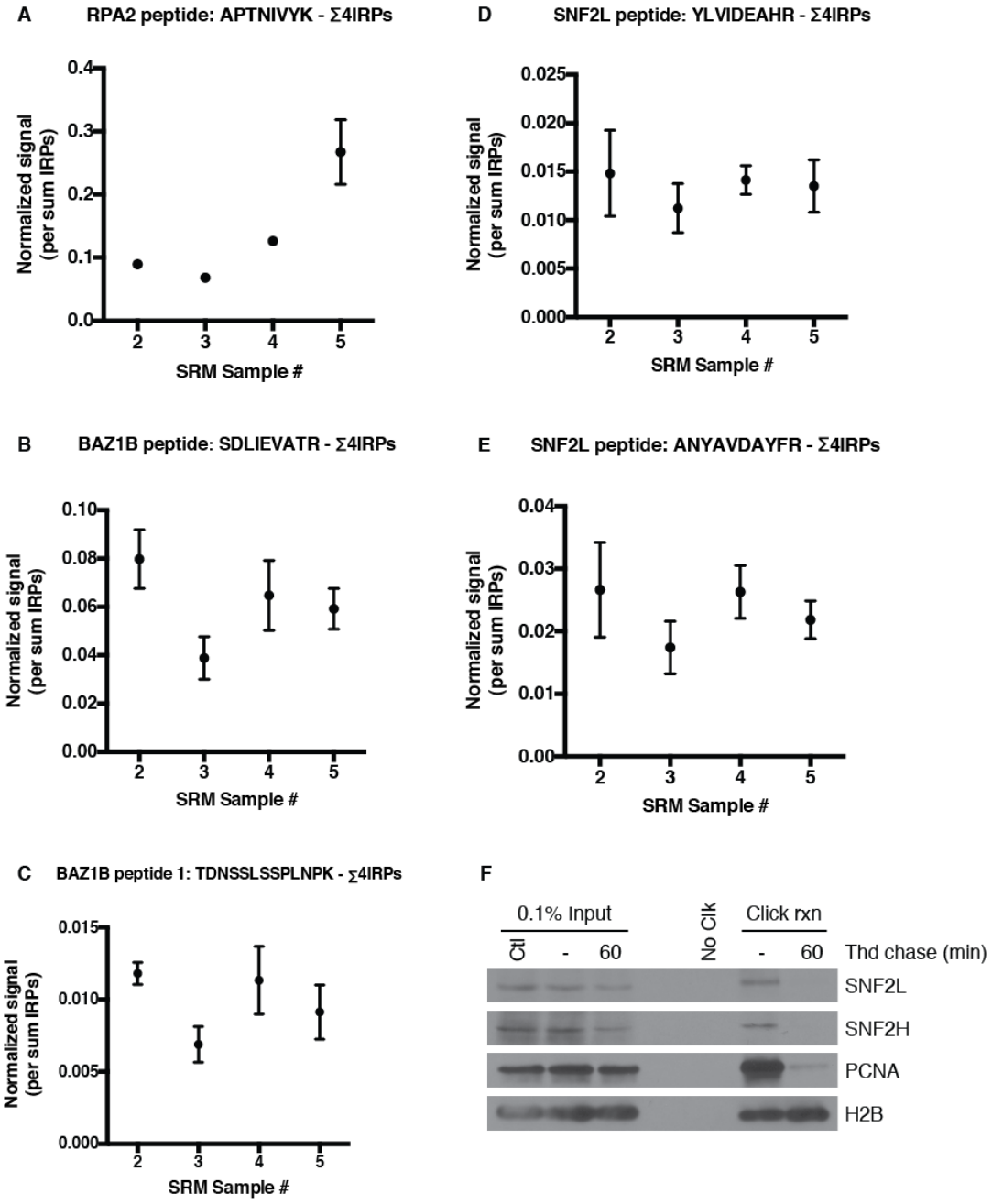

Figure 5.6. Validation of SNF2L association with elongating replication forks. (A–E) Quantitative mass spectrometry in selected reaction monitoring mode (SRM) examined the indicated peptides for RPA2, BAZ1B, and SNF2L after iPOND purifications and was performed by David Friedman in the Vanderbilt Proteomics Core. SRM samples 2, 3, 4, and 5 represent normal replication forks, thymidine chase negative control, HU-treated stalled forks, HU and ATR inhibited collapsed forks, respectively. The signal intensity measured for each peptide is normalized to the sum of the internal reference peptides (Σ4IRPs). (F) Cells labeled with EdU for 10 min were collected or chased into thymidine for 60 mins, iPOND was performed and followed by immunoblotting using antibodies specific to SNF2L and SNF2H.

To test if SNF2L functions in DNA replication, I silenced SNF2L with two siRNAs and examined nascent DNA fiber lengths after short labeling times with the nucleoside analogs IdU and CldU under unperturbed conditions. In one preliminary experiment, cells lacking SNF2L exhibited shorter DNA fibers, consistent with a function for SNF2L in fork progression (data not shown). Collectively, I validated that SNF2H, BAZ1B, and SNF2L localize to moving replication forks and provided preliminary evidence suggesting that SNF2L may promote replication fork progression.

Discussion

In this chapter, I coupled iPOND purification of replication forks with two-dimensional LC-MS/MS to identify the replisome components and nascent DNA-associating proteins under normal and DNA damage conditions. The iPOND-MS screen yielded a total of 290 proteins that were significantly enriched at elongating, HU-stalled, and ATR inhibited replication forks. The dataset included a statistically significant fraction of proteins known to function in DNA damage responses, cell cycle control, DNA repair and replication (Fig. 5.2D).

For example, at normally elongating replication forks, 15 of the top 20 most noteworthy proteins, as measured by fold enrichment and p-value, are established replisome components and chromatin replication factors. These include the replicative polymerases, PCNA, the replication-loading complex RFC (RFC1-5), and the chromatin assembly factors CAF1A and CAF1B. Although the number of positive controls identified at stalled forks is lower than those observed under unperturbed conditions, the dataset still enriched for DDR proteins above random chance of occurrence. Collapsed replication forks exhibited strong enrichment of RPA, double-strand break proteins, fork remodeling helicases, and replisome components.

Although numerous DNA replication and damage proteins were identified, not all components of the replisome were found enriched in my iPOND-MS studies. This may reflect poor fold enrichments of replisome proteins in the iPOND conditions used. Another group successfully identified the majority of the

replisome components using a similar iPOND-MS purification framework, but a different MS approach with a more sensitive MS instrument (see Chapter VI for further discussion on differences in both experimental conditions and MS analyses) [82]. Nonetheless, both screens identified the following 20 replisome components: ATAD5, BAZ1B, CHAF1A, CHAF1B, DNMT1, EXO1, LIG1, MSH2, MSH3, MSH6, PCNA, POLD1, POLE, RFC1-5, UHRF1, and WIZ. While 39 of the additional 48 replication fork proteins identified by the other group are known replication fork proteins, 64 additional proteins from my screen have not been associated with functions during DNA replication. This suggests that the biological false discovery rate in my iPOND-MS screen may be high and will require future optimization to increase the signal to noise ratio (see Chapter VI for further discussion on potential solutions).

Proteins that were observed at normal, stalled, and collapsed replication fork types and have previous links to DNA replication and the DNA damage response are discussed below.

EXO1 and mismatch repair activities at elongating replication forks

The exonuclease EXO1 was one of the highest enriched proteins at unperturbed replication forks in my study and was confirmed in a recently published iPOND-MS screen [82]. EXO1's best-established function is in extending DNA end resection of double-strand breaks after MRE11-dependent nicking [131]. In *S. cerevisiae* and *X. laevis,* EXO1's nucleolytic activity in the 5'-

to-3' direction generates a substrate for Rad51 binding and is essential for homology-directed repair [131-133]. Additionally, Exo1 possesses flap endonuclease activity that facilitates Okazaki fragment maturation [134].

At least in *S. cerevisiae,* EXO1 also functions in mismatch repair (MMR), a repair pathway activated during each S phase to remove bases mis-incorporated by DNA polymerases. EXO1 interacts with the MMR protein MSH2, which localizes in a complex with MSH3 or MSH6 to replication foci in a PCNA-dependent manner [135]. EXO1 excises mismatched bases encountered primarily on the lagging strand produced by the proofreading-deficient polymerase alpha [135, 136]. EXO1's role in MMR surveillance at replication forks is not as crucial as that of MSH2 since deletion of EXO1 causes fewer mutations than does deletion of MSH2 alone or a double knockout EXO1 and MSH2 mutant [137, 138]. It appears that EXO1 becomes most important for MMR when the MSH6-PCNA interaction is disrupted [135]. Perhaps EXO1 is needed when replication forks experience a high burden of base damage that canonical MMR proteins cannot repair alone.

My iPOND-MS results indicate an enrichment of the mammalian MMR proteins MSH2, MSH3 and MSH6 and EXO1, confirming that MMR activity is coupled to replisomes in higher organisms. These findings are further supported by another iPOND-MS screen that identified MMR proteins as the most enriched factors at forks after PCNA [82]. Since iPOND is an ensemble methodology, whether EXO1 and the MMR proteins co-localize and function to repair the same

nascent DNA fragment remains to be determined. Coupling iPOND to single molecule analyses would provide the necessary relative spatial resolution needed to answer this question.

Why such considerable enrichment of MMR at elongating forks? One possible explanation is that the MSH2-MSH3 and MSH3-MSH6 complexes are recruited to forks via interactions with PCNA and CAF1 [139, 140]. Aside from the endogenous base mis-incorporations that occur in each S phase, MMR proteins may recognize EdU labeled nascent DNA. Any damage due to EdU incorporation does not appear to activate the checkpoint as measured by the lack of H2AX phosphorylation at iPOND purified elongating replication forks (see previous chapters).

Fanconi anemia proteins at replication forks

The Fanconi anemia mutated FANCI and FANCD2 genes encode intercrosslink repair proteins and were found highly enriched at stalled and collapsed replication forks (Table 5.3 and 5.4). Current models pose that FANCI and FANCD2 function in complex (the ID complex) during interstrand crosslink repair [46]. These lesions are some of the most difficult to repair substrates, requiring specialized repair mechanisms governed by genes mutated in patients with Fanconi anemia (FA), as well as components of nucleotide excision and DSB repair [28]. Although FA patient-derived cells are hypersensitive to crosslinking reagents such as mitomycin C (MMC), lack of FANC ID renders cells

only mildly sensitive to HU, suggesting that the main function of the ID complex is during ICL repair and not replication stress [141].

Why would the ID complex enrich at stalled and collapsed forks? Perhaps DNA structures generated at stalled and collapsed forks resemble those at ICL repair sites. Indeed, recent structural studies indicate a preference of the ID complex for binding ssDNA-dsDNA junctions [142], a structure likely prevalent at replication forks as a result of polymerase-driven repriming events that promote checkpoint signaling [115, 143]. FANCI also passed the filtering criteria for enrichment at elongating replication forks while FANCD2 did not (Table 5.2-5.4). In support of an ID complex-independent role for FANCD2, recent evidence shows that FANCD2 may promote restart of aphidicholin-stalled replication forks independently of FANCI [144]. Collectively, the ID complex localizes to damaged replication forks and future work is needed to examine the function of this complex at normal, stalled and collapsed forks.

ATAD2 ATPase localization to replication forks

ATAD2 is an oncogene amplified in MYC-driven endometrial cancers [145] that I found localizes to elongating replication forks. Several lines of evidence make ATAD2 an attractive target for further studies. First, ATAD2 encodes an ATPase with a bromo domain that has been shown to bind acetylated H4K5 [146]. A testable hypothesis would pose that ATAD2's bromo domain localizes the protein to nascent chromatin that contains acetylated H4K5. Second, ATAD2

co-localizes with BrdU that marks actively replicating cells [145], although it is difficult to distinguish whether ATAD2 forms distinguishable S-phase foci. Third, ATAD2 depletion sensitizes breast cancer cell lines to the histone deacetylase inhibitor trichostatin-A [145]. This suggests that ATAD2 may be a good prognostic marker for HDAC inhibitors currently in clinical use. However, no publications address a mechanistic role for ATAD2 during DNA replication. Further validation and testing ATAD2 function at the replication fork should be of high interest for future studies.

Fork remodeling enzymes at ATR inhibited and collapsed replication forks

The high enrichment of the heterotrimeric ssDNA-binding protein RPA is a striking feature of stalled replication forks that collapse after ATR inhibition (Table 5.4, first observed independently by Jami FB Couch, unpublished results). Concomitant with RPA accumulation, I observed the enrichment of the disease-associated helicases BLM, CHD1L, SMARCAL1 and WRN, which are all RPA interacting proteins, suggesting that their enrichment at collapsed forks is at least partially due to RPA accumulation.

The formation of excess RPA-coated ssDNA at damaged forks may reflect aberrant fork remodeling activities driven by or normally resolved by these helicases. For example, SMARCAL1 is an SNF2 family ATPase that is activated by complex DNA structures and uses the energy of ATP hydrolysis to re-anneal DNA strands [47]. The WRN helicase unwinds a variety of complex DNA

structures. Both enzymes can catalyze regression of replication forks, generating a Holliday junction on model replication substrates [147-150]. SMARCAL1 and WRN also branch migrate the Holliday junctions, which could restore the normal fork structure via a reversed fork intermediate [39, 148].

Thus, ATR may stabilize a fork and prevent fork collapse and disease by restricting aberrant ATPase-dependent reorganization of DNA structures at stalled replication forks (Fig. 5.7). ATR directly phosphorylates both SMARCAL1 and WRN and cells expressing a non-phosphorylatable WRN mutant exhibit increased fork breakage [151]. DDR kinase phosphorylation of SMARCAL1 also controls the helicase's enzymatic activity (Couch, Bansbach and Cortez, unpublished results). Therefore, the accumulation of RPA and several helicases at stalled forks lacking ATR activity reflects an essential ATR function in blocking fork restructuring to ensure genome stability.

ATR may also restrict ssDNA accumulation by restraining fork movement driven by uncontrolled DNA unwinding. This concept is supported by the fact that ATR phosphorylates several replisome components including the Cdc45-MCM-GINS (CMG) helicase subunits [41, 152-156]. Phosphorylation of CMG may regulate helicase activity to prevent excessive unwinding and is necessary to promote rescue of stalled forks from adjacent origins [155, 156]. In yeast, lack of ATR activity causes ssDNA gaps as visualized by electron microscopy [39]. Such gaps may be the consequence of unproductive DNA polymerization coupled to unrestrained fork movement.

Single and double-strand break repair proteins at collapsed replication forks

I observed the enrichment of double-strand break repair (DSBR) and recombination proteins Rad51 and the MMS22L-TONSL complex at collapsed forks. This observation further supports the model that ATR limits collapse of stalled forks into DSBs, which may be resolved using recombinatiorial mechanisms (Fig. 5.7). Too many recombination events can cause abnormal fork structures, but too few events can prevent proper Rad51-mediated fork restart after DNA damage [39, 87].

In addition to DSBR factors, the single-strand break repair (SSBR) proteins XRCC1 and Ligase III showed significant enrichment (3-fold) when ATR was inhibited (Table 5.4). After IR, the damage-induced localization of these factors depends on PARP1-mediated poly(ADP-ribosyl)ation and the PAR-binding domains of XRCC1 and Ligase III [157, 158]. PARP1-mediated localization of XRCC1 and Ligase III to single-stranded DNA breaks is likely critical for cell survival in the absence of ATR. In support of this idea, knockdown of ATR is synthetic lethal with PARP inhibition [159]. It will be important to examine other synthetic lethal interactions following ATR inhibition to understand the potential mechanisms governing fork collapse. Inhibition of Ligase III may be an interesting therapeutic target given that Ligase III accumulates at ATR inhibited forks and both enzymes are currently being considered as single agent cancer treatments [160].

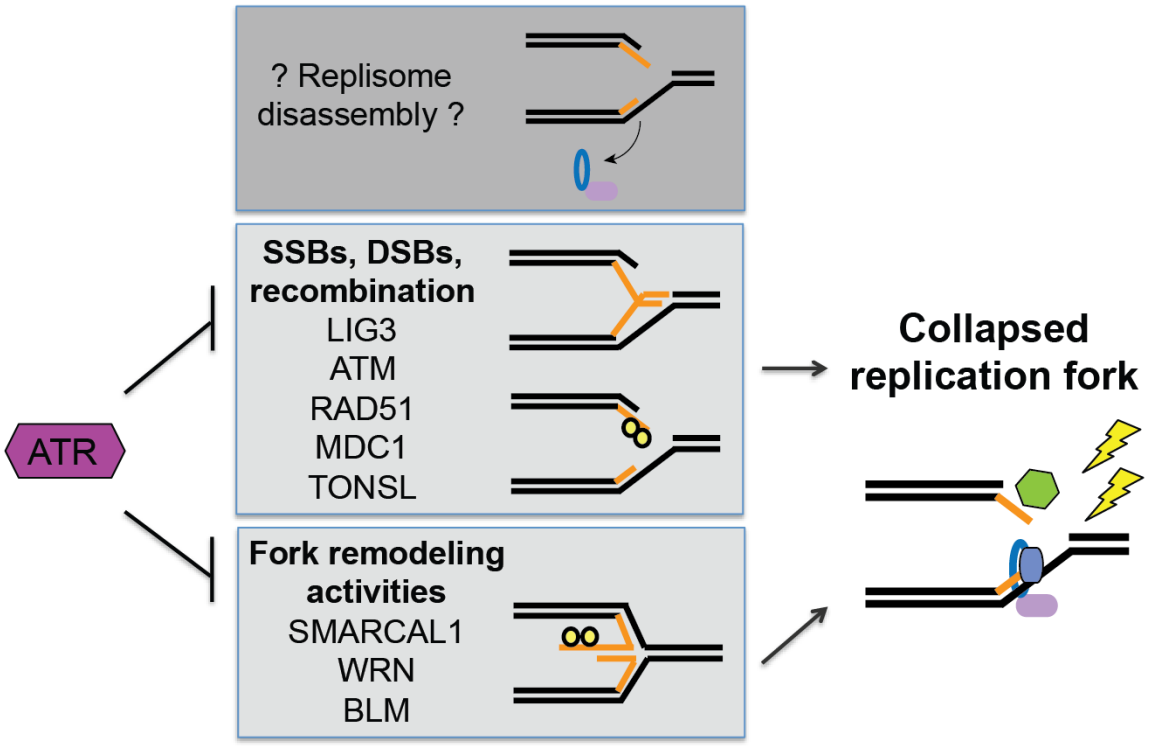

Figure 5.7. Model for how ATR prevents replication fork collapse. ATR prevents the accumulation of single and double-strand breaks and limits recombination and fork remodeling activities. Whether ATR stabilizes stalled replication forks by preventing replisome disassembly remains to be elucidated. Yellow circles represent RPA, which accumulates on nascent ssDNA generated when ATR is inhibited.

Replisome composition without ATR

I observed that ATR inhibited forks exhibit enrichment of the replicative polymerases (POLD1 and POLE) and the clamp loader complex (RFC1-5) similarly to elongating replication forks. Several possibilities may explain these results. One possibility is that a fraction of replication forks are still intact and have not collapsed. Another explanation is that an intact replisome is maintained at collapsed replication forks in mammalian cells. This could suggest that ATR activity is dispensable for replisome stability. Such a scenario would be in contrast to previous findings in yeast and Xenopus reporting loss of at least some replisome components in the absence of ATR function [35-37, 40], although recent biochemical evidence contests these results [156]. A third possibility is that replisomes are enriched on the nascent DNA generated at newly established replication forks. ATR inhibition causes new origin firing (Couch FB et al, publication in press), consistent with the established role of ATR in suppressing new origin firing in the presence of DNA damage. Since some level of origin firing occurs in the absence of ATR activity under these experimental conditions, I cannot determine if the mammalian replisome disassembles without ATR activity (Fig. 5.7).

Replicating and restoring chromatin after replication fork passage

Several SWI/SNF-like chromatin remodeling enzymes were enriched at replication forks including SMARCAD1, SNF2L and SNF2H. SMARCAD1

interacts with PCNA, which localizes the remodeler to replication forks where it promotes deacetylation of histones H3 and H4 [161, 162]. Deacetylation permits subsequent histone methylation of H3K9, a histone modification required to maintain heterochromatin domains and prevent aberrant transcription that threatens genome stability [162-164].

ISWI nucleosome remodelers localize to elongating replication forks

The highly related SNF2H and SNF2L chromatin remodelers represent the human homologs of the Drosophila ISWI complex responsible for regulating transcriptional and replication events [165]. In complex with BAZ1B, SNF2H is recruited to replication forks via an interaction with PCNA to maintain the chromatin landscape through DNA replication [166]. SNF2L's activity at replication forks has not been well described. A discussion of the potential role of SNF2L at replication forks is provided in Chapter VI.

Collectively, the use of iPOND as a screening platform for the identification of novel replication fork proteins could provide a discovery tool to examine the activities that maintain genomic and epigenomic integrity through DNA replication.

CHAPTER VI

SYNOPSIS AND FUTURE DIRECTIONS*

Synopsis

The *in vivo* analysis of dynamic events that protect genomic and epigenomic integrity during DNA replication has been a challenging task. The proteins that ensure the accurate inheritance of the genome act directly at replication forks. Unfortunately, tracking and purifying replication forks has been difficult in mammalian cells because the location of elongating forks is difficult to predict. I have developed the iPOND (isolation of Proteins On Nascent DNA) technique as a tool to isolate, analyze and discover proteins that localize to replication forks during active DNA replication and following conditions of DNA damage. The iPOND technique provides a useful tool to investigate the coordinated mechanisms that maintain the genome and epigenome through DNA replication. These pathways are perturbed in human diseases such as cancer.

Development of iPOND for analysis of normal, stalled and collapsed replication forks

In Chapter III, I described the development of iPOND as a technology to purify nascent DNA and the associated proteins from mammalian cells.

*Excerpts of this chapter are in published in reference [57]. Sirbu BM, Couch FB and Cortez D, *Nature Protocols.*

iPOND is based on the concept that replication forks are sites of active DNA polymerization that can incorporate tagged nucleoside analogs. I showed that labeling of short nascent DNA fragments with the thymidine analog EdU facilitates biotin-tagging of nascent DNA using click chemistry. Nascent DNA fragments with associated proteins are purified using streptavidin-conjugated beads in a single step. To validate this technique, I showed that replication fork proteins PCNA and CAF1 associate specifically with nascent chromatin at elongating replication forks but not with mature chromatin. The sensitivity of the technique permits the detection of low-copy number proteins such as polymerase epsilon, which is undetectable using standard immunofluorescent methods. I further establish iPOND as a tool for monitoring chromatin assembly *in vivo*.

iPOND analysis of chromatin maturation dynamics at elongating replication forks

In Chapter IV, I examined the enzymatic requirements for reestablishing epigenetic marks on nascent chromatin after replication fork passage. Unlike parental histones, new histones contain the evolutionarily conserved di-acetylation mark on histone H4 (H4K5ac/K12ac) [2]. I provide the first *in vivo* evidence that Class 1 histone deacetylases remove H4K5/K12 acetylation at elongating replication forks in mammalian cells. We showed that H4K12 is reacetylated on nascent DNA, suggesting a potential role for this modification independently of H4K5ac/K12ac. Previous circumstantial evidence had suggested that the HAT1 acetyltransferase catalyzes diacetylation of H4K5/K12. In collaboration with Mark Parthun's laboratory, I showed that murine HAT1 is the

acetyltransferase responsible for the replication-coupled di-acetylation of H4K5/K12. Collectively, iPOND analysis of chromatin maturation revealed the timely histone modifications essential for preserving genomic and epigenomic integrity [1, 88].

iPOND reveals changes in proteins and post-translational modifications at stalled and collapsed replication forks

In chapter IV, I furthermore investigated the recruitment dynamics of established DNA damage response proteins and the post-translational modifications (PTMs) to damaged replication forks. I found that replication fork stalling results in rapid phosphorylation of RPA on Serine 33 and is followed by phosphorylation on Serines 4/8, a mark associated with formation of double-strand breaks. An enrichment of double-strand break repair proteins RAD51, MRE11 and KU70/80 was detectable after prolonged treatment with HU, suggesting that DSBs and recombination-based repair occur. At DSBs, MRE11 end-resection facilitates loading of the Rad51 recombinase. Jami Couch showed that Rad51 accumulation at stalled forks is MRE11-dependent after prolonged, but not short exposures to replication stress. This suggests that MRE11 end-resection occurs at persistently stalled replication forks to promote homology-directed DNA repair.

γH2AX spreading from stalled replication forks depends on checkpoint kinases

Phosphorylation of the histone variant H2AX is often considered a marker of DSBs, but I observed γH2AX phosphorylation at stalled forks within 10 mins after replication stress. We detected H2AX phosphorylation in regions distal to the stalled replication fork, supporting the idea that γH2AX spreads from stalled replication forks. Lastly, we provide evidence that ATR catalyzes the early and proximal spreading of γH2AX. During prolonged replication stress, I showed that ATM and DNA-PK contribute to spreading and maintenance of γH2AX in chromosomal regions proximal and distal to the stalled replication fork.

iPOND-MS for discovery of genome and epigenome maintenance activities

To further demonstrate the utility of iPOND as a screening for discovery of genome maintenance activities, I coupled iPOND to spectral counting-based shotgun proteomics to identify new proteins that maintain genomic and epigenomic integrity during DNA replication. I was most interested in identifying proteins at elongating and stalled replication forks. To gain insights into how the ATR kinase prevents fork collapse into toxic DSBs, I also explored the replisome composition in the absence of ATR activity using an ATR inhibitor.

I identified 290 proteins significantly enriched at normal, stalled and collapsed replication forks. Forty-six of these proteins have been previously linked to DNA damage responses, DNA replication and the cell cycle. Several are predicted phosphorylation substrates of ATM/ATR, contain PCNA binding

domains, or have been identified in genomic screens aimed at finding genes that maintain genome stability.

The replisome components identified at unperturbed replication forks included some of the canonical replisome factors such as the replicative polymerases POLD1 and POLE, the processivity factor PCNA, and the clamp loader RFC1-5. Proteins that maintain the epigenomic landscape were also enriched. For example, DNA methyltransferase DNMT1 and the hemimethylated DNA binding protein UHRF1 preserve semiconservative DNA methylation at forks [2]. In contrast to unperturbed forks, iPOND detection of stalled replication forks revealed few expected proteins. Potential explanations for this result are described in the next section.

At collapsed replication forks, I validated previous observations that RPA accumulates on nascent strand ssDNA, a toxic structure that causes genomic instability. I discovered that several replication-fork remodeling enzymes that are found mutated in human diseases enrich at collapsed forks. The helicases SMARCAL1, WRN and BLM localized to collapsed forks, perhaps due to recruitment through RPA binding. ATR directly phosphorylates SMARCAL1 and BLM to regulate their enzymatic activities [151, 167]. This evidence supports the hypothesis that ATR prevents aberrant fork processing by inhibiting the accumulation of fork-remodeling enzymes. Without ATR regulation, these enzymes may drive the formation of aberrant and mutagenic DNA fork structures, causing genome instability. Furthermore, I discovered the enrichment of single-

strand and double-strand break repair proteins such as Ligase III, XRCC1, RAD51, MMS22L and TONSL. Recruitment of these proteins may represent an attempt to maintain competent stalled forks that can restart by initiating recombination-based rescue mechanisms.

Lastly, as validation for the iPOND-MS screen, I showed that the two human homologs of the ISWI chromatin remodeler SNF2L and SNF2H travel with elongating replication forks. While SNF2H has been implicated in replication of heterochromatin, the function of SNF2L during replication has remained unexplored. I provide preliminary genetic evidence that SNF2L facilitates replication fork progression.

Overall, the development of iPOND has provided a powerful biochemical tool to ascertain the mechanisms that maintain genome and epigenome integrity at replication forks. iPOND-MS revealed interesting observations about the proteomic changes as replication forks transition from elongating to stalling to collapsing. Improving the iPOND-MS platform and combining these findings with functional genomics screens should reveal critical targets that maintain replication fork stability.

Understanding the activities that preserve replication-coupled chromatin maintenance and repair is relevant to understanding human disease. Disturbances in these pathways cause mutations and replication stress. This genomic instability is the hallmark of diseases such as cancer. Overall, my thesis work has provided a new biochemical tool that can be exploited to answer

questions about how the genome and epigenome are preserved during DNA replication to prevent disease.

In the future directions section, I discuss (i) testable hypotheses addressing the function of SNF2L during DNA replication, (ii) interpretations of stalled and collapsed replication forks isolated with iPOND, (iii) comparisons to other recent iPOND-MS screens, (iv) potential biochemical improvements the iPOND platform for large-scale screening, (v) ideas for other applications of iPOND to improve spatial resolution and analyze the protein composition of replicating forks in various genomic regions.

Future Directions

(i) Functions of human ISWI chromatin remodelers at replication forks

I have validated the recruitment of the mammalian Imitation Switch (ISWI) chromatin remodeling enzymes SNF2L and SNF2H to elongating replication forks. The remodelers constitute the ATPase motors for several protein complexes that slide and replace histones to facilitate a variety of processes from transcription to preserving higher order chromatin organization to DNA replication [168]. SNF2H is recruited to replication sites in complex with BAZ1B, the gene deleted in the haploinsufficiency Williams-Beuren Syndrome [166, 169]. In this WICH complex, SNF2H promotes replication through heterochromatin and facilitates double-strand break repair [166, 170]. SNF2H also binds ACF1 to regulate replication of pericentromeric DNA, presumably by facilitating chromatin decondensation to allow proper chromatin assembly [171].

While SNF2H's function during DNA replication is well established, the significance of SNF2L recruitment to sites of active replication [172] is unclear. Several lines of evidence suggest a function for SNF2L during replication. First, a fraction of SNF2L is retained longer on chromatin during S phase [172]. Second, *Snf2l* mice expressing a mutant SNF2L with diminished catalytic activity exhibit increased brain sizes due to increased proliferation [173]. Third, I provided preliminary evidence showing that SNF2L depletion causes shorter nascent DNA fibers, suggestive of a role in promoting replication fork progression.

One significant unanswered question is whether SNF2L and SNF2H perform redundant roles during DNA replication. One preliminary piece of genetic data supporting distinct functions for the two remodelers is our observation that silencing of SNF2L but not SNF2H causes DNA damage during replication fork restart (Gina Kavanaugh, unpublished screen results). Also, the yeast ISWI1 and ISW2 complexes exhibit different *in vitro* biochemical activities in spacing of nucleosomes [174]. It is tempting to speculate that such distinct activities render distinct functions *in vivo.*

Despite high sequence similarities between the mammalian ISWIs, small differences in the amino and carboxy termini drive the formation of different protein complexes containing either SNF2L or SNF2H [168]. SNF2L's best-established role is as a component of the nucleosome remodeling NURF complex that functions in transcriptional regulation [175]. SNF2L has not been reported to interact with BAZ1B or ACF1, perhaps due to low protein expression in the cell models used to describe the formation of SNF2H-containing complexes [166, 169]. While SNF2H is expressed in a majority of cell lines and tissues, SNF2L's expression pattern is restricted to undifferentiated cell types and stem-cell like cell types [169, 176]. Therefore, it is plausible that SNF2L and SNF2H may perform similar functions at different developmental stages, but this hypothesis needs to be formally tested.

How does proper nucleosome positioning ensure proper DNA replication? In Figures 6.1-6.2, I present several testable models for SNF2L regulation of

DNA replication. Prior to testing these hypotheses, it will be important to confirm that SNF2L and/or SNF2H affect replication fork progression.

As depicted in Figure 6.1, SNF2L contains a conserved PCNA-interacting motif (PIP box). It is possible that SNF2L localization to replication forks depends on recruitment via PCNA. The localization of SNF2H to sites of heterochromatin replication depends on interaction with BAZ1B and BAZ1B's PIP box [166]. Elucidating the SNF2L-containing protein complexes in HEK 293T cells that were used for the iPOND-MS screen will provide insight into how SNF2L may be recruited to replication forks. Identifying the replication localization domain of SNF2L will be crucial to generate separation-of-function mutants. Such mutants will be necessary to complement any replication defects of SNF2L depletion. Alternatively, a fusion protein that could artificially localize SNF2L to replication forks would be useful. Either the mutant or fusion SNF2L proteins would be useful to test the hypothesis that SNF2L's role during DNA replication is independent of its role in transcription or at other genomic loci.

Further fiber labeling experiments in cells lacking SNF2L should test whether the remodeler could affect DNA replication by promoting origin firing (Fig. 6.2). The yeast Isw2 facilitates replication of late origins [177], perhaps through a role in chromatin remodeling of origins. Clearly, much remains to be studied about SNF2L's role during replication, but these examinations could provide important insights into how ATP-dependent chromatin remodelers maintain genome integrity at the replication fork.

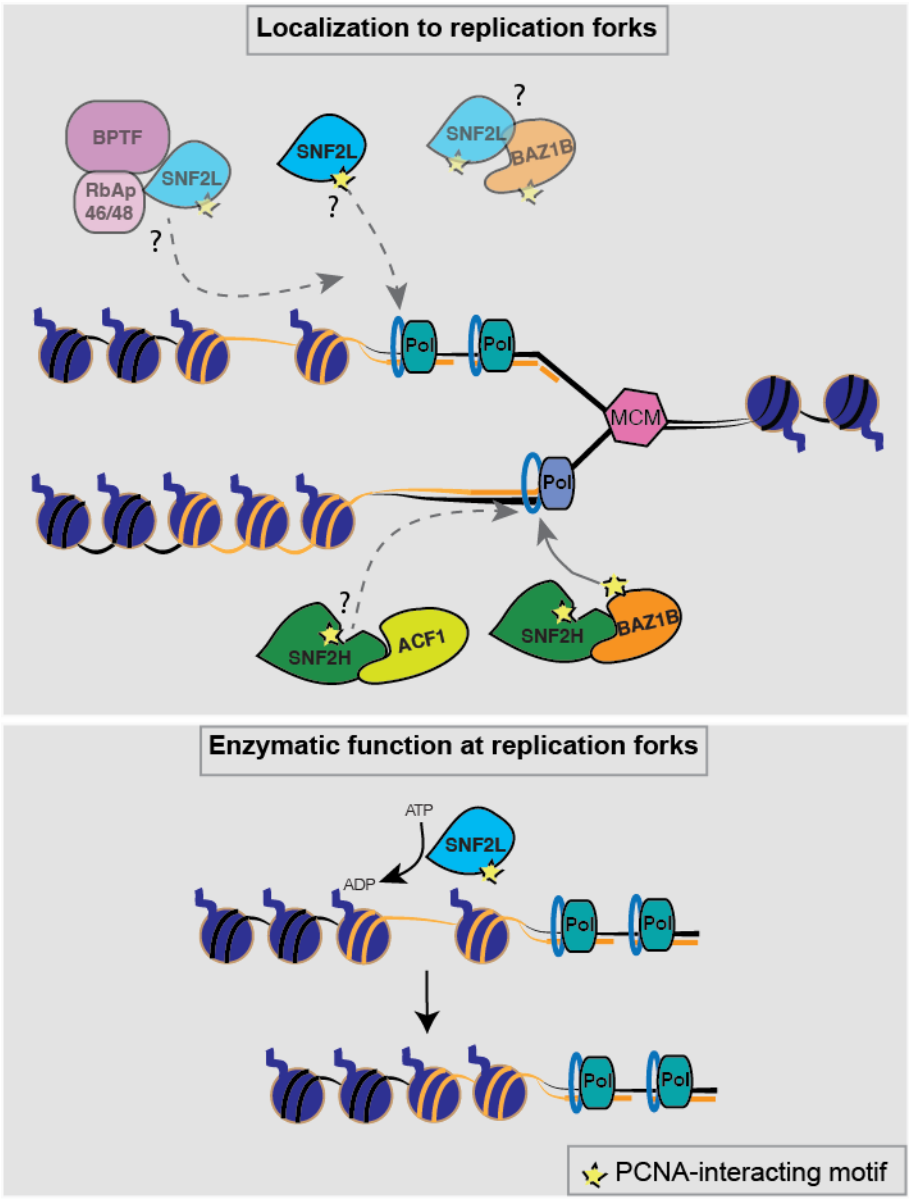

Figure 6.1. Model of SNF2L and SNF2L-containing complex localization to replication forks. SNF2L's PCNA-interacting motif [122] may facilitate SNF2L localization to replication forks, similarly to the recruitment mechanism of the related chromatin remodeler SNF2H [166]. The SNF2L protein complexes that localize with SNF2L to the elongating fork have been unexplored. SNF2H may localize as part of the NURF complex (containing BPTF and RbAp46/48) or in complex with BAZ1B. Once recruited to replication forks, SNF2L likely catalyzes sliding of nucleosomes behind the replication fork on nascent chromatin.

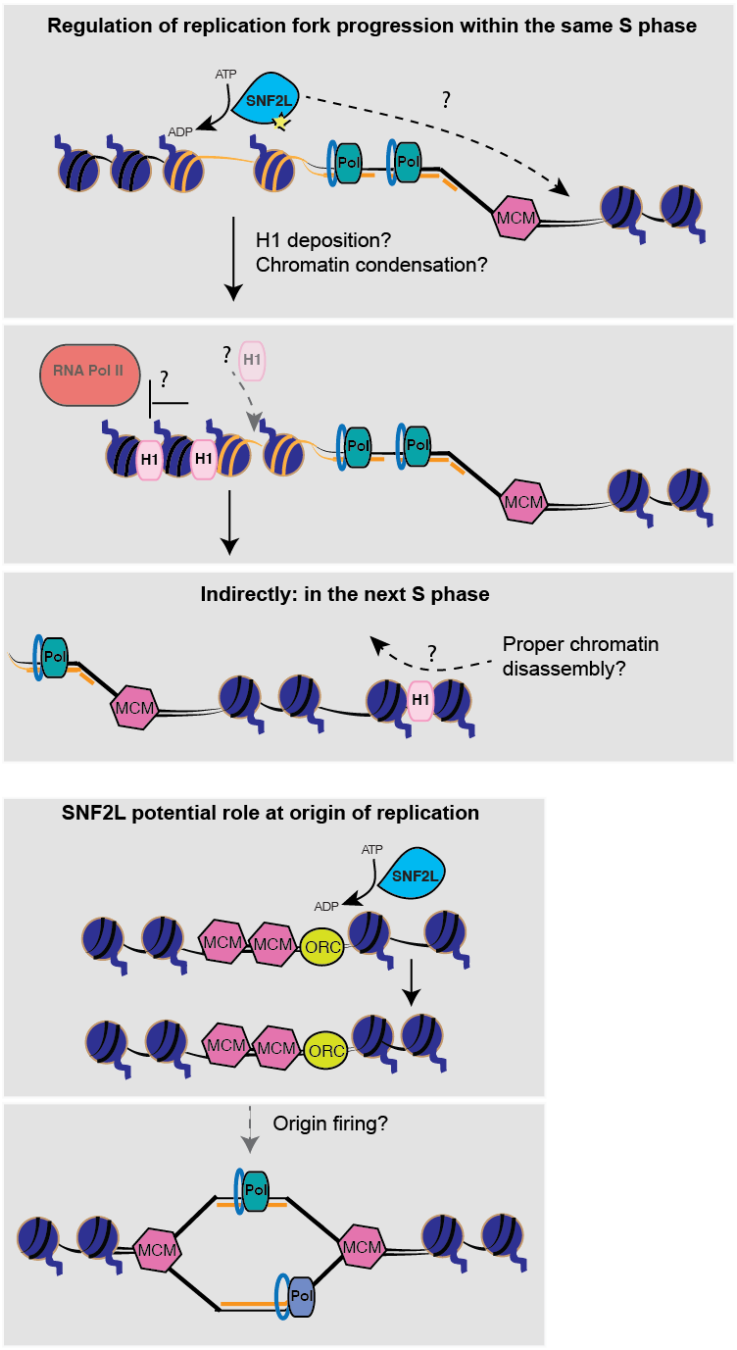

Figure 6.2. Model of SNF2L function in promoting DNA replication. SNF2L may facilitate progression through replication by affecting events within the same S phase in front of the replication fork, such as regulation of DNA topology that may affect fork movement [178]. Alternatively, SNF2L may promote incorporation of histone H1 into nascent chromatin behind the replication fork [179]. At least on the inactive X chromosome, SNF2L maintains chromatin condensation through H1 [180], which prevents aberrant transcription. Proper H1 positioning may affect chromatin disassembly in the next S phase. SNF2L may play a role at replication forks during origin firing by promoting histone sliding to induce an environment conducive for initiation of DNA replication.

(ii) Interpretations of stalled and collapsed replication forks isolated with iPOND

(iia) Stalled replication forks

I observed poor enrichment of known replication stress proteins to HU-stalled forks. This may be attributable to the mechanism by which HU stalls replication forks. HU depletes cellular dNTP pools and causes uncoupling of helicase and polymerase activities [115]. This generates stretches of parental strand RPA-coated ssDNA that signals the recruitment of numerous known replication stress proteins including ATR and the 9-1-1 complex.

Since iPOND purifies nascent DNA fragments, it is possible that HU may not be a feasible reagent to use for isolating replication forks using iPOND (Fig. 4.3D). If polymerase-dependent repriming occurs on the parental DNA strand, iPOND may be able to isolate proteins at HU-stalled forks. Such repriming events have been observed only in *Xenopus* oocytes and not mammalian cells [115]. One way to test whether re-priming occurs in mammalian cells would be to examine if the 9-1-1 clamp loader is enriched in HU-stalled iPOND purifications when EdU is kept in the media. Since 9-1-1 is loaded onto the 5' end of a ssDNA-dsDNA junction, accumulation of the clamp loader may reflect polymerase alpha-dependent 5'-to-3' DNA synthesis. Inhibition of polymerase alpha activity using aphidicholin could further test this hypothesis. Future iPOND experiments designed to identify stalled replication fork proteins may benefit from using another replication stress reagent that blocks both the helicase and replicative polymerase.

(iib) Collapsed replication forks: collapsed or newly fired?

The ATR-dependent mechanisms that promote fork stability are essential for cell viability and yet remain some of the least understood. I used iPOND-MS to gain insights into the function of ATR during replication stress by probing the protein landscape at stalled replication forks lacking ATR activity. I observed the enrichment of several helicases implicated in recombinatorial repair to collapsed forks. One hypothesis is that these helicases catalyze the formation of the toxic ssDNA structures observed without ATR. If this were true, then depletion of SMARCAL1, WRN or BLM should prevent the formation of nascent strand ssDNA observed when ATR is inhibited. Jami FB Couch has provided elegant genetic evidence to support that SMARCAL1 is partially responsible for the toxic accumulation of RPA-ssDNA resulting from ATR inhibition (results in press). However, depletion of WRN or BLM had no apparent effect in these assays.

Throughout my thesis I have used the term 'collapsed' to indicate stalled replication forks that collapse into DSBs and prevent fork restart. ATR restricts such detrimental mechanisms to protect genome integrity. In addition, ATR also limits the initiation of new origins of DNA replication in the presence of DNA damage. We have shown that new origins initiate when cells are treated with the ATR inhibitor, as detected in DNA fiber labeling studies (Jessica Luzwick and Jami Couch, results in press). Therefore, proteins discovered at ATR-inhibited, HU-stalled replication forks may represent proteins at either collapsed or newly fired forks. To distinguish between these scenarios, future iPOND-MS

experiments may benefit from co-treatment of ATR inhibitor with a CDK inhibitor. CDK activity is essential for origin firing. Therefore, proteins enriched at replication forks after ATR and CDK inhibition, as measured relative to levels observed at ATR inhibited cells, may represent proteins that localize to collapsed forks.

Lastly, the nature of the underlying event that causes fork collapse remains elusive. Is fork collapse irreversible? If so, when does this event occur and how? Analysis of the underlying DNA structure purified from ATR inhibited forks may shed light onto these questions.

(iii) Comparison to other iPOND-MS datasets

Two groups have recently employed iPOND and an iPOND-like technique to identify replisome components using proteomics methods [82, 181]. The first group utilized a derivative of iPOND called DmChIP (DNA mediated pulldown) combined with quantitative MS using SILAC. They examined the composition of the replisome during early and late stages of S phase as compared to a sample without tagged nascent DNA and therefore no purified replisomes [181]. The majority of the identified proteins represent chromatin-bound factors that have established roles in chromatin organization.

Another group examined the proteins associated with elongating replication forks in comparison to chromatin-bound proteins using iPOND coupled to label-free proteomics [82]. This methodology identified proteins

known to associate with leading and lagging strand synthesis, as well as proteins implicated in mismatch repair, histone deposition and maturation, nucleosome sliding, and the MRN complex. Interestingly, they identified the components of the MCM2-7 replicative helicase. The GINS3 subunit of the CMG helicase complex was also enriched, perhaps explaining the enrichment of the MCM helicase. Table 6.1 lists the proteins enriched in my iPOND-MS screen compared to the Lopez-Contreras screen.

Table 6.1. Replication fork proteins identified in two independent iPOND-MS screens.

Normal fork proteins in common (Sirbu and Lopez-Contreras)	Sirbu additional normal fork proteins			Lopez-Contreras additional normal fork proteins
ATAD5/ELG1	ACO1	ISYNA1	SNF2H	ATXN10
BAZ1B/WSTF	ANP32A	MRPL13	SMARCAD1	DNAJA1
CHAF1A	ARID3A	MRPL41	SNRPD1	EHMT2
CHAF1B	ARID3B	NAA10	SPTLC2	FEN1
CTF4/WDHD1	ATAD2	NAMPT	SSB	GINS3
DNMT1	ATAD2B	NCAPH	TIMELESS	GTF2I
EHMT1/GLP	ATL3	OSBPL9	TM9SF4	MCM2
EXO1	CA2	PDCD4	TOPBP1	MCM4
LIG1	CBS	PHKB	TRMT6	MCM5
MSH2	CCNH	PIGT	TTC9C	MRE11A
MSH3	CP110	PLOD1	UBA3	POLA1
MSH6	CRTAP	PPIB	UBE2I	POLD3
PCNA	EP400	PSME2	UBE2T	PPM1E
POLD1	FANCI	PTGES2	UBR5	PRIM2
POLE	GMPPB	PUS7	VPS26B	RAD50
RFC1	GRB2	RNASEH2C		RNASEH2B
RFC2	GTPBP5	RPA3		RPA1
RFC3	HAUS7	RPL36AL		RPA2
RFC4	HDAC8	RPL6P10		RPL11
RFC5	HEATR3	SEPT11		SSRP1
SNF2L	HPRT1	SKP1		SUPT16H
UHRF1	HSD17B7	SLC25A15		TCEA1
WIZ	IMMT	SLC4A2		TUBB4A
				ZNF24
	known replication protein			

Overall, Lopez-Contreras identified more known replisome components than my iPOND-MS screen. A direct comparison between the fold enrichments detected in the two screens is difficult given the different analytical MS platforms. Three key factors distinguish the two experimental procedures: cellular scale, chromatin shearing, and proteomic analysis. First, a 10-fold larger cellular scale ($3x10^8$ of 293T cells) was utilized in [82]. A larger scale would improve detection of proteins of lower abundance and should be achievable using suspension 293T cells for label-free quantitative MS. The rationale for my experimental scale was based on the observation that initial MudPIT analyses revealed 2 to 12-fold enrichment of positive controls such as polymerases. However, this enrichment was measured relative to a sample that omitted the biotin azide ('no click' control). A more appropriate negative control for future iPOND optimization experiments will be purification of mature chromatin. Lopez-Contreras performed several such optimization experiments. Using immunoblotting for known proteins and MS approaches, they evaluated the best fold enrichments of iPOND-purified replisomes relative to chromatin chases of varying lengths. Future iPOND optimization experiments would benefit from such optimizations (see *v* below*).*

Second, chromatin was sheared to 80 base pair sizes. This is twice as small as the DNA fragment sizes achievable using original iPOND conditions. Theoretically, smaller fragment sizes should not improve iPOND-MS resolution. In fact, it may be beneficial to increase nascent DNA fragment sizes, perhaps through altering copper(II)sulfate concentrations. The larger the fragment sizes,

the more likely that a piece of nascent chromatin will have been EdU labeled and the associated proteins purified.

Third, the group utilized a completely different label-free proteomics and data analysis approaches. Relative protein abundance was calculated using signal intensities and not spectral counting. Purified replication fork peptides were separated in one dimension for LC-MS/MS analysis using the high performance LTQ Orbitrap Velos mass spectrometer. This instrument is superior because it provides improved capacity to extract ion chromatographs from full-scan spectra [182] (discussed more below). Overall, an improved upfront biochemical iPOND purification technique that increases the signal to noise ratio will benefit the development of a high-throughput iPOND-MS platform.

(iv) iPOND 2.0-improving biochemical purification of replication forks

For future iPOND proteomics screens, it will be critical to minimize the background observed in the chromatin-bound negative control. One of the major challenges I encountered in preparing iPOND samples for MS was not having a quick method to examine the effectiveness of optimizations on reducing the background. Silver staining of purifications showed that the majority of purified proteins were chromatin-bound, but proved to not be a useful method for screening out the background. Identifying a benchmark protein that should not be enriched in iPOND purifications should facilitate such studies.

Future experiments could incorporate: (1) an improved elution using TEV-cleavable biotin azide (currently being tested in our laboratory; (2) a pre-fractionation step to remove cytoplasmic proteins using RIPA buffer has been suggested to be improve the signal of known proteins (personal communication with Cimprich laboratory and lysis described in [181]); (3) further optimization of bead types will be necessary since preliminary MS results revealed that magnetic beads may capture different known proteins than streptavidin-conjugated agarose beads (Appendix A).

Lastly, exploring the possibility of performing comparative proteomics using isobaric chemical labeling (iTRAQ) or metabolic labeling (SILAC) may be of interest. Spectral counting provides depth of proteome coverage, but requires numerous replicates to reproducibly quantify protein changes across samples [119]. Since biochemical sample preparations are performed independently, this may introduce systematic errors that could be eliminated by using SILAC.

Recently, a group compared three quantitative proteomics approaches using the same analytical platform of the LTQ Orbitrap Velos [182]. This study showed that spectral counting methods for protein quantification are less accurate and reproducible than metabolic or isobaric chemical labeling techniques. One advantage to using iTRAQ is the capacity to compare up to 8 samples in one proteomic analysis [183]. This would be valuable for iPOND-MS studies that aim to identify protein changes across numerous samples. One disadvantage of iTRAQ is the necessity of tagging the amine group on lysines

[182]. The current iPOND platform requires formaldehyde crosslinking for protein purification and may complicate the efficiency of iTRAQ tagging. Nonetheless, iTRAQ should be explored as an option for future quantitative iPOND-MS studies. The advent of more quantitative mass spectrometric instruments, protein identification algorithms, scaffolds for protein assembly and improved statistical methods to analyze label-free MS data will prove invaluable to analyses of replication fork proteins purified using iPOND.

(v) Other iPOND applications

One current limitation of iPOND has been the spatial resolution, which is on the order of several kbp. For example, it would be beneficial to distinguish the distribution of proteins relative to one another within the chromosomal space at the replication fork. Such high-resolution mapping has been achieved with *in vitro* replication systems by using T4 DNA polymerase and primer template DNA that contains a position-specific cross-linkable aryl azide [184]. This elegant study provided topographical information about the location of binding of accessory proteins respective to polymerase interaction with and movement along the DNA template. Potential coupling of iPOND to single-molecule analyses [185] of replisome proteins would significantly improve iPOND resolution.

Theoretically, iPOND can be used to study other processes that involve DNA or even RNA synthesis. An example would be DNA repair synthesis outside of S-phase. Synchronized or terminally differentiated cell cultures could be

exposed to DNA damaging agents in the presence of EdU. The late steps in repair of that damage or the re-establishment of chromatin following repair synthesis can be monitored with iPOND. Synchronized cell cultures could also be used to examine the differences in DNA replication, chromatin deposition or DNA repair that occur in early versus late S-phase cells. iPOND could theoretically be adapted to analyze even proteins on nascent RNA, as click chemistry has been used to label newly synthesized RNA with the uridine analog 5-ethynyluridine [186]. A variation of iPOND-MS lacking the crosslinking step would be beneficial for monitoring the substantial variety of post-translational modifications at damaged forks. Lastly, second step purifications of telomere-binding proteins or transcription factors after iPOND-purified replisomes could reveal information about how telomere ends are replicated or what occurs when replication forks encounter the transcriptional machinery. These studies will be important to expand our understanding of how the genome and epigenome is maintained during DNA replication.

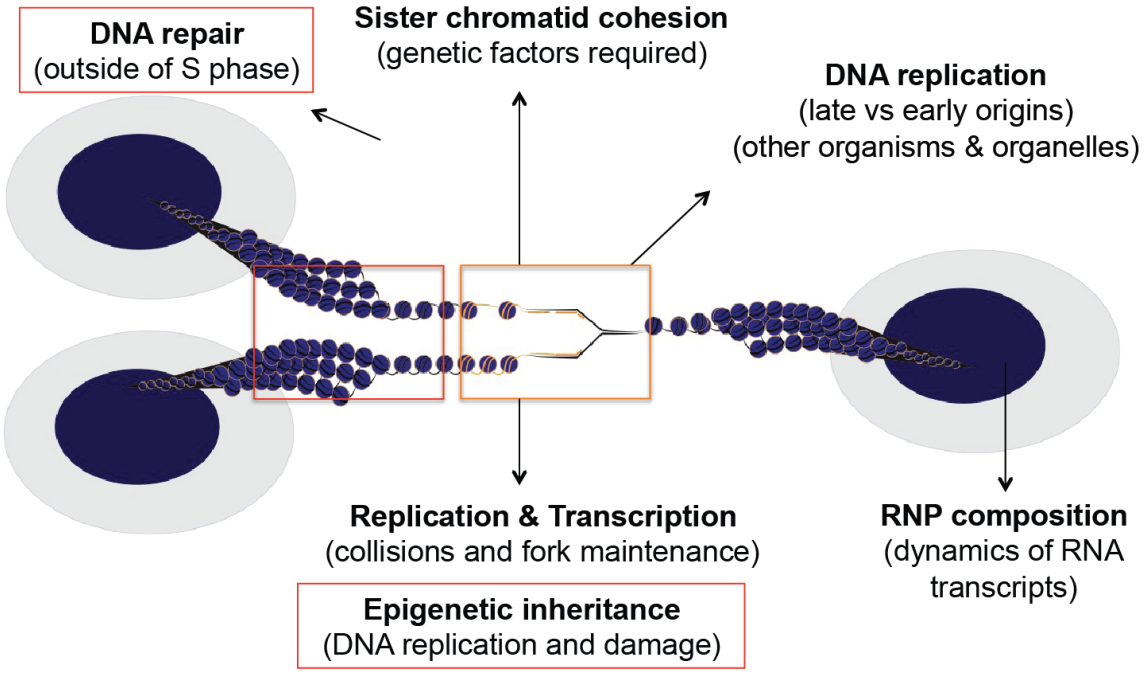

Figure 6.3. Applications of iPOND to studies of genome and epigenome integrity.

APPENDIX A

Preliminary efforts to optimize the iPOND methodology for coupling to MudPIT analyses were performed to decrease the background observed in the negative controls. Proteins bound to nascent DNA were eluted by UV photocleavage, which permits the release of nascent DNA and bound proteins, and compared to proteins eluted under denaturing conditions and high heat using 2x sample buffer. In one experiment, elution by sample buffer as compared to elution by photocleavage proved superior for MudPIT identification of known replisome components (Fig. A1C). Replication proteins such as PCNA, DNA polymerases delta and epsilon, and replication clamp loading proteins (RFC1-5) were enriched 2 to 14-fold relative to the negative control that lacked the click reaction. These results suggested that iPOND-MS worked to detect positive controls. It is important to note that the studies above provided no measurement of biological false positive protein identifications (addressed in Chapter V and VI).

In one experiment, streptavidin conjugated magnetic and agarose beads were used to purify replisome components by iPOND (Fig. A2A). Since a larger cellular scale was used for the magnetic bead purifications, it is difficult to directly compare the MudPIT results. However, agarose and magnetic beads enrich differently for different known proteins (Fig. A2C, D). Future experiments should focus on repeating these results and comparing the elution and bead parameters to a chromatin chase negative control.

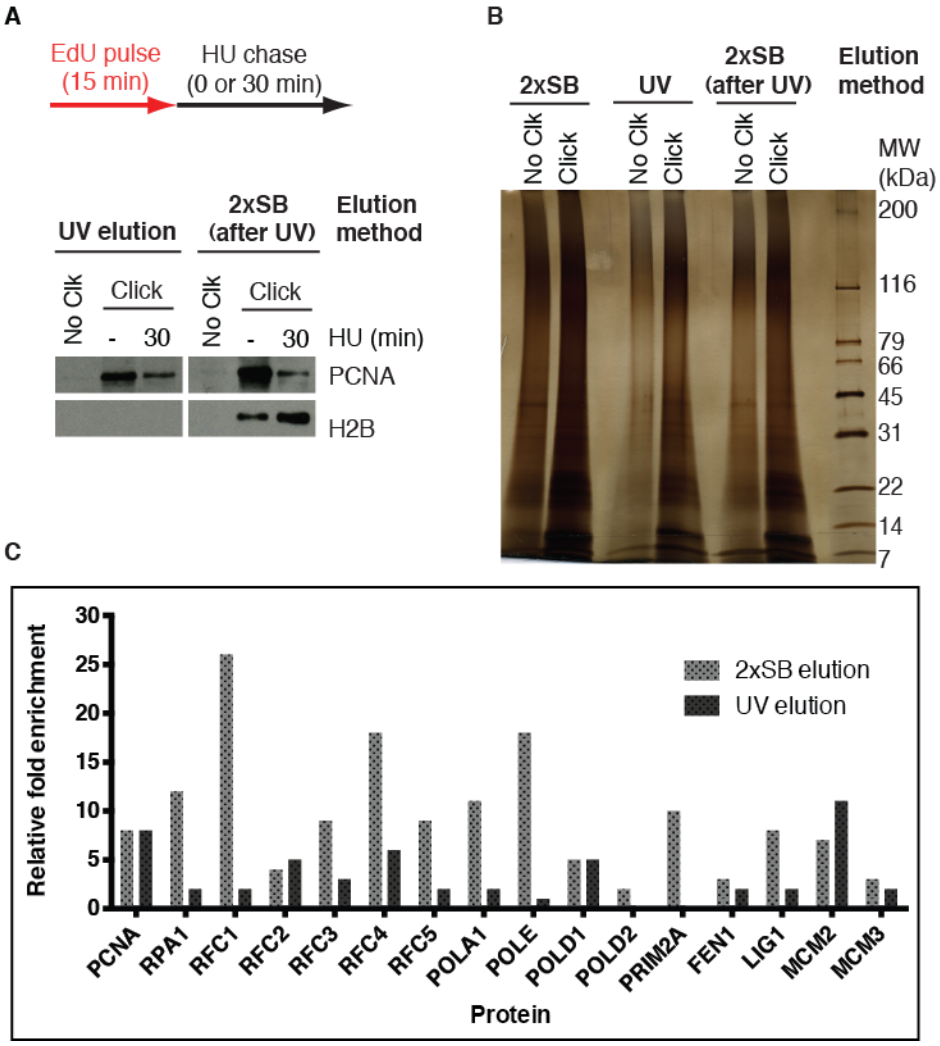

Figure A1. Optimization for iPOND-MS comparing various elution methods. (A) Suspension HEK293T cells were labeled with EdU for 15 mins and collected or chased into HU for 30 mins. Samples were processed by iPOND and eluted for 2h under UV light (365nm). The 2x SB (after UV) represents proteins not eluted by UV but subsequently eluted by boiling in 2x SB. (B) Silver staining of iPOND purifications submitted for MudPIT analyses. (C) Relative fold enrichment of several known replisome components as calculated by dividing raw spectral counts obtained for the experimental sample by the 'no click' negative control. When zero spectral counts were encountered in the negative control, a value of 1 was used.

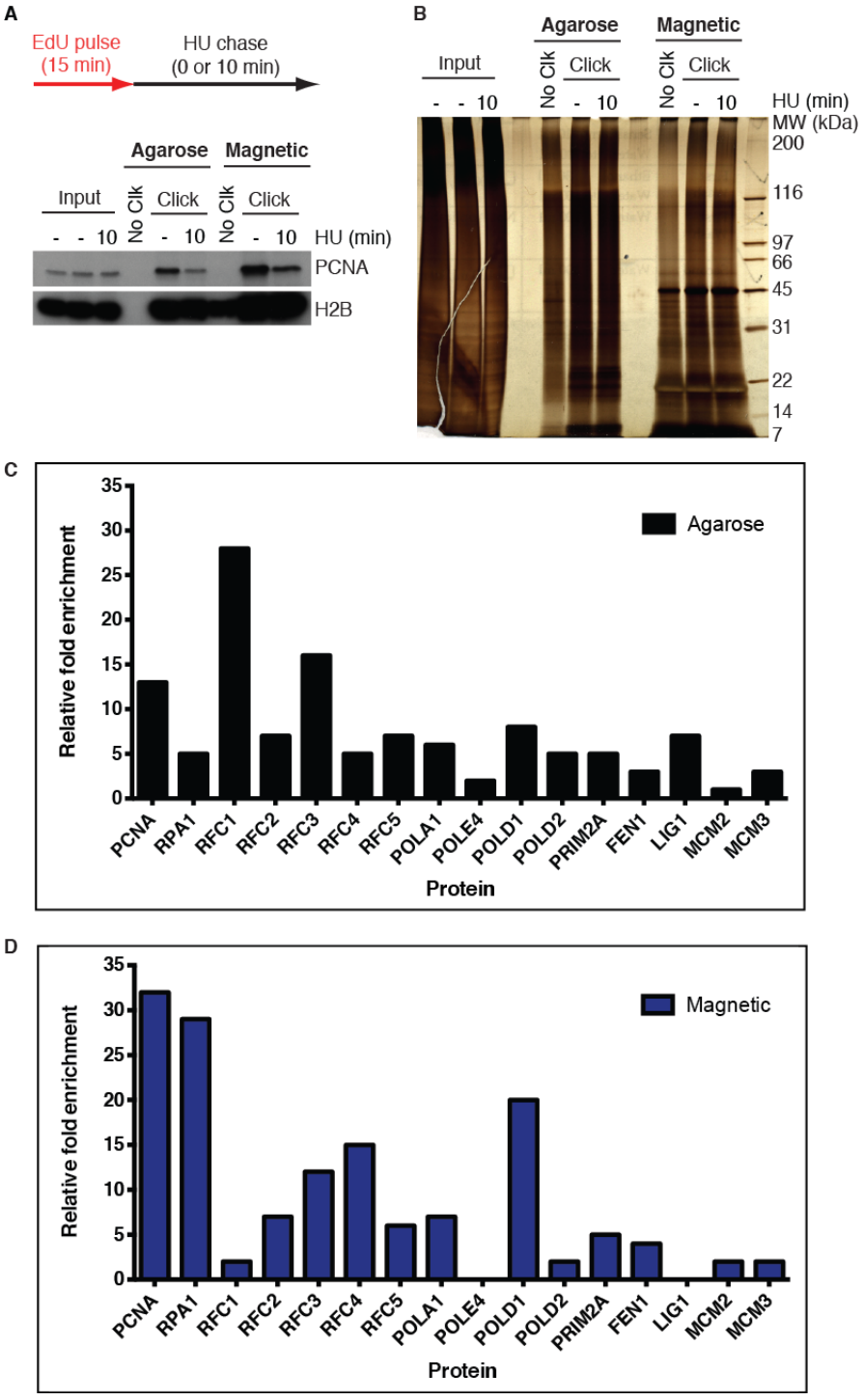

Figure A2. Optimization for iPOND-MS using magnetic and agarose beads. (A) Cells pulsed with EdU for 15 mins were collected or chased into HU for 10 mins and processed by iPOND using streptavidin-conjugated magnetic or agarose beads. (B) Silver staining of samples submitted for MudPIT analyses. (C,D). Relative fold enrichment of known replisome components as calculated by dividing raw spectral counts from the experimental sample by the 'no click' negative control. When zero spectral counts were encountered in the negative control, a value of 1 was used.

APPENDIX B

Table B.1. List of 148 genes examined in functional genomic screen for ATR-like genes.

Gene name	EntrezID	Gene name	EntrezID
AKAP12	9590	FKBP10	60681
ANP32B	10541	FKBP3	2287
ARF5	381	FNBP4	23360
ARHGAP5	394	FXR2	9513
ARID3A	1820	GRWD1	83743
ARID3B	10620	GTF3C3	9330
ARIH1	25820	GTPBP5	26164
ARL6IP5	10550	HAUS7	55559
ASCC3	10973	HDAC8	55869
ATAD2	29028	HEATR3	55027
ATAD2B	54454	HECTD3	79654
ATAD5	79915	HPRT1	3251
ATP6V0D1	9114	INCENP	3619
BAZ1B	9031	ISYNA1	51477
BTAF1	9044	JMJD6	23210
C20ORF3	57136	KBTBD6	89890
C6ORF108	10591	KCTD12	115207
CALR	811	KIAA1598	57698
CBS	875	KIAA2013	90231
CCNH	902	LOH12CR1	118426
CCT3	7203	MAOA	4128
CHD1L	9557	MAP4K4	9448
CMPK1	51727	MAPK7	5598
COMT	1312	MED16	10025
CP110	9738	MELK	9833
CSNK1D	1453	MLL4	9757
DDX11	1663	MMS22L	253714
DHX29	54505	MYCBP	26292
EHMT1	79813	MYO18A	399687
EHMT2	10919	NAA50	80218
EI24	9538	NAMPT	10135
EIF3D	8664	NBAS	51594
EP400	57634	NCAPH	23397
EPB41L2	2037	NDRG1	10397
EXD2	55218	NIN	51199
FAM120A	23196	NT5C	30833
FBXO17	115290	OBSCN	84033
FBXO22OS	26263	OSBPL9	114883
FBXO30	84085	PAPOLA	10914

.

Table B.1 (continued). List of 148 genes examined in functional genomic screen for ATR-like genes.

Gene name	EntrezID	Gene name	EntrezID
PDCD4	27250	SMARCAD1	56916
PDCD6	10016	SMARCC1	6599
PGM3	5238	SMG6	23293
PHF14	9678	SMG8	55181
PHF8	23133	SNRPD1	6632
PIAS1	8554	SNX5	27131
PIGT	51604	SPG11	80208
PLRG1	5356	THUMPD1	55623
PPP1CA	5499	TONSL	4796
PPP1R10	5514	TRAPPC11	60684
PPP2CA	5515	TRMT6	51605
PPP2R1A	5518	TRRAP	8295
PSMA1	5682	TTC27	55622
PSMB3	5691	TTC5	91875
PSMB7	5695	TTC9C	283237
PSMC2	5701	TTI1	9675
PSMD8	5714	UBE2I	7329
PSME2	5721	UBE2T	29089
RAB12	201475	UBR5	51366
RABGAP1L	9910	UHRF1	29128
RAP1B	5908	USP7	7874
RBBP7	5931	VPS26B	112936
RDH14	57665	WASL	8976
RECQL	5965	WDHD1	11169
RIOK1	83732	WDR4	10785
RNASEH2C	84153	WDR87	83889
RPL36AL	6166	WIZ	58525
RRAGB	10325	XRCC1	7515
RSU1	6251	ZC3HAV1L	92092
SART3	9733	ZCCHC6	79670
SBNO2	22904	ZNF22	7570
SCAPER	49855		
SCYL2	55681		
SFXN4	119559		
SIX5	147912		
SKP1	6500		
SLC25A11	8402		
SMARCA1	6594		
SMARCA5	8467		

APPENDIX C

iPOND-MS validation using immunofluorescence detection of tagged protein localization

To examine the subcellular localization of 32 proteins of interest using immunofluorescence, three rotation students helped me generate epitope-tagged cDNAs (Table C.1). Approximately one-third of the purchased cDNA clones lacked the full-length cDNA or exhibited undetectable protein expression.

Table C.1. List of 32 genes cloned into GFP-expressing vectors.

Gene name	OpenBiosystems CloneID
TRMT6	1842 in pDONR223 without stop codon
ASCC3 isoform 2 (short isoform)	11778 in pDONR223
UBE2T	5367 in pDONR223
SNX5	8887 in pDONR223
GRWD1	3222 in pDONR223
FAM120A	53080 in pDONR223
DAK	2753 in pDONR223
PLRG1	13135 in pDONR223
RRAGB	100066617 (with native stop codon) in pENTR221
PDC4	100004275 (with native stop codon) in pENTR221
C6orf108 / RCL	6845 in pDONR223
BTAF1	55143 in pDONR223
MAPK4K4	100004275 (with native stop codon) in pENTR221
KIAA1598	15060 in pDONR223
PIAS1	56382 in pDONR223
NCAPH	100006062 (with native stop codon) in pENTR221
USP7	100066416 (with native stop codon) in pENTR223.1
ZC3HAV1L	5168 in pDONR223
ANP32B	6023 in pDONR223
PPP1CA	3788 in pDONR223
ARID3A	10855 in pDONR223
UBE2I	4616 in pDONR223
ARID3B	10878 in pDONR223
FKBP3	273 in pDONR223
UMPS	2753 in pDONR223
CMPK1	13135 in pDONR223
FKBP10	100066975 (with native stop codon) in pENTR221
ISYNA1	100006095 (with native stop codon) in pENTR221
PP2CA	4071 in pDONR223
RBBP7	56361in pDONR223
ASCC3 isoform 1 (long isoform)	100001999 without stop codon
ATAD2	55166 in pDONR223

problematic	no cDNA or no expression of GFP-taggged protein

The remaining GFP-tagged proteins showed no change in localization following HU-induced replication stress or DNA damage after inhibition of ATR. These negative results are difficult to interpret. Some possibilities include: protein tagging interfered with proper localization, immunofluorescence is not sensitive enough to validate proteins identified using iPOND, or biological false-discovery rate in the iPOND-MS screen is high.

iPOND-MS validation using selected reaction monitoring (SRM)

I attempted to validate proteins identified in the MudPIT proteomics analysis using label-free quantitative mass spectrometry in selected reaction monitoring (SRM) mode. The advantage of SRM to shotgun proteomics is the capacity to schedule a specific window of time for examination of a limited number of spectra. This provides deeper and more accurate quantitative proteomics analyses. In collaboration with David Friedman at the Vanderbilt Proteomics Core, we evaluated the quality of unscheduled runs for 60 proteins (given a minimum of 2 independent peptides with 3 transition states per peptide). A total of 42 proteins were analyzed (Table C.2).

Table C.2. Proteins analyzed by MS in single reaction monitoring mode.

Protein	Name
ARF5	ADP-ribosylation factor 5
ARID3B	AT rich interactive domain 3B (BRIGHT-like)
ATAD2	ATPase family, AAA domain containing 2
ATAD2B	ATPase family, AAA domain containing 2B
ATP6V0D1	ATPase, H+ transporting, lysosomal 38kDa, V0 subunit d1
BAZ1B	bromodomain adjacent to zinc finger domain, 1B
CAT	catalase
CHD1L	Chromodomain Helicase Dna Binding Protein 1-Like
CMPK1	Cytidine Monophosphate (Ump-Cmp) Kinase 1, Cytosolic
EPB41L2	erythrocyte membrane protein band 4.1-like 2
EXD2	Exonuclease 3'-5' Domain Containing 2
FAM120A	Family With Sequence Similarity 120A
FXR2	fragile X mental retardation, autosomal homolog 2
GRB2	growth factor receptor-bound protein 2
GRWD1	Glutamate-Rich Wd Repeat Containing 1
HEATR3	HEAT repeat containing 3
HPRT1	hypoxanthine phosphoribosyltransferase 1
INCENP	Inner Centromere Protein Antigens 135/155Kda
ISYNA1	inositol-3-phosphate synthase 1
MRPL17	Mitochondrial Ribosomal Protein L17
NAMPT	nicotinamide phosphoribosyltransferase
NCAPH	non-SMC condensin I complex, subunit H
NDRG1	N-myc downstream regulated 1
PHF8	Phd Finger Protein 8
PLRG1	Pleiotropic Regulator 1 (Prl1 Homolog, Arabidopsis)
PPP1CA	protein phosphatase 1, catalytic subunit, alpha isoform
PPP2CA	protein phosphatase 2 (formerly 2A), catalytic subunit, alpha isoform
PSMA1	proteasome (prosome, macropain) subunit, alpha type, 1
RBBP7	retinoblastoma binding protein 7
RPA2	replication protein A2, 32kDa
RPL36AL	ribosomal protein L36a-like
SART3	squamous cell carcinoma antigen recognized by T cells 3
SCYL2	SCY1-like 2 (S. cerevisiae)
SLC25A11	solute carrier family 25 (mitochondrial carrier; oxoglutarate carrier), member 11
SNF2L	SWI/SNF related, matrix associated, actin dependent regulator of chromatin, subfamily a, member 1
SNX27	Sorting Nexin Family Member 27
SPG11	spastic paraplegia 11 (autosomal recessive)
UBE2I	ubiquitin-conjugating enzyme E2I (UBC9 homolog, yeast)
UBE2T	ubiquitin-conjugating enzyme E2T (putative)
UGGT1	UDP-glucose ceramide glucosyltransferase-like 1
UNG	Uracil-Dna Glycosylase
ZC3HAV1L	zinc finger CCCH-type, antiviral 1-like

RPA2, SNF2L, BAZ1B, UNG, and 3are highlighted in Table C.2 and exhibited similar patterns of relative enrichment as observed in the MudPIT analyses (Fig. 5.5 and Fig. C.1). Comparing results across different analytical

platforms is difficult, but it should be noted that overall, higher enrichments were observed using MudPIT analyses. For example, whereas RPA2 was enriched 5-fold relative to levels on chromatin (Table 5.4) measured with MudPIT, the intensity observed for one of two peptides by SRM was only 3-fold (Fig. 5.5). Two-dimensional protein separation after iPOND purification reduces the mixture complexity prior to MS analyses and may enhance the dynamic range of detection. Therefore, future iPOND experiments would continue to benefit from MudPIT studies.

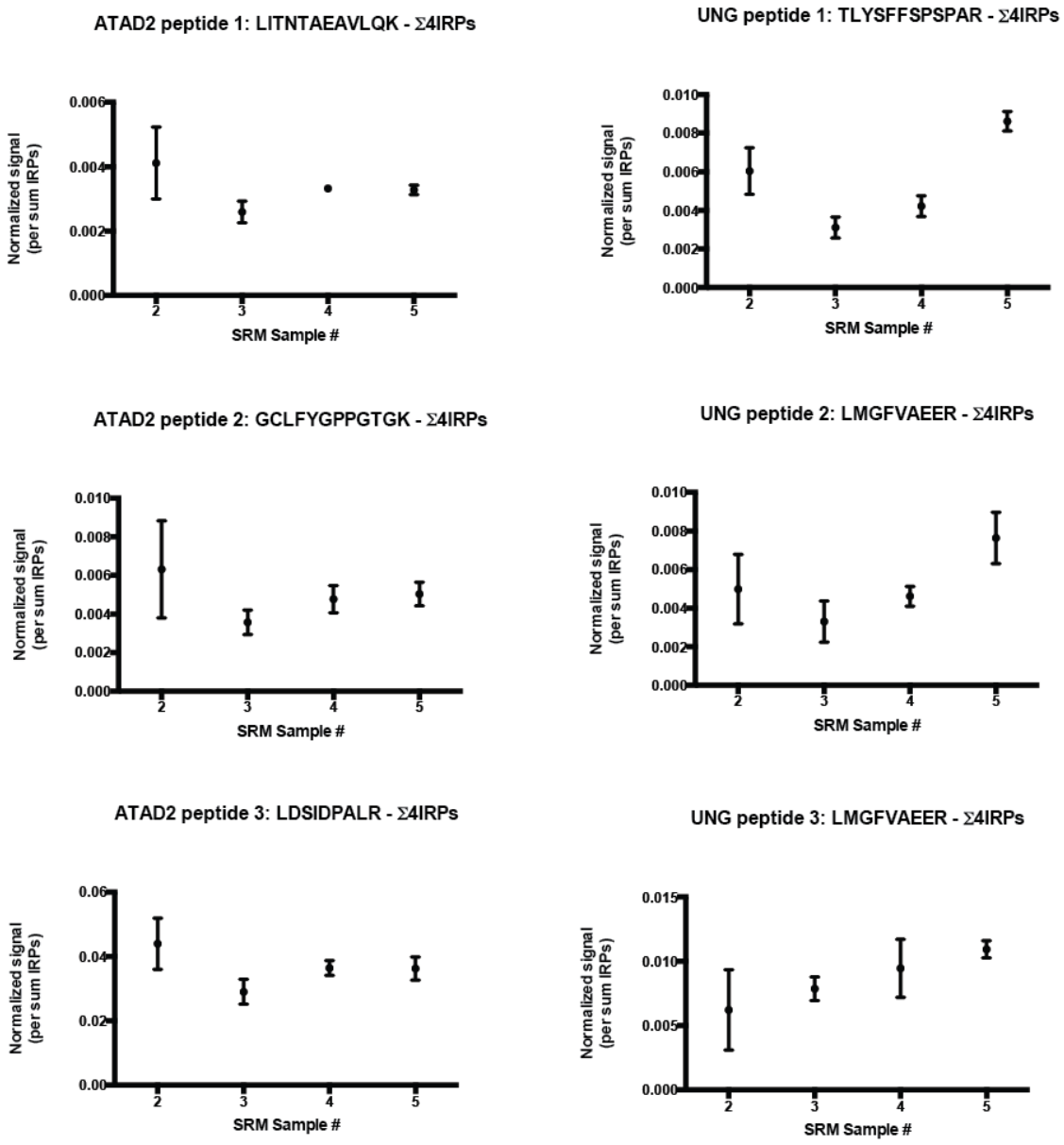

Figure C.1 Validation of ATAD2 and UNG as proteins associated with elongating or collapsed forks, respectively. Quantitative mass spectrometry in selected reaction monitoring mode (SRM) examined the indicated peptides after iPOND purifications and was performed by David Friedman in the Vanderbilt Proteomics Core. SRM samples 2, 3, 4, and 5 represent normal replication forks, thymidine chase negative control, HU-treated stalled forks, HU and ATR inhibited collapsed forks, respectively. The signal intensity measured for each peptide is normalized to the sum of the internal reference peptides (Σ4IRPs).

APPENDIX D

This appendix includes the review publication in Sirbu BM and Cortez D. *DNA damage response: three levels of DNA repair regulation*, 2013. Cold Spring Harbor Perspectives in Biology. doi: 10.1101/cshperspect.a012724.

DNA Damage Response: Three Levels of DNA Repair Regulation

Bianca M. Sirbu and David Cortez

Department of Biochemistry, Vanderbilt University School of Medicine, Nashville, Tennessee 37027

Correspondence: david.cortez@vanderbilt.edu

Cold Spring Harbor Perspectives in Biology
www.cshperspectives.org

Genome integrity is challenged by DNA damage from both endogenous and environmental sources. This damage must be repaired to allow both RNA and DNA polymerases to accurately read and duplicate the information in the genome. Multiple repair enzymes scan the DNA for problems, remove the offending damage, and restore the DNA duplex. These repair mechanisms are regulated by DNA damage response kinases including DNA-PKcs, ATM, and ATR that are activated at DNA lesions. These kinases improve the efficiency of DNA repair by phosphorylating repair proteins to modify their activities, by initiating a complex series of changes in the local chromatin structure near the damage site, and by altering the overall cellular environment to make it more conducive to repair. In this review, we focus on these three levels of regulation to illustrate how the DNA damage kinases promote efficient repair to maintain genome integrity and prevent disease.

The DNA in each of our cells accumulates thousands of lesions every day. This damaged DNA must be removed for the DNA code to be read properly. Fortunately, cells contain multiple DNA repair mechanisms including: base excision repair (BER) that removes damaged bases, mismatch repair (MMR) that recognizes base incorporation errors and base damage, nucleotide excision repair (NER) that removes bulky DNA adducts, and cross-link repair (ICL) that removes interstrand cross-links. In addition, breaks in the DNA backbone are repaired via double-strand break (DSB) repair pathways including homologous recombination (HR) and nonhomologous end joining (NHEJ). Some of these mechanisms can operate independently to repair simple lesions. However, the repair of more complex lesions involving multiple DNA processing steps is regulated by the DNA damage response (DDR). For the most difficult to repair lesions, the DDR can be essential for successful repair.

The DDR consists of multiple pathways, but for the purposes of this review we will focus on the DDR kinase signaling cascades controlled by the phosphatidylinositol 3-kinase-related kinases (PIKK). These kinases include DNA-dependent protein kinase (DNA-PKcs), ataxia telangiectasia-mutated (ATM), and ATM and Rad3-related (ATR). DNA-PKcs and ATM are primarily involved in DSB repair, whereas ATR responds to a wide range of DNA lesions, especially those associated with DNA replication (Cimprich and Cortez 2008). ATR's versatility makes it essential for the viability of replicating cells in mice and humans (Brown and Baltimore

Editors: Errol C. Friedberg, Stephen J. Elledge, Alan R. Lehmann, Tomas Lindahl, and Marco Muzi-Falconi
Additional Perspectives on DNA Repair, Mutagenesis, and Other Responses to DNA Damage available at www.cshperspectives.org

Advanced Online Article. Cite this article as *Cold Spring Harb Perspect Biol* doi: 10.1101/cshperspect.a012724

2000; de Klein et al. 2000; Cortez et al. 2001). In the case of ATM, inherited biallelic mutations cause ataxia-telangiectasia—a disorder characterized by neurodegeneration, immunodeficiency, and cancer (Shiloh 2003; Lavin 2008). *ATM* mutations are also frequently found in several types of tumors (Negrini et al. 2010).

The DDR kinases share several common regulatory mechanisms of activation (Lovejoy and Cortez 2009). All three DDR kinases sense damage through protein–protein interactions that serve to recruit the kinases to damage sites. Once localized, posttranslational modifications and other protein–protein interactions fully activate the kinases to initate a cascade of phosphorylation events. The best-studied substrate of DNA-PKcs is actually DNA-PKcs itself, and autophosphorylation is an important step in direct religation of the DSB via nonhomologous end joining (NHEJ) (Weterings and Chen 2007; Dobbs et al. 2010). ATM and ATR have both unique and shared substrates that participate in DNA repair, checkpoint signaling, and determining cell fate decisions such as apoptosis and sensescence.

THREE LEVELS OF REPAIR REGULATION BY THE DDR KINASES

DDR kinases control DNA repair at three levels (Fig. 1). First, they regulate DNA repair enzymes directly through posttranslational modifications that alter their activity. These modifications appear to be especially important in the repair of complex lesions such as ICLs and repair associated with stalled replication forks. Second, the DDR kinases modify the chromatin near the DNA lesion to create a permissive local environment for repair. This chromatin response also provides a scaffolding function for the recruitment of additional DDR factors regulating both repair and signaling. Finally, the DDR kinases act at a more global level of the nucleus or even the entire cell to provide a cellular environment conducive to repair. This global response includes changes in transcription, the cell cycle, chromosome mobility, and deoxynucleotide (dNTP) levels. Controlling these processes may be most important for repair when damage is persistent.

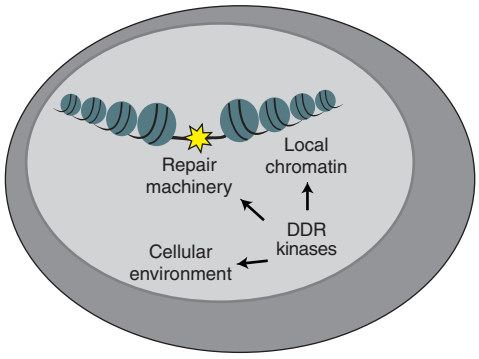

Figure 1. DDR kinases promote efficient DNA repair by directly regulating the DNA repair machinery, changing the local chromatin environment near the DNA lesion, and altering the cellular environment.

This review will highlight examples of each level of regulation. For the direct regulation of repair functions, we will discuss how DDR kinases regulate ICL repair and more general replication fork-associated repair. In discussing the local chromatin environment, we highlight the important role of chromatin modifications surrounding a DSB. Finally, at the global level, we discuss how the DDR alters nuclear architecture and maintains proper cellular dNTP pools to promote repair.

DDR KINASES DIRECTLY REGULATE THE REPLICATION-ASSOCIATED DNA REPAIR MACHINERY

DNA lesions pose an especially important problem when they interfere with DNA polymerases. Errors during DNA replication as well as mistakes in DNA repair cause mutations and chromosomal aberrations that are a source of genetic instability driving tumorigenesis. Additionally, many rare childhood diseases are the result of defects in replication-associated DNA repair. These include Seckel syndrome caused by mutations in ATR and other disorders caused by mutations in ATR substrates like BLM, WRN, and SMARCAL1 (Ciccia and Elledge 2010). Thus, the DNA damage response is particularly critical to ensure complete and accurate duplication of the genome.

ICL Repair during DNA Replication

Interstrand cross-links are perhaps the most difficult lesions to repair, requiring specialized repair mechanisms governed by genes mutated in patients with Fanconi anemia (FA), as well as components of nucleotide excision and DSB repair (Kim and D'Andrea 2012). In the context of DNA replication, interstrand cross-links are potent fork stalling lesions that activate ATR. Perhaps for these reasons, the ATR kinase has an especially critical function in initiating ICL repair (Fig. 2).

When the ICL stalls a replication fork, the DNA structure signals the recruitment of several Fanconi proteins beginning with the FANCM helicase (Meetei et al. 2005; Raschle et al. 2008; Knipscheer et al. 2009). FANCM may remodel the damaged fork to help recruit the FA core complex, a multisubunit ubiquitin ligase. An

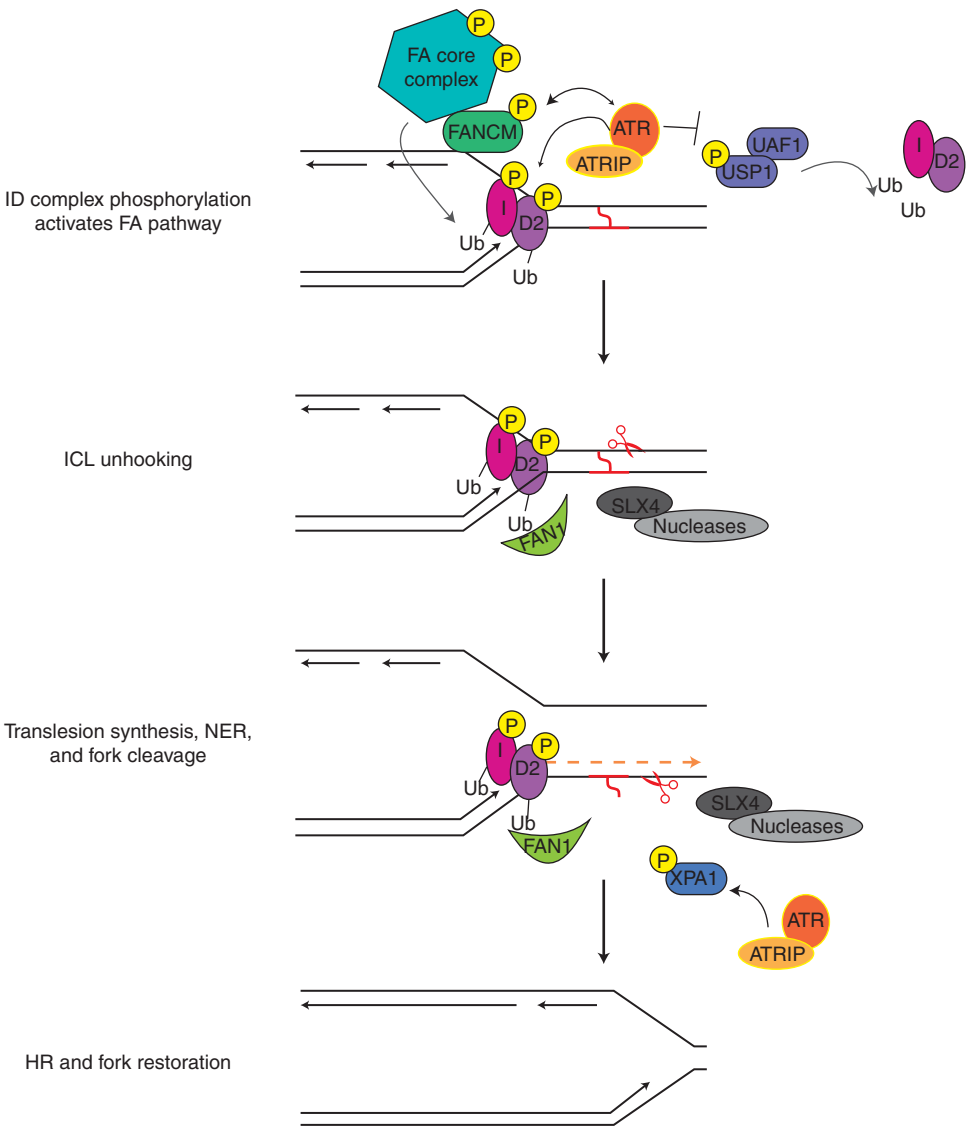

Figure 2. A simplified model of ICL repair indicating steps regulated by ATR phosphorylation.

essential activity of the core complex is monoubiquitination of FANCD2 and FANCI within the FANCI-FANCD2 (ID) complex (Garcia-Higuera et al. 2001). Repair then initiates with synchronized incision on both sides of the cross-link. Incision may be mediated by the flap endonuclease FAN1 whose ubiquitin-binding motif recognizes mono-ub FANCD2 and is essential for ICL repair (Kratz et al. 2010; Liu et al. 2010; Smogorzewska et al. 2010). Additional nucleases such as those associated with SLX4 may also participate in ICL repair given that SLX4 mutations cause FA (Kim et al. 2011). Fork cleavage results in "unhooking" of the cross-link allowing error-prone polymerases to extend past the lesion and NER to remove the cross-linked base. The unhooking reaction also generates a DSB intermediate that is processed by HR to restore the replication fork (Long et al. 2011).

ATR controls the earliest events in the FA pathway and is essential for successful repair. Thus, ATR-deficiency yields high sensitivity to DNA cross-linking agents. ATR phosphorylates several FA proteins including FANCD2, FANCI, FANCA, FANCG, and FANCM (Andreassen et al. 2004; Ishiai et al. 2008; Wilson et al. 2008; Collins et al. 2009; Sobeck et al. 2009). The phosphorylation of FANCI is a particularly critical event for FA pathway activation, as it is needed for monoubiquitination and localization of FANCD2 to sites of damage. FANCI is phosphorylated on several conserved ATR and ATM consensus sites (Matsuoka et al. 2007), and mutants that cannot be phosphorylated prevent FANCD2 mono-ub and cause hypersensitivity to cross-linking reagents (Ishiai et al. 2008). Expression of FANCI mutants that mimic phosphorylation induce FANCD2 monoubiquitination even in the absence of exogenous DNA-damaging agents. These findings suggest that FANCI phosphorylation is a necessary and perhaps sufficient step for FANCD2 monoubiquitination and FA pathway activation. The mechanism by which phosphorylation induces ubiquitylation remains unknown. However, it should be noted that FANCI has WD40 repeats, which might act analogous to F-box proteins to recruit phosphorylated substrates for ubiquitination.

Analysis of the crystal structure of the FANC ID complex has revealed that the ubiquitination sites are buried in the ID interface (Joo et al. 2011). It is possible that ATR phosphorylation of ID in *cis* may inform ID of the presence of dsDNA and ssDNA junctions. A simple model would be that once phosphorylated at the cross-link, the ID complex alters its conformation allowing core complex recognition.

ATR may also regulate FANCD2 ubiquitylation by targeting the FANCD2 deubiquitination complex USP1-UAF1. Consistent with this notion, USP1 was identified as a putative ATM/ATR substrate (Matsuoka et al. 2007), and the interaction of USP1/UAF1 with FANCI is regulated by DNA damage (Yang et al. 2011). Furthermore, in response to DNA damage, USP1 undergoes inactivating autoproteolysis, further promoting FANC ID ubiquitination.

The activities of other FA proteins including FANCA and FANCG are also under the control of the ATR kinase. FANCA is a direct ATR substrate, and mutation of the phosphorylation site creates a protein that cannot fully complement *FANCA*-deficient cells (Collins et al. 2009). FANCG is phosphorylated on multiple sites and at least one (serine 7) is ATR-dependent (Wilson et al. 2008). Phosphorylation of FANCG regulates the interactions of BRCA2 with components of the core complex and FANCD2. FANCG S7 mutants fail to rescue the cross-link sensitivity of *FANCG*-deficient cells (Qiao et al. 2004).

In addition to controlling early events in cross-link repair, the ATR pathway may also regulate later steps. For example, ATR regulates the NER-dependent unhooking reaction pathway by regulating the localization of XPA (Wu et al. 2007; Shell et al. 2009). Also, ATR regulates the HR step by promoting the recruitment of the key RAD51 recombinase (Sorensen et al. 2005).

Thus, ATR regulates nearly every step of the ICL repair process. Why is this necessary? Perhaps the answer lies in the complexity of removing an ICL. ICL repair requires the coordinated activities of multiple repair steps often at a time of maximum vulnerability for the genome (when the replication fork reaches the cross-link). Perhaps ATR signaling provides

a mechanism of ordering the repair steps to prevent undesirable DNA intermediates, which might yield aberrant repair products. In this context, it might be expected that the more difficult a DNA lesion is to repair, the more important the DDR pathways become for success.

DDR Kinase-Dependent Regulation of Replication Fork Repair Pathways

DDR regulation of ICL repair during DNA replication is a specialized version of a more general DDR response that coordinates repair of stalled forks. Base damage, dNTP depletion, and even difficult to replicate sequences that form secondary structures or RNA–DNA hybrids can cause fork damage. A stalled fork itself may not be a particularly devastating event to a cell because DNA replication will usually be completed from an adjacent origin of replication. In such cases, the DDR stabilizes the damaged fork to prevent aberrant DNA processing. In other cases, such as in replication of fragile sites that contain few replication origins, fork stabilization may be insufficient and DDR kinase-dependent restart of the stalled fork becomes essential (Casper et al. 2002).

The fork-stabilization activity of ATR is functionally defined either in terms of the ability to restart replication once a blockage is removed or by the changes in DNA or protein composition at the fork. Yeast mutants deficient in the ATR pathway lose the replicative polymerases from the fork (Cobb et al. 2003, 2005; Lucca et al. 2004) and accumulate abnormal DNA structures including long stretches of ssDNA and reversed fork structures resembling Holliday junctions (Lopes et al. 2001; Sogo et al. 2002). At least in yeast, the Exo1 nuclease is involved in generating the excess ssDNA at the stalled fork when the ATR pathway is inactivated (Cotta-Ramusino et al. 2005). Loss of ATR function in *Xenopus* extracts also causes loss of Pol epsilon and collapse of the fork into a DSB (Trenz et al. 2006).

Thus, one way ATR may stabilize a fork is by preventing dissociation of replisome proteins and thereby inhibiting aberrant enzymatic processing of the DNA. However, a recent paper by the Labib group has challenged this model (De Piccoli et al. 2012). This group monitored replisome stability in budding yeast lacking the $Mec1^{ATR}$ or $Rad53^{Chk2}$ checkpoint kinases by immunoprecipitating a subunit of the replicative helicase and immunoblotting for other replisome proteins. In contrast to expectations, they did not observe disassembly of the replisome, and chromatin immunoprecipitation assays suggested that the replisome remained near origins in cells treated with high doses of hydroxyurea to stall forks. A subset of early origins lacked replisome proteins, but the authors concluded that this was as a result of replisome movement away from the earliest origins in the absence of DDR kinase activity instead of replisome disassembly. Thus, in this case, the ATR pathway may be important for restraining fork movement. If fork movement is not accompanied by productive leading and lagging strand synthesis, it could help generate the ssDNA gaps observed by electron microscopy in $Mec1^{ATR}$-deficient yeast.

Exactly how ATR prevents replisome dissociation, movement, and aberrant fork processing is one of the least understood parts of the DDR. One DDR target is the downstream kinase CHK1, which is activated by ATR phosphorylation and needed to prevent fork collapse and regulate origin firing (Cimprich and Cortez 2008). Note that the mammalian and yeast functions of CHK1 and CHK2 have been reversed during evolution so that human CHK1 is the functional equivalent of yeast Rad53 with respect to replication fork regulation. ATR also directly phosphorylates replisome components including several Cdc45-MCM-GINS (CMG) helicase subunits (Cortez et al. 2004; Yoo et al. 2004; Matsuoka et al. 2007; Shi et al. 2007; Trenz et al. 2008; De Piccoli et al. 2012). Phosphorylation of CMG may regulate helicase activity to prevent excessive unwinding and is important to promote rescue of stalled forks from adjacent origins.

In addition, other replication fork proteins including RPA, CLASPIN, and members of the replication fork-pausing complex like TIMELESS, TIPIN, and AND1 are ATR substrates (Matsuoka et al. 2007). Deficiencies in these proteins cause hypersensitivity to replication

stress agents (Chou and Elledge 2006; Errico et al. 2007; Unsal-Kacmaz et al. 2007; Yoshizawa-Sugata and Masai 2007, 2009; Leman et al. 2010). They act in part through promoting ATR-dependent CHK1 activation but may have additional roles in regulating the repair of damaged forks.

The DDR also targets several repair enzymes that remodel damaged forks including WRN, FANCM, and SMARCAL1. The WRN and FANCM proteins are helicases capable of unwinding a variety of complex DNA structures. SMARCAL1 is an SNF2 family ATPase that is activated by complex DNA structures and uses the energy of ATP hydrolysis to reanneal DNA strands (Yusufzai and Kadonaga 2008). All three enzymes are recruited to damaged forks and can catalyze fork regression generating a Holliday junction on model replication substrates (Machwe et al. 2006; Gari et al. 2008a; Betous et al. 2012; Ciccia et al. 2012). They can also branch migrate the Holliday junction, which could restore the normal fork structure (Gari et al. 2008b; Machwe et al. 2011; Betous et al. 2012). All three are targets of ATR phosphorylation (Yannone et al. 2001; Karmakar et al. 2002; Pichierri et al. 2003; Meetei et al. 2005; Bansbach et al. 2009; Sobeck et al. 2009; Ammazzalorso et al. 2010), and deficiencies in WRN and SMARCAL1 activity lead to MUS81-dependent fork cleavage and DSB formation (Franchitto et al. 2008; Betous et al. 2012).

ATR phosphorylation of WRN and FANCM promotes their recruitment to stalled forks (Sobeck et al. 2009; Ammazzalorso et al. 2010), and cells expressing a nonphosphorylatable mutant WRN show increased fork breakage (Ammazzalorso et al. 2010). SMARCAL1 phosphorylation by DDR kinases does not regulate its localization but does regulate its enzymatic activity (D Cortez, unpubl.). The exact substrates of these fork remodeling enzymes at stalled forks and how their activities promote fork restart in cells is not yet known. Additionally, many other helicases and DNA translocases including BLM have roles at damaged forks and are regulated by ATR phosphorylation (Davalos et al. 2004; Li et al. 2004; Sengupta et al. 2004; Rao et al. 2005; Tripathi et al. 2008).

Clearly, a great deal remains to be learned about how ATR promotes replication fork stability, replication-associated DNA repair, and fork restart. These are likely the most important functions of ATR in maintaining genome stability and cell viability based on results from separation of function mutants in both yeast and human ATR (Paciotti et al. 2001; Cobb et al. 2005; Nam et al. 2011). Yet, they are also arguably the least understood. The development of new reversible ATR inhibitors (Charrier et al. 2011; Reaper et al. 2011; Toledo et al. 2011), as well as new techniques to study DNA replication such as iPOND should accelerate the mechanistic studies (Sirbu et al. 2011, 2012). Such studies will be equally critical in defining the pathways that lead to the elevated levels of replication stress observed in cancer cells (Halazonetis et al. 2008). Combined with defects in other genome-maintenance activities, this stress creates an increased dependency on ATR for successful cell division. Thus, the ATR pathway is a promising target for new cancer drug development. Defining how ATR inhibition alters replication-associated DNA repair will be important for understanding the mechanism of action of these drugs.

DDR REGULATES LOCAL CHROMATIN STRUCTURE TO PROMOTE REPAIR

DNA lesions occur in various chromosomal contexts including compacted and opened chromatin, which influences both the activation of the DDR and DNA repair efficiency. For example, in highly condensed chromatin, repairing the damaged structure is more difficult presumably because repair proteins are physically occluded from accessing the damaged structure. Independently of DDR kinases, an ATP-dependent mechanism induces rapid chromatin relaxation around a DSB, and is required for recruitment of break-sensing proteins (Kruhlak et al. 2006). However, several DDR kinase-dependent local chromatin changes also promote a local environment conducive for repair. These activities include creation of a chromatin platform for recruitment of repair and signaling factors, regulating repair factor accessibility to

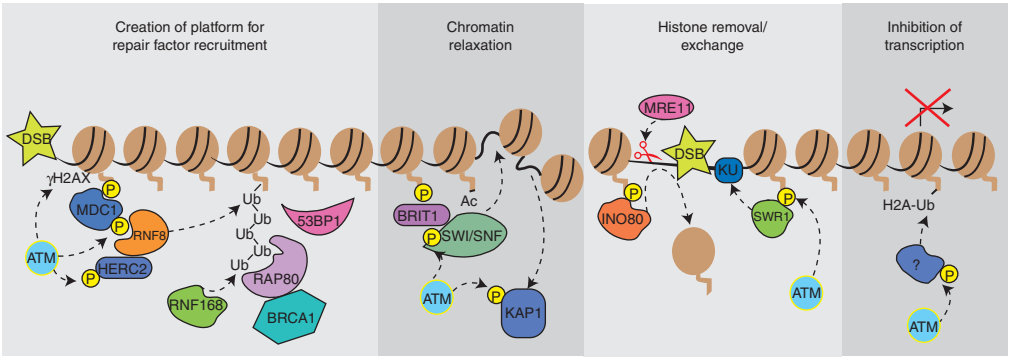

Figure 3. DDR kinases regulate the chromatin near a double-strand break to provide a scaffold for the recruitment of DNA repair proteins, promote repair protein access through nucleosome remodeling, and inhibit local transcription.

the DNA, and inhibition of nearby transcription to prevent potential interference with DNA repair (Fig. 3). Here we discuss the DDR-dependent chromatin response as it relates to DSB repair.

γH2AX as a Platform for DSB Repair

One of the earliest consequences of ATM activation at a DSB is phosphorylation of the histone variant H2AX on an evolutionarily conserved serine (S139) producing γH2AX (Fernandez-Capetillo et al. 2004; Stucki and Jackson 2006; Dickey et al. 2009). A complex of MRN, MDC1, and γH2AX recruits additional ATM to flanking regions of chromatin and facilitates propagation of γH2AX to a large chromatin domain.

γH2AX-MDC1 is a platform for the recruitment of many additional chromatin modifying, DDR signaling, and DNA repair proteins. This scaffold recruits the RING ubiquitin ligases RNF8 and RNF168 to trigger a ubiquitylation cascade surrounding the DSB (Al-Hakim et al. 2010). This recruitment is mediated by ATM-dependent phosphorylation sites on MDC1, which are recognized by the FHA domain of RNF8. Along with the E2 enzyme UBC13, RNF8 catalyzes the formation of Lys63-linked polyubiquitin chains at DSBs (Huen et al. 2007; Kolas et al. 2007; Mailand et al. 2007). Subsequently, RNF168, the protein encoded by the RIDDLIN syndrome gene recognizes and amplifies these ubiquitin chains (Doil et al. 2009; Stewart et al. 2009), whereas another ring finger protein RNF169 antagonizes the ubiquitin cascade (Chen et al. 2012; Poulsen et al. 2012). Another ATM substrate, HERC2, also regulates this process. HERC2 contains an ATM phosphorylation site that binds the RNF8 FHA domain and helps assemble the functional RNF8-UBC13 enzyme (Bekker-Jensen et al. 2010).

Ubiquitylation at the DSB regulates the recruitment of the DSB repair proteins BRCA1 and 53BP1 (Al-Hakim et al. 2010). BRCA1 is itself a ubiquitin ligase and is regulated by ATM and ATR-dependent phosphorylation (Cortez et al. 1999; Tibbetts et al. 2000). BRCA1 is recruited via an interaction with a complex of proteins containing the K63-linked ubiquitin binding protein Rap80 (Kim et al. 2007; Sobhian et al. 2007; Wang et al. 2007; Yan et al. 2007). Three distinct BRCA1 repair complexes (BRCA1-A, BRCA1-B, and BRCA1-C) are recruited, which contain different accessory proteins to regulate checkpoint activation or HR repair (Greenberg et al. 2006). 53BP1 accumulation near the DSB is also dependent on these ubiquitylation events although the mechanism is likely indirect. The overall effect of BRCA1 and 53BP1 recruitment downstream of histone phosphorylation and ubiquitylation is likely regulation of repair choice between NHEJ and HR.

In addition to recruiting repair factors to a DSB, DDR-dependent H2AX phosphorylation also induces changes to chromatin structure by recruiting ATP-dependent chromatin

Cold Spring Harbor Perspectives in Biology
www.cshperspectives.org

remodeling complexes including SWI/SNF, SWR1, and INO80. The SWI/SNF chromatin remodeling activity is targeted to DSBs through interactions with acetylated H3 (Lee et al. 2010) and BRIT1/MCPH1, a protein that binds γH2AX after damage (Wood et al. 2007; Peng et al. 2009). ATM and ATR phosphorylate a SWI/SNF subunit leading to an increased association with BRIT1 and DSBs (Peng et al. 2009). SWI/SNF presumably relaxes chromatin near the break to improve access of DNA repair enzymes to the damaged DNA.

The INO80 and SWR1 complexes are recruited to damage sites through direct interaction with γH2AX. At least in yeast, these complexes promote repair through two distinct mechanisms. INO80 catalyzes histone removal that facilitates Mre11 binding and DNA end resection to promote HR repair, whereas SWR1 promotes KU binding and NHEJ (van Attikum et al. 2007; van Attikum and Gasser 2009). INO80-dependent remodeling may also be important to promote the strand invasion step of HR through displacement of histones at the homologous donor sequences (Tsukuda et al. 2009).

H2AX-Independent but DDR Kinase-Dependent Regulation of Local Chromatin

Besides γH2AX-dependent regulation of repair, ATM controls other chromatin modifications to allow access for repair factors. H2B is monoubiquitylated near DSBs (Moyal et al. 2011). H2B-Ub is catalyzed by an RNF20-RNF40 heterodimer (the human ortholog of yeast Bre1), and this modification is typically associated with actively transcribed genes (Zhu et al. 2005). The levels of H2B-Ub increase near a DSB owing to recruitment of the RNF20-RNF40 proteins through a mechanism that may involve their interaction with ATM and NBS1 (Moyal et al. 2011). Both RNF20 and RNF40 are ATM substrates, and increased H2B-Ub surrounding the break is dependent on RNF20 phosphorylation. Both NHEJ and HR repair are impaired in cells when the damage-induced H2B-Ub is prevented (Moyal et al. 2011). The HR defect was traced to a defect in DNA end resection and could be rescued by experimentally inducing chromatin relaxation. Reduced NHEJ is associated with less XRCC4 and KU80 at the break in the absence of H2B-Ub.

In addition to modulating H2B-Ub, a second mechanism by which ATM relaxes chromatin to promote repair is through phosphorylation of KAP1 (Ziv et al. 2006). KAP1 is a transcriptional corepressor that works with histone methyltransferase and histone deacetylase complexes to promote chromatin compaction. ATM-dependent KAP1 phosphorylation disrupts an interaction between KAP1 and the CHD3 nucleosome remodeler thereby promoting chromatin relaxation (Goodarzi et al. 2011). As a result, ATM is particularly important for repair of DSBs that occur in heterochromatin (Goodarzi et al. 2008a; Noon et al. 2010).

In addition to the examples of local chromatin changes described here, there are changes in other histone modifications regulated by DDR kinases such as an ATM-dependent increase in H2A-Ub that inhibits transcription near DSBs (Shanbhag et al. 2010). There are also changes in the binding of chromatin proteins and the abundance of histone variants. Understanding how the DDR kinases regulate the local chromatin environment to promote repair of other types of DNA lesions, such as those encountered by elongating replication forks, will also be important. Some of the mechanisms may be similar. For example, γH2AX spreads away from stalled forks similarly to the spreading observed at DSBs (Sirbu et al. 2011). However, other mechanisms may be unique, adding to the complexity of the chromatin response to DNA damage.

DDR KINASES FACILITATE REPAIR BY CREATING AN OPTIMAL CELLULAR ENVIRONMENT

In addition to promoting DNA repair through direct regulation of repair proteins and changes in the chromatin near the DNA damage site, the DDR also facilitates repair through more global changes in the cellular environment (Fig. 4). The most obvious example of this mechanism is the checkpoint activity of the DDR kinases, which halts the cell cycle providing time to

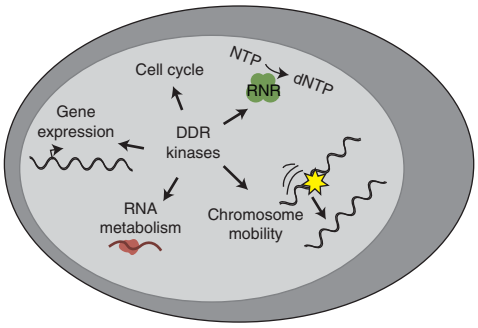

Figure 4. DDR kinases regulate several aspects of nuclear and cellular physiology to provide an environment conducive for successful DNA repair.

repair the DNA damage before DNA replication or mitosis. Checkpoint-dependent changes in cyclin-dependent kinase (CDK) activities also influence DNA repair more directly because many repair proteins are CDK substrates. A second example is the numerous DDR kinase-dependent changes in gene expression that are largely mediated through regulation of p53. In addition to inducing cell cycle arrest and apoptosis, these transcriptional changes can alter the levels of DNA repair proteins, as well as the nucleotides and histones needed for completing repair synthesis and restoring chromatin.

Furthermore, results from functional genomic screens suggest a much broader regulation of cellular physiology by the DDR. For example, proteomic screens for ATM and ATR substrates and genetic screens for new DDR factors based on the level of ATM/ATR activity in undamaged cells identified proteins involved in a wide variety of cellular functions including intracellular protein trafficking, cellular immunity, and RNA metabolism (Matsuoka et al. 2007; Lovejoy et al. 2009; Paulsen et al. 2009; Bansbach and Cortez 2011). In many cases, the connection between these processes and the DDR kinases is likely to promote a cellular environment conducive to DNA repair.

Nuclear Organization and Chromosome Movements Facilitate DNA Repair

One of the important DDR kinase-dependent changes important for repair is regulation of nuclear organization. The nucleus is a highly organized organelle with compartments devoted to specific functions. A long-standing question is whether DNA repair occurs equally well anywhere within the nucleus or whether there are specific repair centers (Misteli and Soutoglou 2009). Recent studies on DSB repair in yeast suggest that repair centers exist and indicate that DDR-dependent changes in chromosome mobility promote HR repair.

Observations of DSBs marked with fluorescent proteins revealed that unrepairable DSBs move to the nuclear periphery and cells with two DSBs merge them into a single repair focus (Nagai et al. 2008; Oza et al. 2009). More recently, the Rothstein and Gasser groups have shown increased chromosomal mobility within the yeast nucleus because of a DSB (Dion et al. 2012; Mine-Hattab and Rothstein 2012). The increased movement depends on the $Mec1^{ATR}$ kinase, resection of the DNA end, and the RAD51 recombinase. Intriguingly, the Rothstein study also showed that the dynamics of unbroken, nonhomologous chromosomes is also increased in the presence of a DSB, suggesting that DDR kinases regulate global nuclear architecture (Mine-Hattab and Rothstein 2012).

The end-result of the increased chromosome mobility is an increase in repair efficiency. Likely this results from an increase in the ability of the RAD51-coated DNA end to find a homologous sequence. Flexibility of the RAD51-coated DNA fiber is important for an efficient homology search (Forget and Kowalczykowski 2012). It is also possible that the movement to or away from a specific nuclear location promotes repair. For example, movement out of a region containing heterochromatin or the nucleolus might increase repair efficiency.

Whether similar changes in chromosome dynamics occur in higher eukaryotes is less clear. Several studies indicate that most DNA ends are largely immobile in mammalian cells (Nelms et al. 1998; Kruhlak et al. 2006; Soutoglou et al. 2007; Jakob et al. 2009). However, deprotected telomere ends have increased mobility compared with protected telomeres (Dimitrova et al. 2008). This increased mobility

depends on both ATM and 53BP1 and these ends are repaired through NHEJ. ATM and 53BP1 also control antigen receptor diversification, and chromosome movement may be needed especially in the context of long-range joining during class switch recombination (Nussenzweig and Nussenzweig 2010). DSBs induced by α particles are also mobile (Aten et al. 2004). Furthermore, breaks in heterochromatin in *Drosophila* cells cause an expansion of the heterochromatin domain followed by movement of the repair focus outside of the heterochromatin (Chiolo et al. 2011). These changes in heterochromatin are dependent on the DDR kinases and seem to be important after the resection step but before the RAD51-dependent homology search for HR repair (Chiolo et al. 2011). Thus, at least in some circumstances the increased mobility of broken chromosomes within the nucleus does occur in metazoan cells.

The mechanism by which the DDR promotes increased chromosome mobility is not known. One clue might be found in the recent observation that DNA attachments to the nuclear pore are regulated by the DDR (Bermejo et al. 2011). In this yeast study, the authors found that DDR kinase modification of nucleoporins releases the interaction between tethered chromosomes and the pore. Another possible mechanism could involve phosphorylation of KAP1, which is observed throughout the nucleus. KAP1 binds the heterochromatin protein HP1 and as mentioned earlier, KAP1 phosphorylation is important for the repair of breaks in heterochromatin (Goodarzi et al. 2008b). Finally, DSB recruitment of chromatin remodeling factors such as INO80 and histone variants such as H2A.Z may be important to promote the increase in mobility (Kalocsay et al. 2009; Neumann et al. 2012). Discovering the mechanisms by which the DDR kinases regulate chromosome dynamics will provide important information about nuclear architecture and how chromosomal domains are maintained. In addition, these studies have significant implications for the mechanisms driving chromosomal translocations and rearrangements that cause cancer.

Control of Cellular Nucleotide Levels for DNA Repair

Perhaps the best-documented example of how the DDR kinases create a cellular environment conducive for repair is through the regulation of nucleotide metabolism. In yeast, the intracellular concentration of dNTPs increases in response to DNA damage, whereas in mammalian cells increased production may be more localized (Chabes et al. 2003; Hakansson et al. 2006b). Higher concentrations of dNTPs cause an increase in mutation frequency (Chabes et al. 2003). Not surprisingly, maintaining an optimal balance of cellular dNTPs is a process strictly controlled at multiple levels by the DDR kinases.

The rate-limiting step in dNTP production is catalyzed by ribonucleotide reductase (RNR) (Nordlund and Reichard 2006). RNR contains two subunits, R1 and R2, encoded by multiple genes in most organisms. DDR kinases regulate RNR at almost every conceivable level. The transcriptional regulation of RNR subunits was one of the first documented functions of the DDR (Elledge et al. 1993). In human cells, a DDR kinase- and p53-dependent pathway induces expression of the catalytic RNR subunit p53R2 after prolonged exposure to DNA damage (Tanaka et al. 2000).

In addition to RNR gene expression, the DDR kinases directly regulate the stability of RNR subunits. For example, ATM phosphorylation of p53R2 increases its stability (Chang et al. 2008). Furthermore, ATR signaling inhibits Cyclin F-dependent R2 degradation, which may be a rapid way of increasing functional RNR enzyme levels (D'Angiolella et al. 2012).

The ATR pathway also controls the localization of the RNR subunits. In yeast, one of the RNR subunits is exported to the cytoplasm after damage to form an active RNR enzyme (Yao et al. 2003). In mammalian cells, RNR subunits may actually be recruited directly to sites of DNA damage to ensure dNTP production right where it is most needed (Niida et al. 2010).

Finally, in budding and fission yeast, small protein inhibitors of RNR including Dif1, Sml1, and Spd1 are regulated by DDR kinases. Dif1 and Spd1 control the localization of RNR sub-

units by regulating nuclear import (Liu et al. 2003; Lee et al. 2008) whereas Sml1 and Spd1 are direct inhibitors of RNR activity (Zhao et al. 1998; Hakansson et al. 2006a). The proteolysis of all three of these proteins is under control of the DDR pathway (Zhao et al. 2001; Liu et al. 2003; Lee et al. 2008; Wu and Huang 2008).

Thus, the DDR kinases control the timely and appropriate production of dNTPs for DNA repair through transcriptional, posttranscriptional, and localization mechanisms targeting RNR. The importance of this pathway to create an optimal cellular environment for repair and replication is illustrated by the observation that, in budding yeast, the lethality associated with deleting $Mec1^{ATR}$ can be rescued by increasing RNR activity (Desany et al. 1998; Zhao et al. 1998). Whether ATR regulation of RNR function is equally important in human cells is unknown.

CONCLUDING REMARKS

The basic DNA repair machinery is often sufficient to reconstitute simple repair reactions in vitro on naked DNA substrates. However, efficient repair often requires regulation by the DNA damage response. The DDR kinases directly modify repair proteins, change chromatin structure around the DNA lesion, and regulate nuclear and cellular environments. Failures at any of these levels cause genome instability and disease. Not surprisingly, the list of DDR kinase substrates is long and our understanding of their regulation is incomplete. Fortunately, new tools for discovery in multiple systems promise to rapidly move us toward an intimate understanding of mechanism. This knowledge may help in the design of cancer therapeutic opportunities based on manipulation of the DNA damage response, epigenetic therapies, and combinations with existing radiation and chemotherapies that work primarily by damaging DNA.

ACKNOWLEDGMENTS

Research in the Cortez laboratory on the DNA damage response and DNA repair is supported by NIH grants R01CA102729 and R01CA136933. B.M.S. is funded by a Department of Defense Breast Cancer Research Program predoctoral fellowship (W81XWH-10-1-0226), and we thank Swim Across America for their support.

REFERENCES

Al-Hakim A, Escribano-Diaz C, Landry MC, O'Donnell L, Panier S, Szilard RK, Durocher D. 2010. The ubiquitous role of ubiquitin in the DNA damage response. *DNA Repair* **9:** 1229–1240.

Ammazzalorso F, Pirzio LM, Bignami M, Franchitto A, Pichierri P. 2010. ATR and ATM differently regulate WRN to prevent DSBs at stalled replication forks and promote replication fork recovery. *EMBO J* **29:** 3156–3169.

Andreassen PR, D'Andrea AD, Taniguchi T. 2004. ATR couples FANCD2 monoubiquitination to the DNA-damage response. *Genes Dev* **18:** 1958–1963.

Aten JA, Stap J, Krawczyk PM, van Oven CH, Hoebe RA, Essers J, Kanaar R. 2004. Dynamics of DNA double-strand breaks revealed by clustering of damaged chromosome domains. *Science* **303:** 92–95.

Bansbach CE, Cortez D. 2011. Defining genome maintenance pathways using functional genomic approaches. *Crit Rev Biochem Mol Biol* **46:** 327–341.

Bansbach CE, Betous R, Lovejoy CA, Glick GG, Cortez D. 2009. The annealing helicase SMARCAL1 maintains genome integrity at stalled replication forks. *Genes Dev* **23:** 2405–2414.

Bekker-Jensen S, Rendtlew Danielsen J, Fugger K, Gromova I, Nerstedt A, Lukas C, Bartek J, Lukas J, Mailand N. 2010. HERC2 coordinates ubiquitin-dependent assembly of DNA repair factors on damaged chromosomes. *Nat Cell Biol* **12:** pp 81–12.

Bermejo R, Capra T, Jossen R, Colosio A, Frattini C, Carotenuto W, Cocito A, Doksani Y, Klein H, Gomez-Gonzalez B, et al. 2011. The replication checkpoint protects fork stability by releasing transcribed genes from nuclear pores. *Cell* **146:** 233–246.

Betous R, Mason AC, Rambo RP, Bansbach CE, Badu-Nkansah A, Sirbu BM, Eichman BF, Cortez D. 2012. SMARCAL1 catalyzes fork regression and Holliday junction migration to maintain genome stability during DNA replication. *Genes Dev* **26:** 151–162.

Brown EJ, Baltimore D. 2000. ATR disruption leads to chromosomal fragmentation and early embryonic lethality. *Genes Dev* **14:** 397–402.

Casper AM, Nghiem P, Arlt MF, Glover TW. 2002. ATR regulates fragile site stability. *Cell* **111:** 779–789.

Chabes A, Georgieva B, Domkin V, Zhao X, Rothstein R, Thelander L. 2003. Survival of DNA damage in yeast directly depends on increased dNTP levels allowed by relaxed feedback inhibition of ribonucleotide reductase. *Cell* **112:** 391–401.

Chang L, Zhou B, Hu S, Guo R, Liu X, Jones SN, Yen Y. 2008. ATM-mediated serine 72 phosphorylation stabilizes ribonucleotide reductase small subunit p53R2 protein

against MDM2 to DNA damage. *Proc Natl Acad Sci* **105:** 18519–18524.

Charrier JD, Durrant SJ, Golec JM, Kay DP, Knegtel RM, Maccormick S, Mortimore M, O'Donnell ME, Pinder JL, Reaper PM, et al. 2011. Discovery of potent and selective inhibitors of ataxia telangiectasia mutated and Rad3 related (ATR) protein kinase as potential anticancer agents. *J Med Chem* **54:** 2320–2330.

Chen J, Feng W, Jiang J, Deng Y, Huen MS. 2012. Ring finger protein RNF169 antagonises the ubiquitin-dependent signaling cascade at sites of DNA damage. *J Biol Chem* **287:** 27715–27722.

Chiolo I, Minoda A, Colmenares SU, Polyzos A, Costes SV, Karpen GH. 2011. Double-strand breaks in heterochromatin move outside of a dynamic HP1a domain to complete recombinational repair. *Cell* **144:** 732–744.

Chou DM, Elledge SJ. 2006. Tipin and timeless form a mutually protective complex required for genotoxic stress resistance and checkpoint function. *Proc Natl Acad Sci* **103:** 18143–18147.

Ciccia A, Elledge SJ. 2010. The DNA damage response: Making it safe to play with knives. *Mol Cell* **40:** 179–204.

Ciccia A, Nimonkar AV, Hu Y, Hajdu I, Achar YJ, Izhar L, Petit SA, Adamson B, Yoon JC, Kowalczykowski SC, et al. 2012. Polyubiquitinated PCNA recruits the ZRANB3 translocase to maintain genomic integrity after replication stress. *Mol Cell* **47:** 396–409.

Cimprich KA, Cortez D. 2008. ATR: An essential regulator of genome integrity. *Nat Rev Mol Cell Biol* **9:** 616–627.

Cobb JA, Bjergbaek L, Shimada K, Frei C, Gasser SM. 2003. DNA polymerase stabilization at stalled replication forks requires Mec1 and the RecQ helicase Sgs1. *EMBO J* **22:** 4325–4336.

Cobb JA, Schleker T, Rojas V, Bjergbaek L, Tercero JA, Gasser SM. 2005. Replisome instability, fork collapse, and gross chromosomal rearrangements arise synergistically from Mec1 kinase and RecQ helicase mutations. *Genes Dev* **19:** 3055–3069.

Collins NB, Wilson JB, Bush T, Thomashevski A, Roberts KJ, Jones NJ, Kupfer GM. 2009. ATR-dependent phosphorylation of FANCA on serine 1449 after DNA damage is important for FA pathway function. *Blood* **113:** 2181–2190.

Cortez D, Wang Y, Qin J, Elledge SJ. 1999. Requirement of ATM-dependent phosphorylation of brca1 in the DNA damage response to double-strand breaks. *Science* **286:** 1162–1166.

Cortez D, Guntuku S, Qin J, Elledge SJ. 2001. ATR and ATRIP: Partners in checkpoint signaling. *Science* **294:** 1713–1716.

Cortez D, Glick G, Elledge SJ. 2004. Minichromosome maintenance proteins are direct targets of the ATM and ATR checkpoint kinases. *Proc Natl Acad Sci* **101:** 10078–10083.

Cotta-Ramusino C, Fachinetti D, Lucca C, Doksani Y, Lopes M, Sogo J, Foiani M. 2005. Exo1 processes stalled replication forks and counteracts fork reversal in checkpoint-defective cells. *Mol Cell* **17:** 153–159.

D'Angiolella V, Donato V, Forrester FM, Jeong YT, Pellacani C, Kudo Y, Saraf A, Florens L, Washburn MP, Pagano M. 2012. Cyclin F-mediated degradation of ribonucleotide reductase M2 controls genome integrity and DNA repair. *Cell* **149:** 1023–1034.

Davalos AR, Kaminker P, Hansen RK, Campisi J. 2004. ATR and ATM-dependent movement of BLM helicase during replication stress ensures optimal ATM activation and 53BP1 focus formation. *Cell Cycle* **3:** 1579–1586.

de Klein A, Muijtjens M, van Os R, Verhoeven Y, Smit B, Carr AM, Lehmann AR, Hoeijmakers JH. 2000. Targeted disruption of the cell-cycle checkpoint gene ATR leads to early embryonic lethality in mice. *Curr Biol* **10:** 479–482.

De Piccoli G, Katou Y, Itoh T, Nakato R, Shirahige K, Labib K. 2012. Replisome stability at defective DNA replication forks is independent of S phase checkpoint kinases. *Mol Cell* **45:** 696–704.

Desany BA, Alcasabas AA, Bachant JB, Elledge SJ. 1998. Recovery from DNA replicational stress is the essential function of the S-phase checkpoint pathway. *Genes Dev* **12:** 2956–2970.

Dickey JS, Redon CE, Nakamura AJ, Baird BJ, Sedelnikova OA, Bonner WM. 2009. H2AX: Functional roles and potential applications. *Chromosoma* **118:** 683–692.

Dimitrova N, Chen YC, Spector DL, de Lange T. 2008. 53BP1 promotes non-homologous end joining of telomeres by increasing chromatin mobility. *Nature* **456:** 524–528.

Dion V, Kalck V, Horigome C, Towbin BD, Gasser SM. 2012. Increased mobility of double-strand breaks requires Mec1, Rad9 and the homologous recombination machinery. *Nat Cell Biol* **14:** 502–509.

Dobbs TA, Tainer JA, Lees-Miller SP. 2010. A structural model for regulation of NHEJ by DNA-PKcs autophosphorylation. *DNA Repair* **9:** 1307–1314.

Doil C, Mailand N, Bekker-Jensen S, Menard P, Larsen DH, Pepperkok R, Ellenberg J, Panier S, Durocher D, Bartek J, et al. 2009. RNF168 binds and amplifies ubiquitin conjugates on damaged chromosomes to allow accumulation of repair proteins. *Cell* **136:** 435–446.

Elledge SJ, Zhou Z, Allen JB, Navas TA. 1993. DNA damage and cell cycle regulation of ribonucleotide reductase. *Bioessays* **15:** 333–339.

Errico A, Costanzo V, Hunt T. 2007. Tipin is required for stalled replication forks to resume DNA replication after removal of aphidicolin in *Xenopus* egg extracts. *Proc Natl Acad Sci* **104:** 14929–14934.

Fernandez-Capetillo O, Lee A, Nussenzweig M, Nussenzweig A. 2004. H2AX: The histone guardian of the genome. *DNA Repair (Amst)* **3:** 959–967.

Forget AL, Kowalczykowski SC. 2012. Single-molecule imaging of DNA pairing by RecA reveals a three-dimensional homology search. *Nature* **482:** 423–427.

Franchitto A, Pirzio LM, Prosperi E, Sapora O, Bignami M, Pichierri P. 2008. Replication fork stalling in WRN-deficient cells is overcome by prompt activation of a MUS81-dependent pathway. *J Cell Biol* **183:** 241–252.

Garcia-Higuera I, Taniguchi T, Ganesan S, Meyn MS, Timmers C, Hejna J, Grompe M, D'Andrea AD. 2001. Interaction of the Fanconi anemia proteins and BRCA1 in a common pathway. *Mol Cell* **7:** 249–262.

Gari K, Decaillet C, Delannoy M, Wu L, Constantinou A. 2008a. Remodeling of DNA replication structures by the

branch point translocase FANCM. *Proc Natl Acad Sci* **105:** 16107–16112.

Gari K, Decaillet C, Stasiak AZ, Stasiak A, Constantinou A. 2008b. The Fanconi anemia protein FANCM can promote branch migration of Holliday junctions and replication forks. *Mol Cell* **29:** 141–148.

Goodarzi AA, Noon AT, Deckbar D, Ziv Y, Shiloh Y, Lobrich M, Jeggo PA. 2008a. ATM signaling facilitates repair of DNA double-strand breaks associated with heterochromatin. *Mol Cell* **31:** 167–177.

Goodarzi AA, Noon AT, Deckbar D, Ziv Y, Shiloh Y, Löbrich M, Jeggo PA. 2008b. ATM signaling facilitates repair of DNA double-strand breaks associated with heterochromatin. *Mol Cell* **31:** 167–177.

Goodarzi AA, Kurka T, Jeggo PA. 2011. KAP-1 phosphorylation regulates CHD3 nucleosome remodeling during the DNA double-strand break response. *Nat Struct Mol Biol* **18:** 831–839.

Greenberg RA, Sobhian B, Pathania S, Cantor SB, Nakatani Y, Livingston DM. 2006. Multifactorial contributions to an acute DNA damage response by BRCA1/BARD1-containing complexes. *Genes Dev* **20:** 34–46.

Hakansson P, Dahl L, Chilkova O, Domkin V, Thelander L. 2006a. The *Schizosaccharomyces pombe* replication inhibitor Spd1 regulates ribonucleotide reductase activity and dNTPs by binding to the large Cdc22 subunit. *J Biol Chem* **281:** 1778–1783.

Hakansson P, Hofer A, Thelander L. 2006b. Regulation of mammalian ribonucleotide reduction and dNTP pools after DNA damage and in resting cells. *J Biol Chem* **281:** 7834–7841.

Halazonetis TD, Gorgoulis VG, Bartek J. 2008. An oncogene-induced DNA damage model for cancer development. *Science* **319:** 1352–1355.

Huen MS, Grant R, Manke I, Minn K, Yu X, Yaffe MB, Chen J. 2007. RNF8 transduces the DNA-damage signal via histone ubiquitylation and checkpoint protein assembly. *Cell* **131:** 901–914.

Ishiai M, Kitao H, Smogorzewska A, Tomida J, Kinomura A, Uchida E, Saberi A, Kinoshita E, Kinoshita-Kikuta E, Koike T, et al. 2008. FANCI phosphorylation functions as a molecular switch to turn on the Fanconi anemia pathway. *Nat Struct Mol Biol* **15:** 1138–1146.

Jakob B, Splinter J, Taucher-Scholz G. 2009. Positional stability of damaged chromatin domains along radiation tracks in mammalian cells. *Radiat Res* **171:** 405–418.

Joo W, Xu G, Persky NS, Smogorzewska A, Rudge DG, Buzovetsky O, Elledge SJ, Pavletich NP. 2011. Structure of the FANCI-FANCD2 complex: Insights into the Fanconi anemia DNA repair pathway. *Science* **333:** 312–316.

Kalocsay M, Hiller NJ, Jentsch S. 2009. Chromosome-wide Rad51 spreading and SUMO-H2A.Z-dependent chromosome fixation in response to a persistent DNA double-strand break. *Mol Cell* **33:** 335–343.

Karmakar P, Piotrowski J, Brosh RM Jr, Sommers JA, Miller SP, Cheng WH, Snowden CM, Ramsden DA, Bohr VA. 2002. Werner protein is a target of DNA-dependent protein kinase in vivo and in vitro, and its catalytic activities are regulated by phosphorylation. *J Biol Chem* **277:** 18291–18302.

Kim H, D'Andrea AD. 2012. Regulation of DNA cross-link repair by the Fanconi anemia/BRCA pathway. *Genes Dev* **26:** 1393–1408.

Kim H, Chen J, Yu X. 2007. Ubiquitin-binding protein RAP80 mediates BRCA1-dependent DNA damage response. *Science* **316:** 1202–1205.

Kim Y, Lach FP, Desetty R, Hanenberg H, Auerbach AD, Smogorzewska A. 2011. Mutations of the SLX4 gene in Fanconi anemia. *Nat Genet* **43:** 142–146.

Knipscheer P, Raschle M, Smogorzewska A, Enoiu M, Ho TV, Scharer OD, Elledge SJ, Walter JC. 2009. The Fanconi anemia pathway promotes replication-dependent DNA interstrand cross-link repair. *Science* **326:** 1698–1701.

Kolas NK, Chapman JR, Nakada S, Ylanko J, Chahwan R, Sweeney FD, Panier S, Mendez M, Wildenhain J, Thomson TM, et al. 2007. Orchestration of the DNA-damage response by the RNF8 ubiquitin ligase. *Science* **318:** 1637–1640.

Kratz K, Schopf B, Kaden S, Sendoel A, Eberhard R, Lademann C, Cannavo E, Sartori AA, Hengartner MO, Jiricny J. 2010. Deficiency of FANCD2-associated nuclease KIAA1018/FAN1 sensitizes cells to interstrand crosslinking agents. *Cell* **142:** 77–88.

Kruhlak MJ, Celeste A, Dellaire G, Fernandez-Capetillo O, Muller WG, McNally JG, Bazett-Jones DP, Nussenzweig A. 2006. Changes in chromatin structure and mobility in living cells at sites of DNA double-strand breaks. *J Cell Biol* **172:** 823–834.

Lavin MF. 2008. Ataxia-telangiectasia: From a rare disorder to a paradigm for cell signalling and cancer. *Nat Rev Mol Cell Biol* **9:** 759–769.

Lee YD, Wang J, Stubbe J, Elledge SJ. 2008. Dif1 is a DNA-damage-regulated facilitator of nuclear import for ribonucleotide reductase. *Mol Cell* **32:** 70–80.

Lee HS, Park JH, Kim SJ, Kwon SJ, Kwon J. 2010. A cooperative activation loop among SWI/SNF, γ-H2AX and H3 acetylation for DNA double-strand break repair. *EMBO J* **29:** 1434–1445.

Leman AR, Noguchi C, Lee CY, Noguchi E. 2010. Human Timeless and Tipin stabilize replication forks and facilitate sister-chromatid cohesion. *J Cell Sci* **123:** 660–670.

Li W, Kim SM, Lee J, Dunphy WG. 2004. Absence of BLM leads to accumulation of chromosomal DNA breaks during both unperturbed and disrupted S phases. *J Cell Biol* **165:** 801–812.

Liu C, Powell KA, Mundt K, Wu L, Carr AM, Caspari T. 2003. Cop9/signalosome subunits and Pcu4 regulate ribonucleotide reductase by both checkpoint-dependent and -independent mechanisms. *Genes Dev* **17:** 1130–1140.

Liu T, Ghosal G, Yuan J, Chen J, Huang J. 2010. FAN1 acts with FANCI-FANCD2 to promote DNA interstrand cross-link repair. *Science* **329:** 693–696.

Long DT, Raschle M, Joukov V, Walter JC. 2011. Mechanism of RAD51-dependent DNA interstrand cross-link repair. *Science* **333:** 84–87.

Lopes M, Cotta-Ramusino C, Pellicioli A, Liberi G, Plevani P, Muzi-Falconi M, Newlon CS, Foiani M. 2001. The DNA replication checkpoint response stabilizes stalled replication forks. *Nature* **412:** 557–561.

Cold Spring Harbor Perspectives in Biology
www.cshperspectives.org

Lovejoy CA, Cortez D. 2009. Common mechanisms of PIKK regulation. *DNA Repair (Amst)* **8:** 1004–1008.

Lovejoy CA, Xu X, Bansbach CE, Glick GG, Zhao R, Ye F, Sirbu BM, Titus LC, Shyr Y, Cortez D. 2009. Functional genomic screens identify CINP as a genome maintenance protein. *Proc Natl Acad Sci* **106:** 19304–19309.

Lucca C, Vanoli F, Cotta-Ramusino C, Pellicioli A, Liberi G, Haber J, Foiani M. 2004. Checkpoint-mediated control of replisome-fork association and signalling in response to replication pausing. *Oncogene* **23:** 1206–1213.

Machwe A, Xiao L, Groden J, Orren DK. 2006. The Werner and Bloom syndrome proteins catalyze regression of a model replication fork. *Biochemistry* **45:** 13939–13946.

Machwe A, Karale R, Xu X, Liu Y, Orren DK. 2011. The Werner and Bloom syndrome proteins help resolve replication blockage by converting (regressed) Holliday junctions to functional replication forks. *Biochemistry* **50:** 6774–6788.

Mailand N, Bekker-Jensen S, Faustrup H, Melander F, Bartek J, Lukas C, Lukas J. 2007. RNF8 ubiquitylates histones at DNA double-strand breaks and promotes assembly of repair proteins. *Cell* **131:** 887–900.

Matsuoka S, Ballif BA, Smogorzewska A, McDonald ER III, Hurov KE, Luo J, Bakalarski CE, Zhao Z, Solimini N, Lerenthal Y, et al. 2007. ATM and ATR substrate analysis reveals extensive protein networks responsive to DNA damage. *Science* **316:** 1160–1166.

Meetei AR, Medhurst AL, Ling C, Xue Y, Singh TR, Bier P, Steltenpool J, Stone S, Dokal I, Mathew CG, et al. 2005. A human ortholog of archaeal DNA repair protein Hef is defective in Fanconi anemia complementation group M. *Nat Genet* **37:** 958–963.

Mine-Hattab J, Rothstein R. 2012. Increased chromosome mobility facilitates homology search during recombination. *Nat Cell Biol* **14:** 510–517.

Misteli T, Soutoglou E. 2009. The emerging role of nuclear architecture in DNA repair and genome maintenance. *Nat Rev Mol Cell Biol* **10:** 243–254.

Moyal L, Lerenthal Y, Gana-Weisz M, Mass G, So S, Wang SY, Eppink B, Chung YM, Shalev G, Shema E, et al. 2011. Requirement of ATM-dependent monoubiquitylation of histone H2B for timely repair of DNA double-strand breaks. *Mol Cell* **41:** 529–542.

Nagai S, Dubrana K, Tsai-Pflugfelder M, Davidson MB, Roberts TM, Brown GW, Varela E, Hediger F, Gasser SM, Krogan NJ. 2008. Functional targeting of DNA damage to a nuclear pore-associated SUMO-dependent ubiquitin ligase. *Science* **322:** 597–602.

Nam EA, Zhao R, Cortez D. 2011. Analysis of mutations that dissociate G_2 and essential S phase functions of human ataxia telangiectasia-mutated and Rad3-related (ATR) protein kinase. *J Biol Chem* **286:** 37320–37327.

Negrini S, Gorgoulis VG, Halazonetis TD. 2010. Genomic instability—An evolving hallmark of cancer. *Nat Rev Mol Cell Biol* **11:** 220–228.

Nelms BE, Maser RS, MacKay JF, Lagally MG, Petrini JH. 1998. In situ visualization of DNA double-strand break repair in human fibroblasts. *Science* **280:** 590–592.

Neumann FR, Dion V, Gehlen LR, Tsai-Pflugfelder M, Schmid R, Taddei A, Gasser SM. 2012. Targeted INO80 enhances subnuclear chromatin movement and ectopic homologous recombination. *Genes Dev* **26:** 369–383.

Niida H, Katsuno Y, Sengoku M, Shimada M, Yukawa M, Ikura M, Ikura T, Kohno K, Shima H, Suzuki H, et al. 2010. Essential role of Tip60-dependent recruitment of ribonucleotide reductase at DNA damage sites in DNA repair during G1 phase. *Genes Dev* **24:** 333–338.

Noon AT, Shibata A, Rief N, Lobrich M, Stewart GS, Jeggo PA, Goodarzi AA. 2010. 53BP1-dependent robust localized KAP-1 phosphorylation is essential for heterochromatic DNA double-strand break repair. *Nat Cell Biol* **12:** 177–184.

Nordlund P, Reichard P. 2006. Ribonucleotide reductases. *Annu Rev Biochem* **75:** 681–706.

Nussenzweig A, Nussenzweig MC. 2010. Origin of chromosomal translocations in lymphoid cancer. *Cell* **141:** 27–38.

Oza P, Jaspersen SL, Miele A, Dekker J, Peterson CL. 2009. Mechanisms that regulate localization of a DNA double-strand break to the nuclear periphery. *Genes Dev* **23:** 912–927.

Paciotti V, Clerici M, Scotti M, Lucchini G, Longhese MP. 2001. Characterization of mec1 kinase-deficient mutants and of new hypomorphic mec1 alleles impairing subsets of the DNA damage response pathway. *Mol Cell Biol* **21:** 3913–3925.

Paulsen RD, Soni DV, Wollman R, Hahn AT, Yee MC, Guan A, Hesley JA, Miller SC, Cromwell EF, Solow-Cordero DE, et al. 2009. A genome-wide siRNA screen reveals diverse cellular processes and pathways that mediate genome stability. *Mol Cell* **35:** 228–239.

Peng G, Yim EK, Dai H, Jackson AP, Burgt I, Pan MR, Hu R, Li K, Lin SY. 2009. BRIT1/MCPH1 links chromatin remodelling to DNA damage response. *Nat Cell Biol* **11:** 865–872.

Pichierri P, Rosselli F, Franchitto A. 2003. Werner's syndrome protein is phosphorylated in an ATR/ATM-dependent manner following replication arrest and DNA damage induced during the S phase of the cell cycle. *Oncogene* **22:** 1491–1500.

Poulsen M, Lukas C, Lukas J, Bekker-Jensen S, Mailand N. 2012. Human RNF169 is a negative regulator of the ubiquitin-dependent response to DNA double-strand breaks. *J Cell Biol* **197:** 189–199.

Qiao F, Mi J, Wilson JB, Zhi G, Bucheimer NR, Jones NJ, Kupfer GM. 2004. Phosphorylation of fanconi anemia (FA) complementation group G protein, FANCG, at serine 7 is important for function of the FA pathway. *J Biol Chem* **279:** 46035–46045.

Rao VA, Fan AM, Meng L, Doe CF, North PS, Hickson ID, Pommier Y. 2005. Phosphorylation of BLM, dissociation from topoisomerase IIIα, and colocalization with γ-H2AX after topoisomerase I-induced replication damage. *Mol Cell Biol* **25:** 8925–8937.

Raschle M, Knipscheer P, Enoiu M, Angelov T, Sun J, Griffith JD, Ellenberger TE, Scharer OD, Walter JC. 2008. Mechanism of replication-coupled DNA interstrand crosslink repair. *Cell* **134:** 969–980.

Reaper PM, Griffiths MR, Long JM, Charrier JD, Maccormick S, Charlton PA, Golec JM, Pollard JR. 2011. Selective killing of ATM- or p53-deficient cancer cells through inhibition of ATR. *Nat Chem Biol* **7:** 428–430.

Sengupta S, Robles AI, Linke SP, Sinogeeva NI, Zhang R, Pedeux R, Ward IM, Celeste A, Nussenzweig A, Chen J, et al. 2004. Functional interaction between BLM helicase and 53BP1 in a Chk1-mediated pathway during S-phase arrest. *J Cell Biol* **166:** 801–813.

Shanbhag NM, Rafalska-Metcalf IU, Balane-Bolivar C, Janicki SM, Greenberg RA. 2010. ATM-dependent chromatin changes silence transcription in *cis* to DNA double-strand breaks. *Cell* **141:** 970–981.

Shell SM, Li Z, Shkriabai N, Kvaratskhelia M, Brosey C, Serrano MA, Chazin WJ, Musich PR, Zou Y. 2009. Checkpoint kinase ATR promotes nucleotide excision repair of UV-induced DNA damage via physical interaction with xeroderma pigmentosum group A. *J Biol Chem* **284:** 24213–24222.

Shi Y, Dodson GE, Mukhopadhyay PS, Shanware NP, Trinh AT, Tibbetts RS. 2007. Identification of carboxyl-terminal MCM3 phosphorylation sites using polyreactive phosphospecific antibodies. *J Biol Chem* **282:** 9236–9243.

Shiloh Y. 2003. ATM and related protein kinases: Safeguarding genome integrity. *Nat Rev Cancer* **3:** 155–168.

Sirbu BM, Couch FB, Feigerle JT, Bhaskara S, Hiebert SW, Cortez D. 2011. Analysis of protein dynamics at active, stalled, and collapsed replication forks. *Genes Dev* **25:** 1320–1327.

Sirbu BM, Couch FB, Cortez D. 2012. Monitoring the spatiotemporal dynamics of proteins at replication forks and in assembled chromatin using isolation of proteins on nascent DNA. *Nat Protoc* **7:** 594–605.

Smogorzewska A, Desetty R, Saito TT, Schlabach M, Lach FP, Sowa ME, Clark AB, Kunkel TA, Harper JW, Colaiacovo MP, et al. 2010. A genetic screen identifies FAN1, a Fanconi anemia-associated nuclease necessary for DNA interstrand crosslink repair. *Mol Cell* **39:** 36–47.

Sobeck A, Stone S, Landais I, de Graaf B, Hoatlin ME. 2009. The Fanconi anemia protein FANCM is controlled by FANCD2 and the ATR/ATM pathways. *J Biol Chem* **284:** 25560–25568.

Sobhian B, Shao G, Lilli DR, Culhane AC, Moreau LA, Xia B, Livingston DM, Greenberg RA. 2007. RAP80 targets BRCA1 to specific ubiquitin structures at DNA damage sites. *Science* **316:** 1198–1202.

Sogo JM, Lopes M, Foiani M. 2002. Fork reversal and ssDNA accumulation at stalled replication forks owing to checkpoint defects. *Science* **297:** 599–602.

Sorensen CS, Hansen LT, Dziegielewski J, Syljuasen RG, Lundin C, Bartek J, Helleday T. 2005. The cell-cycle checkpoint kinase Chk1 is required for mammalian homologous recombination repair. *Nat Cell Biol* **7:** 195–201.

Soutoglou E, Dorn JF, Sengupta K, Jasin M, Nussenzweig A, Ried T, Danuser G, Misteli T. 2007. Positional stability of single double-strand breaks in mammalian cells. *Nat Cell Biol* **9:** 675–682.

Stewart GS, Panier S, Townsend K, Al-Hakim AK, Kolas NK, Miller ES, Nakada S, Ylanko J, Olivarius S, Mendez M, et al. 2009. The RIDDLE syndrome protein mediates a ubiquitin-dependent signaling cascade at sites of DNA damage. *Cell* **136:** 420–434.

Stucki M, Jackson SP. 2006. γH2AX and MDC1: Anchoring the DNA-damage-response machinery to broken chromosomes. *DNA Repair (Amst)* **5:** 534–543.

Tanaka H, Arakawa H, Yamaguchi T, Shiraishi K, Fukuda S, Matsui K, Takei Y, Nakamura Y. 2000. A ribonucleotide reductase gene involved in a p53-dependent cell-cycle checkpoint for DNA damage. *Nature* **404:** 42–49.

Tibbetts RS, Cortez D, Brumbaugh KM, Scully R, Livingston D, Elledge SJ, Abraham RT. 2000. Functional interactions between BRCA1 and the checkpoint kinase ATR during genotoxic stress. *Genes Dev* **14:** 2989–3002.

Toledo LI, Murga M, Zur R, Soria R, Rodriguez A, Martinez S, Oyarzabal J, Pastor J, Bischoff JR, Fernandez-Capetillo O. 2011. A cell-based screen identifies ATR inhibitors with synthetic lethal properties for cancer-associated mutations. *Nat Struct Mol Biol* **18:** 721–727.

Trenz K, Smith E, Smith S, Costanzo V. 2006. ATM and ATR promote Mre11 dependent restart of collapsed replication forks and prevent accumulation of DNA breaks. *EMBO J* **25:** 1764–1774.

Trenz K, Errico A, Costanzo V. 2008. Plx1 is required for chromosomal DNA replication under stressful conditions. *EMBO J* **27:** 876–885.

Tripathi V, Kaur S, Sengupta S. 2008. Phosphorylation-dependent interactions of BLM and 53BP1 are required for their anti-recombinogenic roles during homologous recombination. *Carcinogenesis* **29:** 52–61.

Tsukuda T, Lo YC, Krishna S, Sterk R, Osley MA, Nickoloff JA. 2009. INO80-dependent chromatin remodeling regulates early and late stages of mitotic homologous recombination. *DNA Repair (Amst)* **8:** 360–369.

Unsal-Kacmaz K, Chastain PD, Qu PP, Minoo P, Cordeiro-Stone M, Sancar A, Kaufmann WK. 2007. The human Tim/Tipin complex coordinates an Intra-S checkpoint response to UV that slows replication fork displacement. *Mol Cell Biol* **27:** 3131–3142.

van Attikum H, Gasser SM. 2009. Crosstalk between histone modifications during the DNA damage response. *Trends Cell Biol* **19:** 207–217.

van Attikum H, Fritsch O, Gasser SM. 2007. Distinct roles for SWR1 and INO80 chromatin remodeling complexes at chromosomal double-strand breaks. *EMBO J* **26:** 4113–4125.

Wang B, Matsuoka S, Ballif BA, Zhang D, Smogorzewska A, Gygi SP, Elledge SJ. 2007. Abraxas and RAP80 form a BRCA1 protein complex required for the DNA damage response. *Science* **316:** 1194–1198.

Weterings E, Chen DJ. 2007. DNA-dependent protein kinase in nonhomologous end joining: A lock with multiple keys? *J Cell Biol* **179:** 183–186.

Wilson JB, Yamamoto K, Marriott AS, Hussain S, Sung P, Hoatlin ME, Mathew CG, Takata M, Thompson LH, Kupfer GM, et al. 2008. FANCG promotes formation of a newly identified protein complex containing BRCA2, FANCD2 and XRCC3. *Oncogene* **27:** 3641–3652.

Wood JL, Singh N, Mer G, Chen J. 2007. MCPH1 functions in an H2AX-dependent but MDC1-independent pathway in response to DNA damage. *J Biol Chem* **282:** 35416–35423.

Wu X, Huang M. 2008. Dif1 controls subcellular localization of ribonucleotide reductase by mediating nuclear import of the R2 subunit. *Mol Cell Biol* **28:** 7156–7167.

Wu X, Shell SM, Liu Y, Zou Y. 2007. ATR-dependent checkpoint modulates XPA nuclear import in response to UV irradiation. *Oncogene* **26:** 757–764.

Yan J, Kim YS, Yang XP, Li LP, Liao G, Xia F, Jetten AM. 2007. The ubiquitin-interacting motif containing protein RAP80 interacts with BRCA1 and functions in DNA damage repair response. *Cancer Res* **67:** 6647–6656.

Yang K, Moldovan GL, Vinciguerra P, Murai J, Takeda S, D'Andrea AD. 2011. Regulation of the Fanconi anemia pathway by a SUMO-like delivery network. *Genes Dev* **25:** 1847–1858.

Yannone SM, Roy S, Chan DW, Murphy MB, Huang S, Campisi J, Chen DJ. 2001. Werner syndrome protein is regulated and phosphorylated by DNA-dependent protein kinase. *J Biol Chem* **276:** 38242–38248.

Yao R, Zhang Z, An X, Bucci B, Perlstein DL, Stubbe J, Huang M. 2003. Subcellular localization of yeast ribonucleotide reductase regulated by the DNA replication and damage checkpoint pathways. *Proc Natl Acad Sci* **100:** 6628–6633.

Yoo HY, Shevchenko A, Dunphy WG. 2004. Mcm2 is a direct substrate of ATM and ATR during DNA damage and DNA replication checkpoint responses. *J Biol Chem* **279:** 53353–53364.

Yoshizawa-Sugata N, Masai H. 2007. Human Tim/Timeless-interacting protein, Tipin, is required for efficient progression of S phase and DNA replication checkpoint. *J Biol Chem* **282:** 2729–2740.

Yoshizawa-Sugata N, Masai H. 2009. Roles of human AND-1 in chromosome transactions in S phase. *J Biol Chem* **284:** 20718–20728.

Yusufzai T, Kadonaga JT. 2008. HARP is an ATP-driven annealing helicase. *Science* **322:** 748–750.

Zhao X, Muller EG, Rothstein R. 1998. A suppressor of two essential checkpoint genes identifies a novel protein that negatively affects dNTP pools. *Mol Cell* **2:** 329–340.

Zhao X, Chabes A, Domkin V, Thelander L, Rothstein R. 2001. The ribonucleotide reductase inhibitor Sml1 is a new target of the Mec1/Rad53 kinase cascade during growth and in response to DNA damage. *EMBO J* **20:** 3544–3553.

Zhu B, Zheng Y, Pham AD, Mandal SS, Erdjument-Bromage H, Tempst P, Reinberg D. 2005. Monoubiquitination of human histone H2B: The factors involved and their roles in HOX gene regulation. *Mol Cell* **20:** 601–611.

Ziv Y, Bielopolski D, Galanty Y, Lukas C, Taya Y, Schultz DC, Lukas J, Bekker-Jensen S, Bartek J, Shiloh Y. 2006. Chromatin relaxation in response to DNA double-strand breaks is modulated by a novel ATM- and KAP-1 dependent pathway. *Nat Cell Biol* **8:** 870–876.

REFERENCES

1. Sirbu, B.M., et al., *Analysis of protein dynamics at active, stalled, and collapsed replication forks.* Genes & development, 2011. **25**(12): p. 1320-7.
2. Groth, A., et al., *Chromatin challenges during DNA replication and repair.* Cell, 2007. **128**(4): p. 721-33.
3. Probst, A.V., E. Dunleavy, and G. Almouzni, *Epigenetic inheritance during the cell cycle.* Nat Rev Mol Cell Biol, 2009. **10**(3): p. 192-206.
4. Shibahara, K. and B. Stillman, *Replication-dependent marking of DNA by PCNA facilitates CAF-1-coupled inheritance of chromatin.* Cell, 1999. **96**(4): p. 575-85.
5. Sobel, R.E., et al., *Conservation of deposition-related acetylation sites in newly synthesized histones H3 and H4.* Proc Natl Acad Sci U S A, 1995. **92**(4): p. 1237-41.
6. Leffak, I.M., R. Grainger, and H. Weintraub, *Conservative assembly and segregation of nucleosomal histones.* Cell, 1977. **12**(3): p. 837-45.
7. Ge, Z., et al., *Sites of acetylation on newly synthesized histone H4 are required for chromatin assembly and DNA damage response signaling.* Mol Cell Biol, 2013.
8. Parthun, M.R., *Histone acetyltransferase 1: More than just an enzyme?* Biochim Biophys Acta, 2012. **1819**(3-4): p. 256-63.
9. Chuang, L.S., et al., *Human DNA-(cytosine-5) methyltransferase-PCNA complex as a target for p21WAF1.* Science, 1997. **277**(5334): p. 1996-2000.
10. Arita, K., et al., *Recognition of hemi-methylated DNA by the SRA protein UHRF1 by a base-flipping mechanism.* Nature, 2008. **455**(7214): p. 818-21.
11. Issa, J.P., *CpG island methylator phenotype in cancer.* Nat Rev Cancer, 2004. **4**(12): p. 988-93.
12. Bell, S.P. and A. Dutta, *DNA replication in eukaryotic cells.* Annu Rev Biochem, 2002. **71**: p. 333-74.
13. Diffley, J.F. and K. Labib, *The chromosome replication cycle.* J Cell Sci, 2002. **115**(Pt 5): p. 869-72.
14. Cimprich, K.A. and D. Cortez, *ATR: an essential regulator of genome integrity.* Nat Rev Mol Cell Biol, 2008. **9**(8): p. 616-27.
15. Brown, E.J. and D. Baltimore, *ATR disruption leads to chromosomal fragmentation and early embryonic lethality.* Genes Dev, 2000. **14**(4): p. 397-402.
16. de Klein, A., et al., *Targeted disruption of the cell-cycle checkpoint gene ATR leads to early embryonic lethality in mice.* Curr Biol, 2000. **10**(8): p. 479-82.

17. Cortez, D., et al., *ATR and ATRIP: partners in checkpoint signaling.* Science, 2001. **294**(5547): p. 1713-6.
18. O'Driscoll, M., et al., *A splicing mutation affecting expression of ataxia-telangiectasia and Rad3-related protein (ATR) results in Seckel syndrome.* Nat Genet, 2003. **33**(4): p. 497-501.
19. Alderton, G.K., et al., *Seckel syndrome exhibits cellular features demonstrating defects in the ATR-signalling pathway.* Hum Mol Genet, 2004. **13**(24): p. 3127-38.
20. Shiloh, Y., *ATM and related protein kinases: safeguarding genome integrity.* Nat Rev Cancer, 2003. **3**(3): p. 155-68.
21. Lavin, M.F., *Ataxia-telangiectasia: from a rare disorder to a paradigm for cell signalling and cancer.* Nat Rev Mol Cell Biol, 2008. **9**(10): p. 759-69.
22. Negrini, S., V.G. Gorgoulis, and T.D. Halazonetis, *Genomic instability--an evolving hallmark of cancer.* Nat Rev Mol Cell Biol, 2010. **11**(3): p. 220-8.
23. Lovejoy, C.A. and D. Cortez, *Common mechanisms of PIKK regulation.* DNA Repair (Amst), 2009. **8**(9): p. 1004-8.
24. Casper, A.M., et al., *ATR regulates fragile site stability.* Cell, 2002. **111**(6): p. 779-89.
25. Yeeles, J.T., et al., *Rescuing stalled or damaged replication forks.* Cold Spring Harb Perspect Biol, 2013. **5**(5).
26. Raschle, M., et al., *Mechanism of replication-coupled DNA interstrand crosslink repair.* Cell, 2008. **134**(6): p. 969-80.
27. Ben-Yehoyada, M., et al., *Checkpoint signaling from a single DNA interstrand crosslink.* Mol Cell, 2009. **35**(5): p. 704-15.
28. Kim, H. and A.D. D'Andrea, *Regulation of DNA cross-link repair by the Fanconi anemia/BRCA pathway.* Genes Dev, 2012. **26**(13): p. 1393-408.
29. Meetei, A.R., et al., *A human ortholog of archaeal DNA repair protein Hef is defective in Fanconi anemia complementation group M.* Nat Genet, 2005. **37**(9): p. 958-63.
30. Garcia-Higuera, I., et al., *Interaction of the Fanconi anemia proteins and BRCA1 in a common pathway.* Mol Cell, 2001. **7**(2): p. 249-62.
31. Kratz, K., et al., *Deficiency of FANCD2-associated nuclease KIAA1018/FAN1 sensitizes cells to interstrand crosslinking agents.* Cell, 2010. **142**(1): p. 77-88.
32. Liu, T., et al., *FAN1 acts with FANCI-FANCD2 to promote DNA interstrand cross-link repair.* Science, 2010. **329**(5992): p. 693-6.
33. Smogorzewska, A., et al., *Identification of the FANCI protein, a monoubiquitinated FANCD2 paralog required for DNA repair.* Cell, 2007. **129**(2): p. 289-301.
34. Long, D.T., et al., *Mechanism of RAD51-dependent DNA interstrand cross-link repair.* Science, 2011. **333**(6038): p. 84-7.
35. Cobb, J.A., et al., *DNA polymerase stabilization at stalled replication forks requires Mec1 and the RecQ helicase Sgs1.* EMBO J, 2003. **22**(16): p. 4325-36.

36. Cobb, J.A., et al., *Replisome instability, fork collapse, and gross chromosomal rearrangements arise synergistically from Mec1 kinase and RecQ helicase mutations.* Genes Dev, 2005. **19**(24): p. 3055-69.
37. Lucca, C., et al., *Checkpoint-mediated control of replisome-fork association and signalling in response to replication pausing.* Oncogene, 2004. **23**(6): p. 1206-13.
38. Lopes, M., et al., *The DNA replication checkpoint response stabilizes stalled replication forks.* Nature, 2001. **412**(6846): p. 557-61.
39. Sogo, J.M., M. Lopes, and M. Foiani, *Fork reversal and ssDNA accumulation at stalled replication forks owing to checkpoint defects.* Science, 2002. **297**(5581): p. 599-602.
40. Trenz, K., et al., *ATM and ATR promote Mre11 dependent restart of collapsed replication forks and prevent accumulation of DNA breaks.* EMBO J, 2006. **25**(8): p. 1764-74.
41. Matsuoka, S., et al., *ATM and ATR substrate analysis reveals extensive protein networks responsive to DNA damage.* Science, 2007. **316**(5828): p. 1160-6.
42. Chou, D.M. and S.J. Elledge, *Tipin and Timeless form a mutually protective complex required for genotoxic stress resistance and checkpoint function.* Proc Natl Acad Sci U S A, 2006. **103**(48): p. 18143-7.
43. Unsal-Kacmaz, K., et al., *The human Tim/Tipin complex coordinates an Intra-S checkpoint response to UV that slows replication fork displacement.* Mol Cell Biol, 2007. **27**(8): p. 3131-42.
44. Yoshizawa-Sugata, N. and H. Masai, *Human Tim/Timeless-interacting protein, Tipin, is required for efficient progression of S phase and DNA replication checkpoint.* J Biol Chem, 2007. **282**(4): p. 2729-40.
45. Leman, A.R., et al., *Human Timeless and Tipin stabilize replication forks and facilitate sister-chromatid cohesion.* J Cell Sci, 2010. **123**(Pt 5): p. 660-70.
46. Ciccia, A. and S.J. Elledge, *The DNA damage response: making it safe to play with knives.* Molecular cell, 2010. **40**(2): p. 179-204.
47. Yusufzai, T. and J.T. Kadonaga, *HARP is an ATP-driven annealing helicase.* Science, 2008. **322**(5902): p. 748-50.
48. Betous, R., et al., *Substrate-Selective Repair and Restart of Replication Forks by DNA Translocases.* Cell Rep, 2013.
49. Rudin, N. and J.E. Haber, *Efficient repair of HO-induced chromosomal breaks in Saccharomyces cerevisiae by recombination between flanking homologous sequences.* Mol Cell Biol, 1988. **8**(9): p. 3918-28.
50. Rodrigue, A., et al., *Interplay between human DNA repair proteins at a unique double-strand break in vivo.* EMBO J, 2006. **25**(1): p. 222-31.
51. Soutoglou, E., et al., *Positional stability of single double-strand breaks in mammalian cells.* Nat Cell Biol, 2007. **9**(6): p. 675-82.

52. Berkovich, E., R.J. Monnat, Jr., and M.B. Kastan, *Assessment of protein dynamics and DNA repair following generation of DNA double-strand breaks at defined genomic sites.* Nat Protoc, 2008. **3**(5): p. 915-22.
53. Morrison, A.J. and X. Shen, *Chromatin remodelling beyond transcription: the INO80 and SWR1 complexes.* Nat Rev Mol Cell Biol, 2009. **10**(6): p. 373-84.
54. van Attikum, H., et al., *Recruitment of the INO80 complex by H2A phosphorylation links ATP-dependent chromatin remodeling with DNA double-strand break repair.* Cell, 2004. **119**(6): p. 777-88.
55. Rossetto, D., et al., *Epigenetic modifications in double-strand break DNA damage signaling and repair.* Clin Cancer Res, 2010. **16**(18): p. 4543-52.
56. Venkitaraman, A.R., *Modifying chromatin architecture during the response to DNA breakage.* Crit Rev Biochem Mol Biol, 2010. **45**(1): p. 2-13.
57. Sirbu, B.M., F.B. Couch, and D. Cortez, *Monitoring the spatiotemporal dynamics of proteins at replication forks and in assembled chromatin using isolation of proteins on nascent DNA.* Nat Protoc, 2012. **7**(3): p. 594-605.
58. Gallagher, S.R., *One-dimensional SDS gel electrophoresis of proteins.* Curr Protoc Protein Sci, 2001. **Chapter 10**: p. Unit 10 1.
59. Shevchenko, A., et al., *In-gel digestion for mass spectrometric characterization of proteins and proteomes.* Nat Protoc, 2006. **1**(6): p. 2856-60.
60. Kim, H.Y., et al., *An azido-biotin reagent for use in the isolation of protein adducts of lipid-derived electrophiles by streptavidin catch and photorelease.* Mol Cell Proteomics, 2009. **8**(9): p. 2080-9.
61. Reaper, P.M., et al., *Selective killing of ATM- or p53-deficient cancer cells through inhibition of ATR.* Nat Chem Biol, 2011. **7**(7): p. 428-30.
62. Charrier, J.D., et al., *Discovery of potent and selective inhibitors of ataxia telangiectasia mutated and Rad3 related (ATR) protein kinase as potential anticancer agents.* J Med Chem, 2011. **54**(7): p. 2320-30.
63. MacCoss, M.J., et al., *Shotgun identification of protein modifications from protein complexes and lens tissue.* Proc Natl Acad Sci U S A, 2002. **99**(12): p. 7900-5.
64. Martinez, M.N., et al., *Obesity and altered glucose metabolism impact HDL composition in CETP transgenic mice: a role for ovarian hormones.* J Lipid Res, 2012. **53**(3): p. 379-89.
65. Tabb, D.L., C.G. Fernando, and M.C. Chambers, *MyriMatch: highly accurate tandem mass spectral peptide identification by multivariate hypergeometric analysis.* J Proteome Res, 2007. **6**(2): p. 654-61.
66. Yates, J.R., 3rd, et al., *Method to correlate tandem mass spectra of modified peptides to amino acid sequences in the protein database.* Anal Chem, 1995. **67**(8): p. 1426-36.

67. Chen, Y.Y., et al., *Refining comparative proteomics by spectral counting to account for shared peptides and multiple search engines.* Anal Bioanal Chem, 2012. **404**(4): p. 1115-25.
68. Ma, Z.Q., et al., *IDPicker 2.0: Improved protein assembly with high discrimination peptide identification filtering.* J Proteome Res, 2009. **8**(8): p. 3872-81.
69. UniProt, C., *Reorganizing the protein space at the Universal Protein Resource (UniProt).* Nucleic Acids Res, 2012. **40**(Database issue): p. D71-5.
70. Huang da, W., B.T. Sherman, and R.A. Lempicki, *Systematic and integrative analysis of large gene lists using DAVID bioinformatics resources.* Nat Protoc, 2009. **4**(1): p. 44-57.
71. Huang da, W., B.T. Sherman, and R.A. Lempicki, *Bioinformatics enrichment tools: paths toward the comprehensive functional analysis of large gene lists.* Nucleic Acids Res, 2009. **37**(1): p. 1-13.
72. Li, M., et al., *Comparative shotgun proteomics using spectral count data and quasi-likelihood modeling.* J Proteome Res, 2010. **9**(8): p. 4295-305.
73. Chen, J., et al., *ToppGene Suite for gene list enrichment analysis and candidate gene prioritization.* Nucleic Acids Res, 2009. **37**(Web Server issue): p. W305-11.
74. Warde-Farley, D., et al., *The GeneMANIA prediction server: biological network integration for gene prioritization and predicting gene function.* Nucleic Acids Res, 2010. **38**(Web Server issue): p. W214-20.
75. Uhlen, M. and F. Ponten, *Antibody-based proteomics for human tissue profiling.* Mol Cell Proteomics, 2005. **4**(4): p. 384-93.
76. MacLean, B., et al., *Skyline: an open source document editor for creating and analyzing targeted proteomics experiments.* Bioinformatics, 2010. **26**(7): p. 966-8.
77. Hoeijmakers, J.H., *Genome maintenance mechanisms for preventing cancer.* Nature, 2001. **411**(6835): p. 366-74.
78. Salic, A. and T.J. Mitchison, *A chemical method for fast and sensitive detection of DNA synthesis in vivo.* Proc Natl Acad Sci U S A, 2008. **105**(7): p. 2415-20.
79. Moses, J.E. and A.D. Moorhouse, *The growing applications of click chemistry.* Chem Soc Rev, 2007. **36**(8): p. 1249-62.
80. Koval, O.A., et al., *[Copper-catalyzed cleavage of DNA by arenes].* Bioorg Khim, 2003. **29**(6): p. 632-9.
81. Szychowski, J., et al., *Cleavable biotin probes for labeling of biomolecules via azide-alkyne cycloaddition.* J Am Chem Soc, 2010. **132**(51): p. 18351-60.
82. Lopez-Contreras, A.J., et al., *A Proteomic Characterization of Factors Enriched at Nascent DNA Molecules.* Cell Rep, 2013.
83. Worcel, A., S. Han, and M.L. Wong, *Assembly of newly replicated chromatin.* Cell, 1978. **15**(3): p. 969-77.

84. Herrick, J. and A. Bensimon, *Global regulation of genome duplication in eukaryotes: an overview from the epifluorescence microscope.* Chromosoma, 2008. **117**(3): p. 243-60.
85. Reyes-Lamothe, R., D.J. Sherratt, and M.C. Leake, *Stoichiometry and architecture of active DNA replication machinery in Escherichia coli.* Science, 2010. **328**(5977): p. 498-501.
86. Aladjem, M.I., *Replication in context: dynamic regulation of DNA replication patterns in metazoans.* Nat Rev Genet, 2007. **8**(8): p. 588-600.
87. Petermann, E., et al., *Hydroxyurea-stalled replication forks become progressively inactivated and require two different RAD51-mediated pathways for restart and repair.* Mol Cell, 2010. **37**(4): p. 492-502.
88. Nagarajan, P., et al., *Histone acetyl transferase 1 is essential for Mammalian development, genome stability, and the processing of newly synthesized histones h3 and h4.* PLoS Genet, 2013. **9**(6): p. e1003518.
89. Taddei, A., et al., *Duplication and maintenance of heterochromatin domains.* J Cell Biol, 1999. **147**(6): p. 1153-66.
90. Lusser, A., et al., *Analysis of the histone acetyltransferase B complex of maize embryos.* Nucleic Acids Res, 1999. **27**(22): p. 4427-35.
91. Chang, L., et al., *Histones in transit: cytosolic histone complexes and diacetylation of H4 during nucleosome assembly in human cells.* Biochemistry, 1997. **36**(3): p. 469-80.
92. Ahmad, A., Y. Takami, and T. Nakayama, *WD repeats of the p48 subunit of chicken chromatin assembly factor-1 required for in vitro interaction with chicken histone deacetylase-2.* J Biol Chem, 1999. **274**(23): p. 16646-53.
93. Bhaskara, S., et al., *Hdac3 is essential for the maintenance of chromatin structure and genome stability.* Cancer Cell, 2010. **18**(5): p. 436-47.
94. Furumai, R., et al., *FK228 (depsipeptide) as a natural prodrug that inhibits class I histone deacetylases.* Cancer Res, 2002. **62**(17): p. 4916-21.
95. Anantha, R.W., V.M. Vassin, and J.A. Borowiec, *Sequential and synergistic modification of human RPA stimulates chromosomal DNA repair.* J Biol Chem, 2007. **282**(49): p. 35910-23.
96. Dickey, J.S., et al., *H2AX: functional roles and potential applications.* Chromosoma, 2009. **118**(6): p. 683-92.
97. Mimitou, E.P. and L.S. Symington, *DNA end resection: many nucleases make light work.* DNA Repair (Amst), 2009. **8**(9): p. 983-95.
98. Errico, A. and V. Costanzo, *Differences in the DNA replication of unicellular eukaryotes and metazoans: known unknowns.* EMBO Rep, 2010. **11**(4): p. 270-8.
99. Dupre, A., et al., *A forward chemical genetic screen reveals an inhibitor of the Mre11-Rad50-Nbs1 complex.* Nat Chem Biol, 2008. **4**(2): p. 119-25.
100. Sartori, A.A., et al., *Human CtIP promotes DNA end resection.* Nature, 2007. **450**(7169): p. 509-14.

101. Berkovich, E., R.J. Monnat, Jr., and M.B. Kastan, *Roles of ATM and NBS1 in chromatin structure modulation and DNA double-strand break repair.* Nat Cell Biol, 2007. **9**(6): p. 683-90.
102. Savic, V., et al., *Formation of dynamic gamma-H2AX domains along broken DNA strands is distinctly regulated by ATM and MDC1 and dependent upon H2AX densities in chromatin.* Mol Cell, 2009. **34**(3): p. 298-310.
103. Leahy, J.J., et al., *Identification of a highly potent and selective DNA-dependent protein kinase (DNA-PK) inhibitor (NU7441) by screening of chromenone libraries.* Bioorg Med Chem Lett, 2004. **14**(24): p. 6083-7.
104. Hickson, I., et al., *Identification and characterization of a novel and specific inhibitor of the ataxia-telangiectasia mutated kinase ATM.* Cancer Res, 2004. **64**(24): p. 9152-9.
105. Sarkaria, J.N., et al., *Inhibition of ATM and ATR kinase activities by the radiosensitizing agent, caffeine.* Cancer Res, 1999. **59**(17): p. 4375-82.
106. Masumoto, H., et al., *A role for cell-cycle-regulated histone H3 lysine 56 acetylation in the DNA damage response.* Nature, 2005. **436**(7048): p. 294-8.
107. Tjeertes, J.V., K.M. Miller, and S.P. Jackson, *Screen for DNA-damage-responsive histone modifications identifies H3K9Ac and H3K56Ac in human cells.* EMBO J, 2009. **28**(13): p. 1878-89.
108. Ward, I.M. and J. Chen, *Histone H2AX is phosphorylated in an ATR-dependent manner in response to replicational stress.* J Biol Chem, 2001. **276**(51): p. 47759-62.
109. Gilad, O., et al., *Combining ATR suppression with oncogenic Ras synergistically increases genomic instability, causing synthetic lethality or tumorigenesis in a dosage-dependent manner.* Cancer Res, 2010. **70**(23): p. 9693-702.
110. Dion, V., et al., *Increased mobility of double-strand breaks requires Mec1, Rad9 and the homologous recombination machinery.* Nat Cell Biol, 2012. **14**(5): p. 502-9.
111. Mine-Hattab, J. and R. Rothstein, *Increased chromosome mobility facilitates homology search during recombination.* Nat Cell Biol, 2012. **14**(5): p. 510-7.
112. You, Z., et al., *Rapid activation of ATM on DNA flanking double-strand breaks.* Nat Cell Biol, 2007. **9**(11): p. 1311-8.
113. Ichijima, Y., et al., *MDC1 directs chromosome-wide silencing of the sex chromosomes in male germ cells.* Genes Dev, 2011. **25**(9): p. 959-71.
114. Wang, J., Z. Gong, and J. Chen, *MDC1 collaborates with TopBP1 in DNA replication checkpoint control.* J Cell Biol, 2011. **193**(2): p. 267-73.
115. Byun, T.S., et al., *Functional uncoupling of MCM helicase and DNA polymerase activities activates the ATR-dependent checkpoint.* Genes Dev, 2005. **19**(9): p. 1040-52.

116. Cotta-Ramusino, C., et al., *Exo1 processes stalled replication forks and counteracts fork reversal in checkpoint-defective cells.* Mol Cell, 2005. **17**(1): p. 153-9.
117. Bartek, J., J. Bartkova, and J. Lukas, *DNA damage signalling guards against activated oncogenes and tumour progression.* Oncogene, 2007. **26**(56): p. 7773-9.
118. Halazonetis, T.D., V.G. Gorgoulis, and J. Bartek, *An oncogene-induced DNA damage model for cancer development.* Science, 2008. **319**(5868): p. 1352-5.
119. Bantscheff, M., et al., *Quantitative mass spectrometry in proteomics: a critical review.* Anal Bioanal Chem, 2007. **389**(4): p. 1017-31.
120. Zybailov, B., et al., *Statistical analysis of membrane proteome expression changes in Saccharomyces cerevisiae.* J Proteome Res, 2006. **5**(9): p. 2339-47.
121. Sirbu, B.M., et al., *Analysis of protein dynamics at active, stalled, and collapsed replication forks.* Genes Dev, 2011. **25**(12): p. 1320-7.
122. Gilljam, K.M., et al., *Identification of a novel, widespread, and functionally important PCNA-binding motif.* J Cell Biol, 2009. **186**(5): p. 645-54.
123. Bensimon, A., et al., *ATM-dependent and -independent dynamics of the nuclear phosphoproteome after DNA damage.* Sci Signal, 2010. **3**(151): p. rs3.
124. Lovejoy, C.A., et al., *Functional genomic screens identify CINP as a genome maintenance protein.* Proc Natl Acad Sci U S A, 2009. **106**(46): p. 19304-9.
125. Paulsen, R.D., et al., *A genome-wide siRNA screen reveals diverse cellular processes and pathways that mediate genome stability.* Mol Cell, 2009. **35**(2): p. 228-39.
126. O'Donnell, L., et al., *The MMS22L-TONSL complex mediates recovery from replication stress and homologous recombination.* Mol Cell, 2010. **40**(4): p. 619-31.
127. Duro, E., et al., *Identification of the MMS22L-TONSL complex that promotes homologous recombination.* Mol Cell, 2010. **40**(4): p. 632-44.
128. O'Connell, B.C., et al., *A genome-wide camptothecin sensitivity screen identifies a mammalian MMS22L-NFKBIL2 complex required for genomic stability.* Mol Cell, 2010. **40**(4): p. 645-57.
129. Ciccia, A. and S.J. Elledge, *The DNA damage response: making it safe to play with knives.* Mol Cell, 2010. **40**(2): p. 179-204.
130. Chen, L., et al., *CHD1L promotes hepatocellular carcinoma progression and metastasis in mice and is associated with these processes in human patients.* J Clin Invest, 2010. **120**(4): p. 1178-91.
131. Mimitou, E.P. and L.S. Symington, *Sae2, Exo1 and Sgs1 collaborate in DNA double-strand break processing.* Nature, 2008. **455**(7214): p. 770-4.

132. Nicolette, M.L., et al., *Mre11-Rad50-Xrs2 and Sae2 promote 5' strand resection of DNA double-strand breaks.* Nat Struct Mol Biol, 2010. **17**(12): p. 1478-85.
133. Garcia, V., et al., *Bidirectional resection of DNA double-strand breaks by Mre11 and Exo1.* Nature, 2011. **479**(7372): p. 241-4.
134. Lee, B.I. and D.M. Wilson, 3rd, *The RAD2 domain of human exonuclease 1 exhibits 5' to 3' exonuclease and flap structure-specific endonuclease activities.* J Biol Chem, 1999. **274**(53): p. 37763-9.
135. Hombauer, H., et al., *Visualization of eukaryotic DNA mismatch repair reveals distinct recognition and repair intermediates.* Cell, 2011. **147**(5): p. 1040-53.
136. Liberti, S.E., A.A. Larrea, and T.A. Kunkel, *Exonuclease 1 preferentially repairs mismatches generated by DNA polymerase alpha.* DNA Repair (Amst), 2013. **12**(2): p. 92-6.
137. Tishkoff, D.X., et al., *Identification and characterization of Saccharomyces cerevisiae EXO1, a gene encoding an exonuclease that interacts with MSH2.* Proc Natl Acad Sci U S A, 1997. **94**(14): p. 7487-92.
138. Tran, P.T., J.A. Simon, and R.M. Liskay, *Interactions of Exo1p with components of MutLalpha in Saccharomyces cerevisiae.* Proc Natl Acad Sci U S A, 2001. **98**(17): p. 9760-5.
139. Clark, A.B., et al., *Functional interaction of proliferating cell nuclear antigen with MSH2-MSH6 and MSH2-MSH3 complexes.* J Biol Chem, 2000. **275**(47): p. 36498-501.
140. Schopf, B., et al., *Interplay between mismatch repair and chromatin assembly.* Proc Natl Acad Sci U S A, 2012. **109**(6): p. 1895-900.
141. Kee, Y. and A.D. D'Andrea, *Expanded roles of the Fanconi anemia pathway in preserving genomic stability.* Genes Dev, 2010. **24**(16): p. 1680-94.
142. Joo, W., et al., *Structure of the FANCI-FANCD2 complex: insights into the Fanconi anemia DNA repair pathway.* Science, 2011. **333**(6040): p. 312-6.
143. Van, C., et al., *Continued primer synthesis at stalled replication forks contributes to checkpoint activation.* J Cell Biol, 2010. **189**(2): p. 233-46.
144. Chaudhury, I., et al., *FANCD2 regulates BLM complex functions independently of FANCI to promote replication fork recovery.* Nucleic Acids Res, 2013.
145. Fouret, R., et al., *A comparative and integrative approach identifies ATPase family, AAA domain containing 2 as a likely driver of cell proliferation in lung adenocarcinoma.* Clin Cancer Res, 2012. **18**(20): p. 5606-16.
146. Caron, C., et al., *Functional characterization of ATAD2 as a new cancer/testis factor and a predictor of poor prognosis in breast and lung cancers.* Oncogene, 2010. **29**(37): p. 5171-81.

147. Machwe, A., et al., *The Werner and Bloom syndrome proteins catalyze regression of a model replication fork.* Biochemistry, 2006. **45**(47): p. 13939-46.
148. Betous, R., et al., *SMARCAL1 catalyzes fork regression and Holliday junction migration to maintain genome stability during DNA replication.* Genes & development, 2012. **26**(2): p. 151-62.
149. Gari, K., et al., *Remodeling of DNA replication structures by the branch point translocase FANCM.* Proc Natl Acad Sci U S A, 2008. **105**(42): p. 16107-12.
150. Ciccia, A., et al., *Polyubiquitinated PCNA Recruits the ZRANB3 Translocase to Maintain Genomic Integrity after Replication Stress.* Mol Cell, 2012.
151. Ammazzalorso, F., et al., *ATR and ATM differently regulate WRN to prevent DSBs at stalled replication forks and promote replication fork recovery.* The EMBO journal, 2010. **29**(18): p. 3156-69.
152. Cortez, D., G. Glick, and S.J. Elledge, *Minichromosome maintenance proteins are direct targets of the ATM and ATR checkpoint kinases.* Proc Natl Acad Sci U S A, 2004. **101**(27): p. 10078-83.
153. Yoo, H.Y., et al., *Mcm2 is a direct substrate of ATM and ATR during DNA damage and DNA replication checkpoint responses.* J Biol Chem, 2004. **279**(51): p. 53353-64.
154. Shi, Y., et al., *Identification of carboxyl-terminal MCM3 phosphorylation sites using polyreactive phosphospecific antibodies.* J Biol Chem, 2007. **282**(12): p. 9236-43.
155. Trenz, K., A. Errico, and V. Costanzo, *Plx1 is required for chromosomal DNA replication under stressful conditions.* EMBO J, 2008. **27**(6): p. 876-85.
156. De Piccoli, G., et al., *Replisome stability at defective DNA replication forks is independent of S phase checkpoint kinases.* Mol Cell, 2012. **45**(5): p. 696-704.
157. Kleine, H. and B. Luscher, *Learning how to read ADP-ribosylation.* Cell, 2009. **139**(1): p. 17-9.
158. Caldecott, K.W., *Single-strand break repair and genetic disease.* Nat Rev Genet, 2008. **9**(8): p. 619-31.
159. Turner, N.C., et al., *A synthetic lethal siRNA screen identifying genes mediating sensitivity to a PARP inhibitor.* EMBO J, 2008. **27**(9): p. 1368-77.
160. Chen, X., et al., *Rational design of human DNA ligase inhibitors that target cellular DNA replication and repair.* Cancer Res, 2008. **68**(9): p. 3169-77.
161. Rowbotham, S.P., et al., *Maintenance of silent chromatin through replication requires SWI/SNF-like chromatin remodeler SMARCAD1.* Mol Cell, 2011. **42**(3): p. 285-96.

162. Taddei, A., et al., *Reversible disruption of pericentric heterochromatin and centromere function by inhibiting deacetylases.* Nat Cell Biol, 2001. **3**(2): p. 114-20.
163. Mermoud, J.E., S.P. Rowbotham, and P.D. Varga-Weisz, *Keeping chromatin quiet: how nucleosome remodeling restores heterochromatin after replication.* Cell Cycle, 2011. **10**(23): p. 4017-25.
164. Peters, A.H., et al., *Loss of the Suv39h histone methyltransferases impairs mammalian heterochromatin and genome stability.* Cell, 2001. **107**(3): p. 323-37.
165. Struhl, K. and E. Segal, *Determinants of nucleosome positioning.* Nat Struct Mol Biol, 2013. **20**(3): p. 267-73.
166. Poot, R.A., et al., *The Williams syndrome transcription factor interacts with PCNA to target chromatin remodelling by ISWI to replication foci.* Nat Cell Biol, 2004. **6**(12): p. 1236-44.
167. Bansbach, C.E., et al., *The annealing helicase SMARCAL1 maintains genome integrity at stalled replication forks.* Genes & development, 2009. **23**(20): p. 2405-14.
168. Dirscherl, S.S. and J.E. Krebs, *Functional diversity of ISWI complexes.* Biochem Cell Biol, 2004. **82**(4): p. 482-9.
169. Bozhenok, L., P.A. Wade, and P. Varga-Weisz, *WSTF-ISWI chromatin remodeling complex targets heterochromatic replication foci.* EMBO J, 2002. **21**(9): p. 2231-41.
170. Xiao, A., et al., *WSTF regulates the H2A.X DNA damage response via a novel tyrosine kinase activity.* Nature, 2009. **457**(7225): p. 57-62.
171. Collins, N., et al., *An ACF1-ISWI chromatin-remodeling complex is required for DNA replication through heterochromatin.* Nat Genet, 2002. **32**(4): p. 627-32.
172. Erdel, F., et al., *Human ISWI chromatin-remodeling complexes sample nucleosomes via transient binding reactions and become immobilized at active sites.* Proc Natl Acad Sci U S A, 2010. **107**(46): p. 19873-8.
173. Yip, D.J., et al., *Snf2l regulates Foxg1-dependent progenitor cell expansion in the developing brain.* Dev Cell, 2012. **22**(4): p. 871-8.
174. Tsukiyama, T., et al., *Characterization of the imitation switch subfamily of ATP-dependent chromatin-remodeling factors in Saccharomyces cerevisiae.* Genes Dev, 1999. **13**(6): p. 686-97.
175. Badenhorst, P., et al., *Biological functions of the ISWI chromatin remodeling complex NURF.* Genes Dev, 2002. **16**(24): p. 3186-98.
176. Ye, Y., et al., *Inhibition of expression of the chromatin remodeling gene, SNF2L, selectively leads to DNA damage, growth inhibition, and cancer cell death.* Mol Cancer Res, 2009. **7**(12): p. 1984-99.
177. Vincent, J.A., T.J. Kwong, and T. Tsukiyama, *ATP-dependent chromatin remodeling shapes the DNA replication landscape.* Nat Struct Mol Biol, 2008. **15**(5): p. 477-84.

178. Havas, K., et al., *Generation of superhelical torsion by ATP-dependent chromatin remodeling activities.* Cell, 2000. **103**(7): p. 1133-42.
179. Corona, D.F., et al., *ISWI regulates higher-order chromatin structure and histone H1 assembly in vivo.* PLoS Biol, 2007. **5**(9): p. e232.
180. Deuring, R., et al., *The ISWI chromatin-remodeling protein is required for gene expression and the maintenance of higher order chromatin structure in vivo.* Mol Cell, 2000. **5**(2): p. 355-65.
181. Kliszczak, A.E., et al., *DNA mediated chromatin pull-down for the study of chromatin replication.* Sci Rep, 2011. **1**: p. 95.
182. Li, Z., et al., *Systematic comparison of label-free, metabolic labeling, and isobaric chemical labeling for quantitative proteomics on LTQ Orbitrap Velos.* J Proteome Res, 2012. **11**(3): p. 1582-90.
183. Ow, S.Y., et al., *Quantitative shotgun proteomics of enriched heterocysts from Nostoc sp. PCC 7120 using 8-plex isobaric peptide tags.* J Proteome Res, 2008. **7**(4): p. 1615-28.
184. Capson, T.L., S.J. Benkovic, and N.G. Nossal, *Protein-DNA cross-linking demonstrates stepwise ATP-dependent assembly of T4 DNA polymerase and its accessory proteins on the primer-template.* Cell, 1991. **65**(2): p. 249-58.
185. Loveland, A.B., et al., *A general approach to break the concentration barrier in single-molecule imaging.* Nat Methods, 2012. **9**(10): p. 987-92.
186. Jao, C.Y. and A. Salic, *Exploring RNA transcription and turnover in vivo by using click chemistry.* Proc Natl Acad Sci U S A, 2008. **105**(41): p. 15779-84.